REPORT DOCUMENTATION PAGE

1. Recipient's Reference	2. Originator's Reference	3. Further Reference	4. Security Classification of Document
	AGARD-AG-281	ISBN 92-835-1463-7	UNCLASSIFIED

5. Originator
Advisory Group for Aerospace Research and Development
North Atlantic Treaty Organization
7 rue Ancelle, 92200 Neuilly sur Seine, France

6. Title
TWO-DIMENSIONAL WIND TUNNEL WALL INTERFERENCE

7. Presented at

8. Author(s)/Editor(s)	9. Date
written by M.Mokry, Y.Y.Chan and D.J.Jones edited by L.H.Ohman	November 1983

10. Author's/Editor's Address	11. Pages
National Aeronautical Establishment National Research Council, Canada	194

12. Distribution Statement
This document is distributed in accordance with AGARD policies and regulations, which are outlined on the Outside Back Covers of all AGARD publications.

13. Keywords/Descriptors

Wind tunnels
Subsonic flow
Transonic flow
Walls
Aerodynamic interference
Aerodynamics

14. Abstract

A description and analysis is presented of the more important developments during the past decade in the understanding of the wall interference problem associated with two-dimensional wind tunnel testing at subsonic and transonic speeds. Discussed are wall boundary conditions, asymptotic analysis of wall interference, classical and extended wall interference theories, wall interference corrections from boundary measurements, integral equation formulation of subcritical wall interference, and effects of side wall boundary layer on two-dimensional tests. Unsteady wall interference at subsonic and supersonic flow conditions is reviewed. Recent advances in the adaptive wall technique, which actively reduces or eliminates wall interference, are also described.

This AGARDograph has been produced at the request of the Fluid Dynamics Panel of AGARD.

AGARD-AG-281

AGARD

ADVISORY GROUP FOR AEROSPACE RESEARCH & DEVELOPMENT

7 RUE ANCELLE 92200 NEUILLY SUR SEINE FRANCE

AGARDograph No. 281

Two-Dimensional Wind Tunnel Wall Interference

NORTH ATLANTIC TREATY ORGANIZATION

NORTH ATLANTIC TREATY ORGANIZATION

ADVISORY GROUP FOR AEROSPACE RESEARCH AND DEVELOPMENT, Paris

(ORGANISATION DU TRAITE DE L'ATLANTIQUE NORD)

AGARDograph No.281

TWO-DIMENSIONAL WIND TUNNEL WALL INTERFERENCE

by

M.Mokry, Y.Y.Chan and D.J.Jones
National Aeronautical Establishment
National Research Council, Canada

Edited by

L.H.Ohman
National Aeronautical Establishment
National Research Council, Canada

This AGARDograph has been produced at the request of the Fluid Dynamics Panel of AGARD.

THE MISSION OF AGARD

The mission of AGARD is to bring together the leading personalities of the NATO nations in the fields of science and technology relating to aerospace for the following purposes:

- Exchanging of scientific and technical information;
- Continuously stimulating advances in the aerospace sciences relevant to strengthening the common defence posture;
- Improving the co-operation among member nations in aerospace research and development;
- Providing scientific and technical advice and assistance to the North Atlantic Military Committee in the field of aerospace research and development;
- Rendering scientific and technical assistance, as requested, to other NATO bodies and to member nations in connection with research and development problems in the aerospace field;
- Providing assistance to member nations for the purpose of increasing their scientific and technical potential;
- Recommending effective ways for the member nations to use their research and development capabilities for the common benefit of the NATO community.

The highest authority within AGARD is the National Delegates Board consisting of officially appointed senior representatives from each member nation. The mission of AGARD is carried out through the Panels which are composed of experts appointed by the National Delegates, the Consultant and Exchange Programme and the Aerospace Applications Studies Programme. The results of AGARD work are reported to the member nations and the NATO Authorities through the AGARD series of publications of which this is one.

Participation in AGARD activities is by invitation only and is normally limited to citizens of the NATO nations.

Published November 1983

ISBN 92-835-1463-7

Printed by Specialised Printing Services Limited
40 Chigwell Lane, Loughton, Essex IG10 3TZ

SUMMARY

A description and analysis is presented of the more important developments during the past decade in the understanding of the wall interference problem associated with two-dimensional wind tunnel testing at subsonic and transonic speeds. Discussed are wall boundary conditions, asymptotic analysis of wall interference, classical and extended wall interference theories, wall interference corrections from boundary measurements, integral equation formulation of subcritical wall interference, and effects of side wall boundary layer on two-dimensional tests. Unsteady wall interference at subsonic flow conditions is reviewed. Recent advances in the adaptive wall technique, which actively reduces or eliminates wall interference, are also described.

CONTENTS

1.0 INTRODUCTION

Nearly two decades have passed since the publication of the AGARDograph "Subsonic Wind Tunnel Wall Corrections" by Garner, Rogers, Acum, and Maskell [1.1]. During this time significant advances have taken place, so that a new review of the wall interference topic became a worthwhile project, even if it should cover, as we proposed, only the two-dimensional part of the problem.

In 1975, a discussion concerning the future of wind tunnels was initiated following the appearance of the article "Computers vs. Wind Tunnels" by Chapman, Mark and Pirtle [1.2]. Drawing comparisons with other fields of computational physics, the authors predicted that advances in computer capabilities would eventually provide cheaper and more accurate simulation of flight aerodynamics than the wind tunnels can. The wind tunnels would then perform only a secondary role to computers. As major obstacles to routine computer solution for complete viscous flows identified were the lack of storage and speed of existing computers and the inadequacy of available turbulence models. As noted by Bradshaw [1.3] and Marvin [1.4], more comparisons with well-conceived wind tunnel experiments will in fact be required to guide the development of turbulence models applicable to more complex flows.

So far, there has not been any noticeable decline in wind tunnel activities, even though the computers are gradually taking a relatively bigger share in aircraft design, see Figure 1.1. The unit cost of computer simulations is continually decreasing as a result of improved numerical procedures and advances in computer technology [1.5] and it is foreseen that in perhaps two decades the computer could become an equal partner with the wind tunnel [1.6], [1.7]. On the other hand, the enhancement of wind tunnel capabilities can be realized by integrating wind tunnels and computers as exemplified by the adaptive wall concept. Confidence that wind tunnels will continue to contribute to advances in aircraft design is evidenced by the construction of the new tunnel capabilities in industrialized countries, such as the cryogenic National Transonic Facility at NASA Langley, U.S.A., and the planning for the European Transonic Windtunnel [1.8]. To meet the future challenges, improved correction and wall adjustment schemes for obtaining more reliable wind tunnel data will have to be developed.

In this report we have tried to address all major topics in two-dimensional wall interference, but no attempt has been made to be encyclopedic. In the process of deciding which correction methods to include, preference has been given to those based on the solution of boundary value problems, consisting of a governing differential equation and appropriate boundary conditions. Unlike the empirical corrections, which often apply only to one particular facility (or worse, one model), the techniques based on the boundary value problem approach are lasting contributions in a sense that they represent valid mathematical solutions, even though they may not describe a particular tunnel experiment in all its complexity. In fact, the correction procedures described in this treatise are approximations, based on potential flow methods, external flow field estimations, thin airfoil theories, wind tunnel idealizations, etc. An ultimate tool for analyzing wall interference would be a numerical technique allowing complete solution of viscous flows past airfoils in a wind tunnel. Ironically, this goal has a self-defeating purpose, following from the argument that if we could calculate such flows there would be no need for wind tunnel tests, much less for numerical simulations of the wind tunnel with its complicated boundary conditions. Clearly, exact free air calculations would serve the purpose more than adequately. But as we said earlier, to date such techniques are still outside our reach.

The problem areas which contribute to inaccuracy in wall interference prediction, as summarized by Kemp [1.9], are indicated in Figure 1.2. They are:

(a) nonlinearity of the governing equation at supercritical flow conditions,

(b) nonlinearity of ventilated wall crossflow boundary conditions and difficulties in predicting or measuring them,

(c) wind tunnel geometry features, such as finite ventilated wall length, diffuser entry and presence of a wake survey rake and its support,

(d) boundary layer on tunnel side walls, which causes the flow to deviate from the two-dimensional flow conditions.

An excellent survey of the physical properties of test section walls, particularly the ventilated ones, is given in the book by Goethert [1.10]. The treatment of subject in Chapter 2 of our report is therefore limited to results of more recent developments. Also, the discussion of physical phenomena is restricted to an extent which is needed for the specification of the wall boundary condition in other parts of the report.

Once regarded solely as an engineering approximation, wall interference theory has turned out to be a reputable topic, justifiable as other two Prandtl's concepts — the boundary layer and the lifting line — by singular perturbation analysis. To present this viewpoint at an early stage, the asymptotic analysis of wall interference is placed in Chapter 3, even though it is a relatively new subject.

Chapter 4 is an outline of the subsonic wall interference theory, based on linear homogeneous boundary condition of the walls and the representation of the airfoil far field by concentrated singularities. This theory, providing an insight into the essential features of subsonic wall interference, had been considered the basic correction tool for decades [1.1], [1.11]. The novelty of our approach is the systematization of the correction formulas, which were originally introduced in an ad hoc fashion. Attention is also paid to far field expressions for the wall interference potential, that are useful as upstream and downstream conditions for computations of transonic flows past airfoils at subcritical wall conditions. However, the methods of computational fluid dynamics themselves are outside the scope of the present publication. Regarding the finite difference methods, which are most frequently used to compute transonic flows past airfoils in the idealized wind tunnel environment, the reader is advised to consult References [1.12] to [1.16]. In Chapter 4, additional attention is paid to the effect of the finite test section length and plenum pressure. But even with these extensions, the classical wall interference theory has reached the limits of its usefulness: it has become more and more apparent that the idealization of tunnel boundary conditions cannot produce sufficiently accurate correction formulae for practical use.

The extension of the porous wall theory in Chapter 5, to consider different resistance of porous walls opposing the suction and pressure sides of the airfoil was one of the first attempts to incorporate the actual tunnel wall characteristics in the wall interference evaluation. Using this approach it is possible to retain the advantages of a linear theory and supply the closed form solution with porosity parameters, derived from static pressure measurements on the walls above and below the model. An improved version of the method, based on a more precise concept of different inflow and outflow wall resistances is also presented. Since in this case mixed inflow-outflow regimes are modeled, the wall corrections have to be obtained numerically.

Chapter 6 deals with the evaluation of interference corrections from boundary data, measured either at the walls or some distance from them. The application of measured static pressures and/or flow angles as boundary values ensures that the true physical behaviour of ventilated tunnel walls is taken into account when calculating the corrections. The techniques based on measured static pressures are regarded as the most practical of the discussed methods and are gaining wide acceptance. Naturally, the boundary data have to be taken with each wind tunnel test case, so that they are suitable for on-line or post-test assessment, not for prediction.

Chapter 7 concerns the integral representation of the velocity potential in terms of Green's function. From the point of view of mathematical physics, this seems to be the most natural approach to the wall interference problem. Besides providing an alternative justification of the classical wall interference concept, it allows the formulation of wall interference in terms of the modified Glauert or Oswatitsch integral equations.

Chapter 8 is an outline of unsteady wall interference. A special attention is paid to the phenomenon of transverse resonance which is one of the most severe examples of wall interference. The treatment, which is by no means exhaustive, concentrates on ventilated walls, compressible flow, and thin airfoils undergoing small amplitude harmonic motion. A more systematic presentation has not been attempted in view of an incomplete development of the theory and a lack of reliable experimental data.

Chapter 9 deals with the effect of sidewall boundary layers, which may be as important as the (two-dimensional) wall interference itself. The pressure field around the test airfoil causes variations in the displacement thickness of the boundary layer on the sidewalls, thereby violating the two-dimensionality of the flow. Unless the boundary layer is controlled, post-test corrections are required to be applied to the airfoil data.

Finally, Chapter 10 is concerned with the adaptive wall concept, pointedly characterized as a marriage of state-of-the-art computational and experimental capabilities. Discussed are the operation principles of the adaptive ventilated walls, producing interference-free conditions by controlling the flowfield through suction and blowing, and the self-streamlining walls, effecting the same by assuming streamline shapes in unconfined flow. The minimization of wall interference by adaptive walls is essentially a variational problem, which is no less challenging than the evaluation of corrections for passive walls. Most of the work on adaptive walls is still in the technology-development phase; however the concept has been shown to be feasible, and it is likely that production facilities will be built before long [1.17]. Besides this optimism there are also cautionary views [1.18], that the new technological advances will have to be accompanied by more efficient flow analysis and wall control codes — particularly for transonic flows at the walls — to make the adaptive wall wind tunnel viable. Accordingly, a special attention is paid to the question of initial wall setting and one-step adjustment schemes. The current state of the art of the adaptive wall technology is summarized in Reference [1.19], and a selected, annotated bibliography is given in Reference [1.20].

Since the present monograph is a joint work of three authors and differences in style are apparent, it is appropriate to indicate the individual contributions: Y.Y. Chan prepared Chapters 3 and 9, together with a part of Chapter 2, D.J. Jones is responsible for the second part of Chapter 5, and M. Mokry wrote Chapters 4, 6, 7, 8, 10 and parts of Chapters 2 and 5, the entire manuscript was edited by L.H. Ohman.

Our special thanks are due to Dr. P.R. Ashill of the Royal Aircraft Establishment, England, Professor S. Berndt of the Royal Institute of Technology, Sweden, W.B. Kemp of NASA Langley, U.S.A., Dr. E.M. Kraft of ARVIN/CALSPAN, U.S.A., Dr. N.D. Malmuth of the Rockwell International, U.S.A., Professor E.M. Murman of MIT, U.S.A., H. Sawada of the National Aerospace Laboratory, Japan, and J. Smith of NLR, Netherlands, for reading various parts of the manuscript and offering valuable suggestions. Acknowledged are also the discussions with J.P. Chevallier of ONERA, France and Professor M. Golberg of the University of Nevada.

A note of particular appreciation is due to Mrs. M.H. Cole of the National Research Council Canada, for the meticulous typesetting of the text.

REFERENCES

[1.1] Garner, H.C.; Rogers, E.W.E.; Acum, W.E.A.; Maskell, E.C. *Subsonic Wind Tunnel Wall Corrections.* AGARDograph 109, Oct. 1966.

[1.2] Chapman, D.R.; Mark, H.; Pirtle, M.W. *Computers vs. Wind Tunnels for Aerodynamic Flow Simulations.* Aeronautics and Astronautics, Vol. 13, April 1975, pp. 22-30 and 35.

[1.3] Bradshaw, P. *Computers vs. Wind Tunnels.* Letter, Aeronautics and Astronautics, Vol. 13, Sept. 1975, p. 6.

[1.4] Marvin, J.G. *Turbulence Modeling for Computational Aerodynamics.* AIAA Journal, Vol. 21, 1983, pp. 941-955.

[1.5] Kutler, P. *A Perspective of Theoretical and Applied Computational Fluid Dynamics.* AIAA Paper 83-0037, Jan. 1983.

[1.6] Whitfield, J.D.; Pate, S.R.; Kimzey, W.F.; Whitfield, D.L. *The Role of Computers in Aerodynamic Testing.* Computers and Fluids, Vol. 8, 1980, pp. 71-99.

[1.7] Whitfield, J.D.; Griffith, B.J.; Bang, C.; Butler, R.W. *Overview of Flight and Ground Testing With Emphasis on the Wind Tunnel.* AIAA Paper 81-2474, Nov. 1981.

[1.8] Dietz, R.O. *Windtunnel Capability Related to Test Sections, Cryogenics, and Computer-Windtunnel Integration.* AGARD-AR-174, April 1982, pp. 1-7.

[1.9] Kemp, W.B. *Transonic Assessment of Two-Dimensional Wind Tunnel Wall Interference Using Measured Wall Pressures.* Advanced Technology Airfoil Research, NASA Conference Publication 2045, Vol. 1, pp. 473-486.

[1.10] Goethert, B.H. *Transonic Wind Tunnel Testing.* Pergamon Press, 1961.

[1.11] Pindzola, M.; Lo, C.F. *Boundary Interference at Subsonic Speeds in Wind Tunnels With Ventilated Walls.* AEDC-TR-69-47, May 1969.

[1.12] Murman, E.M. — *Computation of Wall Effects in Ventilated Transonic Wind Tunnels.* AIAA Paper 72-1007, 1972.

[1.13] Kacprzynski, J.J. — *Transonic Flow Field Past 2-D Airfoils Between Porous Wind Tunnel Walls With Nonlinear Characteristics.* AIAA Paper 75-81, 1975.

[1.14] Catherall, D. — *The Computation of Transonic Flows Past Aerofoils in Solid, Porous or Slotted Wind Tunnels.* Wind Tunnel Design and Testing Techniques, AGARD-CP-174, Oct. 1975, pp. 19.1-19.10.

[1.15] Laval, P. — *Méthodes instationnaires de calcul des effets d'interaction de paroi en écoulement bidimensionnel supercritique.* La Recherche Aérospatiale, 1973, pp. 275-288.

[1.16] Stahara, S.S. — *Operational Manual for Two-Dimensional Transonic Code TSFOIL.* NASA CR 3064, 1978.

[1.17] Satyanarayana, B., Schairer, E., Davis, S. — *Adaptive-Wall Wind-Tunnel Development for Transonic Testing.* Journal of Aircraft, Vol. 18, 1980, pp. 273-279.

[1.18] Fonarev, A.S., Sherstyuk, A.V. — *Algorithms and Methods for Computer Simulation of Transonic Flow.* Transl. from Avtomatika i Telemekhanika, No. 7, July 1982, pp. 5-18.

[1.19] Binion, T.W., Chevallier, J.P., Laster, M.L. (ed.) — *Report of the Conveners Group on Transonic Test Sections.* Windtunnel Capability Related to Test Sections, Cryogenics, and Computer-Windtunnel Integration, AGARD-AR-174, April 1982, pp. A1.1-A1.15.

[1.20] Tuttle, Marie H., Plentovich, Elizabeth B. — *Adaptive Wall Wind Tunnels — A Selected, Annotated Bibliography.* NASA TM-84526, Nov. 1982.

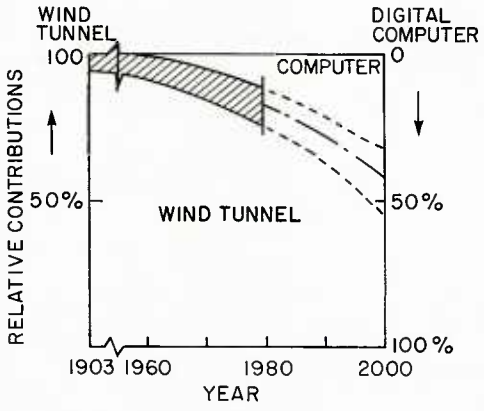

Fig. 1.1 Contributions of the wind tunnel to aeronautical research and development (Ref. [1.6])

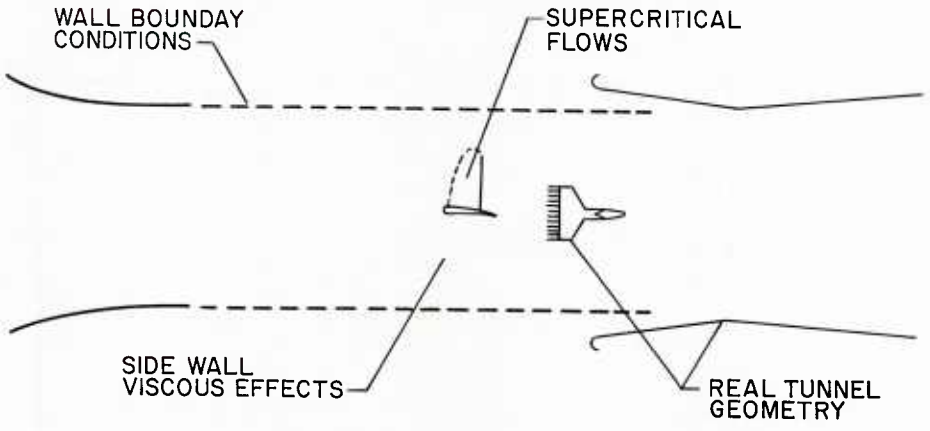

Fig. 1.2 Wall interference problem area (Ref. [1.9])

2.0 WALL BOUNDARY CONDITIONS

2.1 Introductory Remarks

An excellent survey of physical properties of various types of wind tunnel walls is given in the book by Goethert [2.1], published in 1961. The present chapter discusses some newer developments, but concentrates mainly on the specification of wall boundary conditions that are of importance for the calculation of wall interference.

By the wall boundary condition we understand the relation between the normal component V of velocity and the pressure difference across the wall $p - p_{plenum}$, see Figure 2.1. Using the undisturbed values of velocity U_∞, pressure p_∞ and density ρ_∞ far upstream, we form the pressure coefficients

$$C_p = \frac{p - p_\infty}{\frac{1}{2}\rho_\infty U_\infty^2} \tag{2.1}$$

and

$$C_{p_{plenum}} = \frac{p_{plenum} - p_\infty}{\frac{1}{2}\rho_\infty U_\infty^2} \tag{2.2}$$

The velocity ratio V/U_∞ can be expressed in terms of the disturbance velocity potential ϕ as

$$\frac{V}{U_\infty} = \frac{\partial \phi}{\partial n} \tag{2.3}$$

where n is the outward normal to the wall. Supposing that the tested model generates small pressure disturbances at the (distant) wall, then according to the linearized Bernoulli theorem

$$C_p = -\frac{2}{U_\infty}\frac{d\phi}{dt} \tag{2.4}$$

where

$$\frac{d}{dt} = \frac{\partial}{\partial t} + U_\infty \frac{\partial}{\partial x} \tag{2.5}$$

is the linearized total time derivative; x is the co-ordinate tangent to the wall.

Depending on situation, the wall boundary condition thus can be stated in terms of V/U_∞ and C_p, or the derivatives of ϕ. For unsteady flow calculations some authors prefer to use the (linearized) acceleration potential

$$\Psi = -\frac{p - p_\infty}{\rho_\infty}$$

which of course differs from C_p, Equation (2.1), only by a factor.

2.2 Solid (Closed) Walls

The simplest boundary condition is obtained for a solid (closed) wall. Since there is zero mass flux through the wall, normal velocity vanishes at the wall:

$$V = 0 \tag{2.6}$$

Using Equation (2.3), the solid (closed) wall boundary condition takes the form

$$\frac{\partial \phi}{\partial n} = 0 \tag{2.7}$$

For a solid wall wind tunnel, the wall boundary layer growth for a model with moderate lift is close to that on a flat plate as the pressure gradient is very small along the wall. The displacement effect on the tunnel flow can be compensated by setting the wall slightly divergent downstream, so that Equation (2.7) can be applied with a greater confidence along a plane parallel to the undisturbed stream. However, at high lift condition with flow separation at the rear part of the model, the location of the separation point is shown to be sensitive to wall interference and the growth of the wall boundary layer, which is no longer a flat plate type but is modulated by

the strong pressure field generated by the model [2.2]. Nevertheless, the wall boundary layers are in most cases thin compared to the distance from the model and Equation (2.7), as a boundary condition, is considered to be more reliable than those for other types of wind tunnel walls. Assuming that the wall is rigid, Equation (2.7) is also applicable as a solid wall boundary condition for unsteady flows.

If a solid straight wall is used as a wind tunnel boundary, the streamlines forming the flow about the model are squeezed together more than they would be in free air. At transonic speed the reduction in effective tunnel height due to the displacement thickness of the wall boundary layer, at first glance would appear as additional blockage and result in choking at a lower Mach number than if no wall boundary layer was present. However, it has been demonstrated experimentally [2.3] that, due to the "compliant" nature of the boundary layer, its deformation under the influence of the model pressure field actually compensates to some degree for the model blockage, with the net result that the choking Mach number is higher than that theoretically calculated based on the geometric tunnel height. In the most extreme case, as the (subsonic) stream Mach number reaches the critical value, the wind tunnel becomes choked in the test section and thus for an appreciable speed range no transonic testing is possible in a solid wall wind tunnel. In supersonic flow the shock waves generated by the model are reflected from the solid walls again as shock waves. They are a source of unacceptable interference in case they impinge on the model. For the above reasons the test sections with straight solid walls are considered unsuitable for high speed testing. However, it is possible to reduce solid wall interference by contouring the walls to resemble the streamline surfaces in unbounded flow past the same model (wind tunnel with flexible walls).

2.3 Open Jet Walls

An open jet boundary is defined as one on which the pressure perturbation is zero, that is

$$p = p_{plenum}$$

or

$$C_p = C_{p_{plenum}} \tag{2.8}$$

In the theoretical case of an infinitely long jet and constant plenum pressure, $p_{plenum} = p_\infty$ and

$$C_p = 0 \tag{2.9}$$

The substitution of Equation (2.4) in (2.9) yields the homogeneous open jet boundary condition

$$\frac{d\phi}{dt} = 0 \tag{2.10}$$

For steady flow thus

$$\frac{\partial\phi}{\partial x} = 0 \tag{2.11}$$

or simply

$$\phi = 0 \tag{2.12}$$

It is important to point out that an open jet boundary differs from free air because in the latter case the pressure perturbations due to the presence of the model vanish, in general, only at infinity. The curvature of the open jet boundary is greater than that of a corresponding streamline in infinite stream, since there is no outside flow to resist the deformation. A flow pattern will be obtained in which the streamlines are further apart than for free flight. In supersonic flow, the shock waves are reflected from the open jet boundary as expansion waves.

It is general practice to apply Equation (2.10) along the undisturbed jet boundary, assuming that the distortion is small. However, the usability of open jet test sections is rather limited, because of their tendency to develop pulsations, originating in the unstable shear layer of the jet [2.1].

2.4 Mean Boundary Condition for Ventilated Walls

Opposite wall interference effects for solid and open jet boundaries were observed already by Prandtl [2.4]. The desire to minimize the wall interference at subsonic speeds, to avoid choking at transonic speeds and to attenuate shock wave reflections at supersonic speeds has led to the introduction of ventilated (partially open) wind tunnel walls. The principle of using a combination of closed and open jet boundaries to minimize wall interference was established by Theodorsen [2.5], Toussaint [2.6], and Wieselsberger [2.7]; the first contemporary ventilated wind tunnel, using several longitudinal slots, was described by Wright and Ward [2.8]. The tunnel, put in operation in 1947, lived up to its promise concerning the prevention of choking and enabled testing through Mach one. However, as predicted later by Goodman [2.9], improved shock wave cancellation properties for testing at supersonic speeds were possible with small-grain porous walls. This eventually led to the now familiar concept of a perforated wall.

The physics of flow at a ventilated wind tunnel wall is very complex and depends, among other things, on viscous and boundary layer phenomena as well as the construction of the walls themselves. However, at some distance away from the wall, the localized effects of individual holes or slots (by which the wind tunnel is ventilated) will be integrated into more homogeneous effects, thereby permitting the introduction of mean or average boundary conditions, [2.10], [2.11], [2.12], [2.13] and [2.14]. A properly constructed mean boundary condition is expected to reduce to the boundary conditions of the solid and open jet walls if the open area ratio of the ventilated wall is zero and unity, respectively. In accordance with the usual mathematical terminology, we shall speak of a homogeneous boundary condition if the equation is linear and contains no (isolated) constant term. The advantages arising from linearity and superposition in the latter case are considerable.

For perforated walls, the experimental verification of the mean boundary condition concept was provided by Gardenier [2.15], who studied the decay of pressure disturbances generated by the holes, as a function of the distance from the wall. As illustrated in Figure 2.2, for thin boundary layers the Mach number fluctuations are reduced to 0.002 at $M_\infty = 1.2$ at a distance of about 20 hole diameters from the wall. For slotted walls the mean boundary condition concept can be validated theoretically within the framework of potential flow theory [2.1].

As pointed out in Reference [2.16], two types of mean boundary conditions have been proposed, the so-called porous wall boundary condition, based on the viscous effect, and the slotted wall boundary condition, based on the accelerative or mass effect.

2.5 Perforated Walls

The porous wall boundary condition, used for perforated and transversally slotted wind tunnel walls, is obtained by assuming that the average velocity of the flow normal to the wall is a linear function of the pressure drop across the wall. In the nondimensional form, this relationship can be written as

$$\frac{V}{U_\infty} = P\frac{p - p_{plenum}}{\rho_\infty U_\infty^2} \tag{2.13}$$

where the (positive) constant of proportionality P is called the porosity parameter. It is not to be interchanged with the geometrical porosity of the wall (open area ratio). The reciprocal value

$$R = \frac{1}{P} \tag{2.14}$$

is the resistance of the wall to crossflow. In the coefficient form, Equation (2.13) can be written as

$$\frac{V}{U_\infty} = P\frac{C_p - C_{p_{plenum}}}{2} \tag{2.15}$$

or

$$\frac{V}{U_\infty} = P\frac{C_p}{2} \tag{2.16}$$

if $p_{plenum} = p_\infty$.

The boundary condition described by Equation (2.15) represents a viscous mechanism in the sense that force in the form of pressure is proportional to velocity. Sometimes this loosely is referred to as Darcy's law [2.17], drawing analogy with the flow of fluids in porous media, but that does not seem to be an appropriate attribution in the present context [2.16]. Besides, the above relationship can also be derived using the concept of circulation, Section 2.6.

A detailed study of flow through an orifice in the presence of tangent (grazing) flow was given by Rogers and Hersh [2.18]. Using flow visualization by color dyes in a water tunnel, they identified the following distinct regimes of crossflow*:

(1) **Zero Flow** (Fig. 2.3(a))

This regime is characterized by recirculating flow in the cavity, driven by the shear layer of the tunnel stream. Otherwise, the shear layer acts as a barrier to crossflow.

(2) **Low Inflow** (Fig. 2.3(b))

The plenum pressure is sufficient to lift the dividing stream surface. The circulatory motion inside the cavity subsides as orifice flow increases. The detached shear layer acts like a lid, controlling inflow.

(3) **Low Outflow** (Fig. 2.3(c))

The circulatory flow is confined to a separated region off the upstream lip of the orifice. The change of the size of this separated region provides the mechanism for controlling outflow.

(4) **High Inflow** (Fig. 2.3(d))

The shear layer no longer exercises control over inflow. A minimum flow area is established (vena contracta effect).

(5) **High Outflow** (Fig. 2.3(e))

The separated flow region inside the cavity is reduced to minimum (vena contracta) and has no further control over outflow.

From the above physical picture it is sufficiently clear that the linear boundary condition (2.15), based on the viscous flow mechanism is plausible only for low flow regimes. It is generally conceded that one must rely on experiments to establish the resistance (or porosity parameter) for a given wall geometry, Reynolds number and Mach number. Rogers and Hersh [2.18] have shown that the wall resistance measurements can be correlated when plotted in terms of the discharge coefficient vs. orifice velocity, normalized by the tunnel stream velocity.

Using Equations (2.14) and (2.16), we define the orifice resistance

$$R_i = \frac{C_p}{2\frac{V_i}{U_\infty}} \tag{2.17}$$

where V_i is the orifice inlet velocity. Introducing the (incompressible flow) discharge coefficient [2.18]

---

*In agreement with Reference [2.1] and contrary to Reference [2.18], the terms "inflow" and "outflow" are applied with respect to the test section and not plenum.

$$C_d = \frac{V_i}{V_{id}}$$

where

$$V_{id} = U_\infty C_p^{\frac{1}{2}}$$

is the ideal velocity, we obtain

$$R_i = \frac{1}{2} \frac{\frac{V_i}{U_\infty}}{C_d^2}$$

For a perforated wall of small open area ratio, $\delta \ll 1$, the averaged normal velocity can be approximated as

$$V \simeq V_i \frac{\delta}{1 - \delta}$$

so that the total resistance of the wall is

$$R \simeq R_i \frac{1 - \delta}{\delta} \tag{2.18}$$

From crossflow measurements on single orifices [2.18] and clusters of orifices [2.19], it appears that the discharge coefficient for low inflow is proportional to the velocity ratio V_i/U_∞ raised to a power slightly greater than 1/2, but for low outflow the power is slightly less than 1/2, see Figures 2.4 and 2.5. If we accept [2.18]

$$C_d \sim \left(\frac{V_i}{U_\infty}\right)^{\frac{1}{2}}$$

as a fair approximation, then R = constant, and the linear relationship between C_p and V/U_∞ is obtained. So far, a truly linear dependence has been established only for some porous materials, cf. Figure 2.6, where the exponent is 1/2 both for inflow and outflow.

From Figure 2.5, representing a sample of perforated wall with normal holes, another important observation can be made: except for very small velocity ratios, the discharge coefficient for inflow is greater than that for outflow. Denoting by subscripts "in" and "out" inflow and outflow respectively, we can thus write

$$R_{in} < R_{out}$$

or, with respect to Equation (2.14)

$$P_{in} > P_{out}$$

This behaviour of walls with normal perforations was studied in detail by Budoff and Zorumski [2.20] and incorporated into the wall interference corrections by Mokry, Peake and Bowker [2.21], see also Chapter 5.

For high flow rates, we verify from Figures 2.4 to 2.6 that the discharge coefficient reaches its maximum value* and is further independent of V_i/U_∞. According to the above analysis $R_i \sim (V_i/U_\infty)^2$. Fortunately, the high crossflow rates are not typical for the operation of wind tunnels in normal test conditions (small models and plenum pressure close to the free stream static pressure).

The effect of the boundary layer thickness on the orifice discharge is illustrated in Figure 2.7. We can see that by increasing the displacement thickness to orifice diameter ratio, δ^*/d, the discharge increases, that is the resistance is reduced. This applies to both outflow and inflow. As earlier pointed out by Lukasiewicz [2.22], the thicker the boundary layer, the more a wall behaves like a free boundary.

The effect of the orifice depth (wall thickness) to diameter ratio, b/d, on the discharge coefficient is illustrated in Figure 2.8. For outflow, the effect extends throughout a whole range or orifice to grazing flow ratios. The thinner the wall the less stagnation occurs, so that more fluid is deflected and captured by the opening. For inflow, the effect of b/d is for obvious physical reasons much less pronounced.

Regarding the difference between outflow and inflow resistances, it was quite early demonstrated by Chew [2.23] that it can be eliminated by suitably inclining the holes toward the stream. The idea, depicted in Figure 2.9, is to reduce the turning angle for the high momentum air flowing out of the test section. Examples of crossflow curves for walls with normal and inclined holes are given in Figure 2.10. As we can judge from the outflow curves and small available portions of the inflow curves, roughly the same outflow and inflow resistance is achieved for a 6% perforated wall with 60° inclined holes. The open area ratio plays here a very important role: the resistance equalization effect is clearly overdone for the 12% perforated wall with 60° inclined holes.

---

*Close to the discharge coefficient for nongrazing flow, denoted as C_{d_o} in Figure 2.5.

We may also notice that the crossflow curves for walls with inclined holes do not pass through the origin. It is due to the fact that forward inclined holes can scoop certain amount of the test section mass flow at zero pressure difference across the wall. As a result, walls with inclined holes have a tendency to establish a pressure difference between the plenum and the test section when the flow is essentially parallel to the walls [2.1]. It is then logical to modify the linear boundary condition (2.15) to

$$\frac{V - V_o}{U_\infty} = P \frac{C_p - C_{p_{plenum}}}{2} \tag{2.19}$$

where V_o is the normal component of velocity at zero pressure difference.

Substituting from Equations (2.3), (2.4) and (2.5) and dropping the partial time derivative, we obtain the porous wall boundary condition for steady flows

$$\frac{\partial \phi}{\partial x} + \frac{1}{P} \frac{\partial \phi}{\partial n} = C \tag{2.20}$$

where

$$C = \frac{1}{P} \frac{V_o}{U_\infty} - \frac{1}{2} C_{p_{plenum}} \tag{2.21}$$

For perforated walls with normal holes $V_o \simeq 0$ and the constant term takes the form [2.24]

$$C = -\frac{1}{2} C_{p_{plenum}} = \frac{1 - \dfrac{p_{plenum}}{p_\infty}}{\kappa M_\infty^2} \tag{2.22}$$

where κ is the ratio of specific heats (1.4 for air). The homogeneous boundary condition

$$\frac{\partial \phi}{\partial x} + \frac{1}{P} \frac{\partial \phi}{\partial n} = 0 \tag{2.23}$$

corresponding to (2.16), was first applied to wall interference analysis by Goodman [2.10]. The inhomogeneous one, Equation (2.20), suggested by Ebihara [2.25], was used in wall interference computations by Sloof and Piers [2.26] and Sychev and Fonarev [2.24].

Crossflow, subject to the development of wall boundary layers in a nonuniform pressure field, was first systematically studied by Jacocks [2.27]. For a perforated wall wind tunnel the boundary layer development along the wall becomes very complicated due to the inflow and outflow induced by the pressure field. The outflow reduces the boundary layer thickness and the inflow greatly exaggerates its growth. In Jacock's experiment the effect of the airfoil was modeled by contouring the bottom solid wall, as shown in Figure 2.11. Detailed distributions of pressures and flow angles along the upper ventilated wall were measured by a static pressure tube and a laser doppler velocimeter, respectively. A limited number of boundary layer surveys were made with multiple-tube pitot pressure rakes. The obtained crossflow diagram in the lower portion of the same figure shows the inability of any straight line to be an accurate representation of the boundary condition. The geometries of other selected wall contours (bumps) are given in Figure 2.12; the dashed lines represent the boundary layer displacement thickness. The induced static pressure distributions along the perforated wall are in Figure 2.13 and the corresponding crossflow diagrams are in Figure 2.14. The observed nonlinearity and dissimilarity of the crossflow curves, representing the behaviour of perforated walls in actual tunnel test conditions, is more than discouraging. The Mach number effect, documented in Figure 2.15, is relatively consistent. It is seen that the slope of the central portions of the C_p vs. V/U_ω curves is steeper for higher M_∞, which indicates that the porosity parameter decreases as the Mach number grows. However, as pointed out by Jacocks, this is largely due to the reduction of the boundary layer thickness with increased M_∞.

It is not without interest that Kemp [2.28], [2.29] produced crossflow curves of a similar type from actual tunnel measurements, using the measured wall and airfoil pressure distributions and computing the flow angles at the walls. An example of computed pressure-crossflow diagrams for a 20% normal perforated wall from his unpublished work [2.30] is shown in Figure 2.16. Different relative positions of the outflow and inflow branches is achieved by specifying different flow inclination, V_∞/U_∞, far upstream.

From the above flow measurements and computations it would appear that the actual response of a perforated wall is highly nonlinear and "model-dependent" and cannot be described in terms of tunnel stream parameters. Among the missing correlation factors is, of course, the boundary layer development. This problem was addressed by Chan [2.31], [2.32], who performed experimental studies of the variation of the flow parameters along the wall. The boundary layer profile was measured by pitot rakes at three streamwise stations along 20% perforated test section walls with normal holes, in the presence of a transonic airfoil. The wall crossflow characteristics were then calculated from the data by means of a boundary layer computational code [2.33]. The resulting pressure-crossflow relations at the wall are found to be highly nonlinear as shown in Figure 2.17, and are closely similar to those measured by Jacocks [2.27]. It is also interesting to note that the linear pressure-crossflow relation deduced from wall pressure measurements [2.21] passes through all nonlinear curves and presents a relation averaged over the tunnel wall. The normal velocity at the edge of the boundary layer, including the displacement effect and the crossflow in the inflow region of the wall, is shown to be about three times that of the crossflow alone. By taking the boundary layer into account, the pressure-crossflow relations at the wall collapse into a single correlation curve, Figure 2.18. When the boundary layer eventually thickens downstream, the dependence of the wall characteristics on the boundary layer diminishes and the pressure-crossflow relation becomes linear, as shown in Figure 2.19. With these empirical correlations the boundary layer development along the wall can be calculated by an iterative scheme for a given test condition. The normal velocity at the outer edge of the boundary layer then provides the boundary condition for the calculation of the interference flow in the test section. A similar scheme has also been proposed by Freestone and Henington [2.34]. In view of the complexity of the interactive relations between the wall characteristics, the boundary layer growth and the inviscid flow in the tunnel, lengthy calculations are required for post-test estimation of wall interference. It is more practical to bypass the complicated flow development by establishing the boundary condition outside this region, such as measuring the flow parameters a short distance away from the wall, in the axial direction of the tunnel. Correction methods have been well developed for flow with outer boundary conditions specified, see Chapter 6.

The behaviour of perforated walls in unsteady flow conditions is much less understood. Recently, the state of knowledge has been rapidly improving thanks to related research efforts in the reduction of jet engine noise by cavity-backed perforated liners.

For harmonic oscillation with angular frequency ω, we take

$$\phi\,(x,y,t) = \hat{\phi}\,(x,y)\,e^{i\omega t} \tag{2.24}$$

where $\hat{\phi}$ is the complex amplitude of the disturbance velocity potential. A formal substitution of Equations (2.3) to (2.5) in (2.16) yields

$$\left(\frac{\partial}{\partial x} + i\frac{\omega}{U_\infty}\right)\hat{\phi} + \frac{1}{P}\frac{\partial\hat{\phi}}{\partial n} = 0 \tag{2.25}$$

where explicit dependence on the factor exp ($i\omega t$) has been eliminated. This boundary condition, earlier proposed in Reference [2.35], is appropriate to quasi-steady flows (small ω/U_∞).

Based on the acoustic behaviour of cavity-backed orifices (Helmholz resonators), it is reasonable to expect that besides the steady-flow resistance effect there also exists a phase lag between the pressure drop and normal velocity. Accordingly, Equation (2.25) should be modified to

$$\left(\frac{\partial}{\partial x} + i\frac{\omega}{U_\infty}\right)\hat{\phi} + Z\frac{\partial\hat{\phi}}{\partial n} = 0 \tag{2.26}$$

where the complex quantity

$$Z = R + iS \tag{2.27}$$

is the impedance, $R = 1/P$ is the resistance and S is the reactance. The resistance is a viscous phenomenon whereas the reactance is essentially of inviscid nature, related to the inertia of oscillating flow in the neighbourhood of the orifice [2.36].

The experiments of Thurston et al. [2.37] and Ingard and Ising [2.38] with single orifices in nongrazing flow conditions indicate that at low sound pressure levels there is a 90° phase lag of the normal velocity behind the driving pressure. This implies that in such conditions the resistance is very small relative to reactance, $R \ll S$. The relevant experimental results are summarized in Figures 2.20 and 2.21, in terms of orifice resistance* R_i and orifice reactance* S_i plotted against the inlet velocity amplitude V_i. A similar result was also obtained analytically [2.39]. Applying this result to Equations (2.26) and (2.27), we obtain the boundary condition

$$\left(\frac{\partial}{\partial x} + i\frac{\omega}{U_\infty}\right)\hat{\phi} + iS\frac{\partial\hat{\phi}}{\partial n} = 0 \tag{2.28}$$

for highly oscillatory flows (large ω/U_∞).

Based on Ingard's reactance formula [2.38] for a single orifice and the theoretical analysis of the grazing flow effect by Hersh and Rogers [2.36], Mabey [2.40] suggested the following expression for the reactance of the perforated wall

$$S = \frac{\omega}{U_\infty}(0.85\,d + b)\frac{1-\delta}{\delta} \tag{2.29}$$

where d is the orifice diameter and b is the wall thickness. The empirical factor 0.85 represents the mass end correction of the orifice [2.38]. The application of the open area ratio δ is similar to that in Equation (2.18). For larger values of δ we expect acoustic interaction of orifices, so that it is preferable to use the Fok-Melling porosity correction, described in References [2.41] and [2.42].

In order to be able to specify the impedance Z for general oscillatory flow conditions (between the above extreme cases), much more information is needed regarding the interaction of the oscillatory orifice flow and the grazing flow. Earlier, it was theorized [2.43] that orifice reactance is not a function of grazing flow velocity, but this does not seem to be the case [2.42]. Figure 2.22, sketched from the visual studies of Baumeister and Rice [2.44], shows various stages of low amplitude flow through an orifice in the presence of grazing flow. The appreciable difference between the outflow and inflow regimes, which is of the same character as that observed earlier in steady flow, indicates that impedances for the inflow and outflow half-cycles are likely to differ. During the flow reversal, outflow and inflow exist simultaneously in different parts of the orifice, and hence no discontinuity in resistance will exist in an oscillatory system when the average orifice velocity approaches zero from either the outflow or inflow directions [2.44].

With a higher oscillating flow amplitude, Figure 2.23, the dye streamline is seen to be bent at steeper angles towards the orifice plate and the effective flow area of the orifice is increased. In the limit of high orifice flow amplitude the nongrazing flow pattern would eventually be achieved.

2.6 Transversally Slotted Walls

The porous wall boundary condition is also applicable to walls with transversal slots. If the wall is thin, the viscous effects manifest themselves mainly by circulation, so that the force acting on the wall can be determined from the Kutta-Joukowski condition, as for thin airfoils. Since the theoretical case of a thin, transversally slotted wall is important to an understanding of the mean boundary condition concept for a combination of closed and open jet boundaries, it is elaborated on here.

---

*In the absence of grazing flow, $U_\infty = 0$, impedance is defined simply as the ratio of amplitudes of driving pressure and orifice velocity; therefore dimensioned as kg m^{-2} s^{-1}.

Referring to Figure 2.24, we solve for the complex disturbance velocity

$$w(z) = \frac{\partial \phi}{\partial x} - i\frac{\partial \phi}{\partial y}$$

which is an analytic function of

$$z = x + iy$$

in the lower half-plane, $y < 0$, and subject to the boundary conditions

$$\text{Re } w(x) = 0, \qquad n\ell - \frac{a}{2} < x < n\ell + \frac{a}{2}$$

$$\text{Im } w(x) = 0, \qquad n\ell + \frac{a}{2} < x < (n+1)\,\ell - \frac{a}{2}$$

In addition, w satisfies the Kutta-Joukowski condition

$$w(x) = 0, \qquad x = n\ell - \frac{a}{2}$$

which represents the viscous flow mechanism (lift effect). Here a is the slot width and ℓ is the slot spacing. The above mixed boundary value problem is a special case of the Keldysh-Sedov problem [2.45], whose solution is [2.46]

$$w(z) = A\sqrt{\frac{\sin\frac{\pi}{\ell}\left(z+\frac{a}{2}\right)}{\sin\frac{\pi}{\ell}\left(z-\frac{a}{2}\right)}} \tag{2.30}$$

where A is an arbitrary real constant. Similarly to the thin airfoil theory, the velocity is finite at the trailing edges, $z = n\ell - \frac{a}{2}$, but is singular at the leading edges, $z = n\ell + \frac{a}{2}$.

Taking the limit $y \to -\infty$, we obtain

$$w(x - i\infty) = A\, e^{i\frac{\pi}{2}\frac{a}{\ell}}$$

so that far from the wall

$$\frac{\partial \phi}{\partial x} = A\cos\left(\frac{\pi}{2}\frac{a}{\ell}\right)$$

$$\frac{\partial \phi}{\partial y} = -A\sin\left(\frac{\pi}{2}\frac{a}{\ell}\right)$$

Eliminating the unknown constant A, we arrive at the porous wall boundary condition

$$\frac{\partial \phi}{\partial x} + \frac{1}{P}\frac{\partial \phi}{\partial y} = 0 \tag{2.31}$$

cf. Equation (2.23), where

$$P = \tan\left(\frac{\pi}{2}\frac{a}{\ell}\right) \tag{2.32}$$

It is seen that P increases monotonically with the open area ratio a/ℓ and that in the limits $a/\ell \to 0$ and $a/\ell \to 1$ the expected boundary conditions for solid and open jet boundaries are attained. Finally, accounting for compressibility by the transformation $x \to x/\beta$ we obtain

$$P = \beta\tan\left(\frac{\pi}{2}\frac{a}{\ell}\right) \tag{2.33}$$

Within the framework of the linearized potential theory, the value P/β is thus a constant, determined by the open area ratio of the wall. The decrease of the porosity parameter with the increase of the Mach number for transversally slotted wall is similar to the trend observed experimentally for perforated walls in Figure 2.15.

It is important to note that in the present flow model it was assumed that $\partial\phi/\partial x = 0$ in the slots (ideal slot condition) and that the solution in the upper half plane (plenum) was generally of no interest. In fact, a different analytic continuation of w across the slots can be obtained by the selection of the branch of the square root function in Equation (2.30). It can be shown that if the cut is along the negative semi-axis, the solution is discontinuous across the slot, whereas if the cut is along the positive semi-axis, the solution is continuous. In the latter case we can imagine that the wall acts like a lattice of lifting airfoils in unbounded flow. Using this approach, the derivation of the porosity parameter for a transversally slotted wall was given by Goethert [2.1]; the resultant value is, of course, the same.

If the wall is thick, the flow in the transverse slots becomes partly separated and the potential flow modeling is no longer reliable, except perhaps when the slats are shaped as actual airfoils with sharp trailing edges, see Figure 2.25. As shown experimentally by Williams and Parkinson [2.47], [2.48], the crossflow properties of this type of wall, when operated within the unstalled incidence range (low crossflow regime), are predictable from potential flow theory. For transonic or supersonic speeds the transversally slotted wall is unsuitable, since it generates two-dimensional disturbances (plane Mach waves).

2.7 Longitudinally Slotted Walls

In contrast to perforated or transversally slotted walls, the flow through a wall with longitudinal slots is not necessarily dominated by viscosity [2.49]. The boundary condition for a longitudinally slotted wall can thus be derived from the component of Euler's equation normal to the wall. Assuming $V \ll U_\infty$ and approximating the pressure gradient by the finite difference quotient, we obtain

$$\frac{dV}{dt} = \frac{1}{\rho_\infty} \frac{p - p_{plenum}}{K} \tag{2.34}$$

where the constant K, called the slot parameter, has the dimension of length. In two-dimensional wall interference the slot parameter often appears nondimensionalized by half a tunnel height:

$$F = \frac{2K}{h} \tag{2.35}$$

Using Equations (2.1) to (2.3), the slotted wall boundary condition can also be written

$$K \frac{1}{U_\infty} \frac{d}{dt} \left(\frac{\partial\phi}{\partial n} \right) = \frac{1}{2} (C_p - C_{p_{plenum}}) \tag{2.36}$$

Substituting Equation (2.4) in (2.36), we obtain

$$C_p + K \frac{\partial C_p}{\partial n} = C_{p_{plenum}} \tag{2.37}$$

which is particularly suitable for unsteady flow calculations, since the total time derivative is eliminated. For steady flow, Equation (2.3) yields

$$\frac{1}{2} (C_p - C_{p_{plenum}}) = K \frac{\partial^2\phi}{\partial x \partial n} \tag{2.38}$$

This boundary condition expresses linear dependence between the pressure difference and the centrifugal force due to streamline curvature. Accordingly, walls with longitudinal slots, as one of their major advantages, can support an outflow from the test section even when the static pressure in the test section is smaller than that in the plenum chamber [2.51]. Perforated walls are too unyielding in this regard.

An alternative form of Equation (2.38) is

$$\frac{\partial\phi}{\partial x} + K \frac{\partial^2\phi}{\partial x \partial n} = C \tag{2.39}$$

where C is given by Equation (2.22). If $p_{plenum} = p_\infty$, then the constant term vanishes and the boundary condition becomes homogeneous:

$$\frac{\partial\phi}{\partial x} + K \frac{\partial^2\phi}{\partial x \partial n} = 0 \tag{2.40}$$

If the condition $V \ll U_\infty$ is not satisfied, as for a large pressure difference between the undisturbed test section and plenum pressures, it may be necessary to include in Equation (2.34) also quadratic velocity terms [2.50], [2.53], [2.54]. Using an approximate integration of the momentum equation along a suitable path from the slat centre into the plenum, Berndt [2.53], [2.55] proposed the following nonlinear boundary condition

$$\frac{1}{2} (C_p - C_{p_{plenum}}) = K \frac{\partial^2\phi}{\partial x \partial n} + \frac{1}{2} \left(\frac{\ell}{a} \frac{\partial\phi}{\partial n} \right)^2 \tag{2.41}$$

where ℓ is the distance between the slots and a is the slot width, Figure 2.26. The pressure difference across the wall is seen to be the sum of the streamline curvature effect and the crossflow Bernoulli effect.

Since the longitudinal slots introduce periodic flow disturbances normal to the flow plane, a rigorous determination of the slot parameter is rather difficult. A simpler approach is to assume that the flow is quasiplanar, i.e. that the crossflow produced by the slots is only a small perturbation of the basic two-dimensional flow. These flows are considered to be independent, except for a linking through the boundary condition at the wall. The method thus has much in common with the slender body theory [2.14].

Using the co-ordinate system of Figure 2.26, where the y axis is along the outward normal to the wall and the z axis is normal to the slots in the wall plane, the three-dimensional disturbance velocity potential Φ can be decomposed as [2.52].

$$\Phi(x,y,z) \simeq \phi(x,y) + Q(x)\, f(y,z) \tag{2.42}$$

Here ϕ is the two-dimensional potential satisfying the mean boundary condition (2.40), Q is a "slowly varying" function of x and f is the crossflow potential, satisfying

$$\frac{\partial^2 f}{\partial y^2} + \frac{\partial^2 f}{\partial z^2} = 0, \qquad y < 0 \tag{2.43}$$

and the far field condition

$$f \to 0 \quad \text{as} \quad y \to -\infty \tag{2.44}$$

The condition of vanishing pressure disturbances in the slots (open portions of the wall) is

$$\frac{\partial \Phi}{\partial x}(x,0,z) = 0, \qquad n\ell - \frac{a}{2} < z < n\ell + \frac{a}{2}$$

and, similarly, the condition of the vanishing normal component of velocity on the slats (solid portions of the wall) is

$$\frac{\partial \Phi}{\partial y}(x,0,z) = 0, \qquad n\ell + \frac{a}{2} < z < (n+1)\,\ell - \frac{a}{2}$$

Substituting from Equation (2.42), the above conditions become

$$\frac{\partial \phi}{\partial x}(x,0) + Q'(x)\, f(0,z) = 0, \qquad n\ell - \frac{a}{2} < z < n\ell + \frac{a}{2} \tag{2.45}$$

$$\frac{\partial \phi}{\partial y}(x,0) + Q(x)\frac{\partial f}{\partial y}(0,z) = 0, \qquad n\ell + \frac{a}{2} < z < (n+1)\,\ell - \frac{a}{2} \tag{2.46}$$

They can be satisfied only if

$$f(0,z) = f(0,0) = \text{constant}, \qquad n\ell - \frac{a}{2} < z < n\ell + \frac{a}{2} \tag{2.47}$$

$$\frac{\partial f}{\partial y}(0,z) = c = \text{constant}, \qquad n\ell + \frac{a}{2} < z < (n+1)\,\ell - \frac{a}{2} \tag{2.48}$$

From Equations (2.46) and (2.48) thus

$$Q(x) = -\frac{1}{c}\frac{\partial \phi}{\partial y}(x,0)$$

and substituting in Equation (2.45)

$$\frac{\partial \phi}{\partial x}(x,0) - \frac{f(0,0)}{c}\frac{\partial^2 \phi}{\partial x \partial y}(x,0) = 0$$

which is recognized as the slotted wall boundary condition (2.40) with

$$K = -\frac{f(0,0)}{c} \tag{2.49}$$

Taking into account periodicity and symmetry and using Equations (2.43), (2.44), (2.47) and (2.48), the crossflow potential can be constructed as a solution of the following boundary value problem, see the lower portion of Figure 2.26

$$\frac{\partial^2 f}{\partial y^2}(y,z) + \frac{\partial^2 f}{\partial z^2}(y,z) = 0, \qquad -\infty < y < 0, \quad 0 < z < \frac{\ell}{2}$$

$$\frac{\partial f}{\partial z}(0,z) = 0, \qquad 0 < z < \frac{a}{2}$$

$$\frac{\partial f}{\partial y}(0,z) = c, \qquad \frac{a}{2} < z < \frac{\ell}{2}$$

$$\frac{\partial f}{\partial z}(y,0) = 0, \qquad -\infty < y < 0$$

$$\frac{\partial f}{\partial z}(y,\frac{\ell}{2}) = 0, \qquad -\infty < y < 0$$

$$f(-\infty,z) = 0, \qquad 0 < z < \frac{\ell}{2} \tag{2.50}$$

Using conformal mapping, the solution is found as the superposition of parallel flow and source flow [2.52]:

$$f(x,y) = c\,\mathrm{Re}\left\{y+iz + \frac{\ell}{\pi}\log\left[-\sinh\left(\pi\frac{y+iz}{\ell}\right) + \sqrt{\sinh^2\left(\pi\frac{y+iz}{\ell}\right) + \sin^2\left(\frac{\pi a}{2\ell}\right)}\right]\right\} \tag{2.51}$$

The substitution in Equation(2.49) yields the value of the slot parameter

$$K = \frac{\ell}{\pi}\log\frac{1}{\sin\left(\frac{\pi}{2}\frac{a}{\ell}\right)} \tag{2.52}$$

that was first obtained by Lamb, when solving the problem of the propagation of acoustic waves through slotted screens [2.56]. For small open area ratios

$$K \simeq \frac{\ell}{\pi}\log\left(\frac{2}{\pi}\frac{\ell}{a}\right) \tag{2.53}$$

For steady wind tunnel flow, the theoretical values (2.52) or (2.53) were confirmed by several authors [2.11], [2.12], [2.14], [2.46]. A different value of K was obtained by Chen and Mears [2.13], but their crossflow model (generated by doublet rods) is not nearly as meaningful, see for a discussion References [2.57] and [2.58].

Equation (2.52) shows that on the interval $1 \geqslant a/\ell > 0$ the slot parameter is positive and increases monotonically as a/ℓ decreases. In the limit $a/\ell = 1$ we obtain $K = 0$ and Equation (2.37) simplifies to the boundary condition (2.11) for open jet walls. As $a/\ell \to 0$, $K \to \infty$ and Equation (2.40) reduces to

$$\frac{\partial}{\partial x}\frac{\partial \phi}{\partial n} = 0 \tag{2.54}$$

which contains, as a particular case, the boundary condition (2.7) for solid walls. A more detailed picture of the possible values of the slot parameter can be obtained from Figure 2.27. There the nondimensional parameter

$$\psi = \frac{1}{1+F} = \frac{1}{1+\frac{2K}{h}} \tag{2.55}$$

is plotted as a function of the open area ratio, a/ℓ, and the slot spacing/tunnel height ratio, ℓ/h. The limiting values $\psi = 0$ and $\psi = 1$ represent closed wall and open jet conditions respectively. As we shall see in Section 3, a significant part of the incidence correction is just proportional to ψ.

As in the case of transversally slotted walls, there is no need to model the flow outside the test section if the condition of zero pressure disturbance in the slots is used. The solution can be analytically continued across the slots in a variety of ways (i.e. by selection of flow boundaries) without affecting the value of the slot parameter. In theory, the slot parameter (2.52) is thus applicable to both inflow and outflow. Unfortunately, in real physical situations the condition of zero pressure disturbance in the slots, on which the present theory rests, is not necessarily valid.

Using the kinetic energy relations, Davis and Moore [2.11] derived for a longitudinally slotted wall of thickness b the approximate value of the slot parameter

$$K = \ell\,\frac{1}{\pi}\log\frac{1}{\sin\frac{\pi}{2}\frac{a}{\ell}} + \frac{b}{a} \tag{2.56}$$

The importance of the thickness term b/a is appreciated from Figures 2.27 to 2.30, where the parameter ψ is plotted for the cases b/a = 0.0, 0.2, 0.5, and 1.0. However, the formula (2.56) was derived assuming the plenum pressure boundary to be located on the line between the slot edges on the plenum side. As the authors of Reference [2.11] point out, the actual location of the plenum pressure boundary in the slot is a function of the local outflow and inflow.

A more detailed study of the problem was subsequently undertaken by Berndt and Sörensén [2.53]. The value of the slot parameter they arrived at is

$$K = \ell \left[\frac{1}{\pi} \log \frac{1}{\sin\left(\frac{\pi}{2}\frac{a}{\ell}\right)} + \frac{b_p}{a} + k_p \right] \tag{2.57}$$

where [2.49]

$$k_p = \frac{1}{\pi}\left(1 - \log\frac{8}{\pi}\right) \simeq 0.02 \tag{2.58}$$

The quantity b_p, satisfying $0 \leqslant b_p < b$, is the depth of penetration of the test section flow into the slot, Figure 2.31. Since b_p varies with the streamwise co-ordinate x in dependence on the pressure field generated by the airfoil, we can state that K is also a function of x. The situation is thus similar to perforated walls, where the dependence of P on x has been observed experimentally. If $b_p = b$, Equation (2.57) agrees, apart from the (small) constant term k_p, with the earlier given formula by Davis and Moore, Equation (2.56).

It was observed experimentally that for larger outflows, $b_p > b$, the flow remains attached inside the slot, but separates at the slot edges on the plenum side, i.e. the test section air enters the plenum in the form of narrow, high momentum jets. Berndt and Sörensén [2.53] modeled this type of flow on a doubly infinite strip, as illustrated in Figure 2.32(a). The corresponding slot parameter is

$$K = \ell \left[\frac{1}{\pi} \log \frac{1}{\sin\left(\frac{\pi}{2}\frac{a}{\ell}\right)} + \frac{b}{a} + k_s \right] \tag{2.59}$$

where

$$k_s = \frac{1}{\pi}\left(1 - \log\frac{4}{\pi}\right) \simeq 0.24 \tag{2.60}$$

Theoretical analysis of Reference [2.53] also indicates that if the pressure coefficient C_p is formed from the static pressure on the slat centre line, Equation (2.41) remains formally valid, except that

$$k_s = \frac{1}{\pi}\left(1 - \log\frac{2}{\pi}\right) \simeq 0.46 \tag{2.61}$$

There are, however, a number of theoretical outflow models that may give different values of K. For example, treating the constant pressure boundaries as true free jet streamlines (vena contracta effect), Figure 2.32(b), Barnwell [2.57] obtained for a thin, slotted wall and $a \ll \ell$

$$K = \ell \left[\frac{1}{\pi} \log \left(\frac{2}{\pi}\frac{\ell}{a} \right) + k_f \right] \tag{2.62}$$

The constant

$$k_f = \frac{1}{\pi} \log \frac{2+\pi}{8} \simeq -0.14 \tag{2.63}$$

is negative, in contrast to the Berndt-Sörensén formula, Equations (2.59) and (2.60). To retain the same configuration for the inflow with a mere reversal of the crossflow direction is not advisable, since there is a sufficient experimental evidence [2.53] that the low momentum plenum air entering the test section does not form jets, but rather separation bubbles over the slots.

The modeling of the mixed outflow-inflow regimes is even more complicated because of the "history effect" of the jet flow. Depending on tunnel conditions, a small amount of the slot air returns with high momentum to the test section, eventually followed by the low momentum plenum air. This implies that any mathematical formulation of the slot condition must keep track of the flow into and out of the plenum chamber and, possibly, no purely local boundary condition, for example that given by Equation (2.40), could then be adequate [2.34]. Based on slot flow visualization in Reference [2.53], several tentative crossflow patterns have been suggested by Berndt [2.49]. An example amenable to theoretical analysis is shown schematically in Figure 2.33.

More recently, Everhart and Barnwell have suggested [2.59] that the slot parameter, too, should be obtained experimentally for the particular wall geometry and flow conditions. From Equation (2.37)

$$K = \frac{C_{p_{plenum}} - C_p}{\frac{\partial C_p}{\partial n}} \tag{2.64}$$

where the values of C_p and $\partial C_p/\partial n$ can be obtained using the static pressure measurement along two rows of pressure orifices, parallel to the tested wall. Referring to Figure 2.34, midway between two orifices

$$C_p \simeq \frac{1}{2}(C_{p_1} + C_{p_2})$$

and

$$\frac{\partial C_p}{\partial n} \simeq \frac{C_{p_1} - C_{p_2}}{b_2 - b_1}$$

where b_1 and b_2 are the distances of the rows 1 and 2 from the tested wall.

An alternative method for the evaluation of the slot parameter from pressure measurements along the slat centre line, supported by a detailed theoretical analysis of flow in the vicinity of the wall, was suggested by Berndt [2.60].

The comparison of experimental slot parameters, obtained by Everhart and Barnwell [2.59] and Berndt and Sörensén [2.53] in the outflow mode, is shown in Figure 2.35. The values of K/ℓ + the leading logarithmic term, plotted against b/a, are scattered not far from the unit slope line which intercepts the axis of ordinates at 0.46, in accordance with the theoretical prediction of Equations (2.59) and (2.61).

2.8 Porous-slotted Boundary Condition

The homogeneous, steady-flow boundary conditions (2.23) and (2.40) can be combined into the porous-slotted boundary condition

$$\frac{\partial}{\partial x}\left(\phi + K\frac{\partial \phi}{\partial n}\right) + \frac{1}{P}\frac{\partial \phi}{\partial n} = 0 \tag{2.65}$$

which is due to Baldwin, Turner and Knechtel [2.52]. It contains as special cases

(i) solid boundary: $P = 0$

(ii) open jet boundary: $K = 1/P = 0$

(iii) porous boundary: $K = 0$

(iv) slotted boundary: $1/P = 0$

and hence results derived from it will be applicable, in theory, to all possible tunnel conditions.

Furthermore, it was suggested [2.52] to use the porous-slotted boundary condition for longitudinally slotted walls with viscous effects. This hypothesis was partly confirmed by Jacocks [2.27], who for slotted walls detected a strong dependence of V/U_∞ on C_p, similar to that found for perforated walls. An example of a typical experimental result is given in Figure 2.36; unfortunately no reference at all is made to a $\partial^2\phi/\partial x \partial n$ term. Earlier, Parkinson and Lim [2.61] also reported a case of a longitudinally slotted wall that seemed to be better represented by the porous, rather than the slotted wall boundary condition. In contrast, some other authors [2.53], [2.59] feel, based on their own analyses and experiments, that the inclusion of the "porous term" in the slotted wall boundary condition is unjustified. Thus, the influence of viscosity on slotted wall flows seems to remain an unresolved issue [2.51], [2.54].

Löfgren [2.62], following a different line of thought, derived for viscous flow at the longitudinal slots the boundary condition

$$\frac{\partial \phi}{\partial x} + \lambda_1 \frac{\partial^2 \phi}{\partial x \partial n} = \lambda_2 \frac{\partial^3 \phi}{\partial x^3} \tag{2.66}$$

which is consistent with replacing in Equation (2.34) the normal component of the Euler equation by that of the Navier-Stokes equation. As the boundary layer thickness is reduced to zero, the coefficients λ_1 and λ_2 tend to the limits K and 0 respectively, so that the inviscid boundary condition (2.40) is recovered. Unfortunately, further application of Equation (2.66) in wall interference theory does not seem to have been made.

REFERENCES

[2.1] Goethert, B.H. *Transonic Wind Tunnel Testing.* Pergamon Press, 1961.

[2.2] Olson, L.E. Stridsberg, S. *Effect of Viscosity on Wind Tunnel Wall Interference for Airfoils at High Lift.* AIAA Paper 79-1534, July 1979.

[2.3] Petersohn, E.G.M. *Some Experimental Investigations of the Influence of Wall Boundary Layers upon Wind Tunnel Measurements at High Subsonic Speeds.* Rept. 44, The Aeronautical Research Institute of Sweden, May 1952.

[2.4] Prandtl, L. *Tragflügeltheorie II.* Ludwig Prandtl gesammelte Abhandlungen, Springer-Verlag, 1961, pp. 346-372.

[2.5] Theodorsen, T. *Theory of Wind-Tunnel Wall Interference.* NACA Rept. 410, 1931.

[2.6] Toussaint, A. — *Experimental Methods — Wind Tunnels.* Aerodynamic Theory, (Ed. W.F. Durand), Vol. III, J. Springer, 1935, Chpt. III, pp. 280-319.

[2.7] Wieselsberger, C. — *Über den Einfluss de Windkanalbegrenzung auf den Widerstand, insbesondere im Bereiche der kompressiblen Strömung.* Luftfahrtforschung, Vol. 19, May 1942, pp. 124-128.

[2.8] Wright, R.H.; Ward, V.G. — *NASA Transonic Wind Tunnel Sections.* NACA RM L8J06, Oct. 1948; also NACA Rept. 1231, 1955.

[2.9] Goodman, T. — *The Porous Wall Wind Tunnel. Part III. The Reflection and Absorption of Shock Waves at Supersonic Speeds.* AD-706-A-1, Cornell Aeronautical Laboratory, Buffalo, Nov. 1950.

[2.10] Goodman, T. — *The Porous Wall Wind Tunnel. Part II. Interference Effect on a Cylindrical Body in a Two-Dimensional Tunnel at Subsonic Speed.* AD-594-A-3, Cornell Aeronautical Laboratory, Buffalo, 1950.

[2.11] Davis, D.D.; Moore, D. — *Analytical Study of Blockage- and Lift-Interference Corrections for Slotted Tunnels Obtained by the Substitution of an Equivalent Homogeneous Boundary for the Discrete Slots.* NACA RM L53E07b, June 1953.

[2.12] Guderley, G. — *Simplifications of the Boundary Conditions at a Wind-Tunnel Wall With Longitudinal Slots.* TR 53-150, Wright Air Development Center, April 1953.

[2.13] Chen, C.F.; Mears, J.W. — *Experimental and Theoretical Study of Mean Boundary Conditions at Perforated and Longitudinally Slotted Wind Tunnel Walls.* TR-57-20, Arnold Engineering Development Center, Dec. 1957.

[2.14] Woods, L.C. — *On the Theory of Ventilated Wind Tunnels.* Int. J. Mech. Sci., Vol. 1, 1960, pp. 313-321.

[2.15] Gardenier, H.E. — *The Extent and Decay of Pressure Disturbances Created by the Holes in Perforated Walls at Transonic Speeds.* TN-56-1, Arnold Engineering Development Center, April 1956.

[2.16] Fromme, J.; Golberg, M.; Werth, J. — *Two Dimensional Aerodynamic Interference Effects on Oscillating Airfoils With Flaps in Ventilated Subsonic Wind Tunnels.* NASA CR-3210, Dec. 1979.

[2.17] Darcy, H. — *Les fontaines publiques de la ville de Dijon.* V. Dalmont, Paris, 1856.

[2.18] Rogers, T.; Hersh, A.S. — *Effect of Grazing Flow on Steady-State Resistance of Isolated Square-Edged Orifices.* NASA CR-2681, April 1976.

[2.19] Feder, E. — *Effect of Grazing Flow Velocity on the Steady Flow Resistance of Duct Liners.* Rep. 5051, Pratt and Whitney, July 1974.

[2.20] Budoff, M.; Zorumski, E. — *Flow Resistance of Perforated Plates in Tangential Flow.* NASA TM X-2361, Sept. 1971.

[2.21] Mokry, M.; Peake, D.J.; Bowker, A.J. — *Wall Interference on Two-Dimensional Supercritical Airfoils, Using Wall Pressure Measurements to Determine the Porosity Factors for Tunnel Floor and Ceiling.* LR-575, National Research Council Canada, Feb. 1974.

[2.22] Lukasiewicz, J. — *Effects of Boundary Layer and Geometry on Characteristics of Perforated Walls for Transonic Wind Tunnels.* Aerospace Engineering, Vol. 20, April 1961, pp. 22-23 and 62-68.

[2.23] Chew, W.L. — *Experimental and Theoretical Studies on Three-Dimensional Wave Reflection in Transonic Flow — Part III: Characteristics of Perforated Test Section Walls With Different Resistance to Cross-Flow.* TN-55-44, Arnold Engineering Development Center, March 1956.

[2.24] Sychev, V.V.; Fonarev, A.S. — *Bezinduktsionnye aerodinamicheskie truby dlia transzvukovych issledovanii.* Uchenye zapiski TsAGI, Vol. 6, 1975, pp. 1-14.

[2.25] Ebihara, M. — *A Study of Subsonic, Two-Dimensional Wall-Interference Effect in a Perforated Wind Tunnel with Particular Reference to the NAL 2m × 2m Transonic Wind Tunnel — Inapplicability of the Conventional Boundary Condition.* TR-252T, National Aerospace Laboratory, Japan, Jan. 1972.

[2.26] Slooff, J.W.; Piers, W.J. — *The Effect of Finite Test Section Length on Wall Interference in 2-D Ventilated Windtunnels.* Windtunnel Design and Testing Techniques, AGARD-CP-174, 1975, pp. 14.1-14.11.

[2.27] Jacocks, J.L. — *An Investigation of the Aerodynamic Characteristics of Ventilated Test Section Walls for Transonic Wind Tunnels.* Dissertation, The University of Tennessee, Dec. 1976.

[2.28] Kemp, W.B. — *Transonic Assessment of Two-Dimensional Wind Tunnel Wall Interference Using Measured Wall Pressures.* Advanced Technology Airfoil Research, Vol. 1, NASA Conference Publication 2045, Part 2, 1978, pp. 473-486.

[2.29] Kemp, W.B. — *TWINTAN: A Program for Transonic Wall Interference Assessment in Two-Dimensional Wind Tunnels.* NASA Tech. Memo. 81819, May 1980.

[2.30] Kemp, W.B. — *Transonic Post-Test Assessment.* Presented at the Meeting of AGARD Working Group on Design of Transonic Test Sections, NASA Langley, March 1980.

[2.31] Chan, Y.Y. — *Boundary Layer Development on Perforated Walls in Transonic Wind Tunnels.* LTR-HA-47, National Research Council Canada, Feb. 1980.

[2.32] Chan, Y.Y. — *Analysis of Boundary Layers on Perforated Walls of Transonic Wind Tunnels.* Journal of Aircraft, Vol. 18, 1981, pp. 469-473.

[2.33] Chan, Y.Y. — *Compressible Turbulent Boundary Layer Computations Based on Extended Mixing Length Approach.* C.A.S.I. Transactions, Vol. 5, 1972, pp. 21-27.

[2.34] Freestone, M.M. Henington, P. — *A Scheme for Incorporating the Viscous Effects of Perforated Windtunnel Walls in Two-Dimensional Flow Calculations.* Research Memo. Aero 78/7, The City University, London, April 1979.

[2.35] Garner, H.C. Rogers, E.W.E. Acum, W.E.A. Maskell, E.C. — *Subsonic Wind Tunnel Wall Corrections.* AGARDograph 109, October 1966, p. 257.

[2.36] Hersh, A.S. Rogers, T. — *Fluid Mechanical Model of the Acoustic Impedance of Small Orifices.* NASA CR-2682, May 1976.

[2.37] Thurston, G.B. Hargrove, L.E. Cook, B.D. — *Nonlinear Properties of Circular Orifices.* Journal Acoust. Soc. Am., Vol. 29, 1957, pp. 992-1001.

[2.38] Ingard, U. Ising, H. — *Acoustic Nonlinearity of an Orifice.* Journal Acoust. Soc. Am., Vol. 42, 1967, pp. 6-17.

[2.39] Howe, M.S. — *The Influence of Grazing Flow on the Acoustic Impedance of a Cylindrical Wall Cavity.* Journal of Sound and Vibration, Vol. 67, 1979, pp. 533-544.

[2.40] Mabey, D.G. — *The Resonance Frequencies of Ventilated Wind Tunnels.* TR 78038, Royal Aircraft Establishment, April 1978.

[2.41] Melling, T.H. — *The Acoustic Impedance of Perforates at Medium and High Sound Pressure Levels.* Journal of Sound and Vibration, Vol. 29, 1973, pp. 1-65.

[2.42] Hersh, A.S. Walker, B. — *Effect of Grazing Flow on the Acoustic Impedance of Helmholtz Resonators Consisting of Single and Clustered Orifices.* NASA CR-3177, Aug. 1979.

[2.43] Rice, E.J. — *A Theoretical Study of the Acoustic Impedance of Orifices in the Presence of a Steady Grazing Flow.* NASA TM X-71903, April 1976.

[2.44] Baumeister, K.J. Rice, E.J. — *Visual Study of the Effect of Grazing Flow on the Oscillatory Flow in a Resonator Orifice.* NASA TM X-3288, Sept. 1975.

[2.45] Lavrent'ev, M.A. Shabat, B.V. — *Metody teorii funktsii kompleksnogo peremennogo.* Moscow 1958, pp. 284-289.

[2.46] Maeder, P.F. Wood, A.D. — *Transonic Wind Tunnel Sections.* Zeitschrift für angewandte Mathematik und Physik, Vol. 7, 1956, pp. 177-212.

[2.47] Williams, C.D. Parkinson, G.V. — *A Low-Correction Wall Configuration for Airfoil Testing.* Wind Tunnel Design and Testing Techniques, AGARD-CP-174, Oct. 1975, pp. 21.1-21.7.

[2.48] Parkinson, G.V. Williams, C.D. Malek, A. — *Development of a Low-Correction Wind Tunnel Wall Configuration for Testing High Lift Airfoils.* ICAS Proceedings 1978, Vol. 1, Sept. 1978, pp. 355-360.

[2.49] Berndt, S.B. — *Inviscid Theory of Wall Interference in Slotted Test Sections.* AIAA Journal, Vol. 15, Sept. 1977, pp. 1278-1287.

[2.50] Wood, W.W. — *Tunnel Interference from Slotted Walls.* Quart. Journal of Mechanics and Applied Mathematics, Vol. 17, 1964, pp. 125-140.

[2.51] Goethert, B.H. — *Technical Evaluation Report of the AGARD Specialist's Meeting on Wind Tunnel Design and Testing Techniques.* April 1976.

[2.52] Baldwin, B.S. Turner, J.B. Knechtel, E.D. — *Wall Interference in Wind Tunnels With Slotted and Porous Boundaries at Subsonic Speeds.* NACA TN 3176, 1954.

[2.53] Berndt, S.B. Sörensén, H. — *Flow Properties of Slotted Walls for Transonic Test Sections.* Wind Tunnel Design and Testing Techniques, AGARD-CP-174, Oct. 1975, pp. 17.1-17.9.

[2.54] Ramaswamy, M.A. Cornette, E.S. — *Supersonic Flow Development in Slotted Wind Tunnels.* AIAA Journal, Vol. 20, 1982, pp. 805-811.

[2.55] Berndt, S.B. — *Flow Properties of Slotted-Wall Test Sections.* Paper 6, AGARD FDP Specialists' Meeting on Wall Interference in Wind Tunnels, London 1982.

[2.56] Lamb, H. — *Hydrodynamics.* Sixth Ed., Dover Publications, 1945, pp. 533-537.

[2.57] Barnwell, R.W. — *Improvements in the Slotted-Wall Boundary Condition.* Proceedings of the AIAA 9th Testing Conference, June 1976, pp. 21-30.

[2.58] Fairlie, B.D. Pollock, N. *Evaluation of Wall Interference Effects in a Two-Dimensional Transonic Wind Tunnel by Subsonic Linear Theory.* AR-151, Aeronautical Research Laboratories, Melbourne, Feb. 1979.

[2.59] Everhart, J.L. Barnwell, R.M. *A Parametric Experimental Study of the Slotted-Wall Boundary Condition.* Advanced Technology Airfoil Research, Vol. 2, NASA Conference Publication 2045, 1978, pp. 459-471.

[2.60] Berndt, S.B. *Measuring the Flow Properties of Slotted Test-Section Walls.* FFA Rept. 135, The Aeronautical Research Institute of Sweden, May 1982.

[2.61] Parkinson, G.V. Lim, A.K. *On the Use of Slotted Walls in Two-Dimensional Testing of Low Speed Airfoils.* C.A.S.I. Transactions, Vol. 4, 1971, pp. 81-87.

[2.62] Löfgren, P. *Simplifications of the Boundary Condition at a Slotted Wind-Tunnel Wall with a Boundary Layer.* Tech. Note AU-932, The Aeronautical Research Institute of Sweden, March 1975.

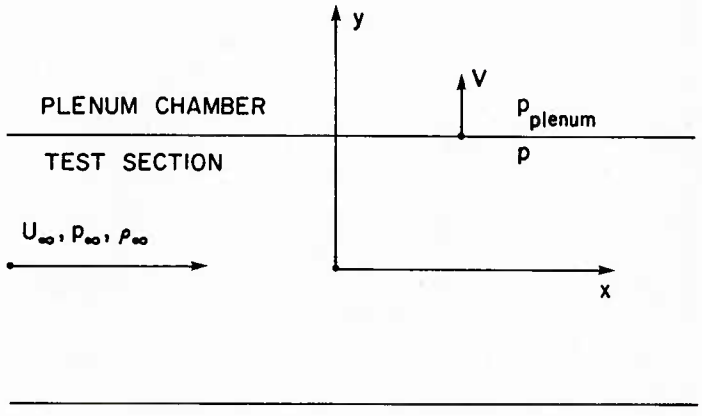

Fig. 2.1 Tunnel co-ordinate system

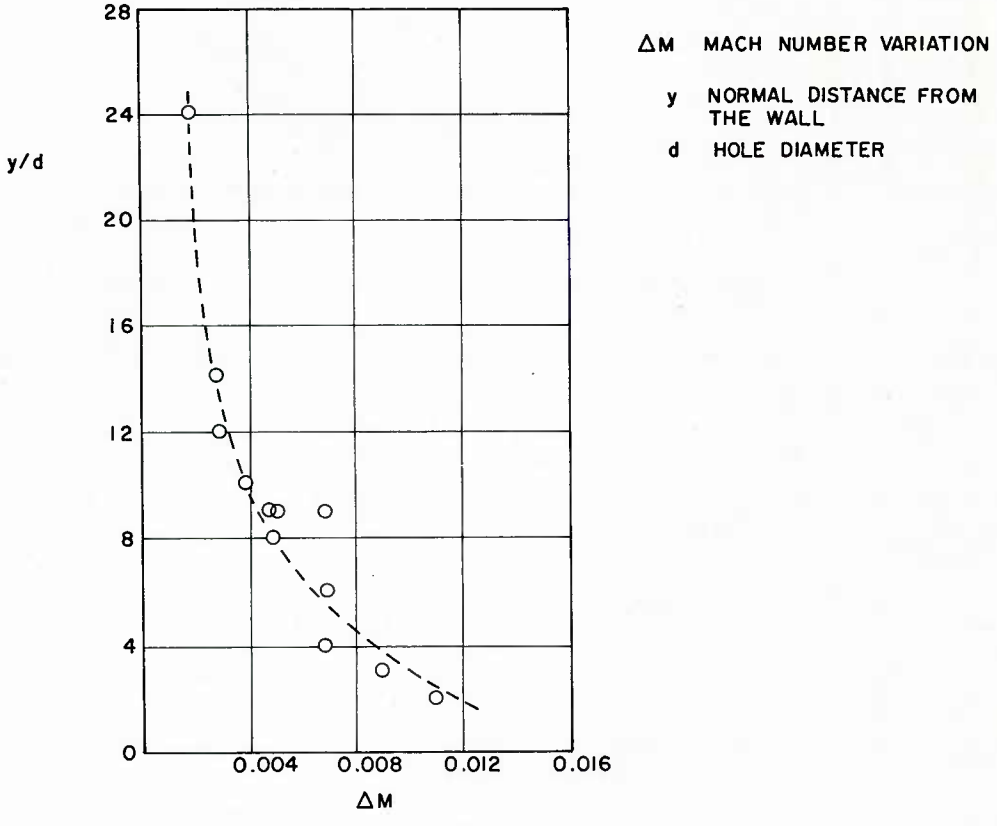

Fig. 2.2 Decay of flow disturbances produced by a perforated wall with normal holes at M = 1.20 (adapted from Ref. [2.15])

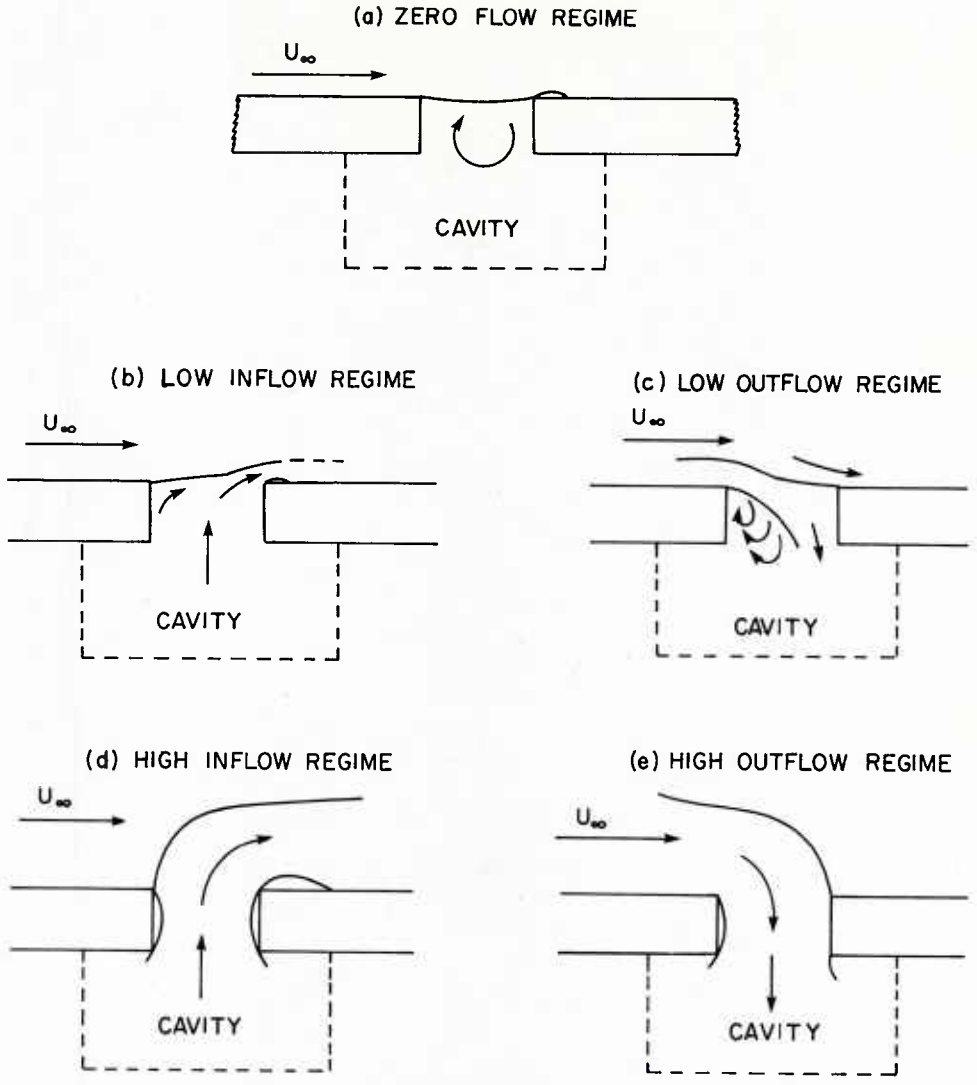

Fig. 2.3 Flow through a normal hole, observed in water tunnel (adapted from Ref. [2.18])

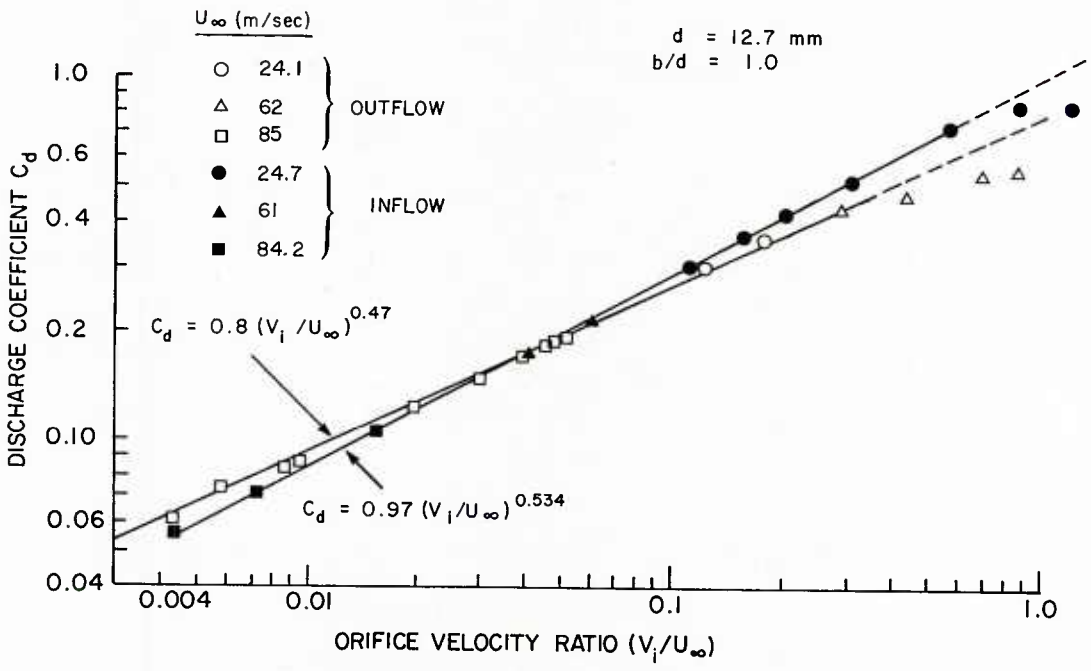

Fig. 2.4 Typical low orifice flow resistance data (adapted from Ref. [2.18])

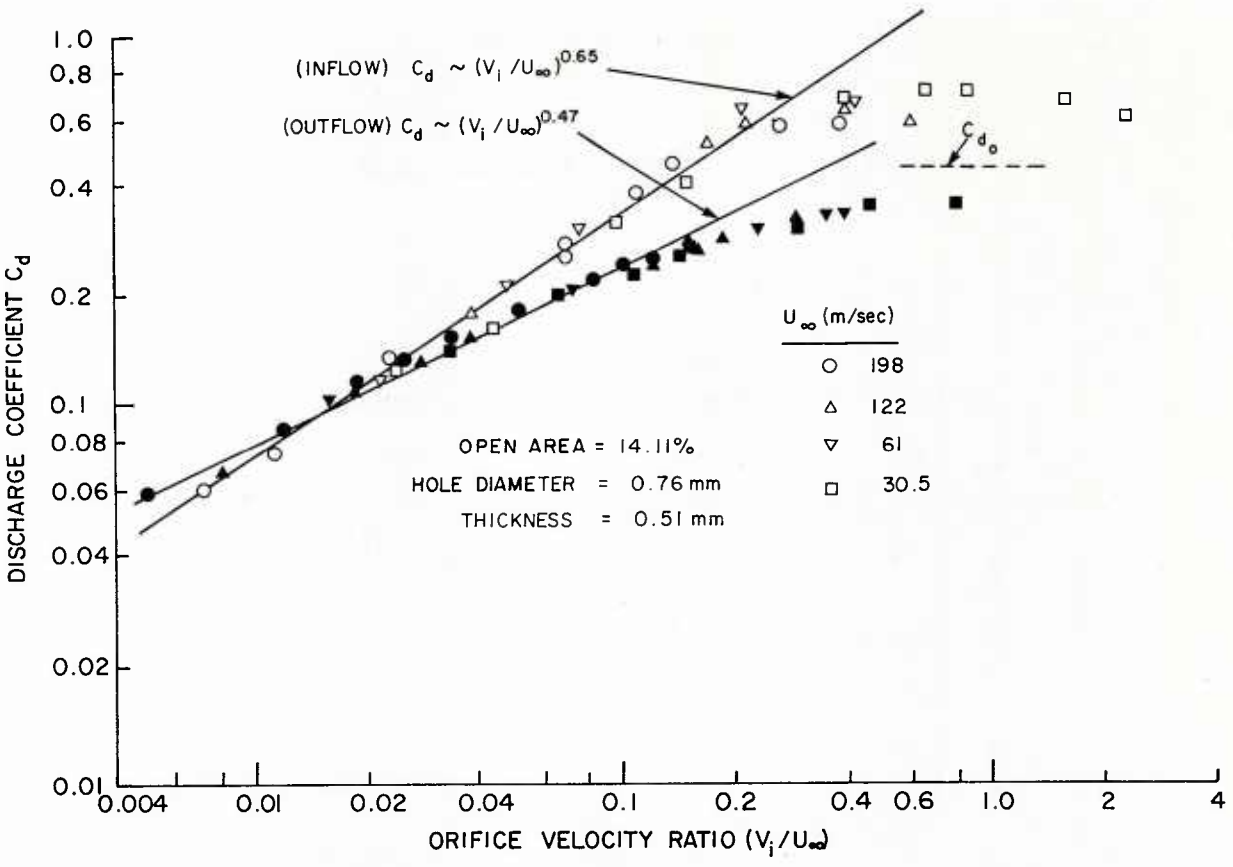

Fig. 2.5 Typical correlation of data for clustered orifices (adapted from Ref. [2.18])

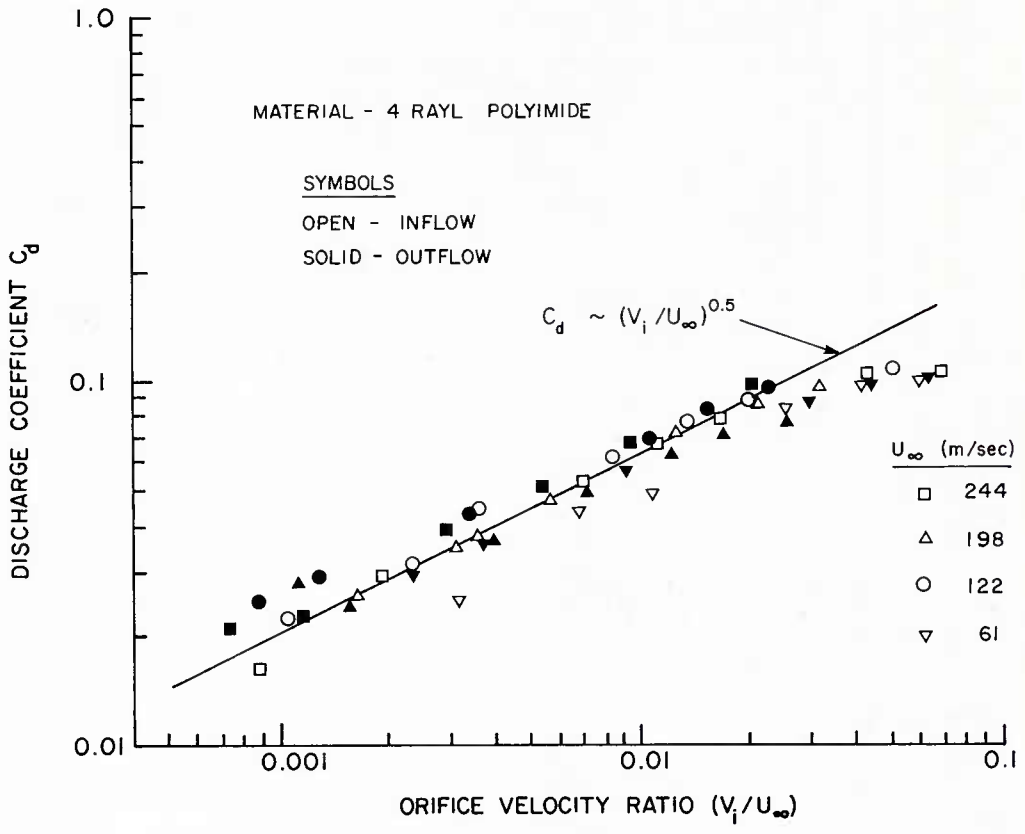

Fig. 2.6 Correlation of data for porous facing material (adapted from Ref. [2.18])

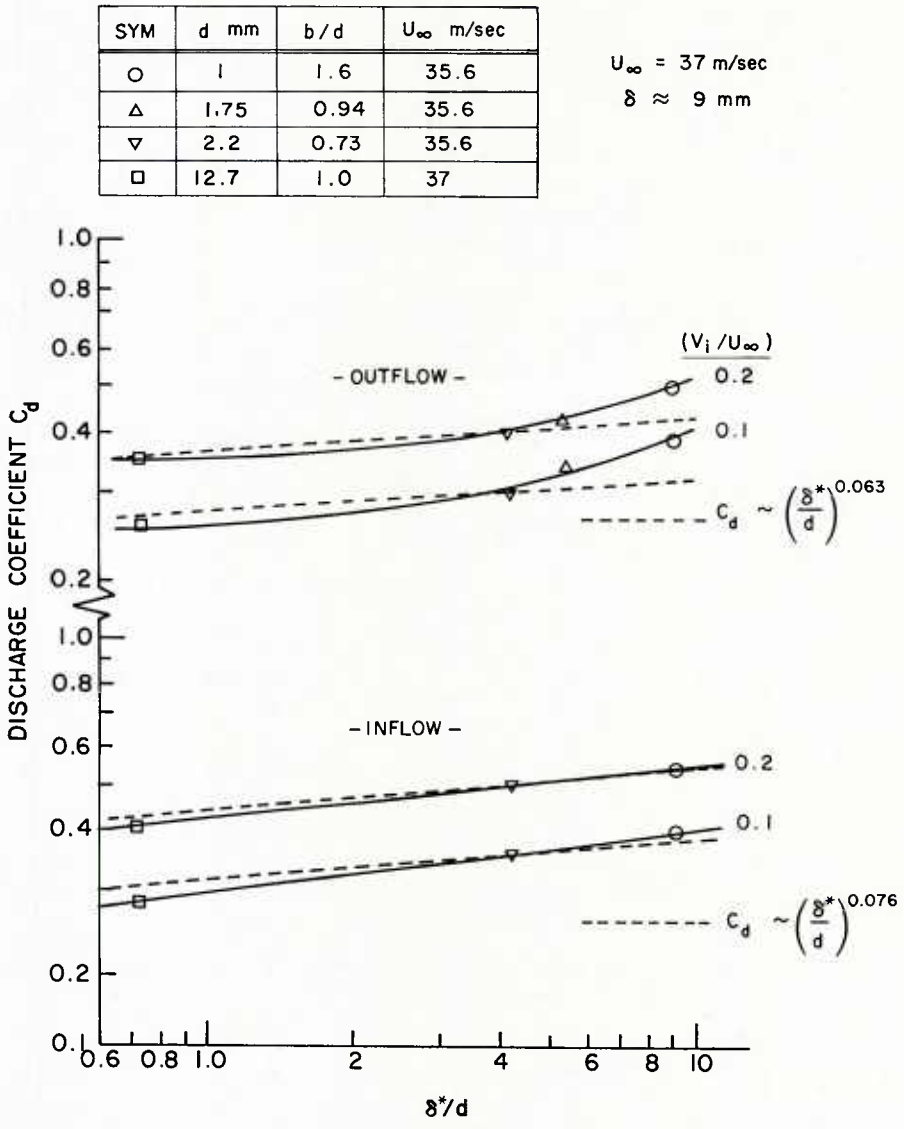

Fig. 2.7 Effect of boundary layer thickness ratio (δ^*/d) on discharge coefficient (C_d) (adapted from Ref. [2.18])

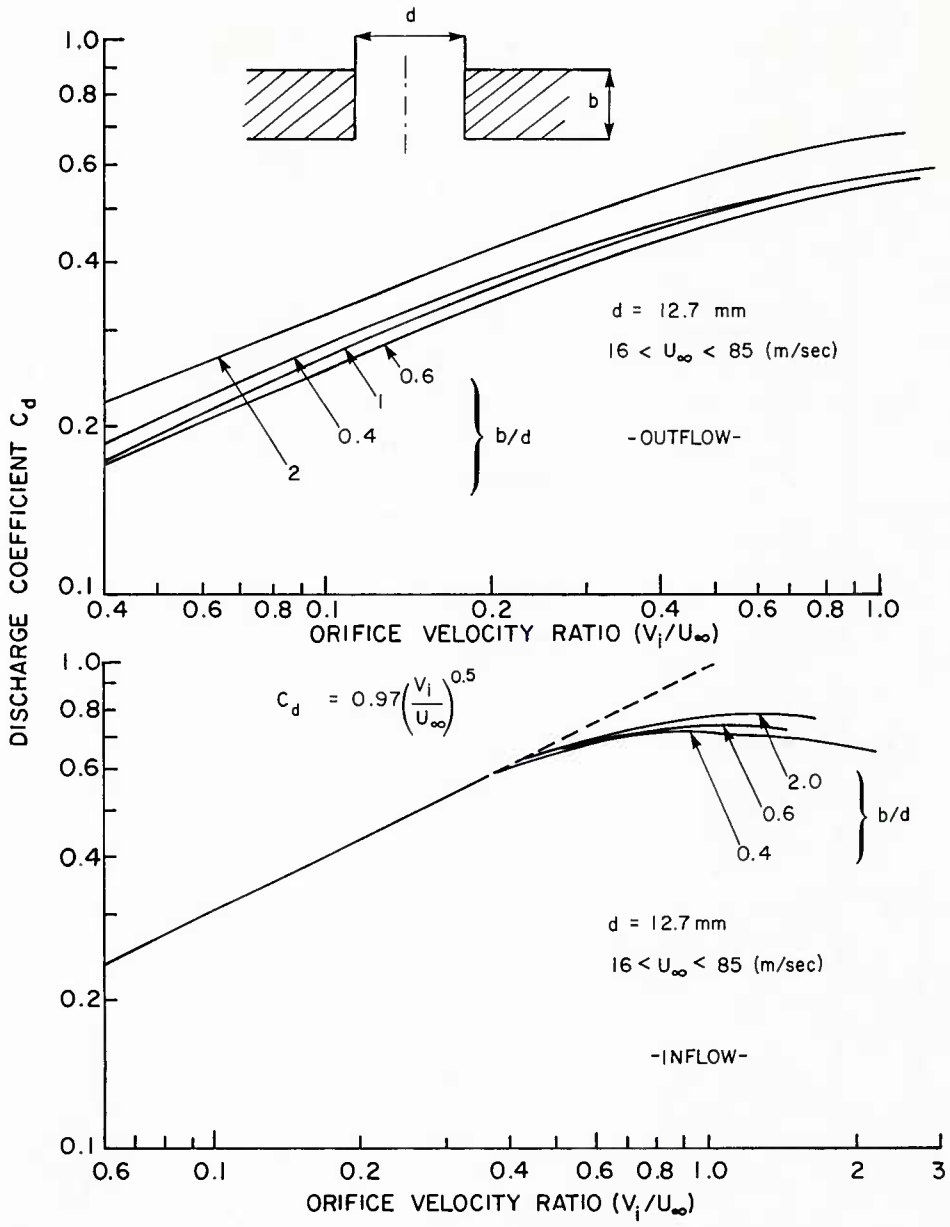

Fig. 2.8 Effect of length — diameter ratio (b/d) discharge coefficient (C_d) (adapted from Ref. [2.18])

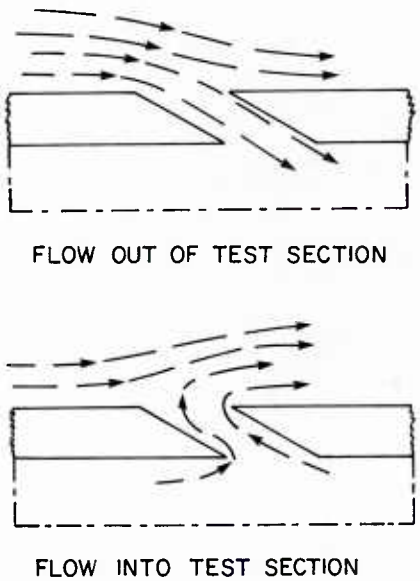

Fig. 2.9 Schematic of flow through a forward inclined hole (adapted from Ref. [2.1])

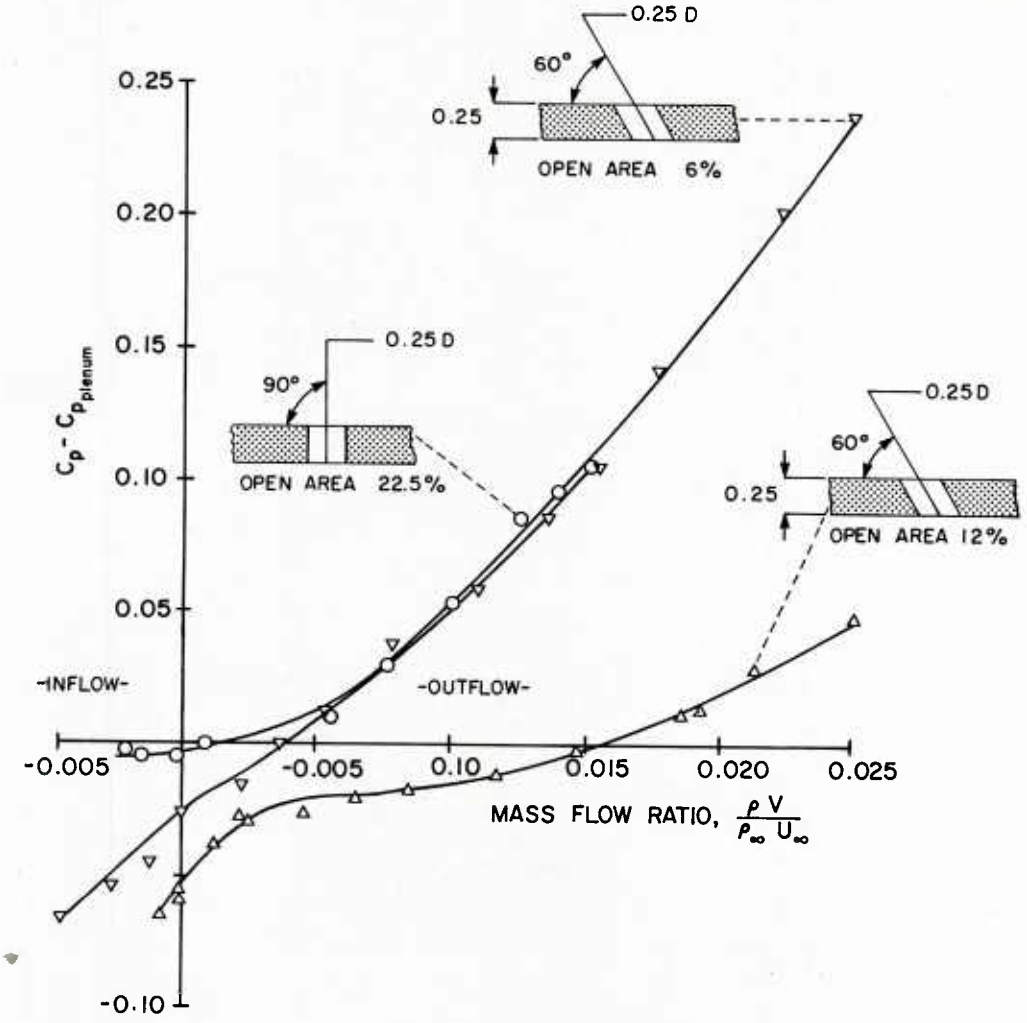

Fig. 2.10 Comparison of crossflow characteristics for walls with normal and inclined holes at M = 1.0 (adapted from Ref. [2.23])

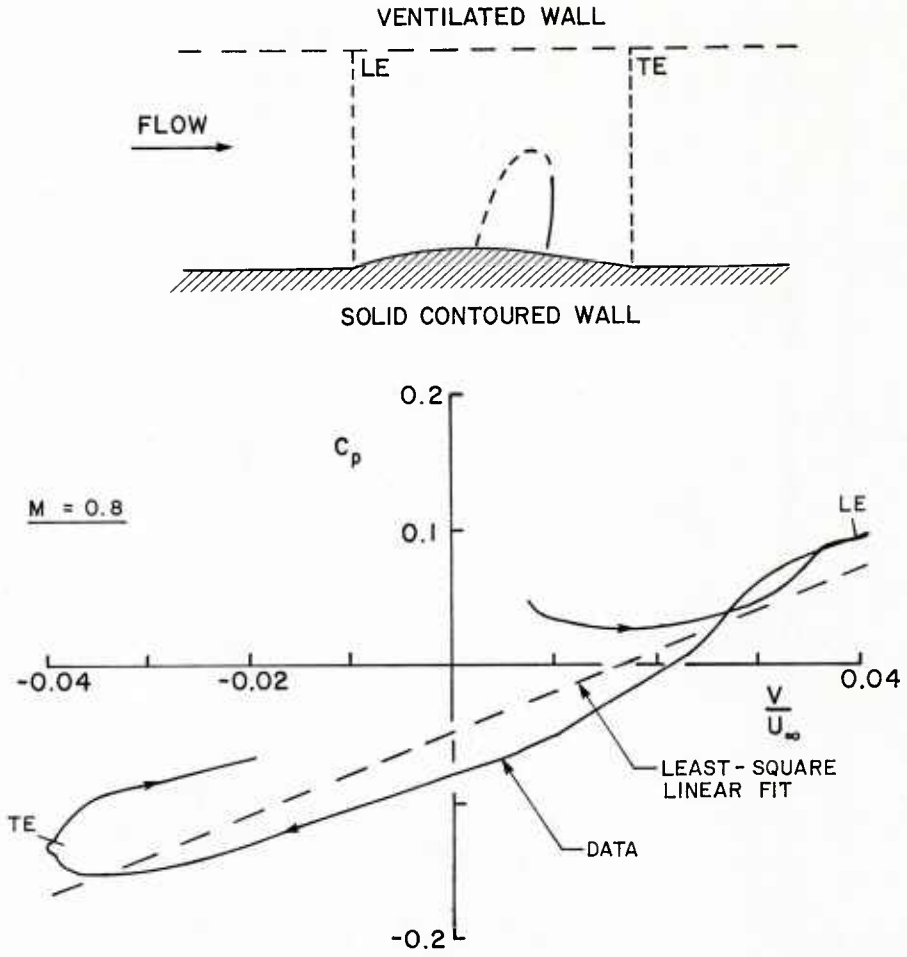

Fig. 2.11 Cross-flow curve based on measurements of C_p and V along a ventilated wall (adapted from Ref. [2.27])

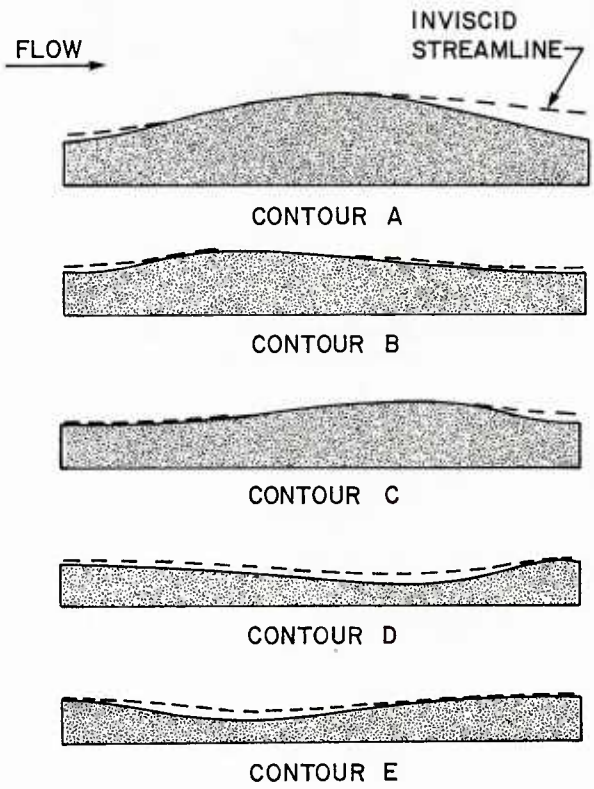

Fig. 2.12 Geometry of wall contours (adapted from Ref. [2.27])

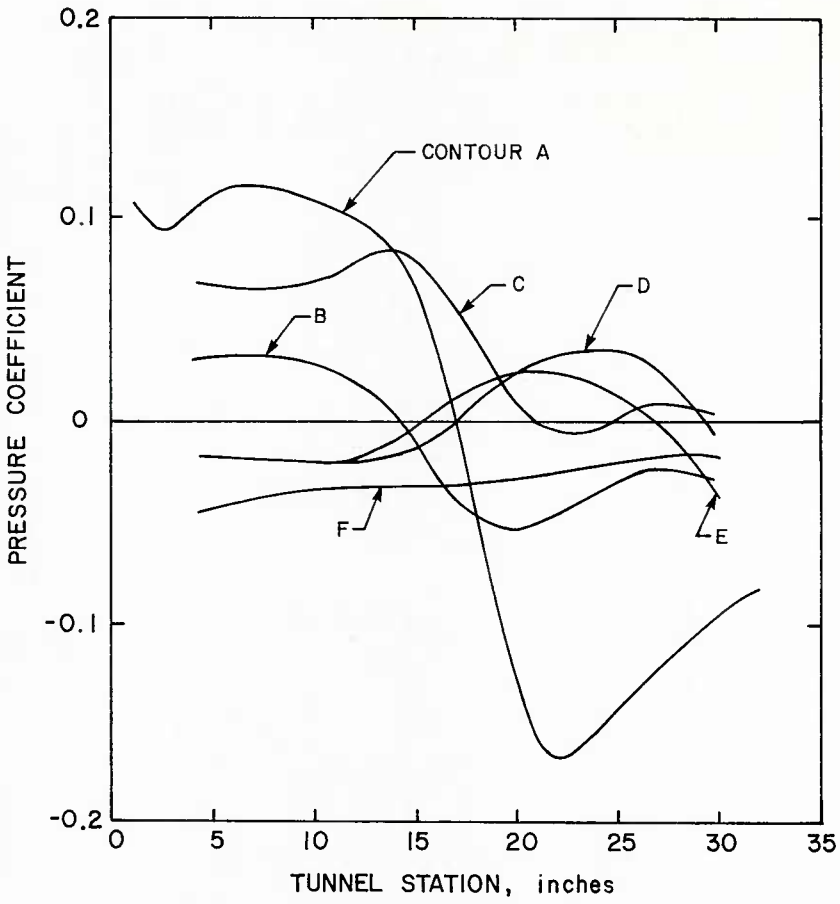

Fig. 2.13 Effect of model shape on static pressure near a perforated wall (adapted from Ref. [2.27])

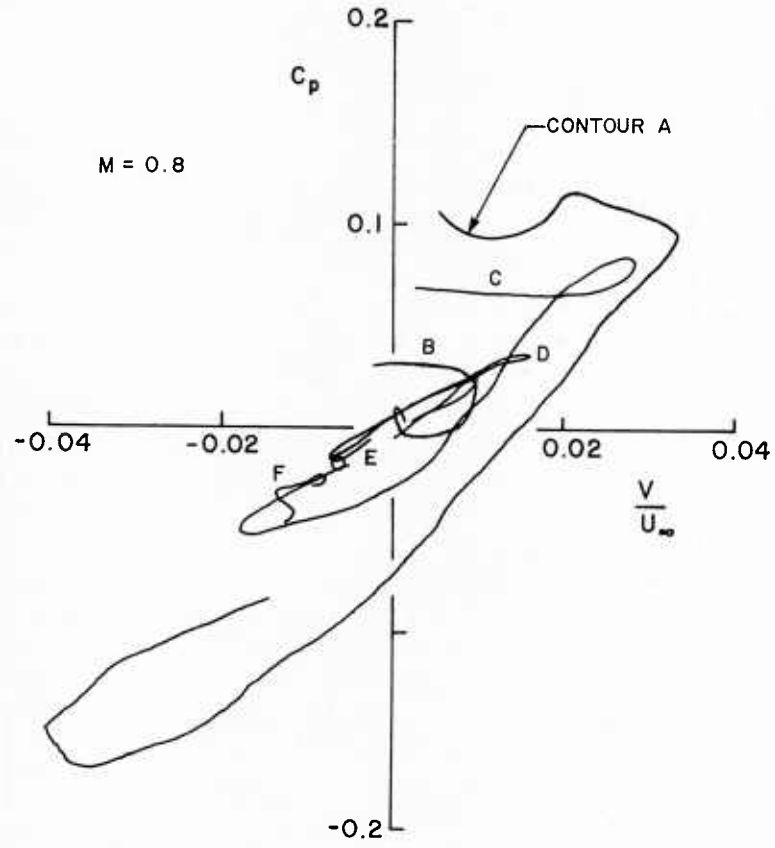

Fig. 2.14 Effect of model shape on the perforated wall characteristic (adapted from Ref. [2.27])

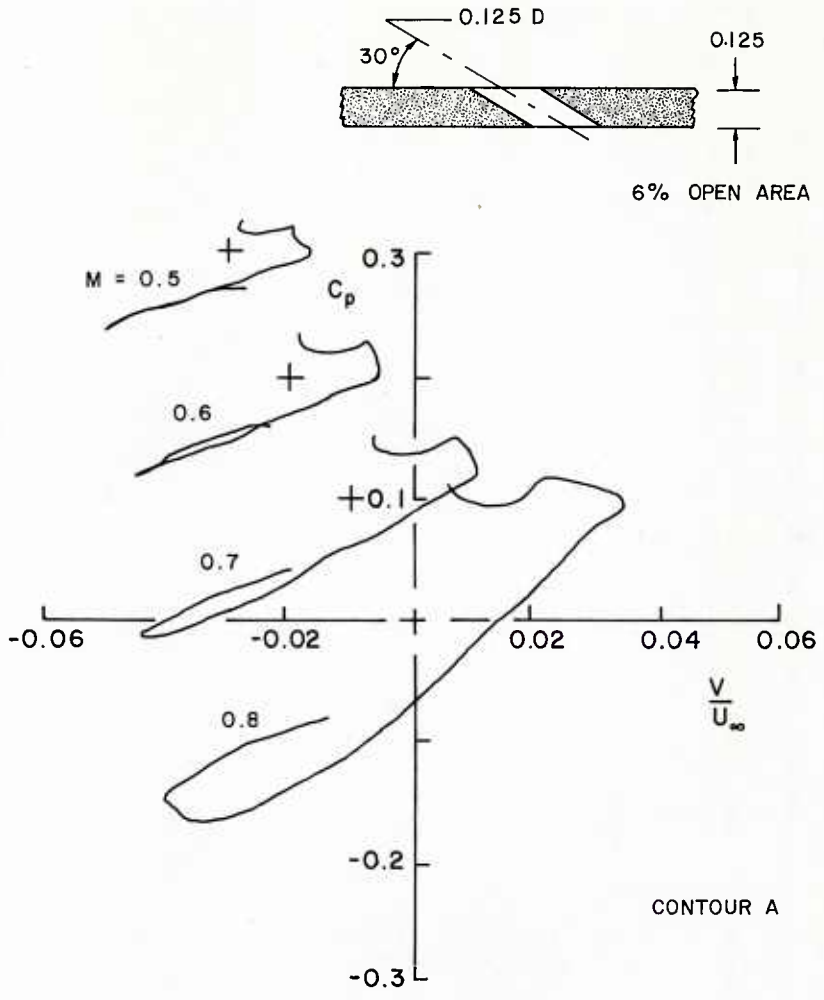

Fig. 2.15 Effect of Mach number on the perforated wall characteristic (adapted from Ref. [2.27])

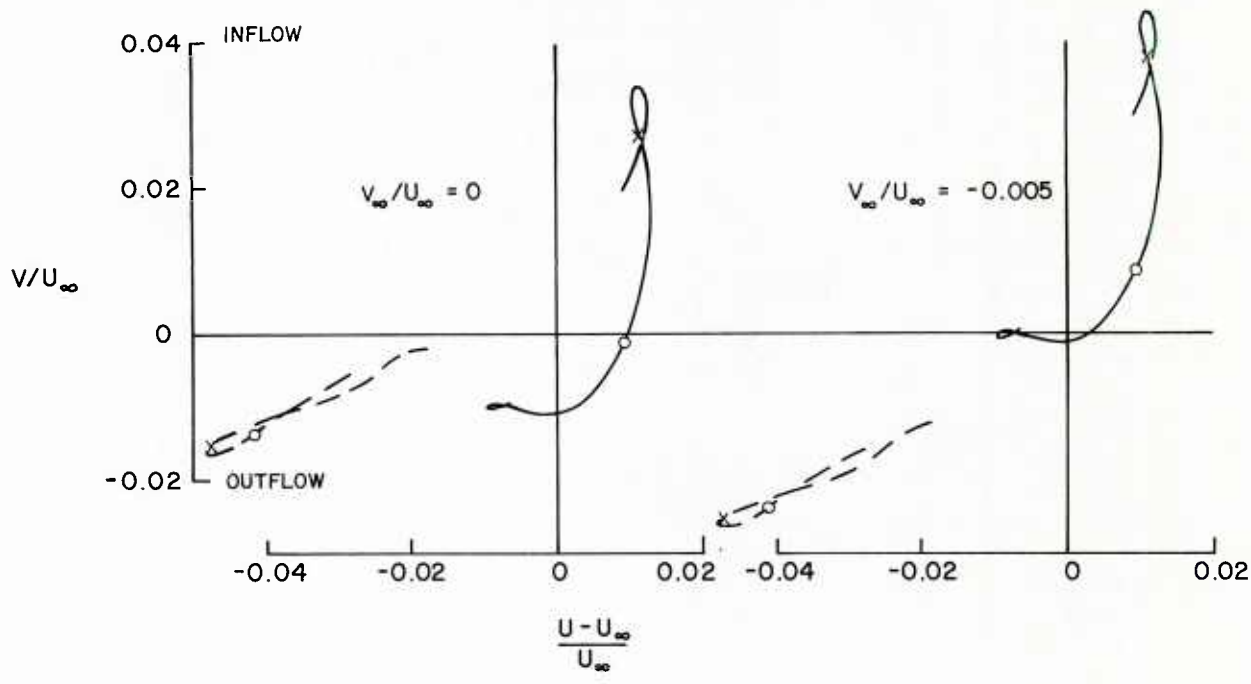

Fig. 2.16 Computed crossflow curves for perforated walls (adapted from Ref. [2.30])

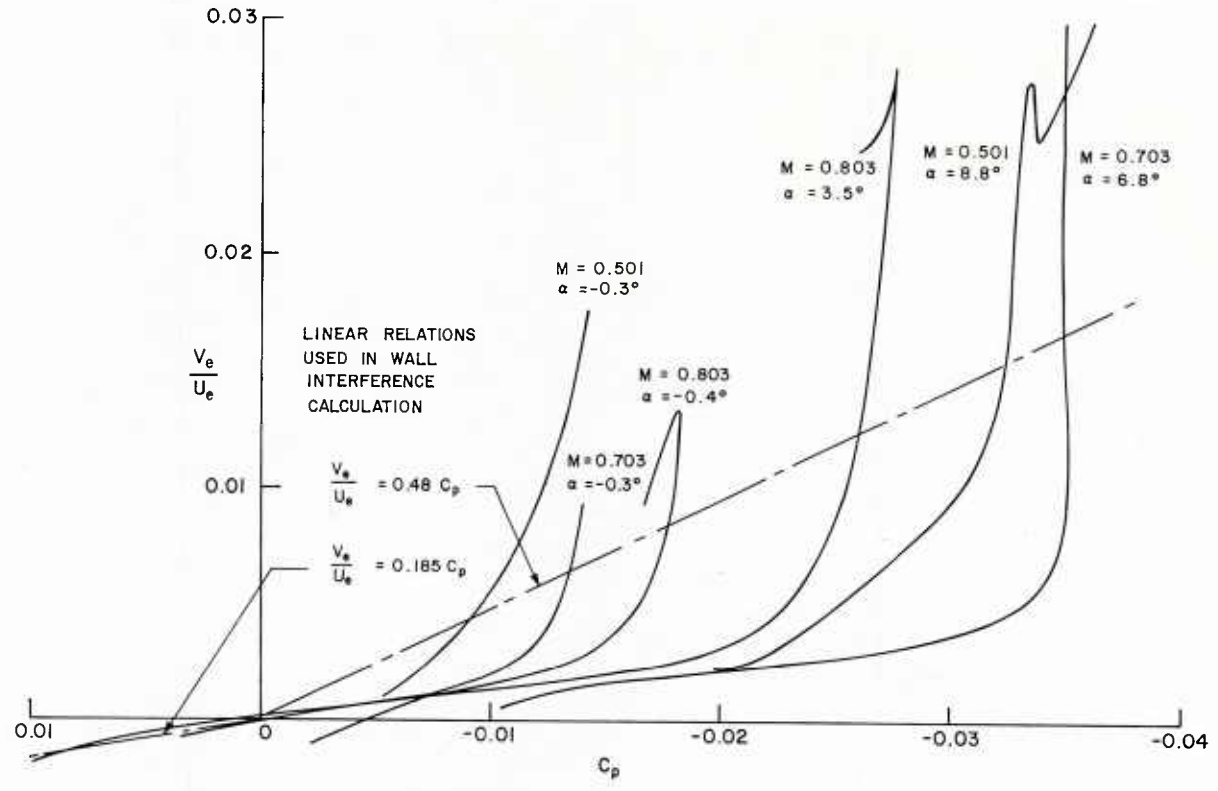

Fig. 2.17 Normal velocity — pressure relations at the edge of the boundary layer of a perforated wall (Ref. [2.32])

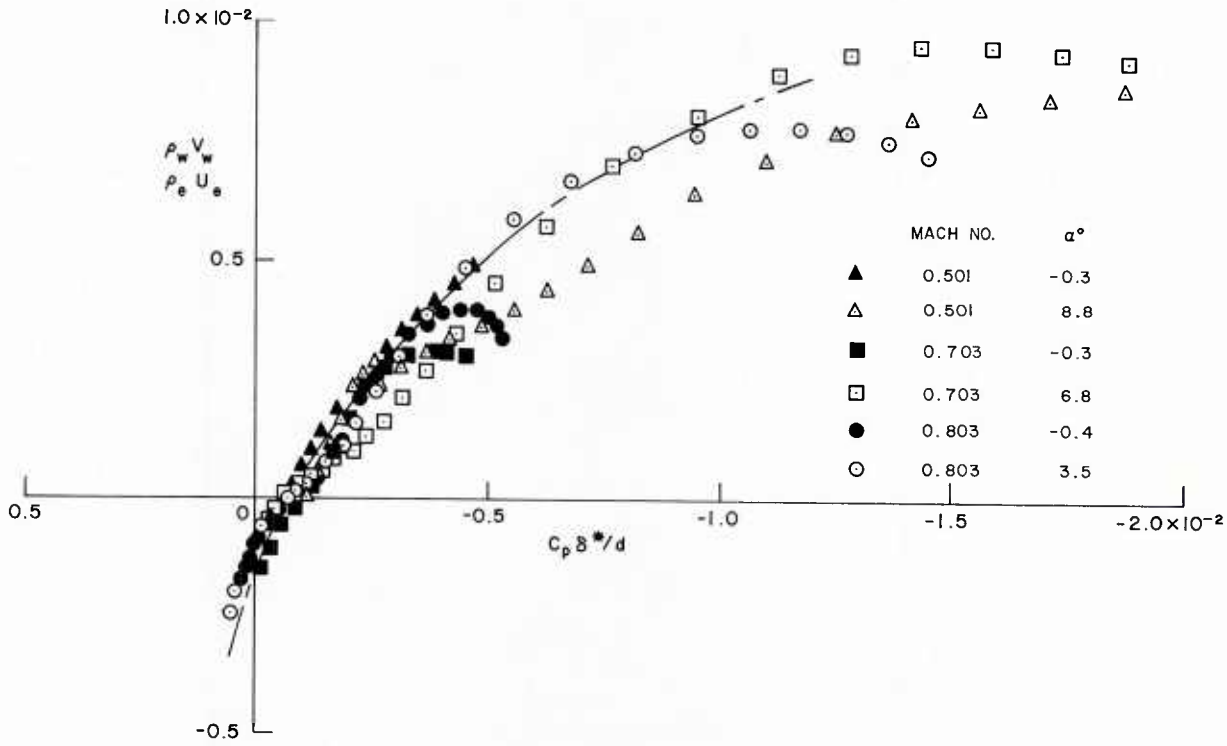

Fig. 2.18 Correlation of normal velocity (mass flow), pressure coefficient and boundary layer displacement thickness of a perforated wall, $\delta^*/d \ll 0.25$ (Ref. [2.32])

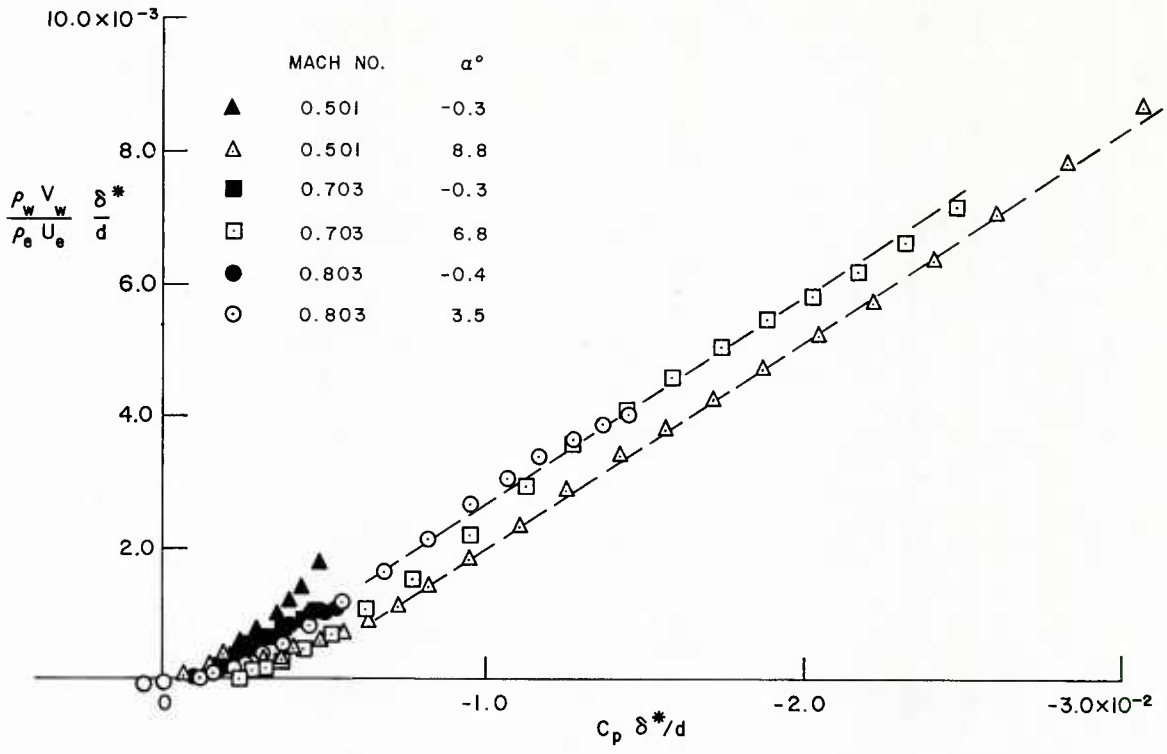

Fig. 2.19 Correlation of normal velocity (mass flow), pressure coefficient and boundary layer displacement thickness at a perforated wall, $\delta^*/d \ll 0.25$ (Ref. [2.32])

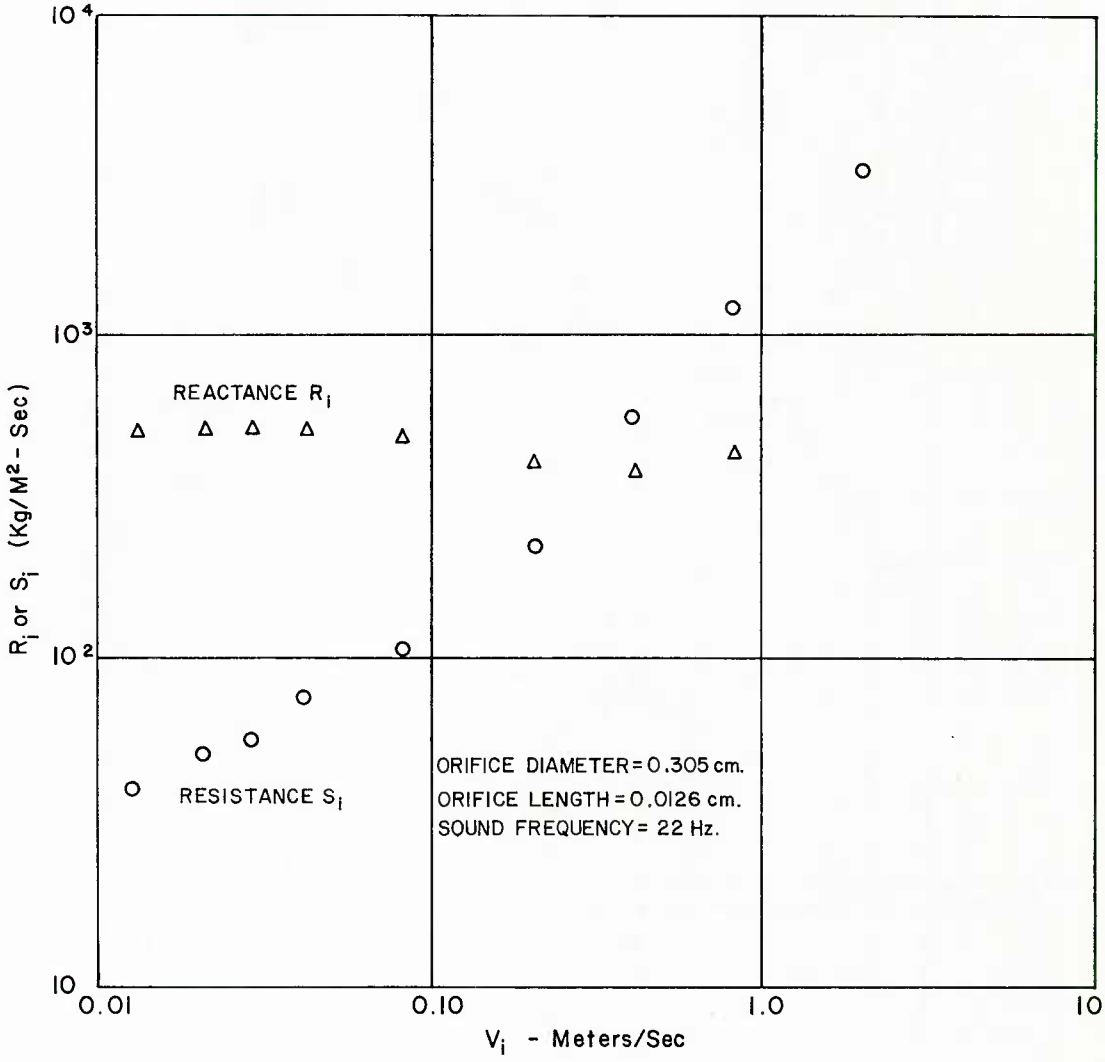

Fig. 2.20 Thurston's et al. measurements of orifice impedance (adapted from Ref. [2.36])

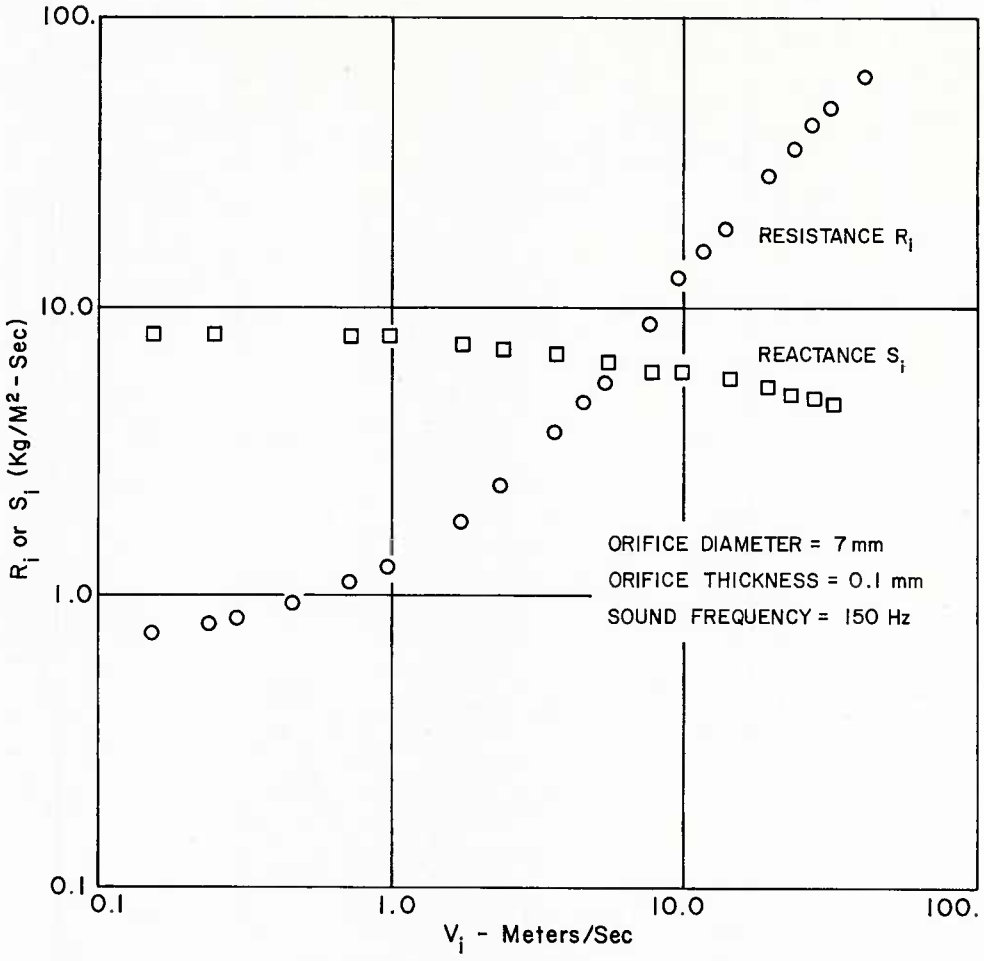

Fig. 2.21 Ingard and Ising's measurements of orifice impedance (adapted from Ref. [2.36])

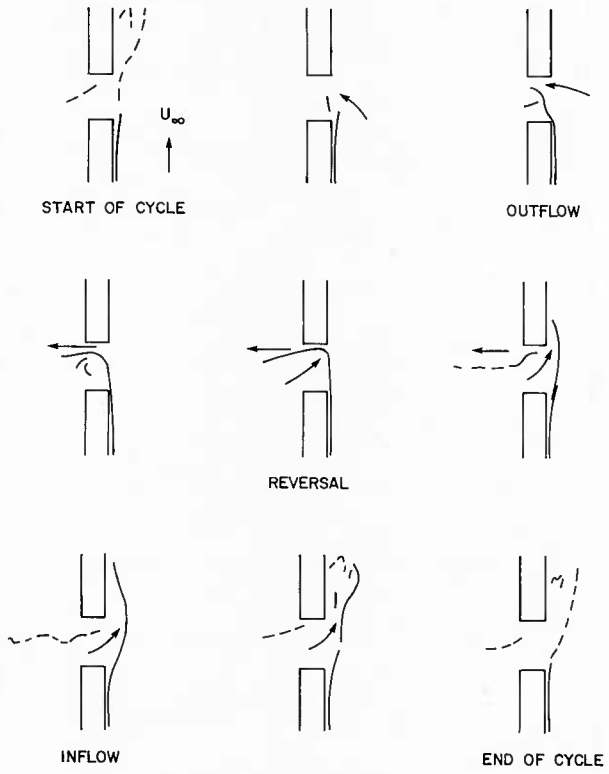

Fig. 2.22 Low amplitude oscillating orifice flow, grazing flow velocity 0.3 m/s (adapted from Ref. [2.44])

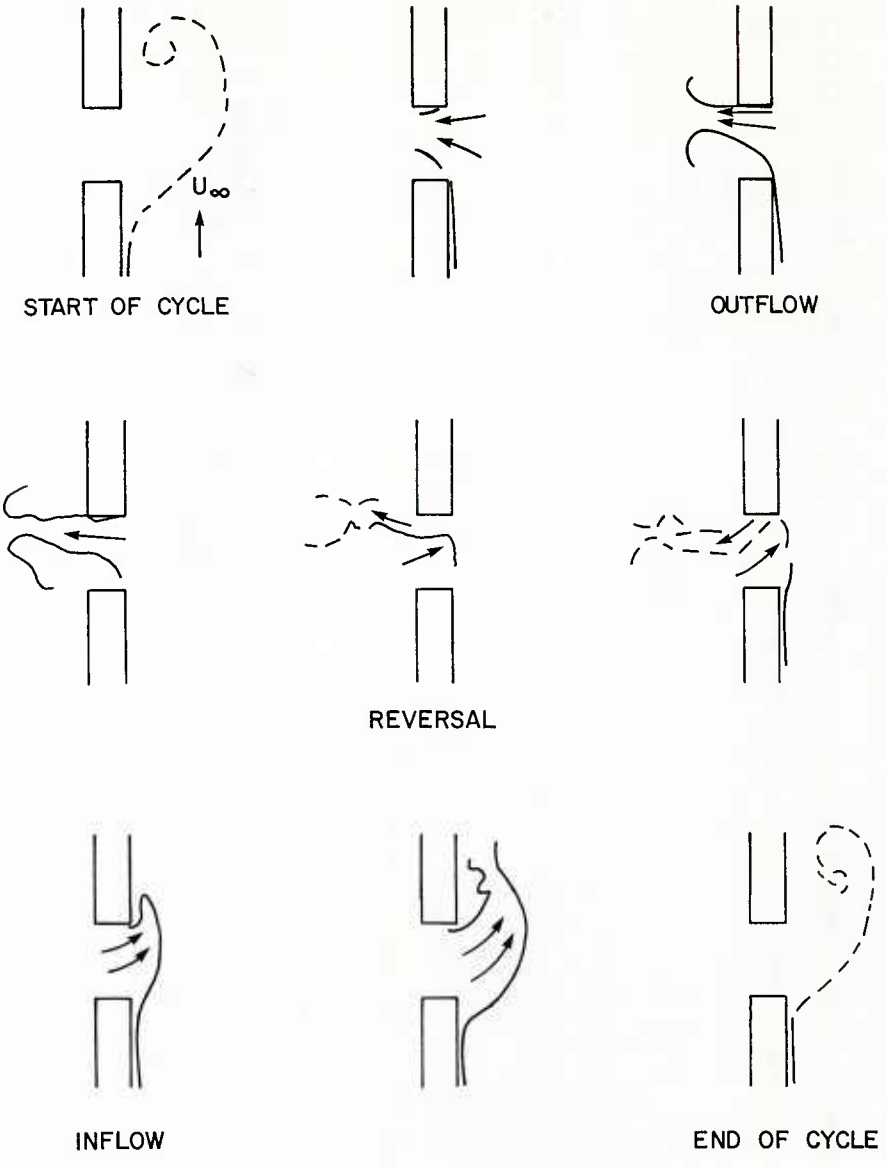

Fig. 2.23 High amplitude oscillating orifice flow, grazing flow velocity 0.3 m/s (adapted from Ref. [2.44])

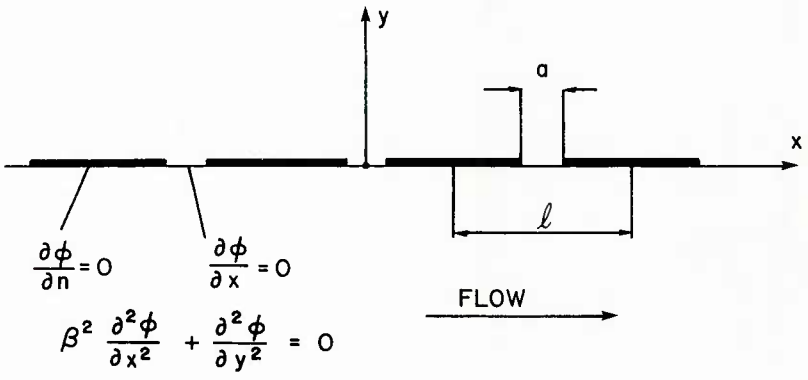

Fig. 2.24 Modeling flow past a transversally slotted wall

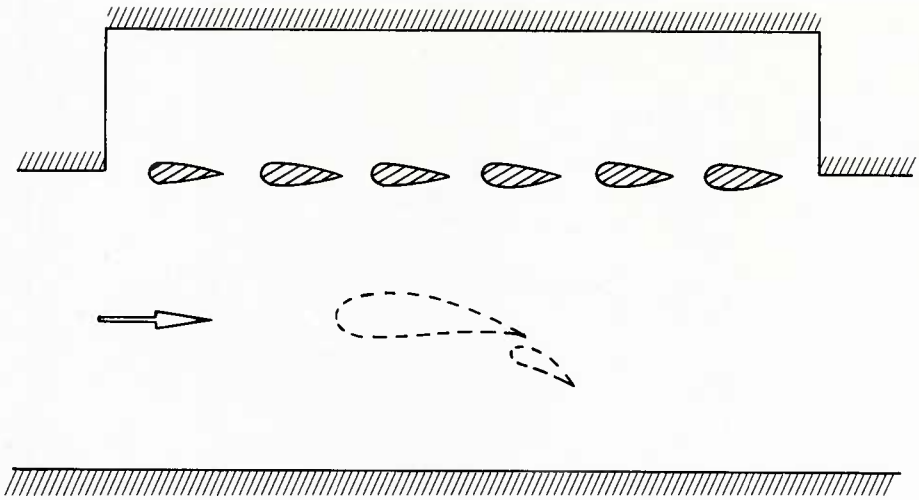

Fig. 2.25 Schematic of the Parkinson-Williams low correction test section

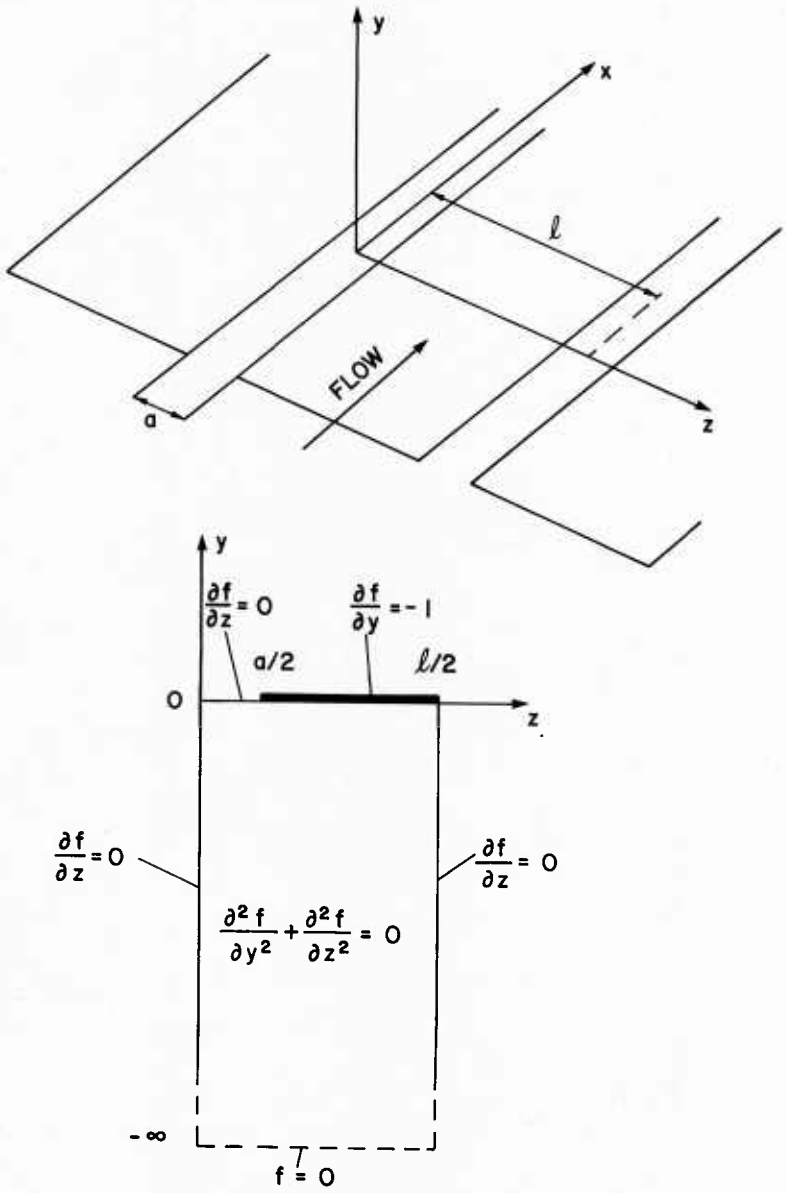

Fig. 2.26 Modeling flow past a longitudinally slotted wall

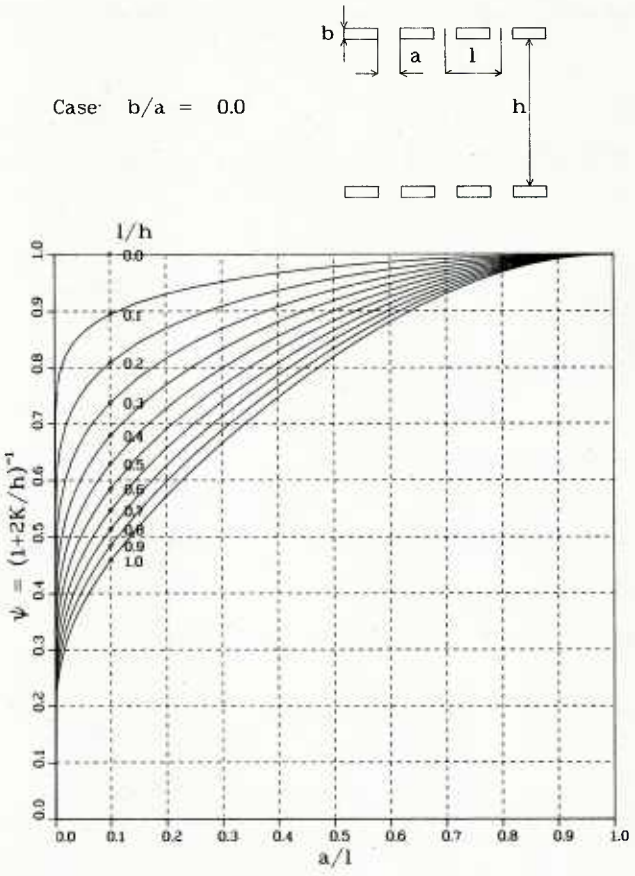

Fig. 2.27 Slot parameter for thin wall, b/a = 0.0

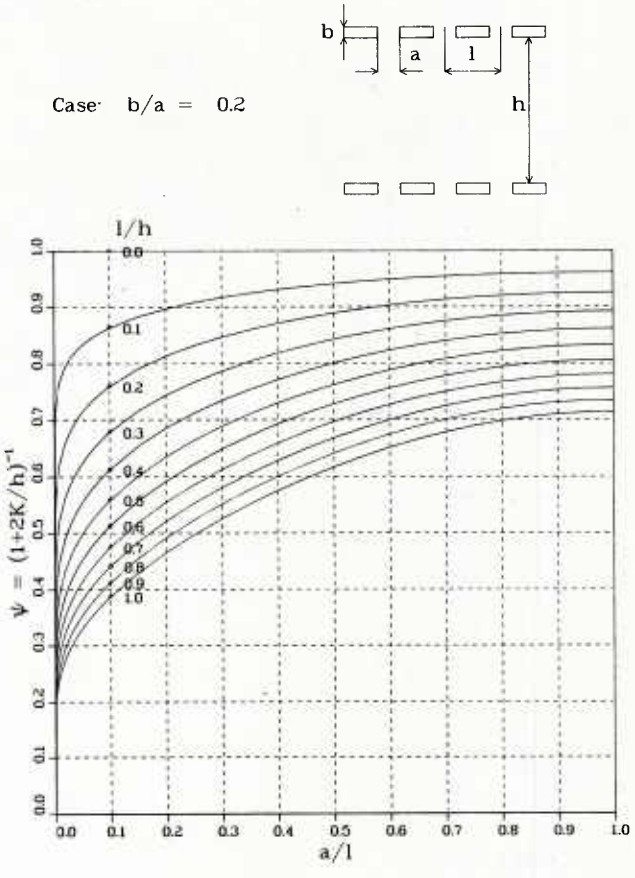

Fig. 2.28 Slot parameter for thick wall, b/a = 0.2

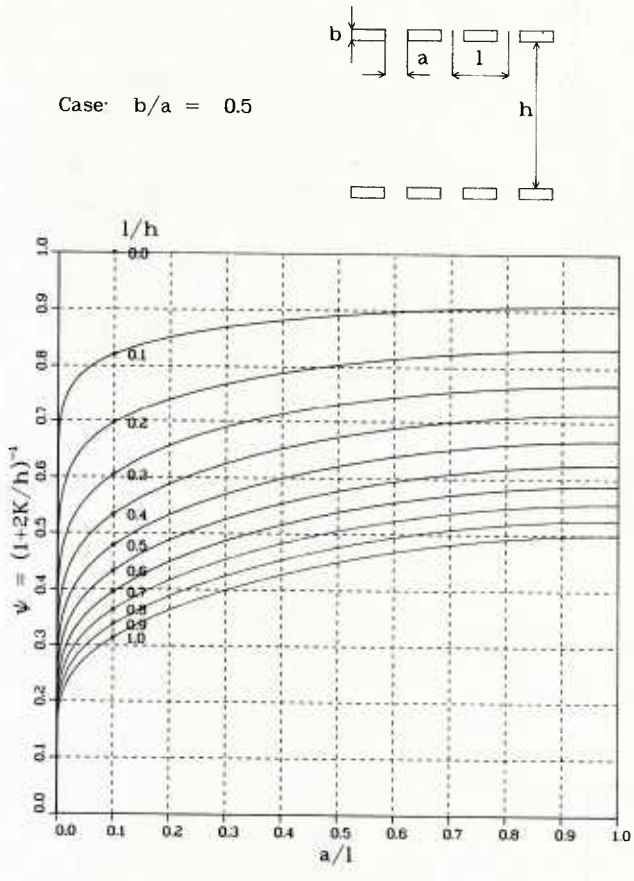

Fig. 2.29 Slot parameter for thick wall, b/a = 0.5

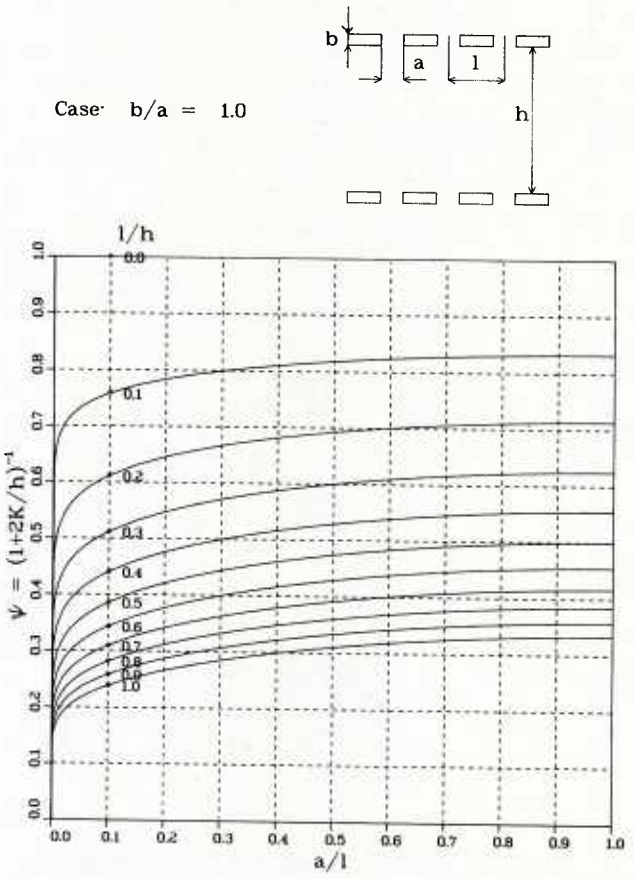

Fig. 2.30 Slot parameter for thick wall, b/a = 1.0

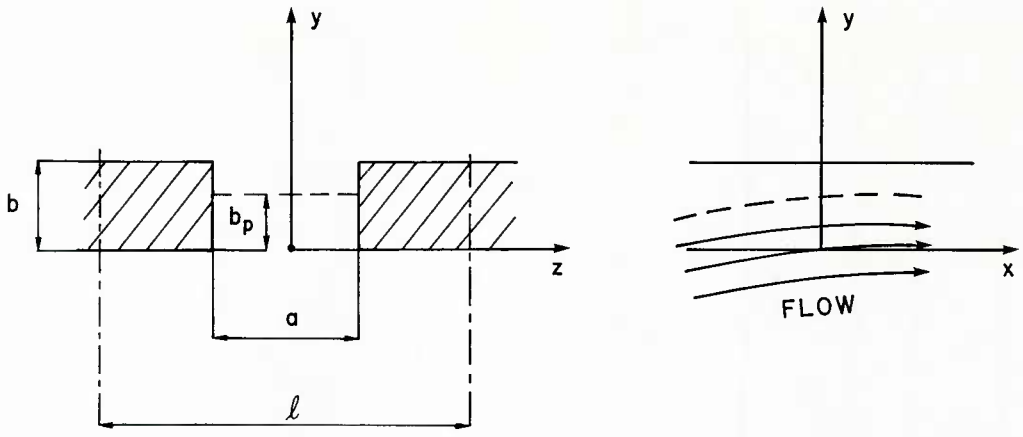

Fig. 2.31 Modeling of flow inside a thick, longitudinally slotted wall

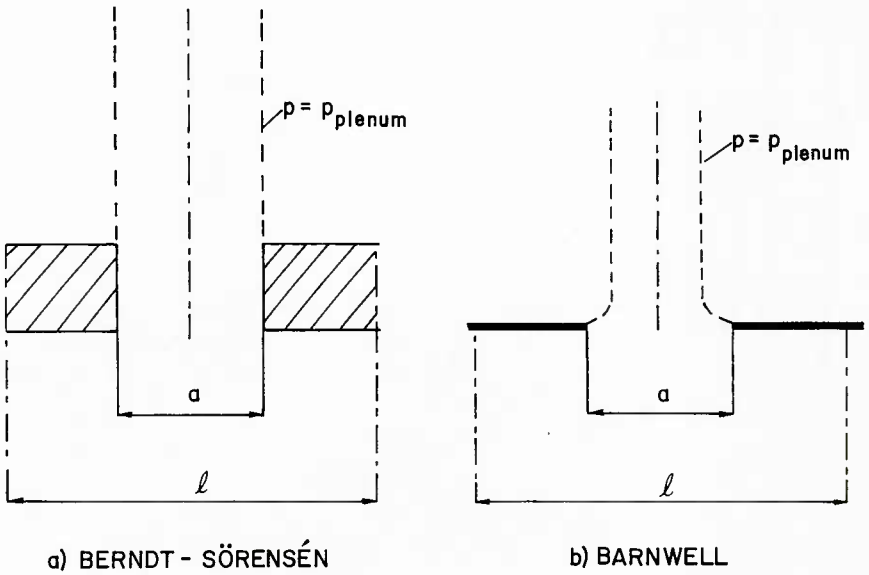

Fig. 2.32 Modeling of slot flow with plenum separation

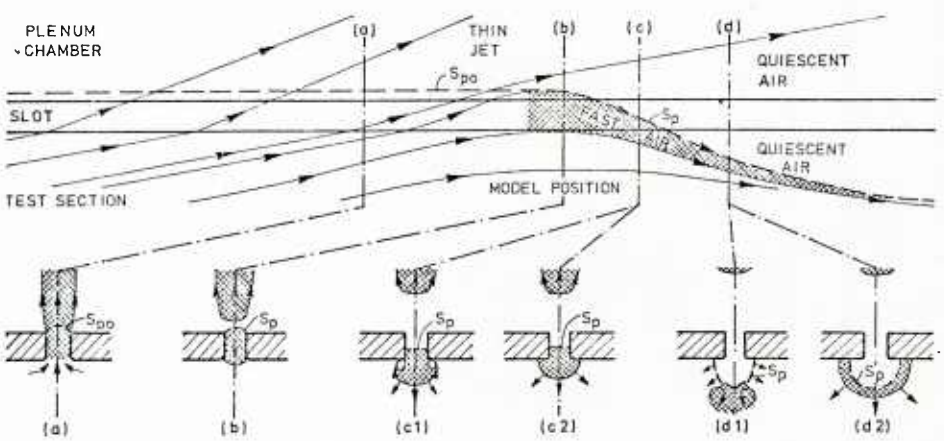

Fig. 2.33 Possible inviscid flow patterns (not to scale)
▨ = fast air from the slot
(adapted from Ref. [2.53])

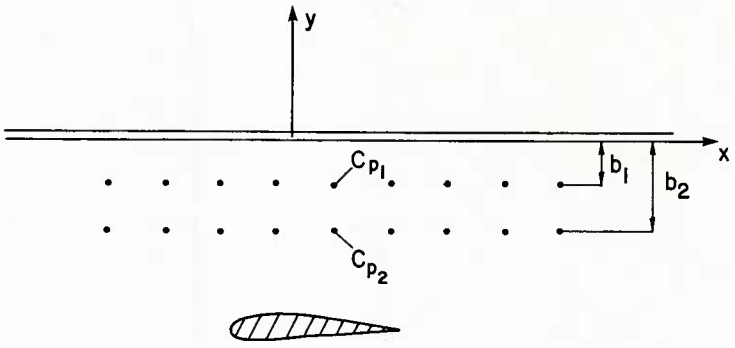

Fig. 2.34 Illustrating the measurement of C_p and $\partial C_p/\partial n$

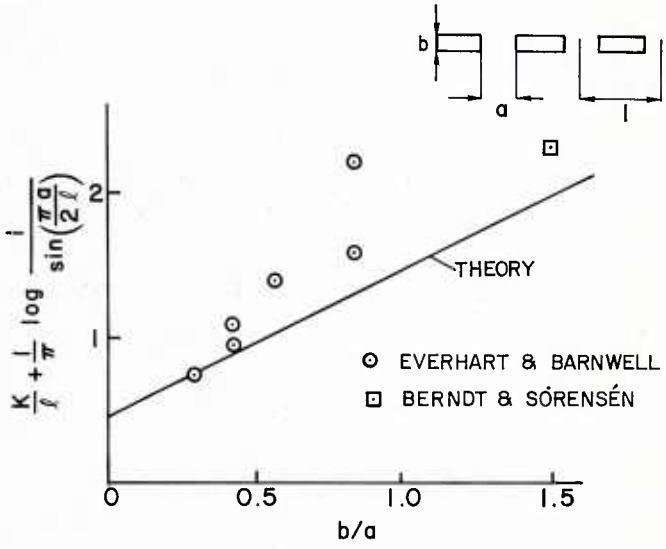

Fig. 2.35 Variation of experimental slot parameter with slot depth to width ratio (adapted from Ref. [2.55])

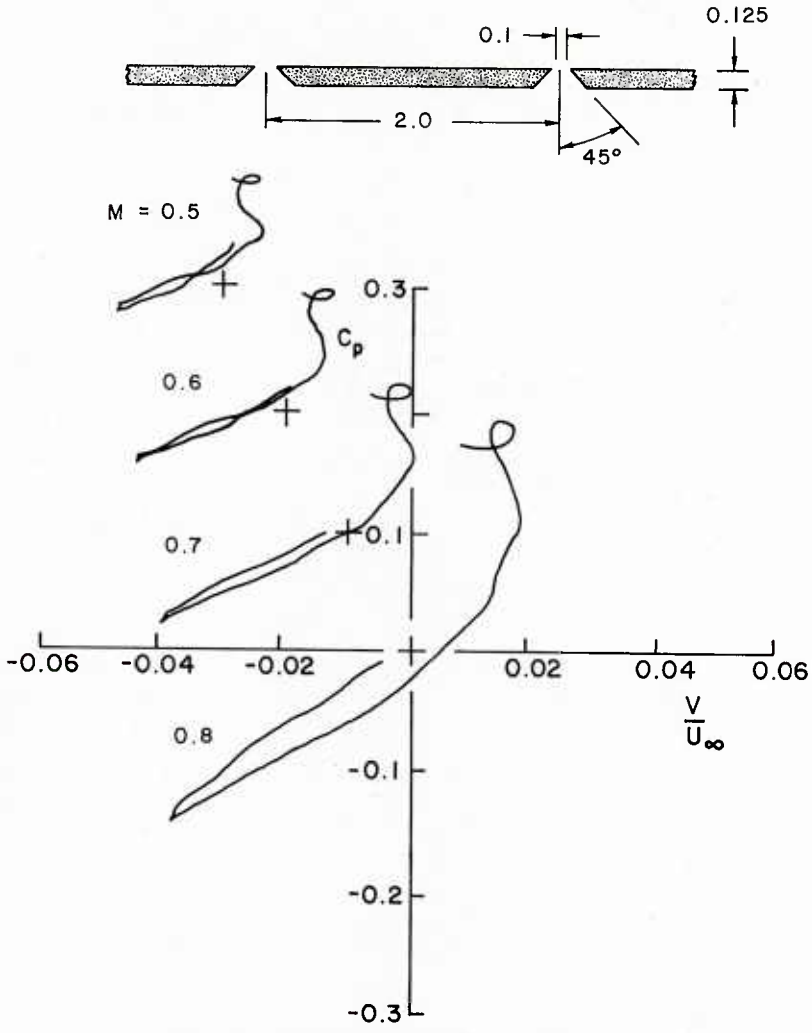

Fig. 2.36 Effect of Mach number on the slotted wall characteristic (adapted from Ref. [2.27])

3.0 ASYMPTOTIC ANALYSIS OF TUNNEL WALL INTERFERENCE

3.1 Introduction

The foundation of the theoretical treatment of wind-tunnel wall interference was laid by Prandtl in 1919 [3.1], [3.2]. He showed that the constraint imposed on the flow by the walls could be defined as an exterior boundary condition. To obtain the actual flow in the wind tunnel it is necessary to superimpose an interference flow to the basic free air flow satisfying the boundary condition at the wall. Since that time a large amount of work on wall interference has been advanced following Prandtl's approach.

Prandtl's approach to the problem is clearly asymptotic in nature. It falls in the same category as that of the two well known asymptotic theories of his, namely the boundary layer theory and the lifting line theory, which led to the development of the method of singular perturbation [3.3]. With this mathematical technique the wall interference problem can be reformulated in the same manner as the other two theories. The singular nature of the problem is shown by the two reference length scales associated with the problem. Away from the airfoil the characteristic length is the tunnel height while near the model its chord becomes the characteristic length. The ratio of these two reference lengths vanishes if the tunnel height is much greater than the chord of the airfoil. The singular nature has indeed been demonstrated by the classical analysis of the problem, in which the far field solutions are obtained for vanishing ratio of chord to tunnel height.

For subsonic linear flow the asymptotic analysis will add little information to the vast existing knowledge of the subject. The merit of the analysis, however, should be based on its systematic approximation of the original problem and providing the means of formulation of the boundary value problems in proper order. The asymptotic analysis delineates explicitly the physical characteristics of the problem without solving it completely. This is particularly important for transonic flows in that the governing equations are non-linear and the solutions can only be obtained by numerical methods with large amounts of computations.

A study in this direction is made by Chan [3.4], [3.5] for a tunnel with perforated walls. The incompressible flow is first treated and the procedure is then applied to transonic flows. The analysis leads to a proper formulation of the boundary value problem for the tunnel wall interference. The result yields explicitly the apparent angle of attack and the blockage due to the wall constraint, and for transonic flow, an effective blockage induced by the nonlinear compressibility. For solid wall interference at transonic speeds a similar analysis was performed by Cole, Malmuth and Zeigler [3.6] including numerical solutions up to the first order. At transonic speeds with free stream Mach number near unity, asymptotic solutions were obtained for perforated walls by Lifshits and Fonarev [3.7] for bodies of revolution and by Blynskaya and Lifshits [3.8] for two-dimensional airfoils.

In this chapter the asymptotic analysis is derived for both the incompressible and the compressible, transonic, flow cases. In each case the outer and inner limits are first discussed, followed by a description of the procedure employed for matching the two.

3.2 Incompressible Flow

3.2.1 Formulation

The wind tunnel wall interference problem is now presented in the formalism of the method of matched asymptotic expansions. Although the flow is assumed to be incompressible the results can be extended to linear subsonic flow with a compressibility transformation. The applications of the procedure to transonic flows with nonlinear governing equations will be presented in Section 3.3.

Within the framework of small perturbation theory the equation governing the flow inside the tunnel can be written in terms of the perturbation velocity potential

$$\phi_{\bar{x}\bar{x}} + \phi_{\bar{y}\bar{y}} = 0 \tag{3.1}$$

where $\bar{x}$ and $\bar{y}$ are the Cartesian co-ordinates normalized by the chord of the model c. The airfoil has a maximum thickness t and is at an angle of attack α. Both t and α are assumed to be small. The boundary condition on the airfoil requires the flow to be tangent to the surface. Thus, within the small disturbance theory, the boundary condition can be written as

$$\phi_{\bar{y}}\,(\bar{x}, \pm 0) = \pm f_{\bar{x}} - \alpha, \qquad -\frac{1}{2} \leqslant \bar{x} \leqslant \frac{1}{2} \tag{3.2}$$

where f is the thickness distribution of the airfoil. The tunnel walls are located at a distance H* above and below the model and are assumed to be perforated for flow ventilation. The boundary condition at the walls is thus

$$\phi_{\bar{x}} \pm \frac{1}{P}\phi_{\bar{y}} = 0 \qquad \text{at} \qquad \bar{y} = \pm H \tag{3.3}$$

where P is the porosity factor and H the tunnel half height normalized by the chord c. In the limits that P tends to zero or infinity, the boundary condition reduces to that of solid walls or a free jet respectively. The perforated wall boundary condition is more general than the limiting cases and part of the results can also be applied to transonic flows analysed in a later section. The other wall configuration such as slotted wall, can also be treated in a similar manner. Far up- and down-stream, the perturbations tend to zero and the boundary conditions become

$$\phi_{\bar{x}}, \phi_{\bar{y}} \to 0 \qquad \text{as} \qquad \bar{x}^2 + \bar{y}^2 \to \infty \tag{3.4}$$

The boundary value problem is fully defined by Equations (3.1) to (3.4). Asymptotic analysis is now applied to the outer region near the tunnel wall and the inner region around the airfoil. The solutions are than matched as these two regions approach each other in the limit.

3.2.2 Outer Limit

Away from the airfoil the characteristic length of the flow is the tunnel half height H. The length variables should therefore be normalized by the reference scale H as

$$x = \frac{\bar{x}}{H}, \quad y = \frac{\bar{y}}{H} \tag{3.5}$$

As $H \to \infty$ with x, y fixed, the airfoil shrinks to a point with all singularities concentrated on it. The potential ϕ can be expanded in an asymptotic series in ascending power of 1/H as

$$\phi\left(x,y;\frac{1}{H}\right) = \phi_0(x,y) + \frac{1}{H}\phi_1(x,y) + \frac{1}{H^2}\phi_2(x,y) + \ldots \tag{3.6}$$

Substituting the series into the governing equation, Equation (3.1), we have

$$\phi_{n_{xx}} + \phi_{n_{yy}} = 0, \qquad n = 0, 1, 2, \ldots \tag{3.7}$$

The zero order solution ϕ_0 is therefore the free air solution and the higher order solutions are the interference solutions. The interference solutions should satisfy the boundary condition at the wall, Equation (3.3)

$$\phi_{0x} \pm \frac{1}{P}\phi_{0y} + \frac{1}{H}\left(\phi_{1x} \pm \frac{1}{P}\phi_{1y}\right) + \frac{1}{H^2}\left(\phi_{2x} \pm \frac{1}{P}\phi_{2y}\right) + \ldots = 0 \qquad \text{at} \qquad y = \pm 1 \tag{3.8}$$

Depending on the order of the singularity of the zero-order solution, we can write

$$\phi_{0x} \pm \frac{1}{P}\phi_{0y} = -\frac{1}{H}\left(\phi_{1x} \pm \frac{1}{P}\phi_{y}\right)$$

$$\phi_{0x} \pm \frac{1}{P}\phi_{0y} = -\frac{1}{H^2}\left(\phi_{2x} \pm \frac{1}{P}\phi_{2y}\right) \tag{3.9}$$

The boundary value problems defined by Equations (3.7) and (3.9) can be identified with the classical formulation of wall interference. The solutions are given in detail in Chapter 4 and for present use, the solution in series form is adopted. The inner expansion of the solution as $r \to 0$ can be written as [3.4]

$$\phi \sim -\frac{\gamma_0}{2\pi}(\theta + a_1 y + a_2 xy) + \frac{1}{H}\left[\frac{d_1}{2\pi}\left(\frac{x}{r^2} + b_2 x\right)\right] + \frac{1}{H}\left[\frac{e_1}{2\pi}\left(-\frac{y}{r^2} + a_2 y\right) - \frac{\gamma_1}{2\pi}\theta\right] + \ldots \tag{3.10}$$

where $r = (x^2+y^2)^{1/2}$ and $\theta = \tan^{-1} y/x$. γ_0 is the vortex strength related to the lift, d_1 the doublet strength based on the cross-sectional area of the profile and e_1 related to the pitching moment of the airfoil. The coefficients a_1, a_2 and b_2 are functions of the porosity parameter P. γ_1 is the circulation induced in the higher order term.

3.2.3 Inner Limit

Near the airfoil, the characteristic length scale is the chord of the model. Thus the variables are scaled accordingly

$$X = Hx, \qquad Y = Hy \tag{3.11}$$

The governing equation, Equation (3.1) and the boundary condition on the airfoil, Equation (3.2) are then written in terms of the inner variables as

$$\phi_{XX} + \phi_{YY} = 0 \tag{3.12}$$

$$\phi_Y(X, \pm 0) = \pm F_X - \alpha \tag{3.13}$$

with X, Y fixed while $H \to \infty$. The potential can be expanded as

$$\phi\left(X,Y;\frac{1}{H}\right) = \Phi_0(X,Y) + \frac{1}{H}\Phi_1(X,Y) + \frac{1}{H^2}\Phi_2(X,Y) + \ldots \tag{3.14}$$

Substituting into the governing equation, Equation (3.12) and the boundary condition Equation (3.13), we have

$$\Phi_{n_{XX}} + \Phi_{n_{YY}} = 0, \qquad n = 0, 1, 2, \ldots \tag{3.15}$$

$$\Phi_{0_Y}(X, \pm 0) = \pm F_X - \alpha \tag{3.16}$$

$$\Phi_{1_Y}(X, \pm 0) = 0, \qquad n = 1, 2, \ldots \tag{3.17}$$

The zero order solution is that of a thin airfoil in free air and can be obtained for the thickness and the lifting cases respectively. The inner solution around the airfoil, however, cannot satisfy the boundary condition at the tunnel wall and has to be matched with the outer solutions. In preparing for the matching process, the inner solution Φ_0 is expanded as $X, Y \to \infty$

$$\Phi_0 \sim -\frac{\Gamma_0}{2\pi}\theta + \frac{D_1}{2\pi}\frac{X}{R^2} + \frac{E_1}{2\pi}\frac{Y}{R^2} + \ldots \tag{3.18}$$

where $\Gamma_0 = \int_{-½}^{½} \Delta u dX$, $D_1 = \int_{-½}^{½} \Delta Y dX$, $E_1 = \int_{-½}^{½} \Delta u X dX$

and $R = (X^2+Y^2)^{½}$

Γ_0 is the circulation, D_1 the displacement and E_1 the pitching moment of the airfoil.

The higher order potential Φ_n, satisfying the homogeneous boundary condition Equation (3.17) on the airfoil surface, can be written in its asymptotic form as $R \to \infty$ [3.10]

$$\Phi_n(X,Y) \sim C_n XY + A_n X + B_n Y - \frac{\Gamma_n}{2\pi}\theta + \ldots, \qquad n = 1, 2, \ldots \tag{3.19}$$

where Γ_n is the circulation which may be induced in the higher order solutions.

3.2.4 Matching Procedure

We have, so far, dealt with the two asymptotic limits of the problem separately. For the outer limit, the tunnel height is fixed and the airfoil shrinks to a singular point and for the inner limit, the airfoil chord is fixed and the tunnel height tends to infinity. In between these two solutions approach each other asymptotically. To match these two expansions we follow Van Dyke's principle that the inner expansion of the outer solution matches the outer expansion of the inner solution [3.3]. The inner expansion of the outer solution, Equation (3.10), is written here as:

$$\phi \sim -\frac{\gamma_0}{2\pi}(\theta + a_1 y + a_2 xy) + \frac{1}{H}\left[\frac{d_1}{2\pi}\left(\frac{x}{r^2} + b_2 x\right)\right] + \frac{1}{H}\left[-\frac{\gamma_1}{2\pi}\theta + \frac{e_1}{2\pi}\left(-\frac{y}{r^2} + a_2 y\right)\right] + \ldots \tag{3.20}$$

The outer expansion of the inner solution written in the outer variables gives

$$\phi \sim -\frac{\Gamma_0}{2\pi}\theta + \frac{D_1}{2\pi H}\frac{x}{r^2} + \frac{E_1}{2\pi H}\frac{y}{r^2} + \left(A_1 x + B_1 y - \frac{\Gamma_1}{2\pi H}\theta\right) + \frac{1}{H}\left(C_2 Hxy + A_2 x + B_2 y - \frac{\Gamma_2}{2\pi H}\theta + \ldots\right) + \ldots \tag{3.21}$$

Comparing these two expressions, we have

$$\gamma_0 = \Gamma_0, \qquad d_1 = D_1, \qquad e_1 = E_1$$

$$-\frac{\gamma_0 a_1}{2\pi} = B_1, \qquad 0 = A_1, \qquad -\frac{\gamma_0 a_2}{2\pi} = C_2,$$

$$\gamma_1 = \Gamma_1, \qquad \frac{d_1 b_2}{2\pi} = A_2, \qquad \frac{e_1 a_2}{2\pi} = B_2 \tag{3.22}$$

The matching procedure relates systematically the flow fields around the airfoil and near the tunnel walls. The zero order inner solution is that of the thin airfoil in free air. The first order outer solution is the classical interference solution with the airfoil shrinking to a singular point, yielding an angle of attack change, $\Delta\alpha$, having a value $-\gamma_0 a_1/2\pi$. This in turn generates additional circulation γ_1 of the same order. The second order solution gives the blockage with the change of free stream velocity Δu equal to $d_1 b_2/2\pi$. In a similar manner, higher order solutions can be obtained. The outer solution forms the outer boundary condition for the inner problem. The inner solution, on the other hand, provides the singularities for the outer problem. The approximate solutions of the original boundary value problem can now be constructed from the asymptotic solutions. The accuracy of approximate solutions can be improved systematically by considering higher order terms.

3.3 Transonic Flow

3.3.1 Formulation

At transonic speeds the governing equation of the flow is nonlinear. Following the procedure presented in the previous section the formulation is again developed within the framework of small disturbance theory. In transonic flows the small disturbance equation can be written as [3.11]

$$[K - (\gamma+1)\,\tilde{\phi}_{\tilde{x}}]\,\tilde{\phi}_{\tilde{x}\tilde{x}} + \tilde{\phi}_{\tilde{y}\tilde{y}} = 0 \tag{3.23}$$

where $K = \dfrac{1 - M^2}{M^{2m}\, t^{2/3}}$

$\tilde{\phi} = t^{-2/3}\, M^n\, \phi$

$\tilde{y} = t^{1/3}\, M^m \bar{y}$

$\tilde{x} = \bar{x}$

K is the transonic similarity parameter, M the free stream Mach number and t the maximum thickness of the airfoil. The velocity potential $\tilde{\phi}$ and the co-ordinates x, y have been scaled by the transonic similarity rule. The boundary condition on the airfoil is

$$\tilde{\phi}_{\tilde{y}}\,(\tilde{x}, \pm 0) = M^{n-m}\left[\pm f_{\tilde{x}} - \frac{\alpha}{t}\right], \qquad -\frac{1}{2} \leqslant \tilde{x} \leqslant \frac{1}{2} \tag{3.24}$$

where f is the thickness distribution of the airfoil. The tunnel walls are considered to be perforated. The boundary conditions at the walls are therefore

$$\tilde{\phi}_{\tilde{x}} \pm \frac{1}{P}\tilde{\phi}_{\tilde{y}} = 0 \qquad \text{at} \qquad \tilde{y} = \pm \tilde{H} \tag{3.25}$$

where $\tilde{H} = t^{1/3} M^m H, \qquad \tilde{P} = t^{-1/3} M^{-m} P$

are the scaled tunnel half height and porosity factors respectively. In transonic flow shock waves may occur in the flow field and the shock condition is specified as

$$[\![(K\tilde{\phi}_{\tilde{x}} - \frac{\gamma+1}{2}\tilde{\phi}_{\tilde{x}}^{\,2}) - (\tilde{\phi}_{\tilde{y}})\,\tilde{x}^{D}_{\tilde{y}}]\!] = 0$$

$$[\![\tilde{\phi}]\!] = 0 \tag{3.26}$$

where the symbol $[\![\ ]\!]$ denotes the difference in the quantities involved across the shock and $\tilde{x}^D$ is the shape of the shock wave.

3.3.2 Outer Limit

Away from the airfoil, the length variables are scaled by $\tilde{H}$ as

$$x = \frac{\tilde{x}}{\tilde{H}}, \qquad y = \frac{\tilde{y}}{\tilde{H}} \tag{3.27}$$

With x, y fixed as $\tilde{H} \to \infty$, the airfoil again shrinks to a point singularity. The potential $\tilde{\phi}$ is expanded in $1/\tilde{H}$ as

$$\phi\left(x,y;\frac{1}{H}\right) = \phi_0\,(x,y) + \frac{1}{H}\phi_1\,(x,y) + \frac{\log H}{H}\phi_2\,(x,y) + \ldots \tag{3.28}$$

where the tilde symbol has been dropped for convenience. For nonlinear compressible flow logarithmic terms exist in the far field solution [3.12] and are included in the expansion for matching with the inner solution. The equations for each order are respectively:

$$K\phi_{0_{xx}} + \phi_{0_{yy}} = 0$$

$$K\phi_{1_{xx}} + \phi_{1_{yy}} = (\gamma+1)\,\phi_{0_x}\,\phi_{0_{xx}}$$

$$K\phi_{2_{xx}} + \phi_{2_{yy}} = 0 \tag{3.29}$$

with the boundary conditions depending on the order of the singularity of the zero order solution,

$$\phi_{0_x} \pm \frac{1}{P}\phi_{0_y} = -\frac{1}{H}\left(\phi_{1_x} \pm \frac{1}{P}\phi_{1_y}\right)$$

$$\phi_{0_x} \pm \frac{1}{P}\phi_{0_y} = -\frac{\log H}{H}\left(\phi_{2_x} \pm \frac{1}{P}\phi_{2_y}\right)$$

(3.30)

The inner boundary condition is now lost and is replaced by matching with the inner solutions. The equations for ϕ_0 and ϕ_2 can be put into the Laplacian form with a transformation in the x-co-ordinate

$$x^* = \frac{x}{\sqrt{K}} \tag{3.31}$$

The boundary value problems of these two terms are therefore similar to those discussed in Chapter 4. The ϕ_1 equation has a non-homogeneous term containing the zero order solution ϕ_0. Its solution provides the nonlinear compressibility contribution to the problem. The inner expansion of the outer solution can be written as [3.4]

$$\phi \sim -\frac{\gamma_0}{2\pi}(\theta + a_1 y + a_2 xy) + \frac{1}{H}\left[\frac{d_1}{2\pi\sqrt{K}}\left(\frac{x}{r^2} + \frac{b_2}{K}x\right)\right] + \frac{\sqrt{K}}{H}\left[\frac{e_1}{2\pi}\left(-\frac{y}{r^2} + \frac{a_2}{K}y\right)\right] + \frac{\log H}{H}\frac{d_2}{2\pi\sqrt{K}}\frac{x}{r^2}$$

$$+\frac{1}{H}\left[\frac{\gamma+1}{4\pi^2 K}\left(\frac{\gamma_0}{2}\right)^2 \frac{\log r}{r}\cos\theta - \frac{r+1}{16\pi^2 K}\left(\frac{\gamma_0}{2}\right)^2 \frac{\cos 3\theta}{r} - \frac{\gamma_1}{2\pi}\theta\right] + \ldots \tag{3.32}$$

where $r = (x^2 + Ky^2)^{1/2}$ and $\theta = \tan^{-1}\dfrac{\sqrt{K}y}{x}$

The first two terms are the solution of the homogeneous equations and are therefore similar to those given in Equation (3.10) for subsonic flows. The other terms come from the nonhomogeneous equation representing the nonlinear compressibility of the outer flow.

3.3.3 Inner Limit

The inner variables are scaled as

$$X = Hx, \qquad Y = Hy \tag{3.33}$$

The inner expansion of the disturbance potential up to the second order has the form

$$\phi\left(X,Y;\frac{1}{H}\right) = \Phi_0(X,Y) + \frac{1}{H}\Phi_1(X,Y) + \frac{1}{H^2}\Phi_2(X,Y) + \ldots \tag{3.34}$$

The corresponding equations are therefore

$$[K - (\gamma+1)\Phi_{0_X}]\Phi_{0_{XX}} + \Phi_{0_{YY}} = 0,$$

$$[K - (\gamma+1)\Phi_{0_X}]\Phi_{1_{XX}} - (\gamma+1)\Phi_{0_{XX}}\Phi_{1_X} + \Phi_{0_{YY}} = 0$$

$$[K - (\gamma+1)\Phi_{0_X}]\Phi_{2_{XX}} - (\gamma+1)\Phi_{0_{XX}}\Phi_{2_X} + \Phi_{2_{YY}} = (\gamma+1)\Phi_{1_X}\Phi_{1_{XX}}$$

(3.35)

and the boundary conditions on the airfoil are

$$\Phi_{0_Y}(X, \pm 0) = F_X - \frac{\alpha}{t}, \qquad -\frac{1}{2} \leqslant X \leqslant \frac{1}{2}$$

$$\Phi_{n_Y}(X, \pm 0) = 0, \qquad n = 1, 2, 3 \ldots$$

(3.36)

The zero order problem consists of the nonlinear small disturbance equation and the corresponding boundary condition on the airfoil. The solution is the free air solution of a thin airfoil in transonic flow. The first order equation is linear with coefficients containing the zero order solution. The inner boundary condition is homogeneous and the outer boundary condition is provided by matching with the outer solution.

The outer expansion of the inner solution up to the second order can be written as [3.4], [3.3]

$$\phi \sim -\frac{\Gamma_0}{2\pi}\theta + \frac{\gamma+1}{4K}\left(\frac{\Gamma_0}{2\pi}\right)^2 \frac{\log R}{R}\cos\theta + \frac{1}{H}\left[\frac{D_1}{2\pi\sqrt{K}}\cos\theta + \frac{E_1}{2\pi\sqrt{K}}\sin\theta - \frac{\gamma+1}{16K}\left(\frac{\Gamma_0}{2\pi}\right)^2 \cos 3\theta\right] + \frac{1}{H}\left[A_1 X + B_1 Y - \frac{\Gamma_1}{2\pi}\theta + \ldots\right] + \frac{1}{H^2}\left[C_2 XY + A_2 X + B_2 Y - \frac{\Gamma_2}{2\pi}\theta + \ldots\right] + \ldots \tag{3.37}$$

where $R = (X^2 + KY^2)^{1/2}$ and $\theta = \tan^{-1}\frac{\sqrt{K}Y}{X}$

Again, Γ_0 is the circulation of the airfoil, D_1 and E_1 are the doublet strength with axes along the X- and Y- direction respectively. The nonlinearity of the transonic equation appears as in the logarithmic and the high degree cosine terms. The first order solutions include the induced flow components A_1 and B_1 and the additional circulation Γ_1.

3.3.4 Matching

The inner expansion of the outer solution, Equation (3.32), is written in terms of x*, y [see Equation (3.31)]

$$\phi \sim -\frac{\gamma_0}{2\pi}(\theta + a_1 y + a_2 xy) + \frac{1}{\sqrt{K}H}\left[\frac{d_1}{2\pi\sqrt{K}}\left(\frac{x^*}{r^{*2}} + b_2 x^*\right)\right] + \frac{1}{\sqrt{K}H}\left[\frac{e_1}{2\pi}\left(-\frac{y}{r^{*2}} + a_1 y\right)\right] + \frac{\log H}{H}\frac{d_2}{2\pi K}\frac{x^*}{r^{*2}} + \frac{1}{H}\left[\frac{\gamma+1}{4\pi^2 K}\left(\frac{\gamma_0}{2}\right)^2 \frac{\log\sqrt{K}r^*}{\sqrt{K}r^*}\frac{\cos 3\theta}{\sqrt{K}r^*} - \frac{\gamma_1}{2\pi}\theta\right] + \ldots \tag{3.38}$$

where $r^* = r/\sqrt{K}$

The outer expansion of the inner solution, Equation (3.36), written in the outer variables x*, y has the form

$$\phi \sim -\frac{\Gamma_0}{2\pi}\theta + \frac{\gamma+1}{4K}\left(\frac{\Gamma_0}{2\pi}\right)^2 \frac{\log\sqrt{K}Hr^*}{\sqrt{K}Hr^*}\cos\theta + \frac{1}{\sqrt{K}H}\left[\frac{D_1}{2\pi\sqrt{K}}\frac{x^*}{r^*} + \frac{E_1}{2\pi\sqrt{K}}\frac{y^*}{r^{*2}} - \frac{\gamma+1}{16K}\left(\frac{\Gamma_0}{2\pi}\right)^2 \frac{\cos 3\theta}{r^*}\right] + \frac{1}{H}\left[A_1\sqrt{K}Hx^* + B_1 Hy - \frac{\Gamma_1}{2\pi}\theta\right] + \frac{1}{H^2}\left[C_2\sqrt{K}H^2 x^* y + A_2\sqrt{K}Hx^* + B_2 Hy - \frac{\Gamma_2}{2\pi}\theta\right] + \ldots \tag{3.39}$$

Comparing these two expressions, we have

$$\gamma_0 = \Gamma_0, \qquad d_1 = D_1, \qquad e_1 = E_1;$$

$$-\frac{\gamma_0 a_1}{2\pi} = B_1, \qquad d_2 = \frac{\gamma+1}{4\sqrt{K}}\frac{\Gamma_0^2}{2\pi}, \qquad -\frac{\gamma_0 a_2}{2\pi\sqrt{K}} = C_2,$$

$$0 = A_1, \qquad \frac{d_1 b_2}{2\pi K^{3/2}} = A_2, \qquad \frac{e_1 a_2}{2\pi K^{1/2}} = B_2 \tag{3.40}$$

Aside from the nonlinear contributions the matching conditions are similar to those of the subsonic flow discussed in Section 3.2.4. The matching condition shows that the wall constraint induces an angle of attack change in the outer region. This additional angle of attack, up to the first order, is the same as that obtained by the linear interference theory. This will in turn generate additional lift with circulation Γ_1 of the same order. The displacement effect due to the wall constraint is of the order 1/H. The matching condition shows contributions from both the linear solution, as in the subsonic flow, and from the transonic nonlinear solution. The nonlinear solutions are shown to be proportional to the square of the circulation γ_0 and do not vanish as the airfoil thickness tends to zero, as long as lift persists. Analysis up to the second order for the solid wall condition can be found in Reference [3.6].

The asymptotic analysis has brought out the essential features of the wall interference at transonic speeds without calculating the flow field completely inside the tunnel. It shows that up to the first order, the angle of attack correction is identical to that for the linear subsonic flow. For blockage correction, aside from the displacement of the doublet based on the cross-sectional area of the airfoil as in the linear subsonic flow, a doublet due to lift is induced resulting from the nonlinear compressibility of the flow. The latter has been grouped with the logarithmic term to form an approximate expression for the effective doublet [3.5]. For moderate and high lift the blockage due to the nonlinear effect can be quite appreciable in comparison with that due to the geometry of the model. In Reference [3.5] it is shown that for a NACA0012 airfoil model in a tunnel with H equal to 3, at Mach number of 0.8 and lift coefficient 0.55, the blockage from the effective doublet is 20% of that due to the geometry of the airfoil.

The results shown by the asymptotic analysis have also been obtained by solving the transonic interference problem numerically [3.14]. In the numerical solution the wall interference is taken as a perturbation to the free air flow and both the free air and the perturbation equations are solved numerically. The results show that the angle of attack correction is practically the same as that obtained by linear subsonic theory and the Mach number correction due to blockage takes a higher value than that of the linear theory. The numerical method, however, is not capable to provide the physical interpretation as clearly as the asymptotic analysis. Interference flow field around the airfoil can also be calculated by the asymptotic method by solving the perturbation equations of the inner limit. These equations are linear with coefficients containing the zero order solutions and can be solved numerically. Detailed calculation of the interference flow field around the airfoil up to the first order is given in Reference [3.6] for solid wall tunnel. Excellent agreement with numerical solutions of the nonlinear equations is obtained for a value of H as low as unity, at the extreme limit of the asymptotic theory.

REFERENCES

[3.1] Prandtl, L. *Tragflügeltheorie, Part II.* Nachrichten der K. Gesellschaft der Wissenschaften zu Göttingen, 1919.

[3.2] Prandtl, L.; Tietjens, O.G. *Applied Hydro- and Aerodynamics.* Dover, N.Y., 1957.

[3.3] Van Dyke, M. *Perturbation Methods in Fluid Mechanics.* Parabolic Press, Palo Alto, California, 1975.

[3.4] Chan, Y.Y. *A Singular Perturbation Analysis of Two-Dimensional Wind Tunnel Interferences.* Journal of Applied Mathematics and Physics (ZAMP), Vol. 31, 1980, pp. 605-619.

[3.5] Chan, Y.Y. *Lift Effect on Transonic Wind Tunnel Blockage.* Journal of Aircraft, Vol. 17, 1980, pp. 915-916.

[3.6] Cole, J.D.; Malmuth, N.D.; Zeigler, F. *An Asymptotic Theory of Solid Tunnel Wall Interference on Transonic Airfoils.* AIAA 82-0933, June 1982.

[3.7] Lifshits, Y.B.; Fonarev, A.S. *Effect of Flow Boundaries on Parameters of Transonic Flows Around Bodies of Revolution.* Fluid Dynamics, Vol. 13, 1978, pp. 393-399.

[3.8] Blynskaya, A.A.; Lifshits, Y.B. *Transonic Flows Around an Airfoil in Wind Tunnels.* Fluid Dynamics, Vol. 15, 1981, pp. 711-718.

[3.9] Mokry, M. *Higher-Order Theory of Two-Dimensional Subsonic Wall Interference in a Perforated Wall Wind Tunnel.* Aero Report LR-553, National Research Council Canada, 1971.

[3.10] Batchelor, G.K. *Introduction to Fluid Dynamics.* Cambridge University Press, 1967, pp. 124-130.

[3.11] Murman, E.M. *Computation of Wall Effects in Ventilated Transonic Wind Tunnel.* AIAA Paper 72-1007, 1972.

[3.12] Ludford, G.S.S. *The Behaviour at Infinity of the Potential Function of a Two-Dimensional Subsonic Compressible Flow.* J. Math. and Physics, Vol. 25, 1951, pp. 117-130.

[3.13] Cook, L.P.; Cole, J.D. *Lifting Line Theory for Transonic Flow.* SIAM J. Applied Mathematics, Vol. 35, 1978, pp. 209-228.

[3.14] Chan, Y.Y. *Perturbation Analysis of Transonic Wind Tunnel Wall Interference.* Journal of Aircraft, Vol. 17, 1980, pp. 409-411.

4.0 CLASSICAL POROUS-SLOTTED WALL THEORY

4.1 General Properties

The theory is based on an infinite test section between two parallel walls, on which the porous-slotted boundary condition (2.65) is satisfied, and the concept of wall interference by Prandtl [4.1]. The latter can be characterized in the following way.

It is assumed that in the vicinity of the walls there is small disturbance flow that may be described by the linearized, subsonic potential flow equation

$$\beta^2 \frac{\partial^2 \phi}{\partial x^2} + \frac{\partial^2 \phi}{\partial y^2} = 0 \tag{4.1}$$

where

$$\beta = \sqrt{1 - M_\infty^2} \tag{4.2}$$

is the Prandtl-Glauert factor and M_∞ is the Mach number far upstream. Experience shows that the linearization is possible up to very high values of $M_\infty < 1$ since the flow is essentially parallel to the tunnel wall.

In the linearized flow region between the contour C, encircling the airfoil, and the wind tunnel walls, see Figure 4.1, the disturbance velocity potential ϕ is decomposed as

$$\phi = \phi_F + \phi_W \tag{4.3}$$

Here ϕ_F denotes the potential due to the airfoil in free air, satisfying Equation (4.1) in the exterior of C and obeying the far field condition

$$\frac{\partial \phi_F}{\partial x}, \frac{\partial \phi_F}{\partial y} \to 0 \qquad \text{as} \qquad r = \sqrt{x^2 + (\beta y)^2} \to \infty \tag{4.4}$$

Since the knowledge of ϕ_F is required only near the walls, the actual airfoil boundary condition does not directly enter the problem and it is sufficient to represent ϕ_F by singularities placed at the airfoil position (origin of the co-ordinate system).

The potential ϕ_W, representing the induced effect of the wind tunnel walls, is called the wall interference potential. It is assumed to be nonsingular inside the test section, i.e. satisfying

$$\beta^2 \cdot \frac{\partial^2 \phi_W}{\partial x^2} + \frac{\partial^2 \phi_W}{\partial y^2} = 0, \qquad |y| < \frac{h}{2} \tag{4.5}$$

where h is the test section height. In other words, the interference flow is assumed to be a perturbation to the mainstream. Accordingly, the derivatives of ϕ_W with respect to x and y, calculated at the airfoil position, are interpreted as corrections to the x and y components of the (unit) tunnel stream velocity. The higher derivatives of ϕ_W describe a nonuniform distortion of the wind tunnel flow that does not exist in free air but, depending on its magnitude and accuracy requirements, the wind tunnel measurement may still qualify as "correctable"; for more discussion see Reference [4.2].

In our specific case, ϕ satisfies the porous-slotted wall boundary condition (2.65). Using Equation (4.3) we have for an airfoil located midway between the tunnel walls

$$\frac{\partial}{\partial x}\left[\left(\phi_F + \phi_W\right) + K\frac{\partial}{\partial y}\left(\phi_F + \phi_W\right)\right] + \frac{1}{P}\frac{\partial}{\partial y}\left(\phi_F + \phi_W\right) = 0, \qquad -\infty < x < \infty, \qquad y = \frac{h}{2} \tag{4.6}$$

$$\frac{\partial}{\partial x}\left[\left(\phi_F + \phi_W\right) - K\frac{\partial}{\partial y}\left(\phi_F + \phi_W\right)\right] - \frac{1}{P}\frac{\partial}{\partial y}\left(\phi_F + \phi_W\right) = 0, \qquad -\infty < x < \infty, \qquad y = -\frac{h}{2} \tag{4.7}$$

where K is the slot parameter and P is the porosity parameter.

Equations (4.5), (4.6) and (4.7) describe the boundary value problem for the wall interference potential ϕ_W. The free air potential ϕ_F, which is assumed known for a given airfoil geometry and aerodynamic force measurements, provides Equations (4.6) and (4.7) with the necessary nonhomogeneous term, so that the solution is in general nontrivial.

Without going into the details of existence and uniqueness, we may note the following properties of the above problem. If $\tilde{\phi}_W$ is its solution, then is also

$$\phi_W = \tilde{\phi}_W + C \tag{4.8}$$

Additional solutions are

$$\phi_W = \tilde{\phi}_W + Ax + C \qquad \text{if} \qquad P = 0 \tag{4.9}$$

and

$$\phi_W = \tilde{\phi}_W + By + C \qquad \text{if} \qquad \frac{1}{P} = 0 \tag{4.10}$$

where A, B and C denote arbitrary constants. As we shall see later, the above properties allow us to satisfy the far upstream condition

$$\phi \to 0 \qquad \text{as} \qquad x \to -\infty \tag{4.11}$$

but not necessarily the far downstream condition

$$\phi \to 0 \qquad \text{as} \qquad x \to \infty \tag{4.12}$$

In any case, Equations (4.3), (4.4) and (4.11) imply that it is possible to achieve

$$\frac{\partial \phi_W}{\partial x}, \frac{\partial \phi_W}{\partial y} \to 0 \qquad \text{as} \qquad x \to -\infty \tag{4.13}$$

i.e. zero tunnel disturbance far upstream, which is convenient from the point of view of interpreting ϕ_W as the wall interference potential.

The most important property follows from linearity of Equations (4.5), (4.6) and (4.7). For a thin airfoil in subsonic flow, we can expand ϕ_F in the multipole expansion [4.3], [4.4]

$$\phi_F = \phi_F{}^{\sigma} + \phi_F{}^{\gamma} + \phi_F{}^{\mu} + \phi_F{}^{\omega} + \ldots \tag{4.14}$$

where the right hand terms denote potentials due to a

source of strength σ

$$\phi_F{}^{\sigma} = \frac{\sigma}{2\pi\beta} \log \sqrt{x^2 + (\beta y)^2} \tag{4.15}$$

vortex of strength γ

$$\phi_F{}^{\gamma} = -\frac{\gamma}{2\pi} \operatorname{atan} \frac{\beta y}{x} \tag{4.16}$$

doublet in the x direction of strength μ

$$\phi_F{}^{\mu} = \frac{\mu}{2\pi\beta} \frac{x}{x^2 + (\beta y)^2} \tag{4.17}$$

doublet in the y direction of strength ω

$$\phi_F{}^{\omega} = \frac{\omega}{2\pi} \frac{\beta y}{x^2 + (\beta y)^2} \tag{4.18}$$

The streamline patterns characterizing the above singularities are schematically shown in Figure 4.2. Since the (complex) velocities derived from potentials (4.15) to (4.18) are terms of a Laurent expansion, the singularity strengths can be easily obtained by contour integration. For a thin airfoil of a small incidence and camber we obtain [4.4]

$$\sigma = \frac{1}{2} c\, C_{DW} \tag{4.19}$$

$$\gamma = \frac{1}{2} c\, C_L \tag{4.20}$$

$$\mu = c^2 A \tag{4.21}$$

$$\omega = \frac{1}{2} c^2 C_M \tag{4.22}$$

where c is the airfoil chord, C_{DW} the wake drag coefficient, C_L the lift coefficient, A the cross-sectional area of the airfoil nondimensionalized by c^2, and C_M is the pitching moment coefficient about the origin of the co-ordinate system. In particular, if the origin is placed at the mid-chord point

$$\omega = \frac{1}{2} c^2 \left(\frac{1}{4} C_L + C_{M_{c/4}} \right) \tag{4.23}$$

where $C_{M_{c/4}}$ is the quarter-chord pitching moment coefficient.

For transonic inviscid flow governed by the small disturbance equation

$$\beta^2 \frac{\partial^2 \phi}{\partial x^2} + \frac{\partial^2 \phi}{\partial y^2} = \frac{\kappa + 1}{2} \frac{\partial}{\partial x} \left(\frac{\partial \phi}{\partial x} \right)^2 \tag{4.24}$$

the far field of a thin airfoil is dominated by the vortex and doublet terms

$$\phi_F = \phi_F{}^{\gamma} + \phi_F{}^{\mu} \tag{4.25}$$

as established from Green's identities by Klunker [4.5]. The vortex strength, determined by circulation around the airfoil, is again given by Equation (4.20). However, the doublet strength contains, besides the airfoil cross-sectional area, also flow field contributions due to the nonlinear term on the right hand side of Equation (4.24). Very far from the airfoil, however, the nonlinear term becomes negligible, so that the far field is again governed by the linearized Equation (4.1).

Using singular perturbation analysis of the problem, Chan [4.6], [4.7] derived an approximate formula for the transonic doublet strength

$$\mu = c^2 (A + \delta A) \tag{4.26}$$

where the nonlinear contribution to the airfoil area is

$$\delta A = \frac{\kappa + 1}{2\pi\beta} M_\infty{}^{\frac{7}{4}} \left(\frac{C_L}{4} \right)^2 \left\{ \frac{7}{4} + \log \left[M_\infty^{\frac{1}{2}} \left(\frac{t}{c} \right)^{\frac{1}{3}} \frac{|y|}{c} \right] \right\} \tag{4.27}$$

Here κ (=1.4) is the ratio of specific heats and t is the (maximum) airfoil thickness. The latter enters the picture through the transonic similarity parameter

$$k = \frac{1 - M_\infty{}^2}{M_\infty \left(\frac{t}{c} \right)^{\frac{2}{3}}} \tag{4.28}$$

It may be observed that δA grows above all limits with increasing the distance $|y|$ from the airfoil. However, this is of little concern, since

$$\frac{\log |y|}{y^2} \to 0 \qquad \text{as} \qquad |y| \to \infty$$

so that the doublet potential vanishes at large distances from the airfoil as for subsonic flow. In practice, $|y|$ is limited by the test section semi-height.

The value δA, Equation (4.27), represents the first order term of an asymptotic expansion (A is its zero order term). The expansion is meaningful only if the perturbation parameter

$$H = M_\infty{}^{\frac{1}{2}} \left(\frac{t}{c} \right)^{\frac{1}{3}} \frac{|y|}{c} \tag{4.29}$$

is greater than one [4.7]. For a given airfoil and Mach number this is the case only if the airfoil chord to tunnel height ratio, c/h, is sufficiently small. Table 4.1, adopted from Reference [4.7], compares δA with A for typical tunnel conditions. It is observed that δA, since it is proportional to $C_L{}^2$, becomes important only for higher values of lift. The transonic contribution to the source strength, depending on the effective thickness of the airfoil at the trailing edge, has been treated by Smithmeyer and Murman [4.8].

Having specified the far field potential ϕ_F, the wall interference problem, Equations (4.5), (4.6) and (4.7), is then solved separately for the singularities (4.15) to (4.18) and the solutions are denoted $\phi_W{}^{\sigma}$, $\phi_W{}^{\gamma}$, $\phi_W{}^{\mu}$ and $\phi_W{}^{\omega}$. In accordance with the aerodynamic parameters determining the singularity strengths (4.19) to (4.22), the wall effects associated with the above potentials are called the wake blockage, lift interference, solid blockage and pitching moment interference, respectively.

By the principle of linear superposition, the wall interference potential corresponding to the free air potential (4.14) is

$$\phi_W = \phi_W{}^{\sigma} + \phi_W{}^{\gamma} + \phi_W{}^{\mu} + \phi_W{}^{\omega} + \ldots \tag{4.30}$$

In the construction of the wall interference potential (4.30), another important property of the solution can be utilized [4.4]. Since

$$\phi_F{}^{\mu} = \frac{\mu}{\sigma} \frac{\partial}{\partial x} \phi_F{}^{\sigma} \tag{4.31}$$

$$\phi_F{}^{\omega} = \frac{\omega}{\gamma} \frac{\partial}{\partial x} \phi_F{}^{\gamma} \tag{4.32}$$

and Equations (4.5), (4.6) and (4.7) permit differentiation with respect to x, it is clear that

$$\phi_W{}^{\mu} = \frac{\mu}{\sigma} \frac{\partial}{\partial x} \phi_W{}^{\sigma} \tag{4.33}$$

$$\phi_W{}^{\omega} = \frac{\omega}{\gamma} \frac{\partial}{\partial x} \phi_W{}^{\gamma} \tag{4.34}$$

so that the wall interference problem needs to be actually solved only for the source and vortex. For solid tunnel walls this property was first utilized by Goldstein [4.3].

It would seem logical to start with analyzing the wake blockage, because the source is a fundamental singularity of the Laplace equation, from which all other singularities of Equation (4.14) are derived. However, since the source solution poses some additional difficulties compared to that of a vortex, we will deal with lift interference first.

4.2 Lift Interference

In free air the potential due to a point vortex at the origin is

$$\phi_F{}^{\gamma}(x,y) = -\frac{\gamma}{2\pi} \operatorname{atan} \frac{\beta y}{x} = -\frac{\gamma}{2\pi} \operatorname{atan} \frac{Y}{X} \tag{4.35}$$

where

$$X = \frac{x}{\beta h}$$

$$Y = \frac{y}{h} \tag{4.36}$$

are nondimensional co-ordinates that reduce Equation (4.5) to Laplace's equation. Applying the Fourier transform technique of Baldwin, Turner and Knechtel [4.9] and Wright [4.10] to the boundary value problem specified by Equations (4.5), (4.6), (4.7) and (4.35), we obtain

$$\tilde{\phi}_W{}^{\gamma}(x,y) = -\frac{\gamma}{2\pi} [J_1(X,Y) + J_2(X,Y)]$$

By the tilde above the symbol we indicate that this is a particular solution, which does not necessarily satisfy the far field condition (4.11). The right-hand side functions are

$$J_1(X,Y) = \int_0^{\infty} \frac{\frac{\beta}{P}}{g_D(s)} \sinh(2Ys) \cos(2Xs) \frac{ds}{s} \tag{4.37}$$

$$J_2(X,Y) = \int_0^{\infty} \frac{g_N(s)}{g_D(s)} \sinh(2Ys) \sin(2Xs) \frac{ds}{s} \tag{4.38}$$

where

$$g_D(s) = \left[\sinh(s) + Fs \cosh(s)\right]^2 + \left[\frac{\beta}{P} \cosh(s)\right]^2 \tag{4.39}$$

$$g_N(s) = \left\{(1 - Fs)\left[\sinh(s) + Fs \cosh(s)\right] - \left(\frac{\beta}{P}\right)^2 \cosh(s)\right\} e^{-s} \tag{4.40}$$

and

$$F = \frac{2K}{h} \tag{4.41}$$

is the nondimensionalized slot parameter.

We are not giving the details of the derivation here, since they may be found in Reference [4.10]. However, a word of caution is in order: as noticed by Catherall [4.11], in the derivation of J_1 one comes across the factor

$$\left\{(1 - Fs)\cosh(s) + \sinh(s) + Fs\cosh(s)\right\} e^{-s}$$

which has a similar structure as g_N except that its value is one. In the original derivation in Reference [4.10] it is not reduced to unity, presumably due to misprinting the last cosh as cos. The reduction is done properly in Reference [4.12], but not in [4.13], where the misprint is reproduced.

For porous walls, F = 0, the expressions (4.37) and (4.38) simplify to

$$J_1(X,Y) = \int_0^\infty \frac{\sin(\pi\tau)}{\cosh(s) + \cos(\pi\tau)} \sinh(Ys)\cos(Xs)\frac{ds}{s} \tag{4.42}$$

$$J_2(X,Y) = -\int_0^\infty \frac{e^{-s} + \cos(\pi\tau)}{\cosh(s) + \cos(\pi\tau)} \sinh(Ys)\sin(Xs)\frac{ds}{s} \tag{4.43}$$

where 2s is replaced by s and

$$\tau = \frac{2}{\pi}\,\mathrm{atan}\,\frac{P}{\beta} \tag{4.44}$$

For a transversally slotted wall it follows from Equation (2.33) that τ is equal to the open area ratio, namely

$$\tau = \frac{a}{\ell}$$

where a is the slot width and ℓ is the slot spacing.

The earlier used factor [4.13]

$$Q = \frac{1}{1 + \frac{\beta}{P}} \tag{4.45}$$

also varies on the interval $<0,1>$, but otherwise lacks physical significance, since it does not follow naturally from the porous wall theory. For comparison, τ and Q are plotted against P/β in Figure 4.3.

In order to make sure that the upstream condition (4.11) is satisfied, we evaluate the upstream limits of J_1 and J_2, Equations (4.37) and (4.38). Since

$$\frac{\beta}{P}\frac{\sinh(2Ys)}{s}$$

is a continuous, finite function on the interval $0 \leqslant s < \infty$, we obtain according to the Riemann-Lebesgue theorem [4.16]

$$\lim_{X \to \pm\infty} J_1(X,Y) = 0$$

The limiting values of J_2 are obtained from the Dirichlet integral [4.16]

$$\lim_{\lambda \to \pm\infty} \int_0^\infty G(s)\frac{\sin(\lambda s)}{s}\,ds = \pm\frac{\pi}{2}G(0+)$$

where G(s) is a function continuous on the interval $0 \leqslant s < \infty$. In our case $\lambda = 2X$ and

$$G(0+) = \lim_{s \to 0+} \left[\frac{g_N(s)}{g_D(s)} \sinh(2Ys) \right] = \begin{cases} 0 & , \quad \frac{1}{P} \neq 0 \\ \frac{2Y}{1+F} & , \quad \frac{1}{P} = 0 \end{cases}$$

Accordingly

$$\lim_{X \to \pm\infty} J_2(X,Y) = \begin{cases} 0 & , \quad \frac{1}{P} \neq 0 \\ \pm \frac{\pi}{1+F} Y & , \quad \frac{1}{P} = 0 \end{cases}$$

In order to make the interference potential vanish far upstream, we thus take

$$\phi_W^{\gamma}(x,y) = -\frac{\gamma}{2\pi} J(X,Y) \tag{4.46}$$

where

$$J(X,Y) = J_1(X,Y) + J_2(X,Y) + \frac{\pi}{1+F} Y \chi\left(\frac{1}{P}\right) \tag{4.47}$$

and χ is a (discontinuous) function defined as

$$\chi\left(\frac{1}{P}\right) = \begin{cases} 1 & , \quad \frac{1}{P} = 0 \\ 0 & , \quad \frac{1}{P} \neq 0 \end{cases} \tag{4.48}$$

Such a modification of the wall interference potential is clearly permissible, cf. Equation (4.10).

The integrals J_1 and J_2 can be converted into infinite series using the method of residues. This approach was first used by Murman [4.17], who was interested in asymptotic expansions of wall interference potentials for large $|x|$. The procedure involves heavy algebraic manipulations, but is in a great detail documented by Catherall [4.11], so that again only the result is presented here:

$$\phi_W^{\gamma}(x,y) = -\phi_F^{\gamma}(x,y) + \frac{\gamma}{2} \sum_{\gamma_j < 0} \frac{\sin(2Y\gamma_j)\, e^{-2X\gamma_j}}{\gamma_j [1 + F\cos^2(\gamma_j)]} , \qquad X < 0 \tag{4.49}$$

$$\phi_W^{\gamma}(x,y) = -\phi_F^{\gamma}(x,y) - \frac{\gamma}{2} \left\{ \sum_{\gamma_j > 0} \frac{\sin(2Y\gamma_j)\, e^{-2X\gamma_j}}{\gamma_j [1 + F\cos^2(\gamma_j)]} + \frac{2Y}{1+F} \chi\left(\frac{1}{P}\right) \right\} , \qquad X > 0 \tag{4.50}$$

where ϕ_F^{γ} is the free air singularity, given by Equation (4.35), and γ_j is the root of the transcendental equation

$$\tan(\gamma_j) = \frac{\beta}{P} - F\gamma_j \tag{4.51}$$

on the interval

$$\left(j - \frac{1}{2}\right)\pi < \gamma_j \leqslant \left(j + \frac{1}{2}\right)\pi$$

We may note that

$$g_D(i\gamma_j) = 0 \quad , \quad i = \sqrt{-1}$$

and thus the values $i\gamma_j$ are the poles of the integrands of J_1 and J_2. In the special case of porous walls we obtain

$$\gamma_j = -\frac{\pi}{2}\tau + \pi\left(j + \frac{1}{2}\right) \tag{4.52}$$

where τ is given by Equation (4.44). The fact that the poles are equidistant results in a great simplicity of the obtained corrections for porous walls, as we shall see in Section 4.6.

Going back to Equations (4.49) and (4.50) we may note that their difference is caused by the selection of different integration contours [4.11] for $X < 0$ and $X > 0$, imposed by the condition

$$e^{-2X\gamma_j} \to 0 \qquad \text{as} \qquad |X| \to \infty$$

If desired, the expression in the curly brackets of Equation (4.50) can be contracted to

$$\sum_{\gamma_j \geq 0} \frac{\sin(2Y\gamma_j)\, e^{-2X\gamma_j}}{\gamma_j\,[1 + F\cos^2(\gamma_j)]}$$

since $\gamma_j = \gamma_0 = 0$ is possible only if $1/P = 0$, in which case

$$\lim_{\gamma_0 \to 0} \frac{\sin(2Y\gamma_0)\, e^{-2X\gamma_0}}{\gamma_0\,[1 + F\cos^2(\gamma_0)]} = \frac{2Y}{1+F}$$

The infinite series formulas (4.49) and (4.50) are particularly suitable for large values of $|X|$, since then only a few terms are needed for achieving required accuracy. However, near $X = 0$, the integral representation (4.46) is more appropriate, particularly if the parameters P and F are close to zero. As experienced in Reference [4.11], in that case the series suffer from poor convergence.

4.3 Wake Blockage

In terms of the reduced co-ordinates, Equations (4.36), the potential due to a point source at the origin of the co-ordinate system can be written as

$$\phi_F{}^{\sigma}(x,y) = \frac{\sigma}{2\pi\beta} \log\sqrt{X^2 + Y^2} \tag{4.53}$$

Admittedly, the right hand sides of Equations (4.15) and (4.53) differ by a constant term, but both expressions have the same derivatives.

Observing that $\phi_F{}^{\sigma}$ is indeterminate as $|X| \to \infty$, it is natural to expect also a few extra complications with the corresponding wall interference potential $\phi_W{}^{\sigma}$. The Fourier solution of the problem described by Equations (4.5), (4.6), (4.7) and (4.53) is [4.10], [4.11]:

$$\tilde{\phi}_W{}^{\sigma}(x,y) = \frac{\sigma}{2\pi\beta}\,[I_1(X,Y) + I_2(X,Y)]$$

where

$$I_1(X,Y) = \int_0^{\infty} \frac{-\frac{\beta}{P}}{f_D(s)} \cosh(2Ys)\sin(2Xs)\,\frac{ds}{s}$$

$$I_2(X,Y) = \int_0^{\infty} \frac{f_N(s)}{f_D(s)} \cosh(2Ys)\cos(2Xs)\,\frac{ds}{s}$$

The denominator and numerator functions are

$$f_D(s) = \left[\cosh(s) + Fs\sinh(s)\right]^2 + \left[\frac{\beta}{P}\sinh(s)\right]^2 \tag{4.54}$$

$$f_N(s) = \left\{(1 - Fs)\,[\cosh(s) + Fs\sinh(s)] - \left(\frac{\beta}{P}\right)^2 \sinh(s)\right\} e^{-s} \tag{4.55}$$

It was again found by Catherall [4.11] that in the original derivation of I_1 in Reference [4.10] the term

$$\left\{(1 - Fs)\sinh(s) + \cosh(s) + Fs\sinh(s)\right\} e^{-s}$$

was not reduced to unity, since the factor $(1 - Fs)$ was dropped by mistake. The error, affecting the wake blockage formulas for slotted walls, is repeated in References [4.12] and [4.13], but not in [4.14].

To analyze the upstream behaviour of $\phi_W{}^\sigma$, we will first examine the far field values of I_1 and I_2. Since

$$\lim_{s\to 0}\left[\frac{-\frac{\beta}{P}}{f_D(s)}\cosh(2Ys)\right] = \begin{cases} 0 & , \quad P = 0 \\ -\frac{\beta}{P} & , \quad P \neq 0 \end{cases}$$

we obtain from the Dirichlet integral formula

$$\lim_{X\to\pm\infty} I_1(X,Y) = \begin{cases} 0 & , \quad P = 0 \\ \mp\frac{\pi}{2}\frac{\beta}{P} & , \quad P \neq 0 \end{cases}$$

In contrast to it, problems arise with I_2. It can be shown that for small values of s

$$\frac{f_N(s)}{f_D(s)}\frac{\cosh(2Ys)}{s} \simeq \frac{1}{s}$$

and thus the integral does not have a finite value. However, it is possible to calculate the far field values of its derivative

$$\frac{\partial I_2}{\partial X}(X,Y) = \int_0^\infty -2s\frac{f_N(s)}{f_D(s)}\cosh(2Ys)\sin(2Xs)\frac{ds}{s}$$

We have

$$\lim_{s\to 0}\left[-2s\frac{f_N(s)}{f_D(s)}\cosh(2Ys)\right] = \begin{cases} 2 & , \quad P = 0 \\ 0 & , \quad P \neq 0 \end{cases}$$

and thus, making use of Dirichlet's integral formula

$$\lim_{X\to\pm\infty}\frac{\partial I_2}{\partial X}(X,Y) = \begin{cases} \pm\pi & , \quad P = 0 \\ 0 & , \quad P \neq 0 \end{cases}$$

This result is consistent with the physical fact that the flux from a source cannot escape the test section if its walls are solid, so that the induced velocity disturbance is felt over the whole test section length. In order to obtain undisturbed velocity far upstream, it is enough to add the term πX to I_2 if $P = 0$, in accordance with Equation (4.9). Physically, the uniform velocity increment in the positive direction is equivalent to placing a sink (source of strength $-\sigma$) infinitely far downstream [4.15]. However, this alone does not make I_2 finite and if we are interested in the values of the interference potential $\phi_W{}^\sigma$, the expression for I_2 has to be modified. Using Catherall's approach [4.11], we set

$$I_1(X,Y) = \int_0^\infty \frac{-\frac{\beta}{P}}{f_D(s)}\left[\cosh(2Ys)\sin(2Xs) - \sin(2s)\right]\frac{ds}{s} \tag{4.56}$$

$$I_2(X,Y) = \int_0^\infty \frac{f_N(s)}{f_D(s)}\left[\cosh(2Ys)\cos(2Xs) - \cos(2s)\right]\frac{ds}{s} \tag{4.57}$$

Such a modification is clearly permissible, since the extra terms in the integrand add only a constant to $\tilde{\phi}_W{}^\sigma$, cf. Equation (4.8). With the help of the additional cosine term, the second integrand becomes zero at $s = 0$; the sine term is added to the first integrand for symmetry purposes.

For porous walls, $F = 0$, the expressions (4.56) and (4.57) reduce to

$$I_1(X,Y) = \int_0^\infty \frac{-\sin(\pi\tau)}{\cosh(s) - \cos(\pi\tau)}\left[\cosh(Ys)\sin(Xs) - \sin(s)\right]\frac{ds}{s} \tag{4.58}$$

$$I_2(X,Y) = \int_0^\infty \frac{e^{-s} - \cos(\pi\tau)}{\cosh(s) - \cos(\pi\tau)}\left[\cosh(Ys)\cos(Xs) - \cos(s)\right]\frac{ds}{s} \tag{4.59}$$

where τ is given by Equation (4.44).

Expanding I_1 and I_2, Equations (4.56) and (4.57), in infinite series, it is possible to show that $\phi_W{}^\sigma$, satisfying the upstream condition (4.11), is

$$\phi_W{}^\sigma (x,y) = \frac{\sigma}{2\pi\beta} I(X,Y) \tag{4.60}$$

where

$$I(X,Y) = I_1(X,Y) + I_2(X,Y) + \pi (X+1)\chi(P) - \pi \frac{\beta}{P}[\chi(P) - 1] - \pi C \tag{4.61}$$

and

$$\chi(P) = \begin{cases} 1 & , \quad P = 0 \\ 0 & , \quad P > 0 \end{cases} \tag{4.62}$$

in accordance with Equation (4.48). The constant C, as will be verified below, has the value

$$C = \sum_{\sigma_j > 0} \frac{e^{-2\sigma_j}}{\sigma_j [1 + F \sin^2(\sigma_j)]} \tag{4.63}$$

The infinite series expansions of $\phi_W{}^\sigma$ are [4.11]

$$\phi_W{}^\sigma (x,y) = -\phi_F{}^\sigma (x,y) + \frac{\sigma}{2\beta} \sum_{\sigma_j < 0} \frac{\cos(2Y\sigma_j)\, e^{-2X\sigma_j}}{\sigma_j [1 + F \sin^2(\sigma_j)]}, \qquad X < 0 \tag{4.64}$$

$$\phi_W{}^\sigma (x,y) = -\phi_F{}^\sigma (x,y) - \frac{\sigma}{2\beta} \left\{ \sum_{\sigma_j > 0} \frac{\cos(2Y\sigma_j)\, e^{-2X\sigma_j}}{\sigma_j [1 + F \sin^2(\sigma_j)]} - 2X\chi(P) + \frac{\beta}{P}[\chi(P) - 1] \right\}, \qquad X > 0 \tag{4.65}$$

where $\phi_F{}^\sigma$ is given by Equation (4.53) and σ_j is the solution of the transcendental equation

$$\cot(\sigma_j) = F\sigma_j - \frac{\beta}{P} \tag{4.66}$$

on the interval

$$(j-1)\pi < \sigma_j \leqslant j\pi$$

We may again note that

$$f_D(i\sigma_j) = 0, \qquad i = \sqrt{-1}$$

and thus $i\sigma_j$ are poles of the integrands of I_1 and I_2. For the porous wall wind tunnel the poles are again equidistant:

$$\sigma_j = -\frac{\pi}{2}\tau + \pi j \tag{4.67}$$

where τ is given by Equation (4.44).

From Equations (4.53) and (4.64) it is seen that the upstream condition (4.11) is satisfied for $\phi^\sigma = \phi_F{}^\sigma + \phi_W{}^\sigma$ but not for $\phi_W{}^\sigma$. As suggested in Reference [4.11], the inconvenient constant term $-\pi C$ in Equation (4.61) can be dropped, but then of course the upstream condition (4.11) is weakened to

$$\phi \to \frac{\sigma}{2\beta} C \qquad \text{as} \qquad x \to -\infty$$

and the infinite series expressions (4.64) and (4.65) have to be modified accordingly.

4.4 Solid Blockage

Using Equations (4.33) and (4.60), the wall interference potential induced by the doublet in the x direction is

$$\phi_W{}^{\mu}(x,y) = \frac{\mu}{2\pi\beta^2 h}\frac{\partial I}{\partial X}(X,Y) \tag{4.68}$$

where

$$\frac{\partial I}{\partial X}(X,Y) = \frac{\partial I_1}{\partial X}(X,Y) + \frac{\partial I_2}{\partial X}(X,Y) + \pi\chi(P) \tag{4.69}$$

This result agrees with the actual solution of the boundary value problem of Equations (4.5), (4.6), (4.7) and (4.17), as may be verified in References [4.9] and [4.11].

Similarly, applying Equation (4.33) to infinite series (4.64) and (4.65), we obtain

$$\phi_W{}^{\mu}(x,y) = -\phi_F{}^{\mu}(x,y) - \frac{\mu}{\beta^2 h}\sum_{\sigma_j<0}\frac{\cos(2Y\sigma_j)\,e^{-2X\sigma_j}}{1+F\sin^2(\sigma_j)}, \qquad X<0 \tag{4.70}$$

$$\phi_W{}^{\mu}(x,y) = -\phi_F{}^{\mu}(x,y) + \frac{\mu}{\beta^2 h}\sum_{\sigma_j\geqslant 0}\frac{\cos(2Y\sigma_j)\,e^{-2X\sigma_j}}{1+F\sin^2(\sigma_j)}, \qquad X>0 \tag{4.71}$$

The value $\sigma_j = \sigma_0 = 0$ comes into question only when $P = 0$, in which case

$$\frac{\cos(2Y\sigma_0)\,e^{-2X\sigma_0}}{1+F\sin^2(\sigma_0)} = 1$$

Again, the results agree with the evaluation of Equation (4.68) by the residue theorem, cf. Reference [4.11].

4.5 Pitching Moment Interference

From Equations (4.34) and (4.46), the wall interference potential induced by the doublet in the y direction is

$$\phi_W{}^{\omega}(x,y) = -\frac{\omega}{2\pi\beta h}\frac{\partial J}{\partial X}(X,Y) \tag{4.72}$$

where

$$\frac{\partial J}{\partial X}(X,Y) = \frac{\partial J_1}{\partial X}(X,Y) + \frac{\partial J_2}{\partial X}(X,Y) \tag{4.73}$$

Applying Equation (4.34) to infinite series (4.49) and (4.50), we obtain

$$\phi_W{}^{\omega}(x,y) = -\phi_F{}^{\omega}(x,y) - \frac{\omega}{\beta h}\sum_{\gamma_j<0}\frac{\sin(2Y\gamma_j)\,e^{-2X\gamma_j}}{1+F\cos^2(\gamma_j)}, \qquad X<0 \tag{4.74}$$

$$\phi_W{}^{\omega}(x,y) = -\phi_F{}^{\omega}(x,y) + \frac{\omega}{\beta h}\sum_{\gamma_j>0}\frac{\sin(2Y\gamma_j)\,e^{-2X\gamma_j}}{1+F\cos^2(\gamma_j)}, \qquad X>0 \tag{4.75}$$

where $\phi_F{}^{\omega}$ is given by Equation (4.18).

The effect of the pitching moment is of lesser importance than that of a lift and has generally been given little attention in the literature, so that it is not too surprising that Equations (4.72) to (4.75) appear to be a new result. With the help of the doublet in the y direction it is possible to place the vortex, representing the lift effect, at the origin of the co-ordinate system and not necessarily at the centre of pressure. This is of particular value for conditions near zero lift.

4.6 Wall Interference Corrections

In most practical cases we will be interested in the following quantities:

velocity (blockage) correction

$$u_W(x,y) = \frac{\partial\phi_W}{\partial x}(x,y) \tag{4.76}$$

incidence correction

$$v_W(x,y) = \frac{\partial \phi_W}{\partial y}(x,y) \tag{4.77}$$

velocity gradient correction

$$\frac{\partial u_W}{\partial x}(x,y) = \frac{\partial^2 \phi_W}{\partial x^2}(x,y) \tag{4.78}$$

streamline curvature correction

$$\frac{\partial v_W}{\partial x}(x,y) = \frac{\partial^2 \phi_W}{\partial x \partial y}(x,y) \tag{4.79}$$

evaluated at the position of the airfoil, x = y = 0. For application of these corrections to measured stream and model quantities, see Section 4.8.

Substituting from Equations (4.30), (4.46), (4.60), (4.68) and (4.72), we obtain

$$u_W(0,0) = \frac{\sigma}{2\pi\beta^2 h}\frac{\partial I}{\partial X}(0,0) + \frac{\mu}{2\pi\beta^3 h^2}\frac{\partial^2 I}{\partial X^2}(0,0) \tag{4.80}$$

$$v_W(0,0) = -\frac{\gamma}{2\pi h}\frac{\partial J}{\partial Y}(0,0) - \frac{\omega}{2\pi\beta h^2}\frac{\partial^2 J}{\partial X \partial Y}(0,0) \tag{4.81}$$

$$\frac{\partial u_W}{\partial x}(0,0) = \frac{\sigma}{2\pi\beta^3 h^2}\frac{\partial^2 I}{\partial X^2}(0,0) + \frac{\mu}{2\pi\beta^4 h^3}\frac{\partial^3 I}{\partial X^3}(0,0) \tag{4.82}$$

$$\frac{\partial v_W}{\partial x}(0,0) = -\frac{\gamma}{2\pi\beta h^2}\frac{\partial^2 J}{\partial X \partial Y}(0,0) - \frac{\omega}{2\pi\beta^2 h^3}\frac{\partial^3 J}{\partial X^2 \partial Y}(0,0) \tag{4.83}$$

where from Equations (4.56) - (4.57) and (4.37) - (4.38)

$$\frac{\partial I}{\partial X}(0,0) = -2\int_0^\infty \frac{\frac{\beta}{P}}{f_D(s)}\,ds + \pi\chi(P) \tag{4.84}$$

$$\frac{\partial^2 I}{\partial X^2}(0,0) = -4\int_0^\infty \frac{f_N(s)}{f_D(s)}\,s\,ds \tag{4.85}$$

$$\frac{\partial^3 I}{\partial X^3}(0,0) = 8\int_0^\infty \frac{\frac{\beta}{P}}{f_D(s)}\,s^2\,ds \tag{4.86}$$

and

$$\frac{\partial J}{\partial Y}(0,0) = 2\int_0^\infty \frac{\frac{\beta}{P}}{g_D(s)}\,ds + \frac{\pi}{1+F}\chi\left(\frac{1}{P}\right) \tag{4.87}$$

$$\frac{\partial^2 J}{\partial X \partial Y}(0,0) = 4\int_0^\infty \frac{g_N(s)}{g_D(s)}\,s\,ds \tag{4.88}$$

$$\frac{\partial^3 J}{\partial X^2 \partial Y}(0,0) = -8 \int_0^\infty \frac{\frac{\beta}{P}}{g_D(s)} s^2 \, ds \tag{4.89}$$

Using Equations (4.39), (4.40), (4.54) and (4.55), the above derivatives of I and J are easily obtained by numerical integration. For a fast orientation they are plotted in Figures 4.4 to 4.9 as functions of τ, Equation (4.44), and

$$\psi = \frac{1}{1+F} = \frac{1}{1+\frac{2K}{h}} \tag{4.90}$$

Concerning Figure 4.4 it should be noted that $\partial I/\partial X$, representing the wake blockage effect, is discontinuous at zero porosity. Introducing an arbitrarily small $\epsilon > 0$, we have

$$\lim_{\tau \to \epsilon} \frac{\partial I}{\partial X}(0,0) = -\pi$$

but

$$\frac{\partial I}{\partial X}(0,0)\Big|_{\tau = 0} = \pi$$

which illustrates one of the most serious deficiencies of the infinite test section theory. This result may first appear somewhat paradoxical, but its explanation is quite simple [4.18]. For the hypothetical, infinitely long test section the discharge from a source, representing the displacement effect of the wake, is transmitted into the surrounding space (plenum) no matter how small the porosity of the walls. If P = 0, the situation changes suddenly since then the wall becomes completely impermeable and all of the discharge is forced to stay inside the test section. In contrast, the actual finite-length test section allows only a portion of the source discharge to escape, and this amount decreases continuously as the porosity of the walls is gradually reduced to zero. Accordingly, for finite-length test sections the wake blockage correction is continuous at zero porosity, cf. Section 4.10. From this we may conclude that the infinite test section theory is an unsuitable mathematical model for low porosity test sections.

For porous walls, F = 0, we obtain from Equations (4.58) - (4.59) and (4.42) - (4.43) the closed form solutions [4.4]

$$\frac{\partial^n I}{\partial X^n}(0,0) = \begin{cases} \pi & , \quad n = 1 \ , \ \tau = 0 \\ \dfrac{(2\pi)^n}{n} B_n\left(\dfrac{\tau}{2}\right) & , \quad \begin{cases} n = 1 \ , \ 0 < \tau \leqslant 1 \\ n > 1 \ , \ 0 \leqslant \tau \leqslant 1 \end{cases} \end{cases} \tag{4.91}$$

and

$$\frac{\partial^n J}{\partial X^{n-1} \partial Y}(0,0) = \frac{(2\pi)^n}{n} B_n\left(\frac{1+\tau}{2}\right) \ , \quad n \geqslant 1 \ , \ 0 \leqslant \tau \leqslant 1 \tag{4.92}$$

The symbol B_n denotes the Bernoulli polynomials

$$\begin{aligned} B_1(T) &= T - \frac{1}{2} \\ B_2(T) &= T^2 - T + \frac{1}{6} \\ B_3(T) &= T^3 - \frac{3}{2}T^2 + \frac{1}{2}T \\ B_4(T) &= T^4 - 2T^3 + T^2 - \frac{1}{30} \\ B_5(T) &= T^5 - \frac{5}{2}T^4 + \frac{5}{3}T^3 - \frac{1}{6}T \\ &\vdots \end{aligned} \tag{4.93}$$

etc., see Reference [4.19]. Substituting in Equations (4.80) to (4.83) we thus obtain for porous walls the correction formulas

$$u_W(0,0) = \frac{\sigma}{\beta^2 h}\left[B_1\left(\frac{\tau}{2}\right) + \chi(P)\right] + \frac{\mu\pi}{\beta^3 h^2} B_2\left(\frac{\tau}{2}\right) \tag{4.94}$$

$$v_W(0,0) = -\frac{\gamma}{h} B_1\left(\frac{1+\tau}{2}\right) - \frac{\omega\pi}{\beta h^2} B_2\left(\frac{1+\tau}{2}\right) \tag{4.95}$$

$$\frac{\partial u_W}{\partial x}(0,0) = \frac{\sigma\pi}{\beta^3 h^2} B_2\left(\frac{\tau}{2}\right) + \frac{4}{3}\frac{\mu\pi^2}{\beta^4 h^3} B_3\left(\frac{\tau}{2}\right) \tag{4.96}$$

$$\frac{\partial v_W}{\partial x}(0,0) = -\frac{\gamma\pi}{\beta h^2} B_2\left(\frac{1+\tau}{2}\right) - \frac{4}{3}\frac{\omega\pi^2}{\beta^2 h^3} B_3\left(\frac{1+\tau}{2}\right) \tag{4.97}$$

where τ is given by Equation (4.44) and χ by Equation (4.62).

The first one to use systematically the Bernoulli polynomials in the porous wall theory was Brescia [4.20], even though he did not identify them as such. Unfortunately, his elegant theoretical result went almost unnoticed and preference was given to special interference factors, discussed in Section 4.7.

From Equations (4.94) to (4.97) we obtain for solid walls, $\tau = 0$,

$$u_W(0,0) = \frac{1}{2}\frac{\sigma}{\beta^2 h} + \frac{1}{6}\frac{\mu\pi}{\beta^3 h^2} \tag{4.98}$$

$$v_W(0,0) = \frac{1}{12}\frac{\omega\pi}{\beta h^2} \tag{4.99}$$

$$\frac{\partial u_W}{\partial x}(0,0) = \frac{1}{6}\frac{\sigma\pi}{\beta^3 h^2} \tag{4.100}$$

$$\frac{\partial v_W}{\partial x}(0,0) = \frac{1}{12}\frac{\gamma\pi}{\beta h^2} \tag{4.101}$$

Equations (4.98) to (4.101) are classical results of closed wall theory. The first term of Equation (4.98) is the wake blockage correction due to Thom [4.15] and Goethert [4.21]; the second term is the solid blockage correction by v.Baranoff [4.22]. Equation [4.99), upon substituting for ω from Equation (4.23), is recognized as the incidence correction according to Allen and Vincenti [4.23]. Equation (4.100) is the velocity gradient correction derived by Thom [4.15]. Finally, Equation (4.101) is the streamline curvature correction given by Prandtl [4.24] in his original work on wall interference.

Similarly, for open jet boundaries, $\tau = 1$,

$$u_W(0,0) = -\frac{1}{12}\frac{\mu\pi}{\beta^3 h^2} \tag{4.102}$$

$$v_W(0,0) = -\frac{1}{2}\frac{\gamma}{h} - \frac{1}{6}\frac{\omega\pi}{\beta h^2} \tag{4.103}$$

$$\frac{\partial u_W}{\partial x}(0,0) = -\frac{1}{12}\frac{\sigma\pi}{\beta^3 h^2} \tag{4.104}$$

$$\frac{\partial v_W}{\partial x}(0,0) = -\frac{1}{6}\frac{\gamma\pi}{\beta h^2} \tag{4.105}$$

Again, these are well-known correction formulas, cf. Pankhurst and Holder [4.25]. It is worth noting that open jet walls do not cause wake blockage, Equation (4.102), but the incidence correction is large, dominated by the term proportional to c/h, see Equations (4.103) and (4.20). The incidence correction for solid walls, as we may verify on Equations (4.99) and (4.23), is an order of magnitude smaller, proportional to $(c/h)^2$.

For ideal slotted walls, $1/P = 0$, $F > 0$, the theory is not nearly as neat as for porous walls. From Equations (4.39, (4.40), (4.54), (4.55) and (4.84) to (4.89) we have

$$\frac{\partial I}{\partial X}(0,0) = 0 \tag{4.106}$$

$$\frac{\partial^2 I}{\partial X^2}(0,0) = -4\int_0^\infty \frac{(1-Fs)\,e^{-s}\,s}{\cosh(s) + Fs\sinh(s)}\,ds \tag{4.107}$$

$$\frac{\partial^3 I}{\partial X^3}(0,0) = 0 \tag{4.108}$$

and

$$\frac{\partial J}{\partial Y}(0,0) = \frac{\pi}{1+F} = \pi\psi \tag{4.109}$$

$$\frac{\partial^2 J}{\partial X \partial Y}(0,0) = 4\int_0^\infty \frac{(1-Fs)\,e^{-s}}{\frac{1}{s}\sinh(s) + F\cosh(s)}\,ds \tag{4.110}$$

$$\frac{\partial^3 J}{\partial X \partial Y}(0,0) = 0 \tag{4.111}$$

Closed form solutions for the integrals (4.107) and (4.110) have been found only in the limit $F \to \infty$; they tend to the solid wall values

$$\frac{\partial^2 I}{\partial X^2}(0,0) = \frac{\pi^2}{3}$$

$$\frac{\partial^2 J}{\partial X \partial Y}(0,0) = -\frac{\pi^2}{6}$$

as may be verified by substituting $\tau = 0$ in Equations (4.91) and (4.92).

4.7 Wall Interference Factors

The earlier treatments on classical wall interference [4.11] to [4.14] employ special wall interference factors in place of our functions I and J, Equations (4.61) and (4.47). The former were introduced for each effect in an ad hoc fashion, as the wall interference theory evolved, making the treatment much less systematic. The relations of the interference factors to the derivatives of I and J are added here to provide continuity with the earlier developments; otherwise this entire section can be skipped.

The following six interference factors appear to be well established:

wake blockage factor

$$\epsilon_W = \frac{1}{2}\frac{\sigma}{\beta^2 h}\Omega_W \tag{4.112}$$

wake blockage ratio

$$\Omega_W = \frac{1}{\pi}\frac{\partial I}{\partial X}(0,0) \tag{4.113}$$

solid blockage factor

$$\epsilon_s = \frac{1}{6}\frac{\mu\pi}{\beta^3 h^2}\Omega_s \tag{4.114}$$

solid blockage ratio

$$\Omega_s = \frac{3}{\pi^2}\frac{\partial^2 I}{\partial X^2}(0,0) \tag{4.115}$$

upwash factor

$$\delta_0 = -\frac{1}{4\pi}\frac{\partial J}{\partial Y}(0,0) \tag{4.116}$$

streamline curvature factor

$$\delta_1 = -\frac{1}{4\pi}\frac{\partial^2 J}{\partial X \partial Y}(0,0) \tag{4.117}$$

The term "blockage ratio" is used for the ratio of the blockage factors in ventilated and solid walls. We readily verify from Equations (4.91) and (4.93) that for solid walls, P = 0, indeed $\Omega_W = \Omega_s = 1$. Graphs and tables of the above factors can be found in References [4.11] to [4.14].

For perforated walls, F = 0

$$\Omega_W = \begin{cases} 1 & , \quad P = 0 \\ 2\,B_1\left(\frac{\tau}{2}\right) & , \quad P > 0 \end{cases} \tag{4.118}$$

$$\Omega_s = 6\,B_2\left(\frac{\tau}{2}\right) \tag{4.119}$$

$$\delta_0 = -\frac{1}{2}B_1\left(\frac{1+\tau}{2}\right) \tag{4.120}$$

$$\delta_1 = -\frac{\pi}{2}B_2\left(\frac{1+\tau}{2}\right) \tag{4.121}$$

The wake blockage ratio is discontinuous at $P = \tau = 0$, in accordance with our earlier discussion in Section 4.6.

For ideal slotted walls, 1/P = 0,

$$\Omega_W = 0 \tag{4.122}$$

$$\delta_0 = -\frac{1}{4\,(1+F)} = -\frac{\psi}{4} \tag{4.123}$$

but Ω_s and δ_1 have to be obtained numerically.

Using Equations (4.112) to (4.115), the velocity correction (4.80) becomes

$$u_W(0,0) = \epsilon_W + \epsilon_s$$

$$= \frac{1}{2}\frac{\sigma}{\beta^2 h}\Omega_W + \frac{1}{6}\frac{\mu\pi}{\beta^3 h^2}\Omega_s \tag{4.124}$$

For solid walls, P = 0, the correction formula (4.98) is obtained.

Using Equations (4.116) and (4.117), the incidence correction (4.81) becomes

$$v_W(0,0) = \frac{2\gamma}{h}\delta_0 + \frac{2\omega}{\beta h^2}\delta_1 \tag{4.125}$$

which upon substituting for the singularity strengths from Equations (4.20) and (4.23) takes the familiar form used in Reference [4.12]. Since the standard wall interference factors are defined up to the second derivatives of I and J, they are sufficient for expressing only the first terms of the velocity gradient and streamline curvature corrections, Equations (4.82) and (4.83):

$$\frac{\partial u_W}{\partial x}(0,0) \simeq \frac{1}{6}\frac{\sigma\pi}{\beta^3 h^2}\Omega_s \tag{4.126}$$

$$\frac{\partial v_W}{\partial x}(0,0) \simeq \frac{2\gamma}{\beta h^2}\delta_1 \tag{4.127}$$

Recently an additional "pressure gradient factor" has been proposed [4.11], which relates to the third derivative of I.

4.8 Corrections to Measured Quantities

The correction to tunnel stream velocity is

$$\Delta U_\infty = U_\infty \, u_W(0,0) \tag{4.128}$$

where the velocity U_∞ is assumed to be measured far upstream*, out of the aerodynamic influence of the airfoil. The correction is to be interpreted in such a way that the pressure distribution measured on the airfoil in the wind tunnel at stream velocity U_∞ corresponds to that which would be obtained if the airfoil were tested in free air at the velocity $U_\infty + \Delta U_\infty$.

In isentropic flow of perfect gas, U_∞ relates to the stream Mach number M_∞ according to

$$U_\infty^2 = \frac{\kappa R T_0}{1 + \frac{\kappa - 1}{2} M_\infty^2} M_\infty^2$$

where $\kappa = 1.4$ (for air) is the ratio of specific heats, R is the gas constant and the stagnation temperature. By differentiating the relation and dividing it by itself we obtain the Mach number correction

$$\Delta M_\infty = \left(1 + \frac{\kappa - 1}{2} M_\infty^2\right) M_\infty \, u_W(0,0) \tag{4.129}$$

From isentropic flow relations corrections can also be made to the stream static pressure and density. Expanding

$$\frac{p}{p_\infty} = \left[1 + \frac{\kappa - 1}{2} M_\infty^2 \left(1 - \frac{U^2}{U_\infty^2}\right)\right]^{\frac{\kappa}{\kappa - 1}}$$

in binomial series, taking the first two terms and interpreting

$$p = p_\infty + \Delta p_\infty$$

$$1 - \frac{U^2}{U_\infty^2} = 1 - \left(\frac{U_\infty + \Delta U_\infty}{U_\infty}\right)^2 \simeq -2 \, u_W(0,0)$$

we obtain the blockage correction to stream static pressure

$$\Delta p_\infty = -\kappa M_\infty^2 \, p_\infty \, u_W(0,0) \tag{4.130}$$

Using the fact that

$$\frac{p}{p_\infty} = \left(\frac{\rho}{\rho_\infty}\right)^\kappa$$

we similarly arrive at the blockage correction to stream density

$$\Delta \rho_\infty = -M_\infty^2 \, \rho_\infty \, u_W(0,0) \tag{4.131}$$

The blockage correction to stream dynamic pressure is then

$$\Delta\left(\frac{1}{2}\rho_\infty U_\infty^2\right) = \rho_\infty U_\infty \Delta U_\infty + \frac{1}{2} U_\infty^2 \Delta \rho_\infty$$

$$= \frac{1}{2} \rho_\infty U_\infty^2 \left(2 - M_\infty^2\right) u_W(0,0) \tag{4.132}$$

and using this result we obtain the blockage corrections to the lift, drag and pitching moment coefficients

$$\Delta C_L = -(2 - M_\infty^2) \, C_L \, u_W(0,0) \tag{4.133}$$

*Since the far upstream velocity is not necessarily equal to the far downstream velocity, it would be more logical to use, as in Reference [4.26], the subscript $-\infty$ instead of ∞.

$$\Delta C_D = - \left(2 - M_\infty^2\right) C_D \, u_W \, (0,0) \tag{4.134}$$

$$\Delta C_M = - \left(2 - M_\infty^2\right) C_M \, u_W \, (0,0) \tag{4.135}$$

The pressure coefficient

$$C_p = \frac{p - p_\infty}{\frac{1}{2} \rho_\infty \, U_\infty^2}$$

on the airfoil surface will also require correction because of changes in both the static and dynamic pressures of the tunnel stream. Thus

$$\Delta C_p = \frac{p - (p_\infty + \Delta p_\infty)}{\frac{1}{2} \rho_\infty \, U_\infty^2 + \Delta\left(\frac{1}{2} \rho_\infty \, U_\infty^2\right)} - C_p$$

from which, using Equations (4.130) and (4.132) and the fact that

$$M_\infty^2 = \frac{U_\infty^2}{\kappa \frac{p_\infty}{\rho_\infty}}$$

we obtain [4.27]

$$\Delta C_p = \left[2 - \left(2 - M_\infty^2\right) C_p\right] u_W \, (0,0) \tag{4.136}$$

Using this expression, the correction formulas (4.133) to (4.135) can be readily verified; the term $2 \, u_W \, (0,0)$ is a constant that drops out when integrating along a closed contour.

In incompressible flow Equation (4.130) is replaced by

$$\Delta p_\infty = - \rho \, U_\infty^2 \, u_W \, (0,0) \tag{4.137}$$

which follows from the Bernoulli equation. Incompressible versions of the other correction formulas, Equations (4.131) to (4.136), are formally obtained by substituting $M_\infty = 0$.

The angle of attack correction (in radians) is directly

$$\Delta\alpha = v_W \, (0,0) \tag{4.138}$$

Again, the correction is to be interpreted in such a way that the pressure distribution on the airfoil measured in the wind tunnel at angle of attack α corresponds to that in free air at angle of attack $\alpha + \Delta\alpha$.

The corrected lift and drag are obtained by resolving the measured aerodynamic force into the directions normal and parallel to the corrected stream velocity vector. Accordingly, the incidence correction to the lift coefficient is

$$\begin{aligned} \Delta C_L &= C_L \, [\cos(\Delta\alpha) - 1] - C_D \sin(\Delta\alpha) \\ &\simeq - C_D \, \Delta\alpha \end{aligned} \tag{4.139}$$

and the incidence correction to the drag coefficient

$$\begin{aligned} \Delta C_D &= C_D \, [\cos(\Delta\alpha) - 1] + C_L \sin(\Delta\alpha) \\ &\simeq C_L \, \Delta\alpha \end{aligned} \tag{4.140}$$

where C_L and C_D are the coefficients of the aerodynamic forces normal and tangent to the wind tunnel axis respectively. Since the correction (4.140) is extremely sensitive to $\Delta\alpha$, it is safer to obtain drag by wake measurements. (C_{D_W} is not subject to incidence correction.)

Regarding the drag correction (4.140), another word of caution is in order. According to the present theory $v_W(x,y) \to 0$ as $x \to \infty$, so that the wake far behind the airfoil is parallel to the oncoming stream (tunnel axis) as it would be in unbounded flow. However, the rotation of the axes of reference through an angle $\Delta\alpha$, on which Equations (4.139) and (4.140) are based, violates the downstream condition and it is clear that there must be some practical limits up to which the incidence correction is applicable. The general consensus [4.28] is that $|\Delta\alpha|$ should not exceed 2°.

The derivatives $\partial u_W/\partial x$ and $\partial v_W/\partial x$ are most undesirable, since they vitiate the purpose of the wind tunnel test, namely the determination of the airfoil performance in uniform flow. However, if they are not large, the effects of flow nonuniformity can be approximated by residual corrections to the force and moment coefficients.

The velocity gradient correction to drag coefficient is approximated as

$$\Delta C_D = -2Ac \frac{\partial u_W}{\partial x}(0,0) \tag{4.141}$$

using the fact that the buoyancy force is the product of the pressure gradient and the (effective) volume of the model; for more rigorous treatment see Glauert [4.29]. Since A is the nondimensional airfoil area and $\partial u_W/\partial x$ is of dimension length^{-1}, the correction is dimensionless as it should be. The buoyancy force is not of viscous nature and therefore the above correction is not to be applied to the drag coefficient from wake traverse measurements, if these are reduced in the usual way [4.27].

The streamline curvature effect is equivalent to a distortion of the airfoil camber [4.29]. Its effects on the lift and pitching moment coefficients can be estimated using the subsonic thin airfoil theory, e.g. Reference [4.30]. For simplicity, we assume that the airfoil is the line segment $x_L < x < x_T$, $y = 0$, where x_L and x_T are the x co-ordinates of the leading and trailing edge respectively and

$$c = x_T - x_L$$

Furthermore, the chordwise distribution of the y component of wall interference velocity is approximated by the first two terms of a Taylor expansion:

$$v_W(x,0) = v_W(0,0) + x \frac{\partial v_W}{\partial x}(0,0)$$

Under such assumptions, the streamline curvature correction to the lift coefficient is derived as

$$\Delta C_L = -\frac{\pi}{2\beta}(3c + 4x_L)\frac{\partial v_W}{\partial x}(0,0) \tag{4.142}$$

If, as recommended by Glauert [4.29], the origin is placed at the mid-chord point,

$$x_L = -\frac{1}{2}c$$

then

$$\Delta C_L = -\frac{\pi}{2\beta} c \frac{\partial v_W}{\partial x}(0,0) \tag{4.143}$$

To the order of approximation employed, the streamline curvature correction to the quarter-chord pitching moment coefficient is found to have a value independent of the location of the origin

$$\Delta C_{M_{c/4}} = \frac{\pi}{8\beta} c \frac{\partial v_W}{\partial x}(0,0) \tag{4.144}$$

Again, the sign convention is such that the correction value is to be added to the measured quantity in order to obtain the corrected one. Comparing Equations (4.143) and (4.144) we arrive at a familiar result, namely that the streamline curvature correction to the quarter-chord pitching moment coefficient is four times less in magnitude than that to the lift coefficient. For practical purposes this correction is often found insignificant.

4.9 Effect of the Reference Station Location

In the previous developments the disturbance velocity was assumed to vanish infinitely far upstream. As discussed in Section 4.6, this approach leads to a discontinuity of the velocity correction at zero porosity, which is not a true physical behaviour of actual, finite-length test sections. However, the problem can be alleviated if as reference a finitely distant upstream point x_{ref}, y_{ref} is considered, see Figure 4.1. In fact, this is in agreement with the usual practice of determining the velocity of the oncoming stream from pressure measurement some distance upstream of the airfoil.

Retaining the symbol U_∞ for the measured stream velocity at the reference point, the velocity correction at the model position x = y = 0 is expressed as

$$\Delta U_\infty = U_\infty \left[u_W (0,0) - u (x_{ref}, y_{ref})\right] \tag{4.145}$$

The term

$$u (x_{ref}, y_{ref}) = \frac{\partial \phi_F}{\partial x} (x_{ref}, y_{ref}) + \frac{\partial \phi_W}{\partial x} (x_{ref}, y_{ref}) \tag{4.146}$$

represents the disturbance velocity at the reference point, due to the presence of the airfoil and wall interference. By subtracting it, we thus measure the wall interference velocity from the undisturbed stream level. In the velocity difference of Equation (4.145) the discontinuity of the wake blockage correction cancels out, as long as x_{ref} is finite, see Reference [4.18].

Without going into details, we mention that the potentials ϕ_F and ϕ_W are given by Equations (4.14) and (4.30) and the x derivative of ϕ_W can be evaluated using the series solutions in Sections 4.2 to 4.5. A similar replacement of u_W (0,0) by the difference u_W (0,0) - u_W (x_{ref}, y_{ref}) is also applicable to correction formulas (4.130) to (4.137).

4.10 Effect of the Test Section Length

The theory of a finite-length test section with porous-slotted boundaries is more complicated and analytic solutions for wall interference corrections are known only in some particular cases. Woods [4.31] studied the case of an airfoil located centrally between two walls which are porous over the length ℓ and solid elsewhere, Figure 4.10. Using the mixed boundary condition

$$\frac{\partial \phi}{\partial x}\left(x, \pm \frac{h}{2}\right) \pm \frac{1}{P} \frac{\partial \phi}{\partial y}\left(x, \pm \frac{h}{2}\right) = 0 \quad , \quad |x| < \frac{\ell}{2}$$

$$\frac{\partial \phi}{\partial y}\left(x, \pm \frac{h}{2}\right) = 0 \quad , \quad |x| > \frac{\ell}{2} \tag{4.147}$$

where ϕ is to be decomposed according to Equation (4.3), the following velocity correction is found [4.31]

$$u_W (0,0) = \frac{1}{2} \frac{\sigma}{\beta^2 h} \left[1 - 2 \tanh \frac{\pi \ell \tau}{\beta h} + \tau \tanh \frac{\pi \ell}{2\beta h}\right]$$

$$+ \frac{1}{6} \frac{\mu \pi}{\beta^3 h^2} \left[1 - 3\tau \tanh \frac{\pi \ell}{2\beta h} \tanh \frac{\pi \ell \tau}{\beta h} + \frac{3}{2} \tau^2 \left(\tanh \frac{\pi \ell}{2\beta h}\right)^2\right] \tag{4.148}$$

Comparing it with Equation (4.124), we see that the terms in square brackets qualify as the blockage ratios for the finite-length test section.

It is easily verified that u_W (0,0) is a continuous function on the interval $0 \leqslant \tau \leqslant 1$ as long as the porous wall length ℓ is finite. If $\ell \to \infty$, then

$$\tanh \frac{\pi \ell}{2\beta h} \to 1$$

$$\tanh \frac{\pi \ell \tau}{\beta h} \to \begin{cases} 0 \quad , & \tau = 0 \\ 1 \quad , & 0 < \tau \leqslant 1 \end{cases}$$

and we arrive at the correction formula (4.94), which is discontinuous at $\tau = 0$.

The effect of the finite length of the porous test section on airfoil lift and pitching moment is treated in Woods' subsequent paper [4.32]. However, as shown by Parkinson and Lim [4.33], for ordinary test sections having $\ell/h > 1.5$, the effect of the upstream and downstream portions on the incidence correction is not significant. For more details of the wall interference on lifting airfoils in a test section with finite-length porous walls the reader is referred to the book by Woods [4.26]. A summary on the length restrictions for ventilated test sections is also given by Vayssaire [4.34].

4.11 Effect of Plenum Pressure

A numerical technique (method of singularity distributions) for the calculation of wall interference in porous wall test sections was presented by Sloof and Piers [4.35]. Their computations show that wall interference depends strongly on the location of the tested airfoil inside the finite-length test section and on the plenum pressure. The latter effect enters the picture by employing the inhomogeneous boundary condition (2.20) instead of (2.23).

An analytic study of the plenum pressure effect on solid blockage between porous walls was recently given by Sayadian and Fonarev [4.36]. In their treatment the porous walls are assumed to be infinite, however the plenum chamber length, ℓ, is finite, see Figure 4.11. Accordingly, the porous wall boundary conditions are

$$\frac{\partial \phi}{\partial x}\left(x, \pm \frac{h}{2}\right) \pm \frac{1}{P} \frac{\partial \phi}{\partial y}\left(x, \pm \frac{h}{2}\right) = \begin{cases} 0 & , \quad |x| > \frac{\ell}{2} \\ -\frac{1}{2} C_{p_{plenum}} & , \quad |x| < \frac{\ell}{2} \end{cases} \tag{4.149}$$

The solid blockage correction, obtained by the Fourier transform method is

$$u_W(0,0) = \frac{\mu \pi}{\beta^3 h^2} B_2\left(\frac{\tau}{2}\right) - \frac{1}{2} C_{p_{plenum}} \left\{ \frac{2}{\pi} \int_0^\infty \frac{\sin\left(\frac{s\ell}{\beta h}\right) \cosh(s)\, ds}{s\left[\cosh^2(s) + \left(\frac{\beta}{P}\right)^2 \sinh^2(s)\right]} \right\} \tag{4.150}$$

The first term is the usual correction for infinite-length test section, cf. Equation (4.94). The second term, which is independent of the doublet strength μ, is the velocity correction for flow between the test section and plenum, caused by the pressure difference $p_\infty - p_{plenum}$. We note that the integral vanishes if $\beta/P = 0$ or $\ell = 0$. In the limit $\ell \to \infty$, the term in curly brackets tends to unity and the correction formula (4.150) reduces to

$$u_W(0,0) = \frac{\mu \pi}{\beta^3 h^2} B_2\left(\frac{\tau}{2}\right) - \frac{1}{2} C_{p_{plenum}}$$

which indicates that the plenum pressure has completely filled the test section. If the plenum pressure is used as reference, $p_\infty = p_{plenum}$, then the pressure term in the velocity correction drops out. This applies to Equation (4.150) as well.

From Equation (4.150) it follows that for given wall porosity and plenum length, the solid blockage can be minimized by adjusting the plenum pressure. If the plenum pressure cannot be controlled, say $C_{p_{plenum}} = 0$, the solid blockage is absent only when the wall porosity is such that $B_2\left(\frac{\tau}{2}\right) = 0$, i.e. $\tau = 1 - 1/\sqrt{3}$ and $P/\beta = 0.782$.

Motivated by Sears' self-correcting wind tunnel [4.37], Sayadian and Fonarev [4.36] also treat the case of top and bottom plenum chambers consisting of two segments each, whose pressures can be adjusted individually. This arrangement allows to eliminate simultaneously the velocity and the velocity gradient corrections.

4.12 Concluding Remarks

The term "classical", adopted in the present Chapter, is in accordance with Reference [4.38], where it is used to categorize a wall interference theory based on the knowledge of the tunnel boundary condition and the representation of the airfoil flow field by singularities.

The present treatment has been limited to the representation of the airfoil by a source, vortex and two doublets, but may be analogously extended to higher-order singularities (quadrupoles, etc.). A question then arises as to whether the representation by the first few singularities is adequate or, more precisely, under what circumstances the derived corrections converge. Using the ratio test and properties of Bernoulli polynomials [4.39], a simple convergence criterion for a thin airfoil between porous walls is derived in Reference [4.4]:

$$\frac{c}{\beta h} < 1 \tag{4.151}$$

where c is the airfoil chord and h is the test section height. As expected, there is an interdependence between the stream Mach number and the ratio c/h. However, as indicated in Reference [4.34], the condition (4.515), based on linearized theory, is not particularly strict; e.g. for c/h = 0.34 (a very large model with respect to the wind tunnel) the limit Mach number is as high as $M_\infty = 0.94$. In many practical situations, however, the flow at the walls would be supercritical at much lower values of M_∞, making the linear theory inapplicable.

REFERENCES

[4.1] Prandtl, L. *Applications of Modern Hydrodynamics to Aeronautics.* Ludwig Prandtl gesammelte Abhandlungen, Vol. 1, Springer-Verlag, 1961, pp. 433-515; also NACA TR-116, 1921.

[4.2] Kemp, W.B. *Toward the Correctable-Interference Transonic Wind Tunnel.* Proceedings of AIAA 9th Aerodynamic Testing Conference, June 1976, pp. 31-38.

[4.3] Goldstein, S. *Two-Dimensional Wind-Tunnel Interference.* ARC R&M 1902, Sept. 1942.

[4.4] Mokry, M. *Higher-Order Theory of Two-Dimensional Subsonic Wall Interference in a Perforated Wall Wind Tunnel.* LR-553, National Research Council of Canada, Oct. 1971.

[4.5] Klunker, E.B. — *Contribution to Methods for Calculating the Flow About Thin Lifting Wings at Transonic Speeds — Analytic Expressions for the Far Field.* NASA TN D-6530, Nov. 1971.

[4.6] Chan, Y.Y. — *A Singular Perturbation Analysis of Two-dimensional Wind Tunnel Interferences.* Journal of Applied Mathematics and Physics, Vol. 31, 1980, pp. 605-619.

[4.7] Chan, Y.Y. — *Lift Effect on Transonic Wind-Tunnel Blockage.* Journal of Aircraft, Vol. 17, 1980, pp. 915-916.

[4.8] Smithmeyer, Marta G. Murman, E.M. — *Far-Field Boundary Conditions for Airfoils in Transonic Wind Tunnels.* Rept. 78, Flow Research Co., Dec. 1976.

[4.9] Baldwin, B.S. Turner, J.B. Knechtel, E.D. — *Wall Interference in Wind Tunnels With Slotted and Porous Boundaries at Subsonic Speeds.* NACA TN 3176, 1954.

[4.10] Wright, R.H. — *The Effectiveness of the Transonic Wind Tunnel as a Device for Minimizing Tunnel-Boundary Interference for Model Tests at Transonic Speeds.* AGARD Rept. 294, March 1959.

[4.11] Catherall, D. — *On the Evaluation of Wall Interference in Two-Dimensional Ventilated Wind Tunnels by Subsonic Linear Theory.* TR-76134, Royal Aircraft Establishment, Sept. 1976.

[4.12] Rogers, E.W.E. — *Wall Interference in Tunnels With Ventilated Walls.* Subsonic Wind Tunnel Wall Corrections, AGARDograph 109, Oct. 1966, pp. 341-430.

[4.13] Pindzola, M. Lo, C.F. — *Boundary Interference at Subsonic Speeds in Wind Tunnels With Ventilated Walls.* AEDC-TR-69-47, May 1969.

[4.14] — *Lift-Interference and Blockage Corrections for Two-Dimensional Subsonic Flow in Ventilated and Closed Wind-Tunnels.* Engineering Sciences Data 76028, Nov. 1976.

[4.15] Thom, A. — *Blockage Corrections in a Closed High-Speed Tunnel.* ARC R&M 2033, Nov. 1943.

[4.16] Sneddon, I.N. — *The Use of Integral Transforms.* McGraw-Hill, 1972, pp. 30-36.

[4.17] Murman, E.M. — *Computation of Wall Effects in Ventilated Transonic Wind Tunnels.* AIAA Paper, No. 72-1007, Sept. 1972.

[4.18] Mokry, M. — *A Wake-Blockage Paradox in a Perforated Wall Wind Tunnel.* AIAA Journal, Vol. 9, 1971, pp. 2462-2464.

[4.19] Abramowitz, M. Stegun, I.A. — *Handbook of Mathematical Functions.* National Bureau of Standards, June 1964, pp. 804-808.

[4.20] Brescia, R. — *Wall Interference in a Perforated Wind Tunnel.* NACA TM-1429, May 1957.

[4.21] Goethert, B. — *Windkanalkorrekturen bei hohen Unterschallgeschwindigkeiten.* Lilienthal-Gesselschaft für Luftfahrtforschung, Bericht 127, 1940, pp. 114-120.

[4.22] v.Baranoff, A. — *Tunnel Corrections for Compressible Subsonic Flow.* NACA TM-1162, July 1947.

[4.23] Allen, H.J. Vincenti, W.G. — *Wall Interference in a Two-Dimensional-Flow Wind Tunnel, With Consideration of the Effect of Compressibility.* NACA Rept. 782, 1944.

[4.24] Prandtl, L. — *Tragflügeltheorie II.* Ludwig Prandtl gesammelte Abhandlungen, Vol. 1, Springer-Verlag, 1961, pp. 346-372.

[4.25] Pankhurst, R.C. Holder, D.W. — *Wind-Tunnel Technique.* Pitman & Sons, 1952, pp. 327-427.

[4.26] Woods, L.C. — *The Theory of Subsonic Plane Flow.* Cambridge at the University Press, 1961.

[4.27] Rogers, E.W.E. — *Blockage Effects in Closed or Open Tunnels.* Subsonic Wind Tunnel Wall Corrections, AGARDograph 109, Oct. 1966, pp. 279-340.

[4.28] Carbonaro, M. — *Review of Some Problems Related to the Design and Operation of Low Speed Wind Tunnels for V/STOL Testing.* Problems in Wind Tunnel Testing Techniques, AGARD-R-601, pp. 1.1-1.24, Nov. 1972.

[4.29] Glauert, H. — *Wind Tunnel Interference on Wings, Bodies and Airscrews.* R.&M. No. 1566, Aeronautical Research Committee, June 1934.

[4.30] Ashley, H. Landahl, M. — *Aerodynamics of Wings and Bodies.* Addison-Wesley, 1965, pp. 88-97.

[4.31] Woods, L.C. — *On the Theory of Two-Dimensional Wind Tunnels with Porous Walls.* Proc. Roy. Soc. of London, Vol. 233, 1955, pp. 74-90.

[4.32] Woods, L.C. — *On the Lifting Aerofoil in a Wind Tunnel with Porous Walls.* Proc. Roy. Soc. of London, Vol. 242, 1957, pp. 341-354.

[4.33] Parkinson, G.V. Lim, A.K. — *On the Use of Slotted Walls in Two-Dimensional Testing of Low Speed Airfoils.* C.A.S.I. Transactions, Vol. 4, 1971, pp. 81-87.

[4.34] Vayssaire, J.-C. *Survey of Methods for Correcting Wall Constraints in Transonic Wind Tunnels.* Problems in Wind Tunnel Testing Techniques, AGARD-R-601, pp. 2.1-2.A9, Nov. 1972.

[4.35] Slooff, J.W. Piers, W.J. *The Effect of Finite Test Section Length on Wall Interference in 2-D Ventilated Windtunnels.* Windtunnel Design and Testing Techniques, AGARD-CP-174, 1975, pp. 14.1-14.11.

[4.36] Sayadian, K.G. Fonarev, A.S. *O maloinduktsionnych rezhimach obtekania profilei i tel vrashchenia v transzvukovych trubach.* Uchenye zapiski TsAGI, Vol. XII, 1981, pp. 51-61.

[4.37] Sears, W.R. *Self-Correcting Wind Tunnels.* The Aeronautical Journal, Vol. 78, 1974, pp. 80-89.

[4.38] Lo, C.F. *Tunnel Interference Assessment by Boundary Measurements.* AIAA Journal, Vol. 16, 1978, pp. 411-413.

[4.39] Lehmer, D.H. *On the Maxima and Minima of Bernoulli Polynomials.* The American Mathematical Monthly, Vol. 47, 1940, pp. 533-538.

Table 4.1 Increment of airfoil area in transonic flow

C_L	A	δA	$\delta A/A$
0.215	0.0823	0.0025	3%
0.370	0.0823	0.0075	9%
0.550	0.0823	0.0165	20%

NACA 0012 airfoil

$M_\infty = 0.8$ $t/c = 0.12$ $h/c = 6$

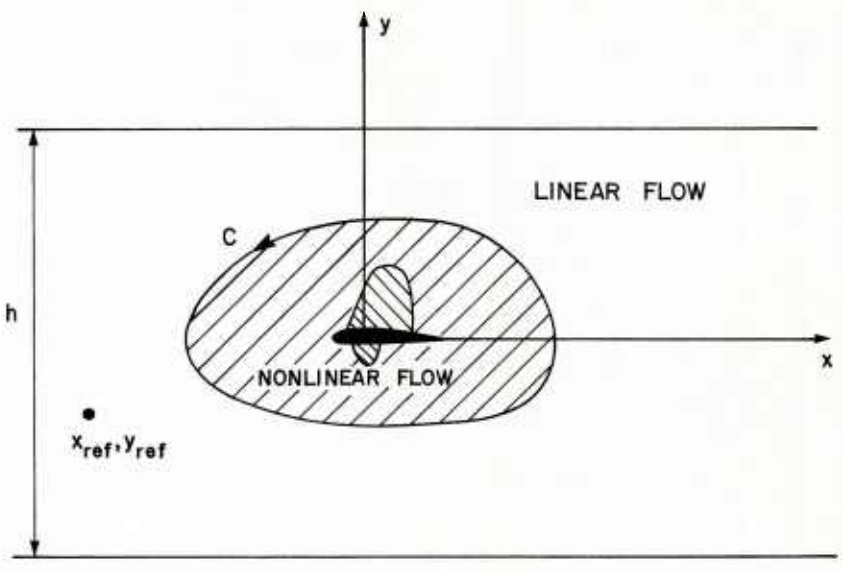

Fig. 4.1 Linear and nonlinear flow regions

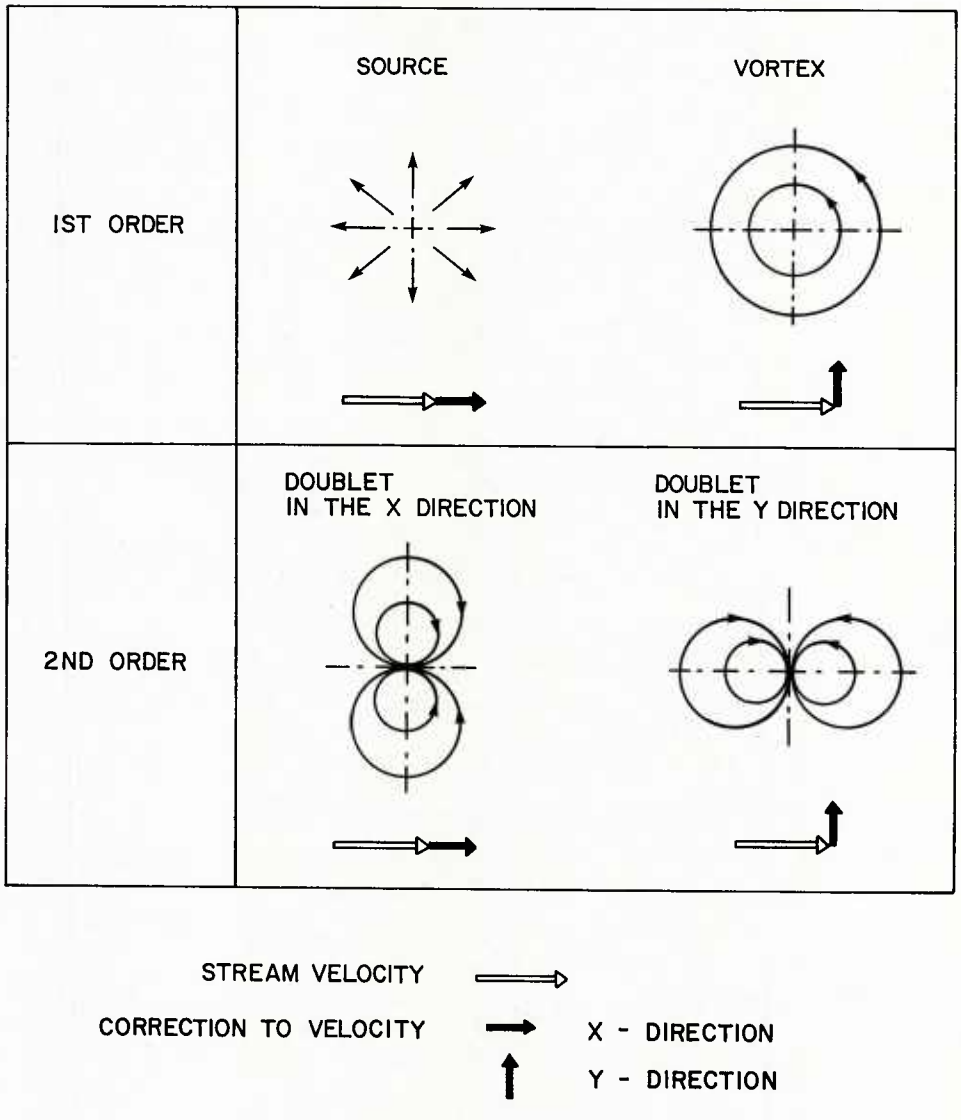

Fig. 4.2 Singularities representing subsonic far field of the airfoil

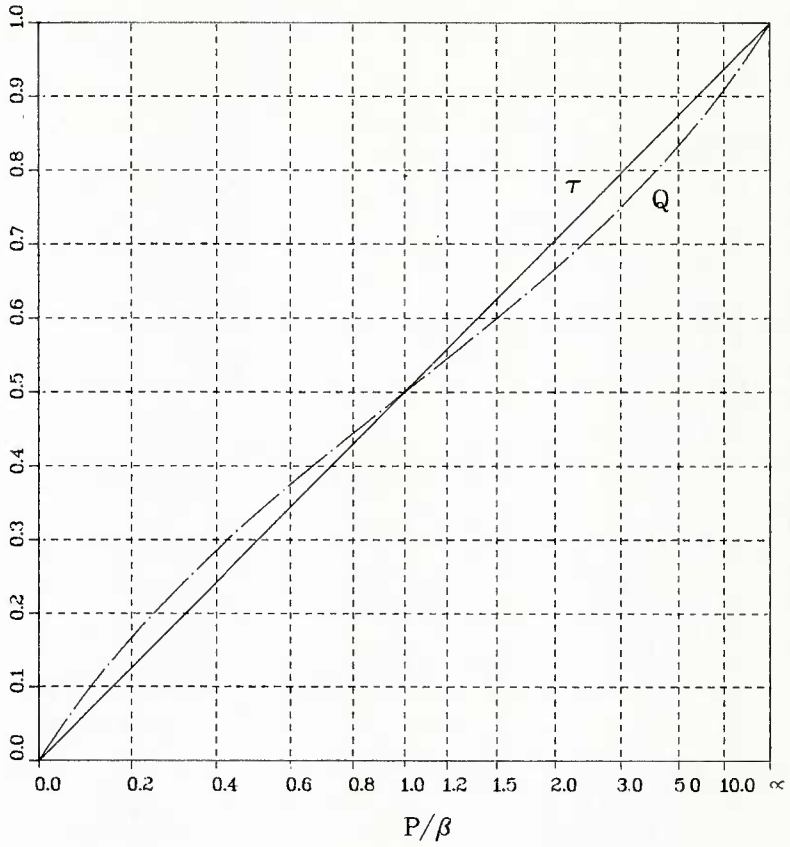

Fig. 4.3 Comparison of porous wall factors

$$\partial I/\partial X\ (0,0) = \pi \quad \text{when } \tau = 0$$

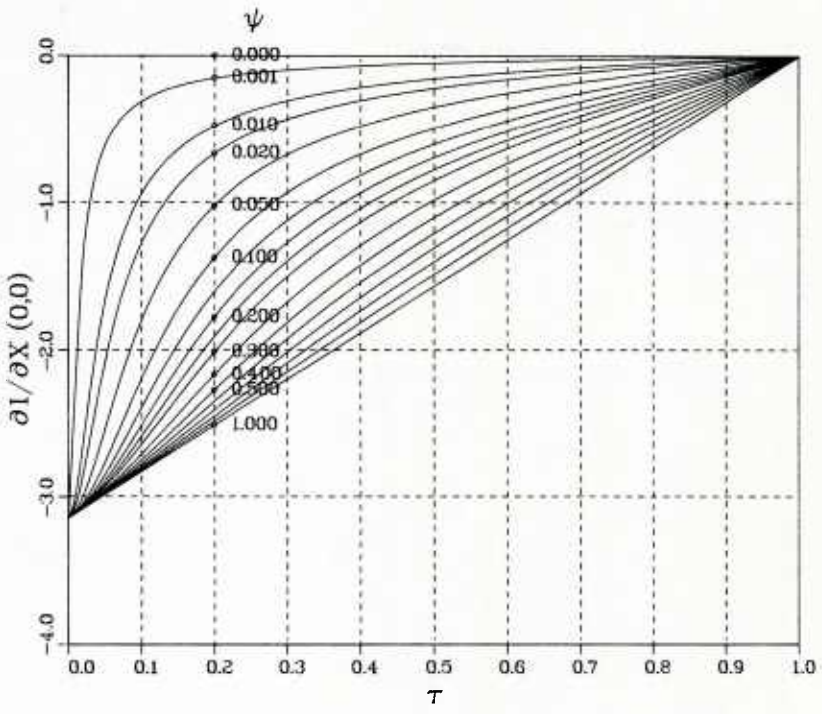

Fig. 4.4 Graph of ∂I/∂X (0,0)

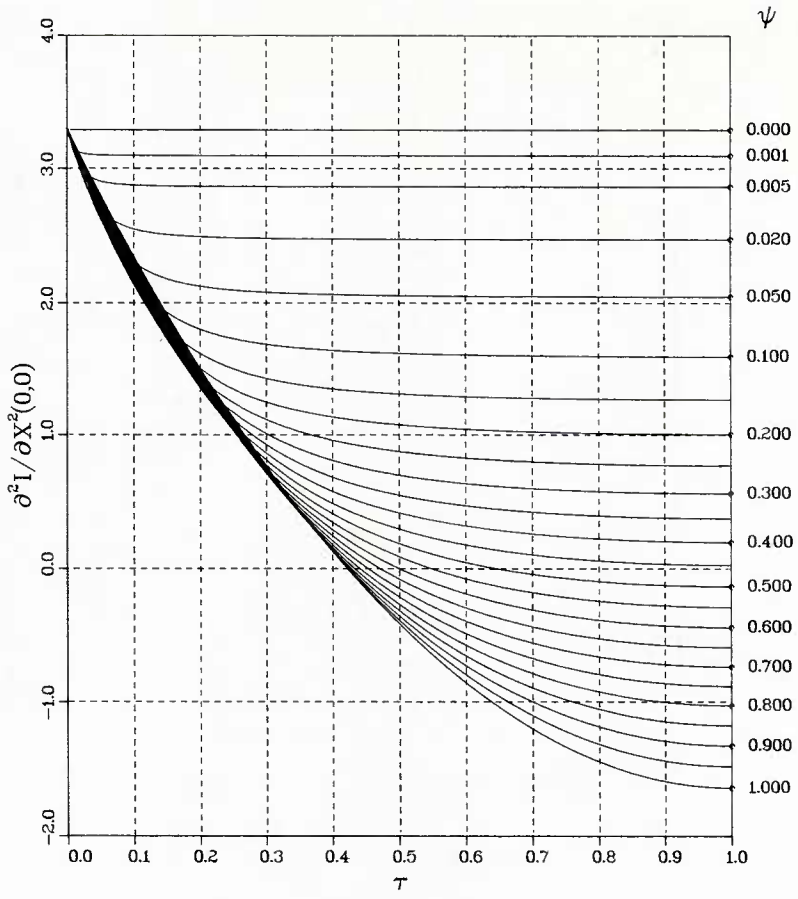

Fig. 4.5 Graph of $\partial^2 I/\partial X^2$ (0,0)

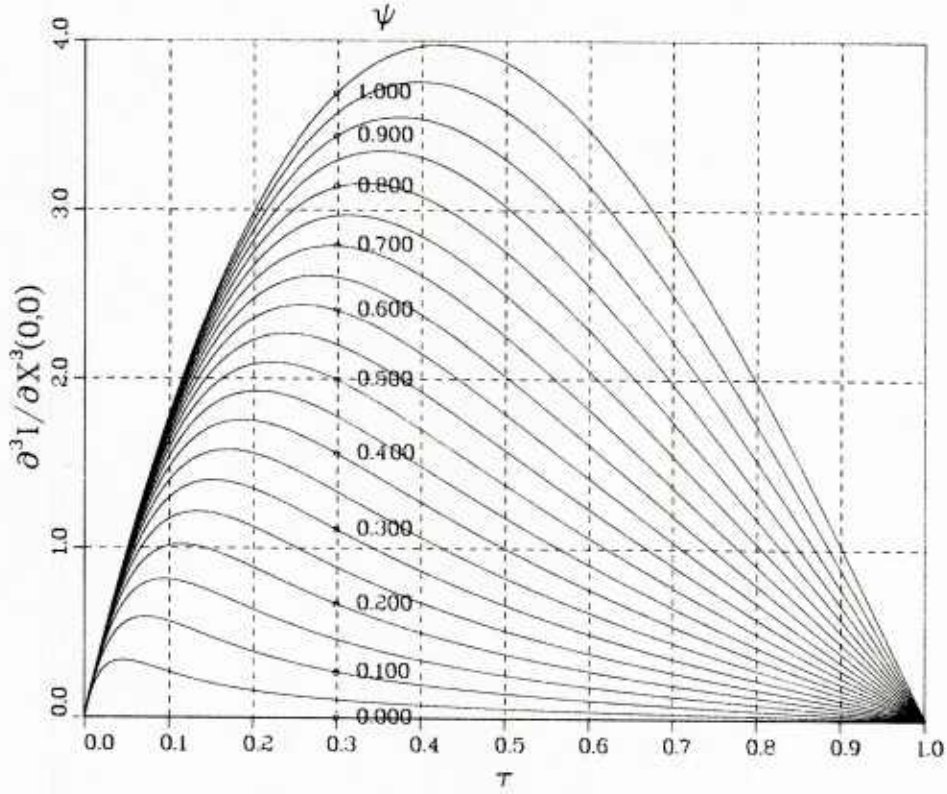

Fig. 4.6 Graph of $\partial^3 I/\partial X^3$ (0,0)

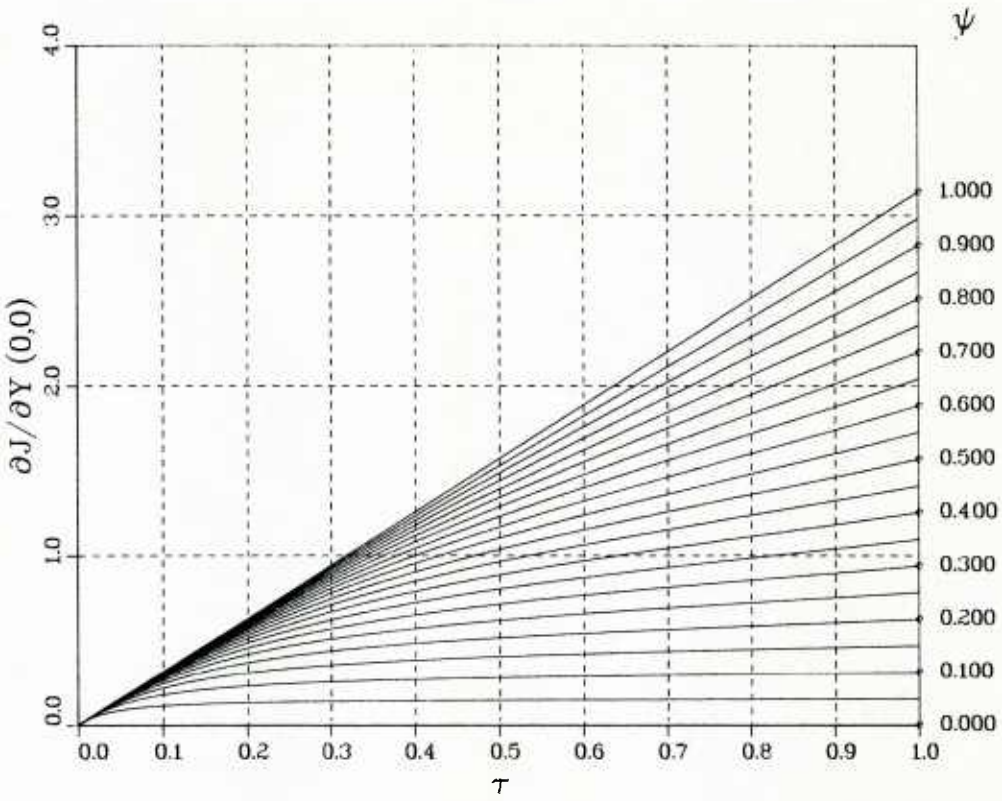

Fig. 4.7 Graph of ∂J/∂Y (0,0)

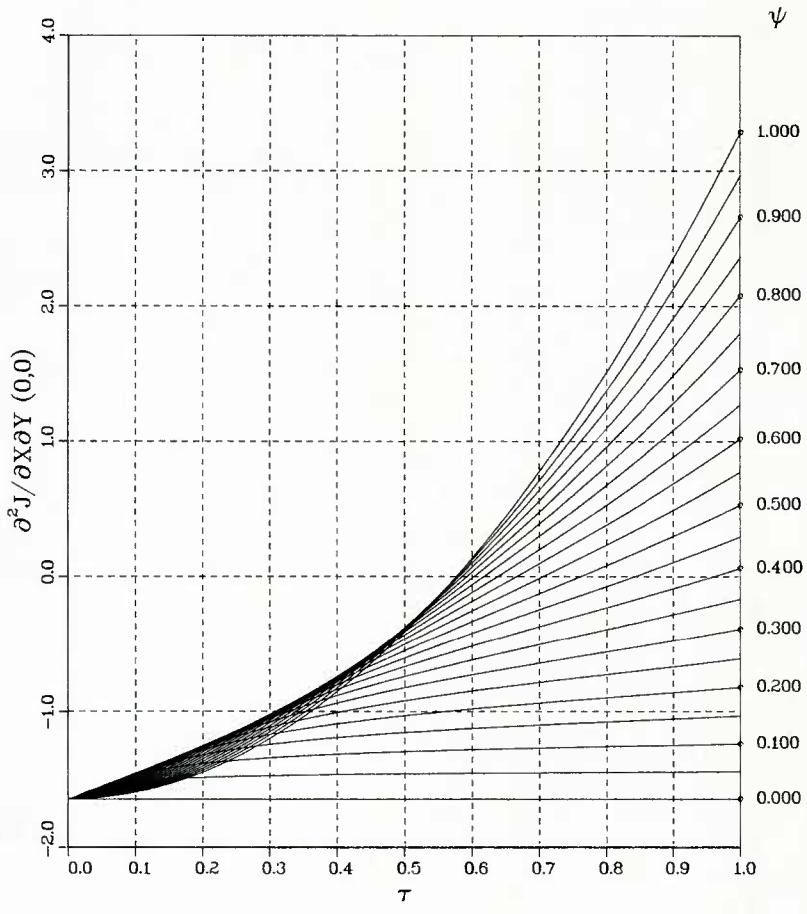

Fig. 4.8 Graph of $\partial^2 J/\partial X \partial Y$ (0,0)

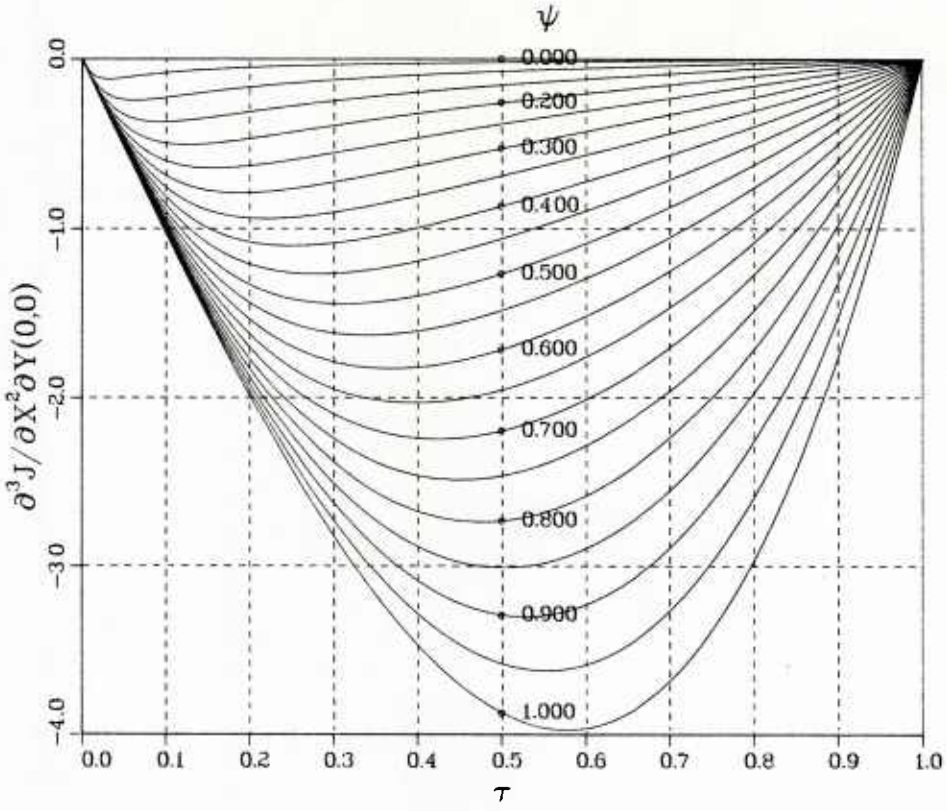

Fig. 4.9 Graph of $\partial^3 J/\partial X^2 \partial Y$ (0,0)

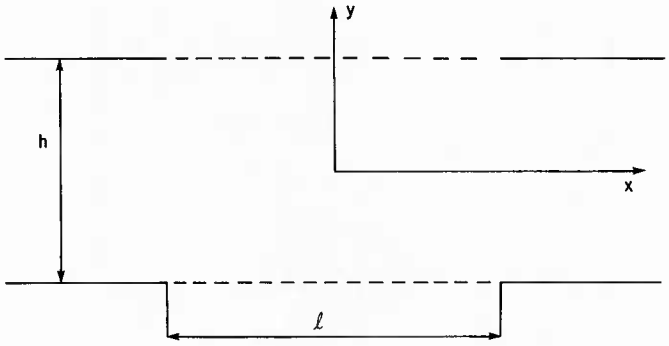

Fig. 4.10 Finite-length ventilated test section

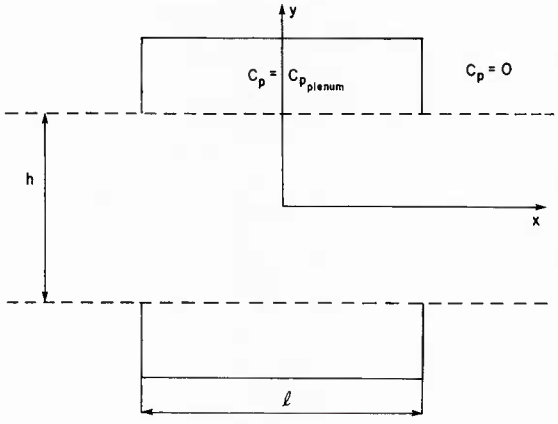

Fig. 4.11 Finite-length plenum chamber

5.0 EXTENDED POROUS WALL THEORY

5.1 Unequal Upper and Lower Porosities / Method of Images

In this section we will consider the extension of the porous wall theory to test sections having unequal upper and lower wall porosity parameters. The case is of relevance if the walls are of different open area ratios or if they are identical, but display unequal resistances to inflow and outflow with respect to the test section, such as the walls with normal perforations, see Chapter 2.

The problem is solved by the method of images which is less general*, but far more effective than the Fourier transform method, since it yields the solutions directly in the infinite series form. The method is applied in the complex plane

$$Z = X + iY \tag{5.1}$$

where

$$X = \frac{x}{\beta h}, \qquad Y = \frac{y}{h} \tag{5.2}$$

are nondimensional co-ordinates, reducing the governing potential equation to the Laplace equation, which is the necessary prerequisite for the use of analytic functions. For generality, we assume that the airfoil is located at an arbitrary position x_0, y_0 in the wind tunnel. The complex co-ordinate of the airfoil location in the transformed plane is thus

$$Z_0 = X_0 + iY_0 \tag{5.3}$$

where

$$X_0 = \frac{x_0}{\beta h}, \qquad Y_0 = \frac{y_0}{h} \tag{5.4}$$

From Equations (4.14) - (4.18), replacing x by $x - x_0$ and y by $y - y_0$, we obtain the complex disturbance velocity

$$W_F(Z) = \frac{\partial \phi_F}{\partial X}(x, y) - i \frac{\partial \phi_F}{\partial Y}(x, y)$$

$$= \frac{\sigma}{\beta} \frac{1}{2\pi (Z - Z_0)} + \gamma \frac{i}{2\pi (Z - Z_0)} + \frac{\mu}{\beta^2 h} \frac{d}{dZ}\left[\frac{1}{2\pi (Z - Z_0)}\right] + \frac{\omega}{\beta h} \frac{d}{dZ}\left[\frac{i}{2\pi (Z - Z_0)}\right] \tag{5.5}$$

The problem then becomes that of finding the complex velocity

$$W_W(Z) = \frac{\partial \phi_W}{\partial X}(x, y) - i \frac{\partial \phi_W}{\partial Y}(x, y) \tag{5.6}$$

which is analytic in the infinite strip $-\infty < X < \infty$, $|Y| \leqslant \frac{1}{2}$ and, according to Equations (4.6) and (4.7), satisfies the porous wall boundary conditions

$$\mathrm{Re}\left[W_F(Z) + W_W(Z)\right] - \frac{\beta}{P_U} \mathrm{Im}\left[W_F(Z) + W_W(Z)\right] = 0, \quad Z = X + \frac{i}{2}, \quad -\infty < X < \infty \tag{5.7}$$

$$\mathrm{Re}\left[W_F(Z) + W_W(Z)\right] + \frac{\beta}{P_L} \mathrm{Im}\left[W_F(Z) + W_W(Z)\right] = 0, \quad Z = X - \frac{i}{2}, \quad -\infty < X < \infty \tag{5.8}$$

where P_U and P_L are the upper and lower wall porosity parameters respectively.

Concerning uniqueness we can, in accordance with Equations (4.9) and (4.10), make the following observations. If $\widetilde{W}_W$ is a solution of the above problem for $P_U = P_L = 0$, then is also

$$W_W(Z) = \widetilde{W}_W(Z) + A \tag{5.9}$$

where A is an arbitrary real constant, Similarly, if $\widetilde{W}_W$ is a solution for $1/P_U = 1/P_L = 0$, then is also

$$W_W(Z) = \widetilde{W}_W(Z) - iB \tag{5.10}$$

where B is an arbitrary real constant. These constants can be fixed by satisfying the upstream condition

*Not applicable to the slotted wall boundary condition because it contains different-order derivatives of the velocity potential.

$$\lim_{X \to -\infty} W_W(Z) = 0 \tag{5.11}$$

As a starting point we consider a unit source

$$W_F(Z) = \frac{1}{2\pi(Z - Z_0)}$$

and construct the function W_W^U analytic in the half plane $Y < \frac{1}{2}$ and satisfying the upper wall boundary condition, Equation (5.7). Since W_F has a simple pole at $Z = Z_0$, we conjecture, by the Schwarz reflection principle and the form of Equation (5.7), that W_W^U has a simple pole at the image point $Z = \bar{Z}_0 + i$, where

$$\bar{Z}_0 = X_0 - iY_0 \tag{5.12}$$

The upper wall image can thus be written

$$W_W^U(Z) = \frac{c}{2\pi(Z - \bar{Z}_0 - i)}$$

where

$$c = a + ib$$

is an unknown pole strength. Substituting in Equation (5.7), we obtain the equation

$$\frac{X - X_0}{\frac{1}{2} - Y_0}\left(1 + a - \frac{\beta}{P_U}b\right) + \left(\frac{\beta}{P_U} - \frac{\beta}{P_U}a - b\right) = 0$$

which, since it holds for an arbitrary X, represents two simultaneous equations for a and b. The solution is

$$a = \frac{\beta^2 - P_U^2}{\beta^2 + P_U^2} = \cos(\pi\tau_U)$$

$$b = \frac{2\beta P_U}{\beta^2 + P_U^2} = \sin(\pi\tau_U)$$

where

$$\tau_U = \frac{2}{\pi}\operatorname{atan}\frac{P_U}{\beta}, \qquad 0 \leqslant \tau_U \leqslant 1 \tag{5.13}$$

in agreement with Equation (4.44). Consequently

$$W_W^U(Z) = \frac{e^{i\pi\tau_U}}{2\pi(Z - \bar{Z}_0 - i)}$$

In a similar fashion we can show that the pole

$$W_F(Z) = \frac{\sigma + i\gamma}{2\pi(Z - Z_0)} \tag{5.14}$$

has the upper wall image

$$W_W^U(Z) = \frac{\overline{\sigma + i\gamma}\, e^{i\pi\tau_U}}{2\pi\,(Z - \bar{Z}_0 - i)}$$

and the lower wall image

$$W_W^L(Z) = \frac{\overline{\sigma + i\gamma}\, e^{-i\pi\tau_L}}{2\pi\,(Z - \bar{Z}_0 + i)}$$

where

$$\tau_L = \frac{2}{\pi}\operatorname{atan}\frac{P_L}{\beta}, \qquad 0 \leqslant \tau_L \leqslant 1 \tag{5.15}$$

The bar above the symbols, denoting complex conjugation, is retained in the above formulas to facilitate the description of images produced by multiple reflections.

Since in complex variables the exponential function defines a simple rotation, we immediately see that the complex disturbance velocity induced by a perforated wall is obtained from that induced by a solid wall by the rotation through the angle $\pi\tau_U$ or $-\pi\tau_L$, depending on whether the upper or lower wall is considered. For open jet walls, $\tau_U = \tau_L = 1$, the rotation angles are π and $-\pi$ respectively, which confirms the well known fact that the solid and open wall images have opposite polarities [5.1]. These findings, making the application of the image method to porous walls possible, were first made by Kassner [5.2]; for further discussion and illustrations also see Goethert [5.3]. We are mentioning these facts to show that the parameter τ, introduced formally in Equation (4.44), has also a physical meaning. The integral form solutions in Chapter 4 are, of course, more difficult to interpret.

In the case of two walls, the boundary conditions (5.7) and (5.8) have to be satisfied simultaneously. By analogy with the formation of optical images by two parallel mirrors, the boundary effect of two walls is given by a sequence of images located at $\overline{Z}_0 + i$, $\overline{Z}_0 - i$, $Z_0 + 2i$, $Z_0 - 2i$, $\overline{Z}_0 + 3i$, and so on, see Figure 5.1. Following the approach of Ebihara [5.4], the boundary effect of the porous walls for the pole (5.14), is then given by infinite series

$$W_W(Z) = \frac{\overline{\sigma + i\gamma}\, e^{i\pi\tau_U}}{2\pi (Z - \overline{Z}_0 - i)} + \frac{\overline{\sigma + i\gamma}\, e^{-i\pi\tau_L}}{2\pi (Z - \overline{Z}_0 + i)} + \frac{\overline{\overline{\sigma + i\gamma}\, e^{-i\pi\tau_L}}\, e^{i\pi\tau_U}}{2\pi (Z - Z_0 - 2i)} + \frac{\overline{\overline{\sigma + i\gamma}\, e^{i\pi\tau_U}}\, e^{-i\pi\tau_L}}{2\pi (Z - Z_0 + 2i)} + \ldots$$

$$= (\sigma + i\gamma)\, B(Z) + \overline{(\sigma + i\gamma)}\, E(Z)$$

$$= \sigma\, [B(Z) + E(Z)] + i\gamma\, [B(Z) - E(Z)] \tag{5.16}$$

where

$$B(Z) = \frac{1}{2\pi} \sum_{m=1}^{\infty} \left[\frac{e^{i\pi m(\tau_U + \tau_L)}}{Z - Z_0 - i\,2m} + \frac{e^{-i\pi m(\tau_U + \tau_L)}}{Z - Z_0 + i\,2m} \right] \tag{5.17}$$

$$E(Z) = \frac{1}{2\pi} \sum_{m=1}^{\infty} \left[\frac{e^{i\pi [m\tau_U + (m-1)\tau_L]}}{Z - \overline{Z}_0 - i(2m-1)} + \frac{e^{-i\pi [(m-1)\tau_U + m\tau_L]}}{Z - \overline{Z}_0 + i(2m-1)} \right] \tag{5.18}$$

These series can be summed using the Fourier expansion of the function exp(tx) on the interval $0 < t < 2\pi$ (Mittag-Leffler theorem), see for details Reference [5.5]:

$$B(Z) = \frac{1}{2} \frac{\exp\left[\pi \frac{\tau_U + \tau_L}{2} (Z - Z_0)\right]}{\exp [\pi(Z - Z_0)] - 1} - \frac{1}{2\pi (Z - Z_0)} \tag{5.19}$$

$$E(Z) = -\frac{1}{2} \frac{\exp\left[\pi \frac{\tau_U + \tau_L}{2} (Z - \overline{Z}_0)\right]}{\exp [\pi (Z - \overline{Z}_0)] + 1} \exp\left[i\pi \frac{\tau_U - \tau_L}{2}\right] \tag{5.20}$$

where

$$0 < \frac{\tau_U + \tau_L}{2} < 1$$

At the end points of the porosity interval, the functions defined by infinite series (5.17) and (5.18) experience jump discontinuities; in other words the series do not converge uniformly on the corresponding closed interval [5.6]. As a result, the values obtained by the substitution

$$\frac{\tau_U + \tau_L}{2} = 0 \text{ or } 1$$

in Equations (5.19) and (5.20) differ from the correct series values (5.19) and (5.10) by constant terms, see Reference [5.4]. However, in view of conditions (5.9) and (5.10) and the requirement to satisfy Equation (5.11), these constants can be disregarded at this point.

The function B has a removable singularity at $Z = Z_0$ and can be expanded in its vicinity in the power series

$$B(Z) = \frac{1}{2} \sum_{n=1}^{\infty} B_n \left(\frac{\tau_U + \tau_L}{2}\right) \frac{[\pi (Z - Z_0)]^{n-1}}{n!}, \qquad |Z - Z_0| < 2 \tag{5.21}$$

where B_n denotes the Bernoulli polynomials

$$B_1(T) = T - \frac{1}{2}$$

$$B_2(T) = T^2 - T + \frac{1}{6}$$

$$B_3(T) = T^3 - \frac{3}{2}T^2 + \frac{1}{2}T \tag{5.22}$$

etc., see Reference [5.7]. Similarly, the function E can be expanded about the point $Z = \overline{Z}_0$ as

$$E(Z) = -\frac{1}{4}\exp\left[i\pi\frac{\tau_U - \tau_L}{2}\right]\sum_{n=0}^{\infty} E_n\left(\frac{\tau_U + \tau_L}{2}\right)\frac{[\pi(Z - \overline{Z}_0)]^n}{n!}, \quad |Z - \overline{Z}_0| < 1 \tag{5.23}$$

where E_n denotes the Euler polynomials

$$E_0(T) = 1$$

$$E_1(T) = T - \frac{1}{2}$$

$$E_2(T) = T^2 - T \tag{5.24}$$

etc., again see Reference [5.7].

Using the result of Equations (5.14) and (5.16), the complex disturbance velocity W_W, corresponding to W_F, Equation (5.5), is constructed as

$$W_W(Z) = \frac{\sigma}{\beta}[B(Z) + E(Z) + \chi(P_U)\chi(P_L)] + i\gamma[B(Z) - E(Z)] + \frac{\mu}{\beta^2 h}\frac{d}{dZ}[B(Z) + E(Z)] + i\frac{\omega}{\beta h}\frac{d}{dZ}[B(Z) - E(Z)] \tag{5.25}$$

The term

$$\chi(P_U)\chi(P_L) = \begin{cases} 1\ , & P_U = P_L = 0 \\ 0\ , & \text{otherwise} \end{cases}$$

(for definition see Equation (4.62)), is added to the source contribution in order to satisfy the upstream condition (5.11).

Using Equations (5.2) and (5.6), the wall interference corrections at the model position $Z = Z_0$ are obtained as follows:

velocity (blockage) correction

$$u_W(x_0, y_0) = \frac{1}{\beta h}\,\mathrm{Re}\,[W_W(Z_0)] \tag{5.26}$$

incidence correction

$$v_W(x_0, y_0) = -\frac{1}{h}\,\mathrm{Im}\,[W_W(Z_0)] \tag{5.27}$$

velocity gradient correction

$$\frac{\partial u_W}{\partial x}(x_0, y_0) = \frac{1}{\beta^2 h^2}\,\mathrm{Re}\left[\frac{d\,W_W}{dZ}(Z_0)\right] \tag{5.28}$$

streamline curvature correction

$$\frac{\partial v_W}{\partial x}(x_0, y_0) = -\frac{1}{\beta h^2}\,\mathrm{Im}\left[\frac{d\,W_W}{dZ}(Z_0)\right] \tag{5.29}$$

The detailed correction formulas can be worked out by substituting from Equations (5.20), (5.21) and (5.25). However, in order to avoid cumbersome expressions, it is advisable to adhere to complex variables and let the computer find the real and imaginary parts.

Although situating the airfoil off axis may have certain potential benefits, cf. Wieselsberger [5.8], the most common test arrangement is to place the airfoil on the tunnel axis. Putting $Z = Z_0$, we obtain from Equations (5.21), (5.23) and (5.25) the following corrections for unequal upper and lower wall porosities:

$$u_W(0,0) = \frac{\sigma}{\beta^2 h}\left[\frac{1}{2}B_1\left(\frac{\tau_U+\tau_L}{2}\right) - \frac{1}{4}\cos\left(\pi\frac{\tau_U-\tau_L}{2}\right) + \chi(P_U)\,\chi(P_L)\right] - \frac{\gamma}{4\beta h}\sin\left(\pi\frac{\tau_U-\tau_L}{2}\right)$$
$$+ \frac{\mu\pi}{4\beta^3h^2}\left[B_2\left(\frac{\tau_U+\tau_L}{2}\right) - E_1\left(\frac{\tau_U+\tau_L}{2}\right)\cos\left(\pi\frac{\tau_U-\tau_L}{2}\right)\right] - \frac{\omega\pi}{4\beta^2h^2}E_1\left(\frac{\tau_U+\tau_L}{2}\right)\sin\left(\pi\frac{\tau_U-\tau_L}{2}\right) \qquad (5.30)$$

$$v_W(0,0) = \frac{\sigma}{4\beta h}\sin\left(\pi\frac{\tau_U-\tau_L}{2}\right) - \frac{\gamma}{h}\left[\frac{1}{2}B_1\left(\frac{\tau_U+\tau_L}{2}\right) + \frac{1}{4}\cos\left(\pi\frac{\tau_U-\tau_L}{2}\right)\right]$$
$$+ \frac{\mu\pi}{4\beta^2h^2}E_1\left(\frac{\tau_U+\tau_L}{2}\right)\sin\left(\pi\frac{\tau_U-\tau_L}{2}\right) - \frac{\omega\pi}{4\beta h^2}\left[B_2\left(\frac{\tau_U+\tau_L}{2}\right) + E_1\left(\frac{\tau_U+\tau_L}{2}\right)\cos\left(\pi\frac{\tau_U-\tau_L}{2}\right)\right] \qquad (5.31)$$

$$\frac{\partial u_W}{\partial x}(0,0) = \frac{\sigma\pi}{4\beta^3h^2}\left[B_2\left(\frac{\tau_U+\tau_L}{2}\right) - E_1\left(\frac{\tau_U+\tau_L}{2}\right)\cos\left(\pi\frac{\tau_U-\tau_L}{2}\right)\right] - \frac{\gamma\pi}{4\beta^2h^2}E_1\left(\frac{\tau_U+\tau_L}{2}\right)\sin\left(\pi\frac{\tau_U-\tau_L}{2}\right)$$
$$+ \frac{\mu\pi^2}{\beta^4h^3}\left[\frac{1}{6}B_3\left(\frac{\tau_U+\tau_L}{2}\right) - \frac{1}{4}E_2\left(\frac{\tau_U+\tau_L}{2}\right)\cos\left(\pi\frac{\tau_U-\tau_L}{2}\right)\right] - \frac{\omega\pi^2}{4\beta^3h^2}E_2\left(\frac{\tau_U+\tau_L}{2}\right)\sin\left(\pi\frac{\tau_U-\tau_L}{2}\right) \qquad (5.32)$$

$$\frac{\partial v_W}{\partial x}(0,0) = \frac{\sigma\pi}{4\beta^2h^2}E_1\left(\frac{\tau_U+\tau_L}{2}\right)\sin\left(\pi\frac{\tau_U-\tau_L}{2}\right) - \frac{\gamma\pi}{4\beta h^2}\left[B_2\left(\frac{\tau_U+\tau_L}{2}\right) + E_1\left(\frac{\tau_U+\tau_L}{2}\right)\cos\left(\pi\frac{\tau_U-\tau_L}{2}\right)\right]$$
$$+ \frac{\mu\pi^2}{4\beta^3h^3}E_2\left(\frac{\tau_U+\tau_L}{2}\right)\sin\left(\pi\frac{\tau_U-\tau_L}{2}\right) - \frac{\omega\pi^2}{\beta^2h^3}\left[\frac{1}{6}B_3\left(\frac{\tau_U+\tau_L}{2}\right) + \frac{1}{4}E_2\left(\frac{\tau_U+\tau_L}{2}\right)\cos\left(\pi\frac{\tau_U-\tau_L}{2}\right)\right] \qquad (5.33)$$

Setting $\tau_U = \tau_L = \tau$ we recover the earlier derived formulas (4.94) - (4.97) for equal porosities. However, if $\tau_U \neq \tau_L$, the usual symmetry and antisymmetry flow conditions no longer apply and we notice that γ and ω also contribute to the velocity correction and σ and μ affect the incidence correction. For larger differences between τ_U and τ_L the magnitude of the velocity correction due to lift overshadows the wake and solid blockage terms. This leads to difficulties, if it is desired to test airfoils at varying incidence and constant Mach number.

Having Equations (5.30) - (5.33) at hand, it is easy to obtain the corrections for the special case $\tau_U = 1$, $\tau_L = 0$, which is complementary to the earlier analyzed cases $\tau_U = \tau_L = 0$, Equations (4.98) - (4.101), and $\tau_U = \tau_L = 1$, Equations (4.102) - (4.105). For the lower wall solid and the upper wall open we thus have

$$u_W(0,0) = -\frac{\gamma}{4\beta h} - \frac{1}{48}\frac{\mu\pi}{\beta^3h^2} \qquad (5.34)$$

$$v_W(0,0) = \frac{\sigma}{4\beta h} + \frac{1}{48}\frac{\omega\pi}{\beta h^2} \qquad (5.35)$$

$$\frac{\partial u_W}{\partial x}(0,0) = -\frac{1}{48}\frac{\sigma\pi}{\beta^3h^2} + \frac{1}{16}\frac{\omega\pi^2}{\beta^3h^3} \qquad (5.36)$$

$$\frac{\partial v_W}{\partial x}(0,0) = \frac{1}{48}\frac{\gamma\pi}{\beta h^2} - \frac{1}{16}\frac{\mu\pi^2}{\beta^2h^3} \qquad (5.37)$$

From the point of view of the design of minimum correction test sections, this case is of considerable interest since at high Mach numbers the flow is not prone to choking on the upper (suction) side of the airfoil and yet the incidence correction (5.35) remains small. The lift-dependent velocity correction (5.34) is unfortunately large. A low correction wind tunnel, utilizing one wall solid and one wall with transversal slots, has been designed by Williams and Parkinson, References [5.9] and [5.10], with encouraging results for testing of high lift systems.

The practical importance of the derived corrections (5.30) - (5.33) is that they account for the difference of porosity factors on the walls opposing the suction and pressure sides of the airfoil, regardless of whether the difference is caused by unequal open area ratios of the walls or different physics of inflow and outflow. The porosity parameters can be estimated by comparing the theoretical pressure coefficients.

$$C_p(x, y) = -2 \frac{\partial \phi}{\partial x}(x, y)$$

$$= -\frac{2}{\beta h} \mathrm{Re}\left[W_F(Z) + W_W(Z)\right] \tag{5.38}$$

with the measured ones near the walls [5.5].

5.2 Least Squares Method to Determine P_U, P_L

The preceding section shows how the theoretical wall boundary pressure distribution (5.38) can be calculated for given values of P_U and P_L. In a practical situation, though, we do not know what values should be used for P_U and P_L. However, if we know the wall boundary pressures from measurement, C_P^M, we can then compare this measured value to the computed value C_p^C and minimize

$$S = \sum_{i=1}^{N} \left(C_{p_i}^M - C_{p_i}^C\right)^2$$

where N is the total number of pressures taken on (or near) both the upper and lower walls. The minimization of S is achieved by varying P_U and P_L.

To carry out the process numerically we differentiate S with respect to P_U and P_L and set the derivatives to zero, thus giving two simultaneous nonlinear algebraic equations, which are solved by Newton's method. The partial derivatives

$$\frac{\partial C_{p_i}^C}{\partial P_U} \quad \left(\text{or } \frac{\partial C_{p_i}^C}{\partial P_L}\right)$$

which are needed for the method are approximated by differences

$$\frac{C_{p_i}^C (P_U + \Delta P_U) - C_{p_i}^C (P_U)}{\Delta P_U}$$

Here ΔP_U is taken to be 0.05, while we assume as a starting point $P_U = 1.0, P_L = 0.5$.

Results of a typical optimization are shown in Table 5.1. The initial porosity parameters give $\Delta\alpha = -0.67°$ and $\Delta M_\infty = -0.0060$ with the sum $S = 0.0102$. After only 2 Newton steps we arrive at the optimum $P_U = 1.53, P_L = 0.54$ with $\Delta\alpha = -0.72°$, $\Delta M_\infty = -0.0083$ and $S = 0.0068$. The final wall pressure distribution after optimization is shown in Figure 5.2.

5.3 Variable Porosity Method

So far it has been assumed that the porosity along the walls is constant, although it can be different for the upper and lower walls. However, in practice it can be seen in some cases that one or both walls experience both inflow ($C_p < 0$) and outflow ($C_p > 0$), see Figure 5.2 for example. Thus it is desirable to ascribe a constant P_{in} to the inflow portions of the walls and different constant P_{out} to the outflow portions. The disadvantage of such an approach is that an analytic solution is not available and a numerical solution must be sought.

The numerical solution has been described in Reference [5.11]. Here we present only a brief outline of the technique.

We again assume that the total disturbance potential is made up of the free air disturbance potential and the wall disturbance potential:

$$\phi = \phi_F + \phi_W$$

where ϕ_F is given in Equation (4.14) and includes contributions due to lift, cross-sectional area, pitching moment and wake drag, Equations (4.15) - (4.18). The problem reduces to that of solving Laplace's equation

$$\frac{\partial^2 \phi_W}{\partial X^2} + \frac{\partial^2 \phi_W}{\partial Y^2} = 0$$

subject to

$$\phi_W = -\phi_F$$

at an upstream line $X = -X_\infty$ and

$$\frac{\partial \phi_W}{\partial X} = -\frac{\partial \phi_F}{\partial X}$$

at a downstream line $X = X_\infty$, where X and Y denote the transformed variables, Equations (5.2). Also on the upper and lower walls we have

$$\frac{P}{\beta}\frac{\partial \phi_W}{\partial X} \pm \frac{\partial \phi_W}{\partial Y} = -\left(\frac{P}{\beta}\frac{\partial \phi_F}{\partial X} \pm \frac{\partial \phi_F}{\partial Y}\right) \qquad \text{for} \qquad Y = \pm\frac{1}{2}$$

In the preceding porous wall boundary condition we choose P according to whether there is inflow or outflow at the particular X location. Thus

$$P = P_{in} \qquad \text{for} \qquad C_p < 0$$

and

$$P = P_{out} \qquad \text{for} \qquad C_p > 0$$

Since we do not know in advance from the theory whether there is inflow or outflow, we assume, for the first iteration, that the upper wall has an inflow condition, while the lower wall has complete outflow. Thus on the first iteration we recover the constant porosity solution and can compare our numerical solution with the analytical solution obtained in the previous section. Table 5.2 shows such a comparison: it can be seen that the numerical solution is very good as judged by the pressure distributions on the upper and lower walls and the Mach number and angle of attack corrections at the quarter chord point.

Also shown in Table 5.2 is the variable porosity solution obtained after 2 iterations of adjusting the porosity to be an inflow or an outflow value (in this case 1.5 or 0.5 respectively). The corrections ΔM_∞ and $\Delta\alpha$ in the bottom portion of the table are seen to be affected very little.

The variable porosity method just described, in combination with the least squares optimization process, has been used to determine P_{in} and P_{out} for some typical test cases in the NAE 20% perforated wall test section. The results are summarized in Table 5.3, which also shows the results for constant optimum porosities. We see that there are hardly any differences in ΔM_∞ and only very small differences in $\Delta\alpha$. This seems to indicate that the basic method utilizing unequal, constant porosities for upper and lower walls is a very satisfactory approximation. In Table 5.3 are for comparison also shown the corrections obtained directly from measured wall pressures using the fast Fourier transform technique (FFT), which will be described in Section 6.3.

REFERENCES

[5.1] Prandtl, L. — *Tragflügeltheorie II.* Ludwig Prandtl gesammelte Abhandlungen, Springer-Verlag, 1961, pp. 346-372.

[5.2] Kassner, R.R. — *Subsonic Flow Over a Body Between Porous Walls.* TR 52-9, Wright Air Development Center, Feb. 1952.

[5.3] Goethert, B.H. — *Transonic Wind Tunnel Testing.* Pergamon Press, 1961, pp. 92-103.

[5.4] Ebihara, M. — *A Study of Subsonic, Two-Dimensional Wall-Interference Effect in a Perforated Wind Tunnel with Particular Reference to the NAL 2m x 2m Transonic Wind Tunnel — Inapplicability of the Conventional Boundary Condition.* TR-252T, National Aerospace Laboratory, Japan, 1972.

[5.5] Mokry, M.; Peake, D.J.; Bowker, A.J. — *Wall Interference on Two-Dimensional Supercritical Airfoils, Using Wall Pressure Measurements to Determine the Porosity Factors for Tunnel Floor and Ceiling.* LR-575, National Research Council Canada, Feb. 1974.

[5.6] Mokry, M. — *A Wake-Blockage Paradox in a Perforated Wall Wind Tunnel.* AIAA Journal, Vol. 9, Dec. 1971, pp. 2462-2464.

[5.7] Abramowitz, M.; Stegun, I.A. — *Handbook of Mathematical Functions.* National Bureau of Standards, June 1964, pp. 804-808.

[5.8] Wieselsberger, C. — *Über den Einfluss der Windkanalbegrenzung auf den Widerstand, insbesondere im Bereiche der kompressiblen Strömung.* Luftfahrtforschung, Vol. 19, May 1942, pp. 124-128.

[5.9] Williams, C.D.; Parkinson, G.V. — *A Low-Correction Wall Configuration for Airfoil Testing.* AGARD-CP-174, London, Oct. 1975, pp. 21.1-21.7.

[5.10] Parkinson, G.V.; Williams, C.D.; Malek, A. — *Development of a Low-Correction Wind Tunnel Wall Configuration for Testing High Lift Airfoils.* ICAS Proceedings 1978, Vol. 1, Lisbon 1978, pp. 355-360.

[5.11] Jones, D.J. — *A Method for Computing 2-D Wind Tunnel Wall Interference Effects Allowing for Variable Porosity along Floor and Ceiling.* LTR-HA-37, National Aeronautical Establishment, National Research Council Canada, Feb. 1979.

Table 5.1 Optimization process for wall pressure distributions, Figure 5.2

Newton step	P_U	P_L	$\Delta\alpha$	ΔM_∞	S
0	1.00	0.50	-0.67	-0.0060	0.0102
	1.05	0.50	-0.67	-0.0064	0.0094
	1.00	0.55	-0.70	-0.0054	0.0111
1	1.47	0.56	-0.74	-0.0078	0.0069
	1.54	0.56	-0.74	-0.0080	0.0069
	1.47	0.61	-0.77	-0.0072	0.0073
2	1.53	0.54	-0.72	-0.0083	0.0068

Table 5.2 Theoretical wall pressure distributions and corrections

$M_\infty = 0.758, C_L = 0.58, A = 0.08, C_D = C_M = 0, h/c = 6, P_{in} = 1.5, P_{out} = 0.5$

x/c	C_{P_U}				C_{P_L}			
	constant porosity	exact	variable porosity	free air	constant porosity	exact	variable porosity	free air
-21.133	-0.000	0.000	0.000	-0.000	0.000	0.000	0.000	0.000
-18.613	0.000	0.000	0.000	-0.000	0.000	0.000	0.000	0.001
-16.324	0.000	0.000	0.000	-0.001	0.000	0.000	0.000	0.001
-14.253	0.000	0.000	0.000	-0.001	0.000	0.000	0.000	0.001
-12.383	0.000	0.000	0.001	-0.001	0.000	0.000	0.001	0.001
-10.698	0.000	0.000	0.001	-0.001	0.000	0.000	0.001	0.002
-9.184	0.000	0.000	0.002	-0.002	0.001	0.001	0.002	0.002
-7.824	0.001	0.001	0.003	-0.002	0.001	0.001	0.003	0.003
-6.604	0.001	0.001	0.004	-0.003	0.002	0.002	0.004	0.004
-5.508	0.002	0.002	0.006	-0.004	0.004	0.004	0.006	0.006
-4.520	0.003	0.003	0.008	-0.006	0.007	0.007	0.009	0.009
-3.625	0.004	0.004	0.010	-0.009	0.011	0.011	0.013	0.012
-2.807	0.006	0.005	0.011	-0.014	0.017	0.016	0.019	0.017
-2.051	0.006	0.006	0.008	-0.022	0.026	0.025	0.028	0.023
-1.341	0.003	0.002	0.002	-0.035	0.038	0.037	0.040	0.030
-0.663	-0.008	-0.008	-0.009	-0.050	0.051	0.051	0.053	0.035
0.000	-0.025	-0.024	-0.026	-0.057	0.061	0.061	0.062	0.037
0.663	-0.035	-0.035	-0.036	-0.050	0.065	0.065	0.066	0.035
1.341	-0.035	-0.035	-0.035	-0.035	0.062	0.063	0.063	0.030
2.051	-0.029	-0.029	-0.030	-0.022	0.054	0.054	0.055	0.023
2.807	-0.023	-0.023	-0.023	-0.014	0.044	0.044	0.044	0.017
3.625	-0.017	-0.018	-0.018	-0.009	0.034	0.034	0.034	0.012
4.520	-0.013	-0.013	-0.013	-0.006	0.025	0.025	0.025	0.009
5.508	-0.009	-0.009	-0.009	-0.004	0.018	0.018	0.018	0.006
6.604	-0.006	-0.006	-0.006	-0.003	0.013	0.013	0.013	0.004
7.824	-0.004	-0.004	-0.004	-0.002	0.008	0.008	0.008	0.003
9.184	-0.003	-0.003	-0.003	-0.002	0.005	0.005	0.005	0.002
10.698	-0.002	-0.002	-0.002	-0.001	0.003	0.003	0.003	0.002
12.282	-0.001	-0.001	-0.001	-0.001	0.002	0.002	0.002	0.001
14.253	-0.000	-0.000	-0.001	-0.001	0.001	0.001	0.001	0.001
16.324	-0.000	-0.000	-0.000	-0.001	0.000	0.000	0.001	0.001
18.613	-0.000	-0.000	-0.000	-0.000	0.000	0.000	0.000	0.001
21.133	-0.000	-0.000	-0.000	-0.000	0.000	0.000	0.000	0.000

	constant porosity	exact	variable porosity
ΔM_∞	-0.0084	-0.0084	-0.0087
$\Delta\alpha$	-0.71°	-0.70°	-0.75°

Table 5.3 Corrections for the BGK1 airfoil, h/c = 6, 20% perforated walls

M_∞	α(deg)	C_L	ΔM_∞			$\Delta\alpha$(deg)		
			constant porosity	variable porosity	FFT	constant porosity	variable porosity	FFT
0.758	-3.63	-0.21	-0.001	-0.001	-0.001	0.29	0.25	0.15
0.758	-0.38	0.28	-0.002	-0.003	-0.003	-0.48	-0.48	-0.55
0.758	1.50	0.58	-0.008	-0.008	-0.008	-0.72	-0.76	-0.83
0.758	2.55	0.75	-0.011	-0.011	-0.012	-0.88	-0.93	-1.01
0.758	3.58	0.90	-0.014	-0.014	-0.014	-0.99	-1.06	-1.15
0.758	4.60	0.94	-0.014	-0.015	-0.015	-1.03	-1.09	-1.18

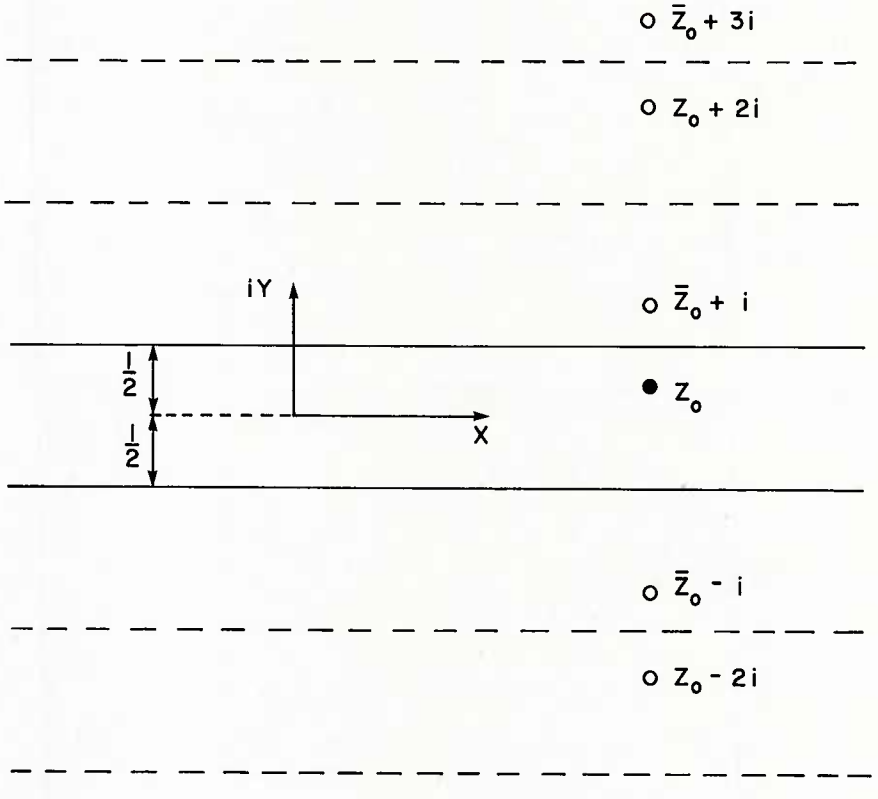

Fig. 5.1 Sequence of images of Z_0

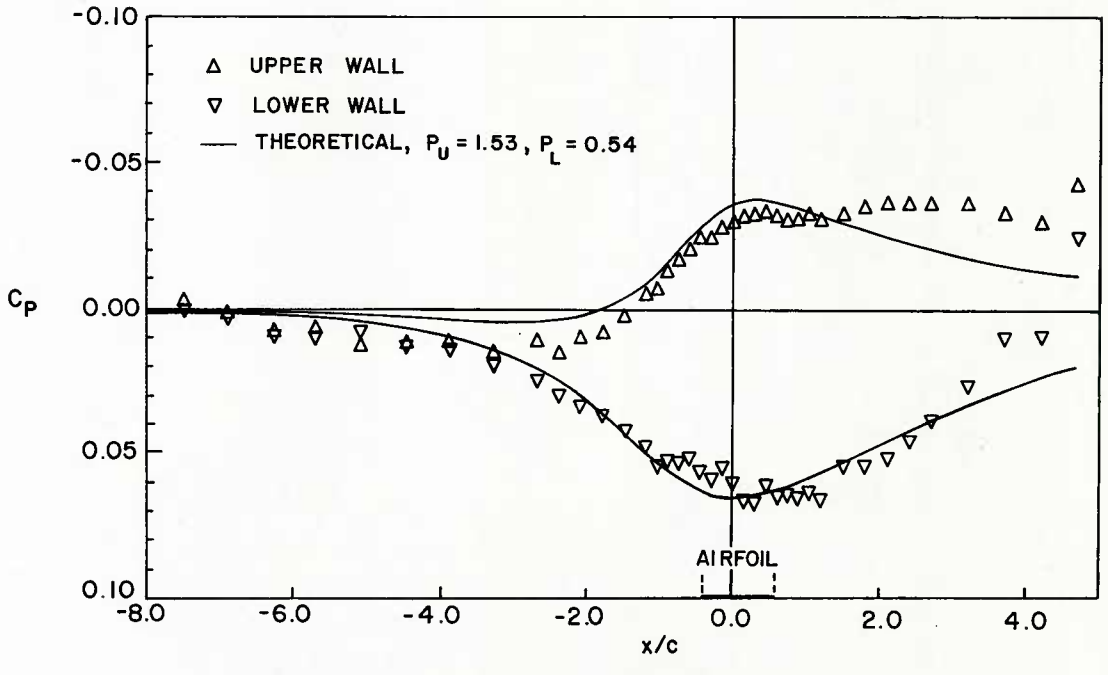

Fig. 5.2 Experimental and theoretical wall pressure distributions, $M_\infty = 0.758$, $C_L = 0.58$, $C_{M_{c/4}} = -0.116$, $C_D = 0.0085$, h/c = 6, 20% perforated walls

6.0 WALL INTERFERENCE CORRECTIONS FROM BOUNDARY MEASUREMENTS

6.1 Early Blockage Corrections for Solid Walls

To utilize wall pressures for the evaluation of wall interference corrections was proposed by Franke and Weinig [6.1], Goethert [6.2], Thom [6.3], Mair and Gamble [6.4] and possibly by others; for a brief description see also References [6.5] and [6.6]. The development of the method was motivated by observations that the determination of solid wall corrections from the classical solid wall theory became unreliable at high speeds and incidences, mainly due to uncertainties in the determination of singularity strengths, representing the far field of model. The use of measured wall pressure data made the estimation of singularity strengths unnecessary.

The method is reviewed here using the theoretical results of Chapter 5. We assume that the airfoil is located on the tunnel axis and that the static pressures are measured along both tunnel walls, $y = \pm h/2$. The asymmetry effect of the lift and pitching moment is eliminated by taking the mean of the upper and lower wall readings, at each streamwise station x.

Introducing the disturbance velocity

$$u(x,y) = \frac{1}{\beta h} \operatorname{Re}\left[W_F(Z) + W_W(Z)\right]$$

we obtain, upon substituting $Z = X \pm i/2$, $Z_0 = 0$ and $\tau_U = \tau_L = 0$ into Equations (5.5), (5.19), (5.20) and (5.25), the following formula

$$\frac{1}{2}\left[u\left(x,\frac{h}{2}\right) + u\left(x,-\frac{h}{2}\right)\right] = \frac{\sigma}{\beta^2 h}\frac{e^{2\pi X}}{1+e^{2\pi X}} + \frac{\mu\pi}{\beta^3 h^2}\frac{2e^{2\pi X}}{(1+e^{2\pi X})^2} \tag{6.1}$$

where

$$X = \frac{x}{\beta h} \tag{6.2}$$

is the reduced streamwise co-ordinate. Alternatively, Equation (6.1) can be written as

$$\frac{1}{2}\left[u\left(x,\frac{h}{2}\right) + u\left(x,-\frac{h}{2}\right)\right] = \frac{\sigma}{2\beta^2 h}\left[1+\tanh(\pi X)\right] + \frac{\mu\pi}{2\beta^3 h^2}\operatorname{sech}^2(\pi X) \tag{6.3}$$

which for the case $\beta = 0$ was earlier given by Rogers [6.6] on basis of Goldstein's theory [6.7].

Substituting $x = 0$, we obtain

$$\frac{1}{2}\left[u\left(0,\frac{h}{2}\right) + u\left(0,-\frac{h}{2}\right)\right] = \frac{1}{2}\frac{\sigma}{\beta^2 h} + \frac{1}{2}\frac{\mu\pi}{\beta^3 h^2} \tag{6.4}$$

Comparing this with the velocity correction (4.98), we see that the mean velocity increment at the wall locations opposite the airfoil is equal to the velocity correction due to the wake blockage plus three times the velocity correction due to the solid blockage, at the position of the airfoil. This simple rule was discovered and experimentally verified by Thom [6.3].

In the absence of wake blockage, $\sigma = 0$, we obtain by comparing Equations (4.98) and (6.1) the correction formula of Franke and Weinig [6.1]

$$u_W(0,0) = \frac{1}{6}\left[u\left(0,\frac{h}{2}\right) + u\left(0,-\frac{h}{2}\right)\right] \tag{6.5}$$

If $\sigma \neq 0$, additional pressure points have to be provided. Mair and Gamble [6.4] utilize for this purpose the infinitely distant point downstream. Taking the limit $x \to \infty$, we obtain from Equation (6.1)

$$\frac{1}{2}\left[u\left(\infty,\frac{h}{2}\right) + u\left(\infty,-\frac{h}{2}\right)\right] = \frac{\sigma}{\beta^2 h} \tag{6.6}$$

which shows that the velocity increment far downstream is twice the velocity correction at the airfoil position due to wake blockage. Substituting Equations (6.5) and (6.6) in (4.98), we obtain the velocity corrections

$$u_W(0,0) = \frac{1}{6}\left[u\left(0,\frac{h}{2}\right) + u\left(0,-\frac{h}{2}\right) + u\left(\infty,\frac{h}{2}\right) + u\left(\infty,-\frac{h}{2}\right)\right] \tag{6.7}$$

This formula is applicable only if the downstream measurement is performed far enough from the model, where a constant pressure level is attained, see Figure 6.1.

Of course, it is not difficult to generalize the above procedure to the case of two finite wall locations, which is more relevant in practice. Since we measure pressures, it is also convenient to work directly with the (linearized) pressure coefficient

$$C_p(x,y) = -2\,u(x,y) \tag{6.8}$$

and rewrite Equation (6.1) as

$$a(x)\,\frac{\sigma}{\beta^2 h} + b(x)\,\frac{\mu\pi}{\beta^3 h^2} = -\frac{1}{2}\left[C_p\left(x,\frac{h}{2}\right) + C_p\left(x,-\frac{h}{2}\right)\right] \tag{6.9}$$

where

$$a(x) = 2\,\frac{e^{2\pi X}}{1+e^{2\pi X}} \tag{6.10}$$

$$b(x) = 4\,\frac{e^{2\pi X}}{(1+e^{2\pi X})^2} \tag{6.11}$$

Knowing the static pressures at $x = x_1$ and $x = x_2$, see Figure 6.2, we set up two linear equations from which the expressions

$$\frac{\sigma}{\beta^2 h} \quad \text{and} \quad \frac{\mu\pi}{\beta^3 h^2}$$

can be evaluated. Substituting in Equations (4.98) and (4.100), we obtain the required velocity and velocity gradient corrections.

As mentioned at the beginning, this correction does not require the knowledge of the singularity strengths σ and μ. This makes it extremely attractive for correcting wind tunnel tests of bluff bodies and airfoils at high incidence, where the direct determination of σ and μ from Equations (4.19) and (4.21) is uncertain because of the presence of flow separation. For example, separation bubbles increase the airfoil cross-section that is hard to estimate [6.8], [6.9], unless the flow is visualized. Further information on blockage corrections for bluff bodies in solid wall test sections can be found in Reference [6.10].

In principle, there are no difficulties in extending the analysis to the asymmetric part of the pressure disturbance

$$C_p\left(x,\frac{h}{2}\right) - C_p\left(x,-\frac{h}{2}\right)$$

Using wall pressures at two streamwise stations x_1 and x_2, we can analogously set up two linear equations in

$$\frac{\gamma}{\beta h} \quad \text{and} \quad \frac{\omega\pi}{\beta^2 h^2}$$

and evaluate the incidence and streamline curvature corrections from Equations (4.99) and (4.101). We are not going into details, since the method is superseded by that of Section 6.5, where the entire wall pressure distributions can be taken into account.

6.2 Method of Capelier, Chevallier and Bouniol

This method utilizes the measured boundary pressures differently from that of Section 6.1. In what we have seen so far, it was always the wall boundary condition that was supposed to be known; the novelty of the approach of Capelier, Chevallier and Bouniol [6.11] is that the measured pressures are directly taken as the boundary values so that the cross-flow properties of the walls do not enter the picture at all. This makes the method particularly suited for the evaluation of wall corrections in test sections with ventilated walls, whose cross-flow properties, as we have seen in Chapter 2, are extremely difficult to model mathematically. However, as in the classical wall interference concept, the far field representation of the model by singularities is still required.

The idea of the method is very simple, resting again upon the existance of the linearized flow at the walls and the concept of splitting the disturbance velocity potential into the free air and wall interference parts, Equation (4.3). The flow is investigated in the infinite strip $-\infty < x < \infty$, $y_1 < y < y_2$, where the wall interference potential is supposed to satisfy Equation (4.5). The lines $y = y_1 < 0$ and $y = y_2 > 0$, see Figure 6.3, along which the static pressures are measured and which bound the analyzed tunnel flow region, are sometimes called the interfaces. Usually, they are placed some distance from the walls (inside the test section), in order to avoid wall viscous effects and smooth out discrete disturbances caused by the open and closed portions of the walls. In this regard the reasoning is very similar to that in Chapter 2, which lead to the introduction of the mean boundary condition concept.

Along the boundaries $y = y_1$ and $y = y_2$, where the flow is assumed to be linearized, the pressure coefficient can be expressed as

$$C_p(x,y) = -2\,\frac{\partial\phi}{\partial x}(x,y)$$

$$= -2\left[\frac{\partial\phi_F}{\partial x}(x,y) + \frac{\partial\phi_W}{\partial x}(x,y)\right] \tag{6.12}$$

For the x component of the wall interference velocity

$$u_W(x,y) = \frac{\partial \phi_W}{\partial x}(x,y) \tag{6.13}$$

we can set up from Equations (4.5) and (6.12) the following Dirichlet problem, see Figure 6.4

$$\beta^2 \frac{\partial^2 u_W}{\partial x^2}(x,y) + \frac{\partial^2 u_W}{\partial y^2}(x,y) = 0, \qquad -\infty < x < \infty, \qquad y_1 < y < y_2 \tag{6.14}$$

$$u_W(x,y_1) = f_1(x) \quad , \quad -\infty < x < \infty$$

$$u_W(x,y_2) = f_2(x) \quad , \quad -\infty < x < \infty \tag{6.15}$$

The boundary values

$$f_1(x) = -\frac{1}{2} C_p(x,y_1) - \frac{\partial \phi_F}{\partial x}(x,y_1)$$

$$f_2(x) = -\frac{1}{2} C_p(x,y_2) - \frac{\partial \phi_F}{\partial x}(x,y_2) \tag{6.16}$$

are obtained from measured static pressures* and by substitution for ϕ_F from Equation (4.14) or (4.25).

The Fourier transform solution of the above Dirichlet problem is [6.12]

$$u_W(x,y) = \frac{1}{2\beta h} \sin\left(\pi \frac{y - y_1}{h}\right) \left[\int_{-\infty}^{\infty} \frac{f_2(\xi)\, d\xi}{\cosh\left(\pi \frac{x - \xi}{\beta h}\right) + \cos\left(\pi \frac{y - y_1}{h}\right)} + \int_{-\infty}^{\infty} \frac{f_1(\xi)\, d\xi}{\cosh\left(\pi \frac{x - \xi}{\beta h}\right) - \cos\left(\pi \frac{y - y_1}{h}\right)} \right] \tag{6.17}$$

where

$$h = y_2 - y_1 \tag{6.18}$$

is the distance between the boundaries.

To find the y component of the interference velocity

$$v_W(x,y) = \frac{\partial \phi_W}{\partial y}(x,y) \tag{6.19}$$

we use the condition of irrotationality

$$\frac{\partial v_W}{\partial x}(x,y) = \frac{\partial u_W}{\partial y}(x,y) \tag{6.20}$$

Thus

$$v_W(x,y) = \int \frac{\partial u_W}{\partial y}(x,y)\, dx + C$$

where C is an arbitrary constant. It can be determined from the condition

---

*If along the interface lines the flow angles were measured instead, an identical Dirichlet problem could be set up for the y component of interference velocity, v_W. However, since u_W and v_W are interdependent (they obey the flow irrotationality condition), a simultaneous specification of both boundary value problems might lead to contradiction. In the case that both static pressures and flow angles are available, it is recommended to use the method described in Section 6.5.

$$\lim_{x \to -\infty} v_W(x,y) = v_\infty \tag{6.21}$$

where v_∞ is the flow angle (in radians) far upstream*, known from empty tunnel calibrations. Ideally, $v_\infty = 0$.

We have no difficulties in verifying that the solution satisfying Equations (6.20) and (6.21) is [6.13]

$$v_W(x,y) = v_\infty + \frac{1}{2h}\left[\int_{-\infty}^{\infty} \frac{e^{\pi\frac{x-\xi}{\beta h}} + \cos\left(\pi\frac{y-y_1}{h}\right)}{\cosh\left(\pi\frac{x-\xi}{\beta h}\right) + \cos\left(\pi\frac{y-y_1}{h}\right)} f_2(\xi)\,d\xi \right.$$

$$\left. - \int_{-\infty}^{\infty} \frac{e^{\pi\frac{x-\xi}{\beta h}} - \cos\left(\pi\frac{y-y_1}{h}\right)}{\cosh\left(\pi\frac{x-\xi}{\beta h}\right) - \cos\left(\pi\frac{y-y_1}{h}\right)} f_1(\xi)\,d\xi \right] \tag{6.22}$$

Using Equations (6.13) and (6.15) it can be shown that

$$\lim_{x \to \infty} v_W(x,y) = v_\infty + \frac{1}{h}\int_{-\infty}^{\infty} \left[f_2(\xi) - f_1(\xi)\right] d\xi$$

$$= v_\infty + \frac{1}{h}\left[\phi_W(\xi,y_2) - \phi_W(\xi,y_1)\right]_{\xi=-\infty}^{\xi=\infty}$$

$$= v_\infty$$

except for open jet boundaries in which case ϕ_W is nonvanishing far downstream, see Equation (4.50), and

$$\lim_{x \to \infty} v_W(x,y) = v_\infty - \frac{c}{h} C_L$$

In Reference [6.11] the conjugate functions u_W and v_W are obtained in one operation using analytic functions. The corresponding Schwarz problem [6.14]** is solved by mapping the infinite strip onto the (upper) half plane and invoking the Cauchy integral formula. The result is also known as Palatini's formula [6.15].

Assuming the airfoil midway between the boundaries, i.e.

$$y_2 = -y_1 = \frac{h}{2}$$

we obtain from Equations (6.17) and (6.22) the following corrections at the airfoil position

$$u_W(0,0) = \frac{1}{2\beta h}\int_{-\infty}^{\infty} \frac{f_2(\xi) + f_1(\xi)}{\cosh\left(\frac{\pi\xi}{\beta h}\right)} d\xi \tag{6.23}$$

$$v_W(0,0) = v_\infty + \frac{1}{h}\int_{-\infty}^{\infty} \frac{f_2(\xi) - f_1(\xi)}{1 + \exp\left(\frac{2\pi\xi}{\beta h}\right)} d\xi \tag{6.24}$$

*The subscript $-\infty$ would be more appropriate.

**The problem of determining an analytic function inside a domain from its defined real part on the boundary. The real part is determined uniquely, the imaginary part to within an arbitrary constant.

$$\frac{\partial u_W}{\partial x}(0,0) = \frac{\pi}{2\beta^2 h^2} \int_{-\infty}^{\infty} \frac{f_2(\xi) + f_1(\xi)}{\cosh^2\left(\frac{\pi\xi}{\beta h}\right)} \sin h\left(\frac{\pi\xi}{\beta h}\right) d\xi \tag{6.25}$$

$$\frac{\partial v_W}{\partial x}(0,0) = \frac{\pi}{2\beta h^2} \int_{-\infty}^{\infty} \frac{f_2(\xi) - f_1(\xi)}{\cosh^2\left(\frac{\pi\xi}{\beta h}\right)} d\xi \tag{6.26}$$

The corrections to measured stream and model quantities are then evaluated using the standard procedures as described in Section 3.7.

As discussed in Reference [6.11], the application of the above correction formulas requires in principle the knowledge of the pressure distributions along the boundaries $y = \pm h/2$, from upstream infinity to downstream infinity. Fortunately, the presence of cosh in the denominators of expressions (6.23), (6.25) and (6.26) makes the weight of f_1 and f_2 diminish rapidly as $|\xi|$ increases. The same does not apply to the incidence correction (6.24): the respective denominator tends to unity as $\xi \to -\infty$ and it is thus required to provide the pressure data up to the point where the difference $f_2 - f_1$ is negligibly small. In fact, numerical experimentation [6.16] with actual tunnel data indicates that the incidence correction is quite sensitive to contributions far upstream. Since the length available for measuring wall pressures is quite often insufficient, a simple extrapolation based on the exponential decay of f_1 and f_2 proves to be helpful, at least in a sense that the integral (6.24) exists and that the residual error is systematic from one tunnel test to another. On the downstream end, f_1 and f_2 tend to a limit which is not necessarily zero [6.17]. Presumably, the extrapolation is less crucial there, but it should be kept in mind that the zero circulation condition

$$\int_{-\infty}^{\infty} \left[f_2(\xi) - f_1(\xi)\right] d\xi = 0$$

has to be satisfied if the flow is expected to be parallel to the tunnel axis far upstream and downstream. Other helpful suggestions concerning the truncation of wall pressure signatures were made by Vaucheret [6.19].

As pointed out in References [6.11] and [6.13], one of the most attractive features of the method is that the velocity (Mach number) correction compensates automatically for small errors of the reference velocity (Mach number). We shall call it the autocorrection property. To illustrate its principle, we denote by the symbol δ the perturbations (errors) of pertinent stream quantities. Starting with the perturbation δp_∞ of the reference pressure p_∞, we obtain the perturbation of any pressure coefficient C_p based on p_∞ as

$$\delta C_p = \frac{-\delta p_\infty}{\frac{1}{2}\rho_\infty U_\infty^2}$$

The perturbation of the boundary values (6.16) is then

$$\delta f_1(x) = \delta f_2(x) = -\frac{1}{2}\delta C_p = \text{constant}$$

and since any constant is a solution of Equation (6.14), we obtain, without the need of actual evaluating Equation (6.17), the perturbation of the velocity correction

$$\delta \Delta u_W(x,y) = -\frac{1}{2}\delta C_p$$

The relative perturbation of the reference stream velocity U_∞, evaluated from p_∞, is however exactly opposite:

$$\frac{\delta U_\infty}{U_\infty} = -\frac{\delta p_\infty}{\rho_\infty U_\infty^2} = \frac{1}{2}\delta C_p$$

Using Equation (4.128), the corrected stream velocity at the model position is then

$$(U_\infty + \delta U_\infty)\left[1 + u_W(0,0) + \delta u_W(0,0)\right] \simeq U_\infty\left[1 + u_W(0,0)\right]$$

i.e. to the first approximation independent of δp_∞. For incompressible flow, the autocorrection property applies exactly, see Paquet [6.13].

Considering the total amount of work that went into the ventilated wall research during the last thrity years, it is quite amazing that a method as basic and powerful as this had to wait for its discovery until 1977: all the necessary experimental and theoretical tools had been available for a while. Then, it is perhaps no coincidence that the right time came with the advent of the self-correcting wind tunnel, when the importance of the boundary pressure measurements became newly appreciated and the problem of wall interference was given another perspective.

In conclusion we also mention that the boundary value problem described by Equations (6.14) and (6.15) can also be solved numerically, for example by the panel method [6.17], finite difference or finite element techniques. This may be convenient if it is required to calculate the whole interference velocity field and not just the corrections at the model position. Also, the numerical methods are applicable to more complex test section geometries or combinations of pressure and normal velocity boundary conditions. In the latter case, which is appropriate to the solid wall wind tunnel with a finite-length ventilated test section [6.17], care must be taken since we are no longer on the safe ground of the Dirichlet, respectively the Schwarz boundary value problem. The mixed boundary value problem of the Keldysh-Sedov type has a solution only when u_W and v_W are permitted to be unbounded at the solid wall edges. A unique solution exists if Kutta-like conditions are satisfied at either the upstream or downstream solid wall edges [6.18].

6.3 Method of Mokry and Ohman

This method, described in detail in Reference [6.20] and also independently proposed in Reference [6.13], is a variant of the wall correction method discussed in Section 6.2. Instead of using the infinite strip solution, the problem is formulated for a rectangle $x_1 < x < x_2$, $y_1 < y < y_2$, see Figure 6.7, which is more appropriate to testing in actual, finite-length test sections. The method is again of the "Schwarz type", indicating that by using the measured wall pressures the velocity correction is determined uniquely, whereas the flow angle correction is obtained only to within an arbitrary constant. Regarding the autoconvergence of the velocity correction, the same remains valid as in Section 6.2.

Following Reference [6.20], we first employ the transformation

$$\xi = \frac{x - x_1}{\beta}$$
$$\eta = y - y_1 \tag{6.27}$$

that reduces Equation (4.5) to the Laplace equation and the investigated flow region to the rectangle $0 < \xi < a$, $0 < \eta < b$, where

$$a = \frac{x_2 - x_1}{\beta}$$
$$b = y_2 - y_1 \tag{6.28}$$

are the sides of the transformed rectangle.

For the transformed x component of interference velocity

$$\tilde{u}_W(\xi,\eta) = \frac{\partial \phi_W}{\partial \xi}(x,y) = \beta\, u_W(x,y) \tag{6.29}$$

we can set up the following Dirichlet problem

$$\frac{\partial^2 \tilde{u}_W}{\partial \xi^2}(\xi,\eta) + \frac{\partial^2 \tilde{u}_W}{\partial \eta^2}(\xi,\eta) = 0, \qquad 0 < \xi < a, \qquad 0 < \eta < b \tag{6.30}$$

$$\begin{aligned}
\tilde{u}_W(\xi,0) &= f^{(1)}(\xi), \qquad 0 < \xi < a \\
\tilde{u}_W(\xi,b) &= f^{(2)}(\xi), \qquad 0 < \xi < a \\
\tilde{u}_W(0,\eta) &= g^{(1)}(\eta), \qquad 0 < \eta < b \\
\tilde{u}_W(a,\eta) &= g^{(2)}(\eta), \qquad 0 < \eta < b
\end{aligned} \tag{6.31}$$

as illustrated in Figure 6.8. The boundary values

$$\begin{aligned}
f^{(1)}(\xi) &= -\beta\left[\frac{1}{2} C_p(x,y_1) + \frac{\partial \phi_F}{\partial x}(x,y_1)\right] \\
f^{(2)}(\xi) &= -\beta\left[\frac{1}{2} C_p(x,y_2) + \frac{\partial \phi_F}{\partial x}(x,y_2)\right]
\end{aligned} \tag{6.32}$$

are obtained from measured static pressures along the rectangle sides $y = y_1$ and $y = y_2$ and by substituting for ϕ_F from Equation (4.14). Since it is impractical to measure pressures across the stream, the remaining boundary values are obtained by linear interpolation of the corner values:

$$g^{(1)}(\eta) = f^{(1)}(0) + \frac{f^{(2)}(0) - f^{(1)}(0)}{b}\eta$$

$$g^{(2)}(\eta) = f^{(1)}(a) + \frac{f^{(2)}(a) - f^{(1)}(a)}{b}\eta \tag{6.33}$$

Using the method of separation of variables, the solution of the boundary value problem specified by Equations (6.30) and (6.31) is found to be [6.21]

$$\tilde{u}_W(\xi,\eta) = \sum_{k=1}^{\infty}\left[A_k^{(1)}\frac{\sinh\mu_k(b-\eta)}{\sinh\mu_k b} + A_k^{(2)}\frac{\sinh\mu_k\eta}{\sinh\mu_k b}\right]\sin\mu_k\xi$$

$$+ \sum_{k=1}^{\infty}\left[B_k^{(1)}\frac{\sinh\nu_k(a-\xi)}{\sinh\nu_k a} + B_k^{(2)}\frac{\sinh\nu_k\xi}{\sinh\nu_k a}\right]\sin\nu_k\eta \tag{6.34}$$

where the eigenvalues are

$$\mu_k = \frac{k\pi}{a}$$

$$\nu_k = \frac{k\pi}{b} \tag{6.35}$$

The series coefficients are given by the integrals

$$A_k^{(\ )} = \frac{2}{a}\int_0^a f^{(\ )}(\xi)\sin\mu_k\xi\,d\xi$$

$$B_k^{(\ )} = \frac{2}{b}\int_0^b g^{(\ )}(\eta)\sin\nu_k\eta\,d\eta \tag{6.36}$$

where the empty superscript ( ) stands either for (1) or (2).

The above solution is uniformly convergent within the rectangle except near the corners, where it would have to be modified [6.22]. For a model located near the test section centre, Equation (6.34) can be approximated by a truncated series. This can be accomplished by using the following procedure: defining the odd extensions of the boundary functions $f^{(\ )}$ on the interval $0 < \xi < 2a$ and dividing 2a into m equal length intervals, see Figure 6.9, the coefficients $A_k^{(\ )}$ can be approximated according to the rectangular rule as

$$A_k^{(1)} = \frac{2}{m}\sum_{j=0}^{m-1} f^{(1)}\left(a\frac{2j+1}{m}\right)\sin\frac{2\pi jk}{m}$$

$$A_k^{(2)} = \frac{2}{m}\sum_{j=0}^{m-1} f^{(2)}\left(a\frac{2j+1}{m}\right)\sin\frac{2\pi jk}{m} \tag{6.37}$$

If m is selected as an integer power of 2, the above sums can be efficiently calculated by the fast Fourier transform algorithm for the indices $k = 1, 2, \ldots, m/2 - 1$. Accordingly, the upper limit of the first series of (6.34) has to be $m/2 - 1$.

The evaluation of the coefficients $B_k^{(\ )}$ is even simpler; using Equations (6.33) we obtain their closed form integrals

$$B_k^{(1)} = \frac{2}{k\pi}\left[f^{(1)}(0) - (-1)^k f^{(2)}(0)\right]$$

$$B_k^{(2)} = \frac{2}{k\pi}\left[f^{(1)}(a) - (-1)^k f^{(2)}(a)\right] \tag{6.38}$$

Using Equations (6.27) and (6.29), the velocity correction at the model position x = y = 0 is obtained as

$$u_W(0,0) = \frac{1}{\beta}\tilde{u}_W\left(-\frac{x_1}{\beta}, -y_1\right) \tag{6.39}$$

In order to express the incidence correction

$$v_W(0,0) = \frac{\partial \phi_W}{\partial y}(0,0)$$

we form the total differential of $\partial\phi_W/\partial y$ and integrate it along the path $x_{ref}, y_{ref} \to 0, y_{ref} \to 0,0$, where x_{ref}, y_{ref} is a selected interior point of the rectangle, inside the linearized flow region, see Figure 6.7. The integration gives

$$\frac{\partial \phi_W}{\partial y}(0,0) - \frac{\partial \phi_W}{\partial y}(x_{ref}, y_{ref}) = \tilde{v}_W\left(-\frac{x_1}{\beta}, -y_1\right) - \tilde{v}_W\left(\frac{x_{ref} - x_1}{\beta}, y_{ref} - y_1\right)$$

where $\tilde{v}_W$ is the conjugate velocity function

$$\tilde{v}_W(\xi,\eta) = \int \frac{\partial \tilde{u}}{\partial \eta}(\xi,\eta)\, d\xi = -\int \frac{\partial \tilde{u}}{\partial \xi}(\xi,\eta)\, d\eta$$

$$= \sum_{k=1}^{\infty}\left[A_k^{(1)}\frac{\cosh \mu_k (b-\eta)}{\sinh \mu_k b} - A_k^{(2)}\frac{\cosh \mu_k \eta}{\sinh \mu_k b}\right]\cos \mu_k \xi$$

$$+ \sum_{k=1}^{\infty}\left[-B_k^{(1)}\frac{\cosh \nu_k (a-\xi)}{\sinh \nu_k a} + B_k^{(2)}\frac{\cosh \nu_k \xi}{\sinh \nu_k a}\right]\cos \nu_k \eta \tag{6.40}$$

Using Equation (4.3) we can further split

$$\frac{\partial \phi_W}{\partial y}(x_{ref}, y_{ref}) = \theta(x_{ref}, y_{ref}) - \frac{\partial \phi_F}{\partial y}(x_{ref}, y_{ref})$$

where

$$\theta(x_{ref}, y_{ref}) = \frac{\partial \phi}{\partial y}(x_{ref}, y_{ref})$$

is the flow angle (in radians) at the reference station.

Consequently

$$v_W(0,0) = \tilde{v}_W\left(-\frac{x_1}{\beta}, -y_1\right) - \tilde{v}_W\left(\frac{x_{ref} - x_1}{\beta}, y_{ref} - y_1\right) + \theta(x_{ref}, y_{ref}) - \frac{\partial \phi_F}{\partial y}(x_{ref}, y_{ref}) \tag{6.41}$$

The first two right hand terms are evaluated from Equation (6.40) and the last term from Equation (4.14). The only unknown term in Equation (6.41) is the flow angle θ, which has to be measured (yawmeter, laser velocimeter) or estimated by other means. If the distance $|x_1|$ between the airfoil and the upstream side of the rectangle is sufficiently large and the pressure measurements show that

$$C_p(x_1, y_1) \simeq C_p(x_1, y_2) \simeq 0$$

we may assume that the flow at the entrance to the test section is practically undisturbed, select

$$x_{ref} = x_1 \quad , \quad y_{ref} = 0 \tag{6.42}$$

and take

$$\theta\,(x_1,0) = 0 \tag{6.43}$$

or, more exactly, set the flow angle equal to the value known from empty tunnel calibration.

Using Equation (6.29), we similarly obtain the velocity gradient correction

$$\frac{\partial u_W}{\partial x}(0,0) = \frac{1}{\beta^2}\,\frac{\partial \tilde{u}_W}{\partial \xi}\left(-\frac{x_1}{\beta}, - y_1\right) \tag{6.44}$$

and the streamline curvature correction

$$\frac{\partial v_W}{\partial x}(0,0) = \frac{1}{\beta}\,\frac{\partial \tilde{u}_W}{\partial \eta}\left(-\frac{x_1}{\beta}, - y_1\right) \tag{6.45}$$

These corrections are evaluated by summing the differentiated series (6.34); the coefficients $A_k^{(\ )}$ and $B_k^{(\ )}$ remain of course the same as before.

6.4 Method of Paquet

In this method the wall interference corrections are derived from the boundary pressure measurements, utilizing the solution of the Schwarz problem for a semi-infinite strip, Figures 6.5 and 6.6. It may well be the best combination of the two above methods, since the flow angle reference point can be put comfortably far upstream and yet the uncertainty of the downstream extrapolation avoided by performing the measurement (or interpolation) across the stream at a finite distance behand the model. The acquisition of boundary values for the three methods, treated collectively in Paquet's thesis [6.13], is shown schematically in Figure 6.10.

In the co-ordinate system of Figures 6.5 and 6.6, the Dirichlet part of the problem to be solved is

$$\beta^2\,\frac{\partial^2 u_W}{\partial x^2}(x,y) + \frac{\partial^2 u_W}{\partial y^2}(x,y) = 0, \qquad -\infty < x < \ell, \qquad -\frac{h}{2} < y < \frac{h}{2} \tag{6.46}$$

$$\begin{aligned} u_W\left(x, -\frac{h}{2}\right) &= f_1(x), \qquad -\infty < x < \ell \\ u_W\left(x, \frac{h}{2}\right) &= f_2(x), \qquad -\infty < x < \ell \\ u_W(\ell, y) &= g(y), \qquad -\frac{h}{2} < y < \frac{h}{2} \end{aligned} \tag{6.47}$$

where, in accordance with Equations (6.16)

$$\begin{aligned} f_1(x) &= -\frac{1}{2}\,C_p\left(x, -\frac{h}{2}\right) - \frac{\partial \phi_F}{\partial x}\left(x, -\frac{h}{2}\right) \\ f_2(x) &= -\frac{1}{2}\,C_p\left(x, \frac{h}{2}\right) - \frac{\partial \phi_F}{\partial x}\left(x, \frac{h}{2}\right) \\ g(y) &= -\frac{1}{2}\,C_p(\ell, y) - \frac{\partial \phi_F}{\partial x}(\ell, y) \end{aligned} \tag{6.48}$$

Mapping conformally the semi-infinite strip onto the upper half plane and employing the Poisson formula, Paquet [6.13] obtained for $y = 0$ the solution

$$u_W(x,0) = \frac{\sinh\left(\pi\,\frac{\ell - x}{\beta h}\right)}{\beta h}\left\{ \int_{-\infty}^{\ell} \frac{\left[f_2(\xi) + f_1(\xi)\right]\sinh\left(\pi\,\frac{\ell - \xi}{\beta h}\right)}{\cosh\left(\pi\,\frac{2\ell - x - \xi}{\beta h}\right)\cosh\left(\pi\,\frac{x - \xi}{\beta h}\right)}\,d\xi + \beta \int_{-\frac{h}{2}}^{\frac{h}{2}} \frac{g(\eta)\cos\left(\pi\,\frac{\eta}{h}\right)}{\sinh^2\left(\pi\,\frac{\ell - x}{\beta h}\right) + \sin^2\left(\pi\,\frac{\eta}{h}\right)}\,d\eta \right\} \tag{6.49}$$

and the conjugate solution

$$v_W(x,0) = \frac{1}{2h}\left\{ \int_{-\infty}^{\ell} \frac{\left[f_2(\xi) - f_1(\xi)\right] \sinh\left(2\pi \frac{\ell - \xi}{\beta h}\right)}{\cosh\left(\pi \frac{2\ell - x - \xi}{\beta h}\right) \cosh\left(\pi \frac{x - \xi}{\beta h}\right)} d\xi + \beta \int_{-\frac{h}{2}}^{\frac{h}{2}} \frac{g(\eta) \sin\left(2\pi \frac{\eta}{h}\right)}{\sinh^2\left(\pi \frac{\ell - x}{\beta h}\right) + \sin^2\left(\pi \frac{\eta}{h}\right)} d\eta \right\} + v_\infty \qquad (6.50)$$

The velocity gradient and streamline curvature corrections are obtained by differentiating Equations (6.49) and (6.50) with respect to x. Equations (6.23) to (6.26) are recovered by putting $x = 0$ and taking the limit $\ell \to \infty$.

6.5 Method of Ashill and Weeks

The specification of the singularity strengths representing the far field of the airfoil becomes unnecessary if both the pressure and flow angle distributions are known along the test section boundary.* Wall corrections can then be calculated directly from these wall quantities, without knowing anything about the crossflow properties of the walls and the flow in the neighbourhood of the model [6.23]. Near the model the flow can be separated, supercritical, etc., but near the tunnel walls it is assumed to be attached and subcritical.

Ashill and Weeks were among the first researchers who fully realized the great potential of this approach, deriving the general correction formula first from Green's theorem [6.24] and then, more concisely, from Cauchy's integral formula [6.25]. The idea of correcting the model data from measured two components of velocity at a control surface near tunnel walls was independently also pursued by Lo [6.26], who derived the blockage formula for symmetrical flow past an airfoil between solid tunnel walls by solving the linearized boundary value problem using the Fourier transform method. The more straightforward Cauchy integral (or residue) approach was subsequently also adopted by Smith [6.17], [6.27] and by Draft and Dahm [6.28], who pointed out the connection with Lo's blockage formula [6.26].

Using the complex variable approach, we form the complex disturbance velocity

$$w(z) = \beta u(x,y) - iv(x,y) \qquad (6.51)$$

in the region of subsonic linearized flow surrounding the airfoil. Here

$$z = \frac{x}{\beta} + iy \qquad (6.52)$$

is the complex co-ordinate and

$$u(x,y) = \frac{\partial \phi}{\partial x}(x,y)$$
$$v(x,y) = \frac{\partial \phi}{\partial y}(x,y) \qquad (6.53)$$

are the disturbance velocity components. In accordance with the classical wall interference concept we decompose the complex disturbance velocity as

$$w(z) = w_F(z) + w_W(z) \qquad (6.54)$$

where w_F and w_W are analytic in the test section exterior and interior respectively. Applying the Cauchy integral formula to the closed contour L shown in Figure 6.11, we obtain for an interior point z

$$0 = \frac{1}{2\pi i} \int_L \frac{w_F(\zeta)}{\zeta - z} d\zeta \qquad (6.55)$$

and

$$w_W(z) = \frac{1}{2\pi i} \int_L \frac{w_W(\zeta)}{\zeta - z} d\zeta \qquad (6.56)$$

*In fact, the problem would be overdetermined.

where

$$\zeta = \frac{\xi}{\beta} + i\eta \tag{6.57}$$

is the complex co-ordinate of the running (dummy) point. Adding Equations (6.55) and (6.56), we obtain with the help of Equation (6.54) the correction formula [6.27]

$$w_W(z) = \frac{1}{2\pi i} \int_L \frac{w(\zeta)}{\zeta - z} d\zeta \tag{6.58}$$

The velocity and incidence corrections immediately follow as

$$u_W(x,y) = \frac{1}{\beta} \operatorname{Re} w_W(z) \tag{6.59}$$

$$v_W(x,y) = -\operatorname{Im} w_W(z) \tag{6.60}$$

and the velocity gradient and streamline curvature as

$$\frac{\partial u_W}{\partial x}(x,y) = \frac{1}{\beta^2} \operatorname{Re} \frac{dw_W}{dz}(z) \tag{6.61}$$

$$\frac{\partial v_W}{\partial x}(x,y) = -\frac{1}{\beta} \operatorname{Im} \frac{dw_W}{dz}(z) \tag{6.62}$$

The above correction formulas are applicable to arbitrary (simply closed) contours, including those formed by flexible test section walls. For two parallel interface lines at $y = \pm h/2$, Figure 6.12, Equation (6.58) gives [6.25]

$$w_W(z) = -\frac{1}{2\pi i} \int_{-\infty}^{\infty} \frac{w\left(\frac{\xi}{\beta} + i\frac{h}{2}\right)}{\frac{\xi}{\beta} + i\frac{h}{2} - z} \frac{d\xi}{\beta} + \frac{1}{2\pi i} \int_{-\infty}^{\infty} \frac{w\left(\frac{\xi}{\beta} - i\frac{h}{2}\right)}{\frac{\xi}{\beta} - i\frac{h}{2} - z} \frac{d\xi}{\beta} \tag{6.63}$$

At $x = y = 0$ the components of the wall interference velocity are thus

$$u_W(0,0) = \frac{\beta\frac{h}{2}}{2\pi} \int_{-\infty}^{\infty} \frac{u\left(\xi, \frac{h}{2}\right) + u\left(\xi, -\frac{h}{2}\right)}{\xi^2 + \left(\beta\frac{h}{2}\right)^2} d\xi + \frac{1}{2\pi\beta} \int_{-\infty}^{\infty} \left[v\left(\xi, \frac{h}{2}\right) - v\left(\xi, -\frac{h}{2}\right)\right] \frac{\xi}{\xi^2 + \left(\beta\frac{h}{2}\right)^2} d\xi \tag{6.64}$$

$$v_W(0,0) = \frac{\beta\frac{h}{2}}{2\pi} \int_{-\infty}^{\infty} \frac{v\left(\xi, \frac{h}{2}\right) + v\left(\xi, -\frac{h}{2}\right)}{\xi^2 + \left(\beta\frac{h}{2}\right)^2} d\xi - \frac{\beta}{2\pi} \int_{-\infty}^{\infty} \left[u\left(\xi, \frac{h}{2}\right) - u\left(\xi, -\frac{h}{2}\right)\right] \frac{\xi}{\xi^2 + \left(\beta\frac{h}{2}\right)^2} d\xi \tag{6.65}$$

The velocity gradient and streamline curvature correction can be worked out in a similar fashion from Equations (6.61) and (6.62).

For symmetrical flow conditions

$$u\left(\xi, -\frac{h}{2}\right) = u\left(\xi, \frac{h}{2}\right)$$

$$v\left(\xi, -\frac{h}{2}\right) = -v\left(\xi, \frac{h}{2}\right)$$

we obtain from Equation (6.64) the velocity correction

$$u_W(0,0) = \frac{\beta\frac{h}{2}}{\pi}\int_{-\infty}^{\infty}\frac{u\left(\xi,\frac{h}{2}\right)}{\xi^2+\left(\beta\frac{h}{2}\right)^2}\,d\xi+\frac{1}{\pi\beta}\int_{-\infty}^{\infty}v\left(\xi,\frac{h}{2}\right)\frac{\xi}{\xi^2+\left(\beta\frac{h}{2}\right)^2}\,d\xi \tag{6.66}$$

that was first given by Lo [6.26].

Of course, to be able to evaluate the corrections from Equations (6.64) and (6.65), both components of the disturbance velocity, u and v, have to be known at the walls. Within small disturbance theory, they can be obtained from experiment as

$$u\left(\xi,\pm\frac{h}{2}\right) = -\frac{1}{2}C_p\left(\xi,\pm\frac{h}{2}\right)$$
$$v\left(\xi,\pm\frac{h}{2}\right) = \theta\left(\xi,\pm\frac{h}{2}\right) \tag{6.67}$$

where C_p is the pressure coefficient and θ is the flow angle (in radians).

In the case of solid walls, to which the method of Ashill and Weeks is mainly addressed, the flow angle is essentially defined by the condition of no flow through the walls, and so only static pressures need be measured. To the order of accuracy of the small disturbance theory, the flow angles can be estimated from the wall shape adjustment (adaptive walls) and boundary layer development [6.29].

For ventilated walls, the technical problem of measuring flow angles is an obstacle to the routine application of the method. However, there has been a steady progress in applications of laser doppler technology [6.30] and developments of flow angle probes [6.31] and double orifice static pipes [6.32], which eventually will make this powerful correction technique applicable to all types of test sections.

6.6 Methods of Kemp and Murman

A rather different approach to the correction of transonic two-dimensional wind tunnel data is the one taken in the method by Kemp [6.33], [6.34], [6.35] and in the related method by Murman [6.36]. The method is attractive and of practical interest, since it does not require boundary flow angle measurements. It uses experimental pressures at the model and the walls and transonic computational codes to determine whether the airfoil pressure data is correctable in the sense that they can be (with a reasonable accuracy) reproduced computationally by an optimized search of the free air Mach number and angle of attack.

First, an inverse problem is solved to determine the values of the normal component of velocity on the upper and lower surfaces, from which the effective contour S_e of the tested model can be constructed. The use of measured pressures on the model ensures that the boundary layer effects are included in the calculation providing the pressure gradient across the boundary layer is small: the effective contour contains the actual airfoil (at given geometrical incidence) augmented by the displacement area of the boundary layer. Boundary conditions used for the inverse problem include the measured pressure at the tunnel wall, the measured pressure at the model and suitable upstream and downstream boundary conditions. As demonstrated by Kemp [6.37] on the example of the BGK 1 airfoil, shown here in Figure 6.13, a special care should be taken in establishing the flow direction far upstream. Under the assumption that the front portions of the effective and actual contours should coincide (the boundary layer is thin there), it is found that in this particular case the flow far upstream should be inclined - 0.25° with respect to the tunnel axis ($v_\infty \simeq -0.005$). The wall crossflow results earlier shown in Figure 2.16 seem to support this finding in the sense that the crossflow results for upper and lower walls lie on a single curve, having a smooth variation in slope.

Next, the direct problem is solved for free air flow past the effective airfoil contour. Kemp adjusts the free stream Mach number to obtain at a control (match) point on the airfoil the computed pressure equal to that measured in the wind tunnel. Experience has shown that this control point should be selected just upstream of the shock wave. The angle of attack is subsequently adjusted to produce computationally the test lift coefficient, corrected for blockage (change in reference dynamic pressure). The difference between the obtained free air Mach number and the wind tunnel Mach number is then identified with the Mach number correction; a similar rule applies to the angle of attack correction. The data is considered correctable if the difference between the computed and measured surface pressures remains small all over the airfoil. Murman [6.36] formalizes the procedure by defining the error integral

$$E^2 = \frac{1}{q^2}\int_S [p(s)-p_c(s)]^2\,ds \tag{6.68}$$

where p is the measured pressure, p_c is the pressure calculated on the effective airfoil contour in free air, and q is the dynamic pressure for the test. The integral is taken over the actual airfoil contour S and the unconstrained minimization problem is solved to minimize E by varying M_∞ and α. Clearly, if E is zero, the measured pressure distribution corresponds exactly to the calculated stream conditions at the corrected Mach number and angle of attack. In practice, E will not be zero; but if it is small enough, the data will be considered correctable. It is indicated that the values of order 0.01 would likely be acceptable but, apparently, the concept needs to be further quantified on a reliable experimental sample. Since any discrepancy in shock positions produces a large value of E, the minimization procedure is expected to produce nearly identical shock positions for measured and computed data, which is a prerequisite for matching the experiment and computation.

There appear to be several advantages to the Kemp-Murman method over previously outlined wall correction procedures. The method does not require the flow angle measurement along the walls and yet disposes with the far field approximation of the potential

of the airfoil in free air. It accounts for the nonlinearity of transonic flow and incorporates the boundary layer effect, unlike the majority of methods based on potential flow calculation, through the use of the effective airfoil contour. Another feature, as we have seen, is that the comparison of the effective and actual airfoil shape allows to set correctly the flow angle far upstream. However, since it requires more computer time than other methods discussed in this Chapter, it is recommended for benchmark experiments where accurate results are important, or to use it as a base method to validate more approximate correction procedures which may suffice for routine testing [6.36].

6.7 Comparison of Methods on an Experimental Example

As a test case for comparing the various correction methods based on wall pressure measurements, data were selected from an investigation of the BGK 1 airfoil in the NAE 15″ × 60″ two-dimensional test facility with 20% perforated top and bottom walls. The chord to tunnel height ratio was c/h = 1/6 and the airfoil was set at 2.56° incidence relative to the tunnel axis and tested at a reference Mach number of 0.784 and a Reynolds number of 21.03×10^6. Based on earlier analyses, the transition point can be assumed to be near the leading edge at about 7% chord of the airfoil. The airfoil pressure distribution is listed in Table 6.1 and the wall pressure distribution in Table 6.2. These data were submitted to various authors who kindly performed the correction calculations. The results of their efforts are collected in Table 6.3 in the form of evaluated corrections to Mach number and angle of attack.

The NAE (Mokry, Ohman) and the ONERA (Capelier, Chevallier, Bouniol) methods produced identical corrections (within three digits of accuracy). Both methods are based on analytic solutions, utilizing the same principle, cf. Sections 6.2 and 6.3, and if the length over which the wall pressures are scanned is sufficiently large, the different handling of the data on the far ends (extrapolation versus interpolation) should not indeed matter. However, more recently Gopinath [6.16] produced with the ONERA method, supplemented by an exponential fit of the pressure data, a more negative value of ΔM_∞ (− 0.017 versus − 0.015). We may mention that very satisfactory agreement between experiment and free air calculation was achieved using the Bauer-Garabedian-Korn-Jameson program [6.38] and applying the $\Delta M_\infty = -0.015$ correction, see Figure 6.14. The free air computation, performed at the corrected Mach number of 0.769 and the experimental lift coefficient of 0.764, indicates the change of incidence $\Delta\alpha = 1.73° - 2.56° = -0.83°$, which is somewhat larger in amplitude than the angle of attack correction − 0.67° obtained on the assumption of zero flow angle far upstream. On the other hand, a need for a Mach number correction more negative than − 0.015 was called for by Melnik [6.39], who correlated the NAE measurement with viscous-code computations [6.40] that produce more rearward shock locations (mainly because of conservative differencing) than the method of Reference [6.38]. This may also serve as an illustration of the difficulties that are often encountered in the correlation of tunnel measurements with computations.

The NLR (Smith) method is very similar to that of ONERA, but utilizes singularity distributions to solve the Dirichlet problem. It yields the same Mach number correction, but departs slightly in the angle of attack correction. However, this value is supported by the NAL (Sawada) method, which will be described in Chapter 7.

The NASA (Kemp) method gives the angle of attack correction of − 0.64°, close to that obtained by the ONERA and NAE methods. If, however, the airfoil effective contour calculated in the tunnel flow solution is plotted and compared with the actual BGK 1 airfoil shape at 2.56° incidence, Figure 6.13, it appears that the correspondence between contours is improved by superimposing a downwash − 0.25° to the tunnel flow solution. The corresponding angle of attack correction is − 0.89°, close to that obtained indirectly in Figure 6.14. The Mach number correction − 0.017 obtained by Kemp's method agrees with Gopinath [6.16].

REFERENCES

[6.1] Franke, A. Weinig, F. — *The Correction of the Speed of Flow and the Angle of Incidence Due to Blockage by Aerofoil Models in a High Speed Wind Tunnel with Closed Working Section.* F.B. 1171, Rep. & Transl. 259, British M.A.P., April 1946.

[6.2] Goethert, B. — *Wind-Tunnel Corrections at High Subsonic Speeds Particularly for an Enclosed Circular Tunnel.* NACA TM 1330, Feb. 1952.

[6.3] Thom, A. — *Blockage Corrections in a Closed High-Speed Tunnel.* ARC R&M 2033, Nov. 1943.

[6.4] Mair, W.A. Gamble, H.E. — *The Effect of Model Size on Measurements in the R.A.E. High Speed Tunnel. Drag of Two-dimensional Symmetrical Airfoils at Zero Incidence.* ARC R&M 2527, Dec. 1944.

[6.5] Pankhurst, R.C. Holder, D.W. — *Wind-Tunnel Technique.* Pitman & Sons, 1952, pp. 386-388.

[6.6] Rogers, E.W.E. — *Blockage Effects in Closed or Open Tunnels.* Subsonic Wind Tunnel Wall Corrections, AGARDograph 109, Oct. 1966, pp. 311-313.

[6.7] Goldstein, S. — *Two-Dimensional Wind-Tunnel Interference.* ARC R&M 1902, Sept. 1942.

[6.8] Horton, H.P. — *A Semi-Empirical Theory for the Growth and Bursting of Laminar Separation Bubbles.* C.P. No. 1073, Aeronautical Research Council, June 1967.

[6.9] Williams, B.R. — *The Prediction of the Bursting of Laminar Separation Bubbles in the Design of Two-Dimensional High-Lift Aerofoils.* TR 80060, Royal Aircraft Establishment, May 1980.

[6.10] — *Blockage Corrections for Bluff Bodies in Confined Flows.* Item No. 80024, Engineering Sciences Data, Nov. 1980.

[6.11] Capelier, C. Chevallier, J.P. Bouniol, F. — *Nouvelle méthode de correction des effets de parois en courant plan.* La recherche Aérospatiale, Jan.-Feb. 1978, pp. 1-11.

[6.12] Sneddon, I.N. — *The Use of Integral Transforms.* McGraw-Hill, 1972, pp. 93-94.

[6.13] Paquet, J.B. — *Perturbations induites par les parois d'une soufflerie, méthodes intégrales.* Thèse Doc. Ing., Université de Lille, juin 1979.

[6.14] Gakhov, F.D. — *Boundary Value Problems.* Pergamon Press, 1963, pp. 208-210.

[6.15] Lavrent'ev, M.A. Shabat, B.V. — *Metody teorii funktsii kompleksnogo peremennogo.* Moscow 1958, pp. 212-213.

[6.16] Gopinath, R. — *Wall Interference Evaluation from Pressure Measurements on Control Surfaces.* Journal of Aircraft, Vol. 19, 1982, pp. 1097-1098.

[6.17] Smith, J. — *A Method for Determining 2D Wall Interference on an Aerofoil from Measured Pressure Distributions near the Walls and on the Model.* NLR TR 81016 U, National Aerospace Laboratory NLR, Jan. 1981.

[6.18] Lavrent'ev, M.A. Shabat, B.V. — *Metody teorii funktsii kompleksnogo peremennogo.* Moscow 1958, pp. 284-289.

[6.19] Vaucheret, X. — *Reévaluation des resultats corrigés du profil CAST 7 â S3MA.* Annex to the GARTEUR Action Group on Two-Dimensional Transonic Testing Methods (Elsenaar, A. and Stanewsky, E.), 1982.

[6.20] Mokry, M. Ohman, L.H. — *Application of the Fast Fourier Transform to Two-Dimensional Wind Tunnel Wall Interference.* Journal of Aircraft, Vol. 17, June 1980, pp. 402-408.

[6.21] Powers, D.L. — *Boundary Value Problems.* 2nd. Ed., Academic Press, 1979, pp. 179-183.

[6.22] Budak, B.M. Samarskii, A.A. Tikhonov, A.N. — *A Collection of Problems on Mathematical Physics.* Pergamon Press, 1964, pp. 445-447.

[6.23] Rubbert, P.E. — *Some Ideas and Opportunities Concerning Three-Dimensional Wind-Tunnel Wall Corrections.* Wind-Tunnel/Flight Correlation — 1981, NASA Conference Publication 2225, Nov. 1981, pp. 217-229.

[6.24] Ashill, P.R. Weeks, D.J. — *An Experimental Investigation of the Drag of Thick Supercritical Aerofoils — a Progress Report.* TM Aero 1765, Royal Aircraft Establishment, 1978.

[6.25] Ashill, P.R. Weeks, D.J. — *Techniques Developed in Europe for Tunnel-Wall Corrections Using Measured Boundary Conditions.* AGARD FDP Proceedings Integration of Computers and Wind Tunnel Testing, Feb. 1980.

[6.26] Lo, C.F. — *Tunnel Interference Assessment by Boundary Measurements.* AIAA Journal, Vol. 16, 1978, pp. 411-413.

[6.27] Smith, J. — *Measured Boundary Conditions Methods for 2D Flow.* Wall Interference in Wind Tunnels, AGARD-CP-335, 1982, pp. 9.1-9.15.

[6.28] Kraft, E.M. Dahm, W.J.A. — *Direct Assessment of Wall Interference in a Two-Dimensional Subsonic Wind Tunnel.* AIAA Paper 82-0187, Jan. 1982.

[6.29] Ashill, P.R. Weeks, D.J. — *A Method for Determining Wall-Interference Corrections in Solid-Wall Tunnels from Measurements of Static Pressure at the Walls.* Wall Interference in Wind Tunnels, AGARD-CP-335, 1982, pp. 1.1-1.12.

[6.30] Satyanarayana, B. Schairer, E. Davis, S. — *Adaptive-Wall Wind Tunnel Development for Transonic Testing.* Journal of Aircraft, Vol. 18, 1981, pp. 273-279.

[6.31] Sawada, H. Hagii, H. Komatsu, Y. Nakamura, M. — *An Experiment with Special Yawmeters.* TM-409, National Aerospace Laboratory, March 1980.

[6.32] Nenni, J.P. Erickson, J.C. Wittliff, C.E. — *Measurement of Small Normal Velocity Components in Subsonic Flows by Use of a Static Pipe.* AIAA Journal, Vol. 20, 1982, pp. 1077-1083.

[6.33] Kemp, W.B. — *Toward the Correctable-Interference Transonic Wind Tunnel.* Proceedings of the AIAA 9th Aerodynamic Testing Conference, 1976, pp. 31-38.

[6.34] Kemp, W.B. — *Transonic Assessment of Two-Dimensional Wind Tunnel Wall Interference Using Measured Wall Pressures.* Advanced Technology Airfoil Research, NASA Conference Publication 2045, Vol. 1, March 1978, pp. 473-486.

[6.35] Kemp, W.B. — *TWINTAN: A Program for Transonic Wall Interference Assessment in Two-Dimensional Wind Tunnels.* NASA TM-81819, May 1980.

[6.36] Murman, E.M. — *A Correction Method for Transonic Wind Tunnel Wall Interference.* AIAA Paper No. 79-1533, July 1979.

[6.37] Kemp, W.B. — *Transonic Post-Test Assessment.* Presented at the meeting of AGARD Working Group on Design of Transonic Test Sections, NASA Langley, March 1980.

[6.38] Bauer, F. Garabedian, P. Korn, D. Jameson, A. — *Supercritical Wing Sections II.* Springer-Verlag, 1975, pp. 173-191 and 202-240.

[6.39] Melnik, R.E. Private communication, Nov. 1979.

[6.40] Melnik, R.E. Mead, H.R. *A Multi-Grid Method for the Computation of Viscid-Inviscid Interaction on Airfoils.* AIAA Paper 83-0234, Jan. 1983.

Table 6.1 Test case — airfoil pressure distributions

x/c	y/c	C_p	
0.69969	-0.02259	0.1344	
0.65058	-0.01049	0.0496	
0.60088	0.00174	-0.0440	
0.55143	0.01309	-0.1454	
0.50184	0.02316	-0.2454	
0.45197	0.03187	-0.3707	
0.40225	0.03923	-0.5369	
0.37239	0.04299	-0.8942	
0.35257	0.04526	-1.1343	
0.33280	0.04733	-1.1416	
0.31296	0.04922	-1.1347	
0.27317	0.05248	-1.1127	
0.25306	0.05393	-1.1120	
0.23300	0.05523	-1.1004	
0.21308	0.05641	-1.0952	
0.19296	0.05749	-1.0828	
0.17208	0.05841	-1.0691	
0.15320	0.05920	-1.0623	
0.13294	0.05991	-1.0534	
0.11296	0.06048	-1.0656	
0.09301	0.06091	-1.0476	
0.05280	0.06147	-1.0593	
0.03278	0.06155	-1.0338	
0.01276	0.06151	-1.0446	
-0.00727	0.06127	-1.0371	$M_\infty = 0.784$
-0.02741	0.06091	-1.0378	
-0.04735	0.06039	-1.0327	$\alpha = 2.56^\circ$
-0.06750	0.05966	-1.0224	
-0.08736	0.05874	-1.0317	$R_c = 21 \times 10^6$
-0.10754	0.05756	-1.0309	
-0.12757	0.05610	-1.0194	$C_L = 0.764$
-0.14753	0.05423	-0.9919	
-0.15738	0.05318	-0.9759	$A = 0.075$
-0.16771	0.05172	-0.9334	
-0.17764	0.05010	-0.8791	$c/h = 1/6$
-0.18784	0.04810	-0.7686	
-0.19816	0.04562	-0.7074	20% perforated walls
-0.20810	0.04280	-0.5856	
-0.21846	0.03927	-0.5275	
-0.22356	0.03725	-0.4455	Note: Origin of the co-ordinate system at airfoil quarter-chord point.
-0.22866	0.03504	-0.4285	
-0.23686	0.03084	-0.3585	
-0.23892	0.02956	-0.2657	
-0.24098	0.02818	-0.2345	
-0.24307	0.02617	-0.0976	
-0.24532	0.02414	0.0821	
-0.24734	0.02027	0.3467	
-0.24975	0.01117	1.0781	
-0.24827	0.00629	1.1130	
-0.24653	0.00258	0.9789	
-0.24435	-0.00021	0.8023	
-0.24247	-0.00210	0.6979	
-0.24056	-0.00488	0.6230	
-0.23085	-0.00929	0.4226	
-0.22089	-0.01382	0.3077	
-0.20113	-0.02082	0.1443	
-0.17622	-0.02775	0.0396	
-0.15134	-0.03329	-0.0498	
-0.10156	-0.04161	-0.1415	
-0.05206	-0.04730	-0.1906	
-0.00219	-0.05124	-0.2088	
0.09725	-0.05485	-0.2049	
0.19792	-0.05327	-0.1172	
0.29859	-0.04729	-0.0072	
0.39908	-0.03739	0.1695	
0.49957	-0.02754	0.3345	
0.59926	-0.02320	0.4078	
0.69947	-0.02760	0.3795	

Table 6.2 Test case — wall pressure distributions

Upper wall			Lower wall		
x/c	y/c	C_{p_U}	x/c	y/c	C_{p_L}
-8.10	2.90	-0.0063	-8.10	-2.90	-0.0064
-4.50	2.90	0.0034	-6.00	-2.90	0.0145
-3.60	2.90	0.0135	-4.50	-2.90	0.0235
-3.00	2.90	0.0200	-3.60	-2.90	0.0290
-2.70	2.90	0.0235	-3.00	-2.90	0.0358
-2.40	2.90	0.0191	-2.70	-2.90	0.0377
-2.10	2.90	0.0070	-2.40	-2.90	0.0422
-1.80	2.90	0.0156	-2.10	-2.90	0.0463
-1.50	2.90	0.0064	-1.80	-2.90	0.0572
-1.20	2.90	-0.0011	-1.50	-2.90	0.0553
-1.05	2.90	0.0005	-1.35	-2.90	0.0569
-0.90	2.90	-0.0049	-1.20	-2.90	0.0642
-0.75	2.90	-0.0084	-1.05	-2.90	0.0732
-0.60	2.90	-0.0128	-0.90	-2.90	0.0721
-0.45	2.90	-0.0225	-0.75	-2.90	0.0738
-0.30	2.90	-0.0173	-0.60	-2.90	0.0806
-0.15	2.90	-0.0212	-0.45	-2.90	0.0782
0.00	2.90	-0.0386	-0.30	-2.90	0.0810
0.15	2.90	-0.0382	-0.15	-2.90	0.0842
0.30	2.90	-0.0230	0.00	-2.90	0.0770
0.45	2.90	-0.0277	0.15	-2.90	0.0875
0.60	2.90	-0.0281	0.30	-2.90	0.0975
0.75	2.90	-0.0249	0.45	-2.90	0.0954
0.90	2.90	-0.0239	0.60	-2.90	0.0902
1.05	2.90	-0.0246	0.75	-2.90	0.0900
1.20	2.90	-0.0263	0.90	-2.90	0.0935
1.35	2.90	-0.0239	1.05	-2.90	0.0949
1.50	2.90	-0.0299	1.20	-2.90	0.0938
1.80	2.90	-0.0228	1.35	-2.90	0.0917
2.10	2.90	-0.0274	1.50	-2.90	0.0905
2.40	2.90	-0.0262	1.80	-2.90	0.0826
2.70	2.90	-0.0232	2.10	-2.90	0.0797
3.00	2.90	-0.0190	2.40	-2.90	0.0813
3.30	2.90	-0.0196	2.70	-2.90	0.0688
3.60	2.90	-0.0179	3.00	-2.90	0.0641
3.90	2.90	-0.0172	3.30	-2.90	0.0591
4.50	2.90	-0.0221	3.60	-2.90	0.0430
			3.90	-2.90	0.0396
			4.50	-2.90	0.0257

Table 6.3 Corrections for the NAE test case obtained by several methods

Method	Ref.	ΔM_∞	$\Delta\alpha$
NAE Mokry, Ohman	[6.20]	-0.015	-0.67°
ONERA Capelier, Chevallier, Bouniol	[6.11]	-0.015	-0.67°
NASA Gopinath	[6.16]	-0.017	-0.67°
NLR Smith	[6.17]	-0.015	-0.59°
NAL Sawada	[7.5], [7.16]	———	-0.58°
NASA Kemp	[6.34]	-0.017	-0.64° -0.89°*

* with adjustment of upstream flow angle

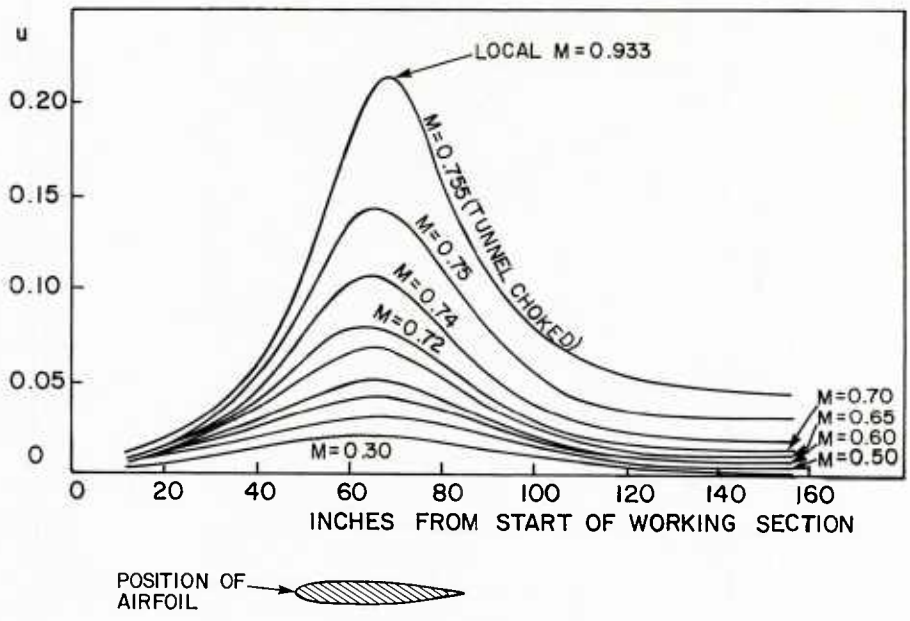

Fig. 6.1 Velocity increment at tunnel wall due to a NACA 0015 airfoil, $\alpha = 0^\circ$, $Re = 3.4 \times 10^6$, $c/h = 0.3125$ (adapted from Ref. [6.4])

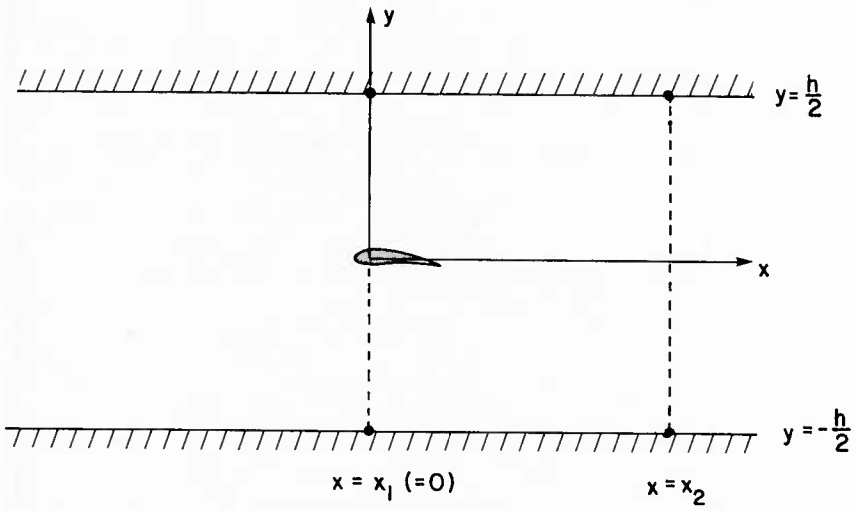

Fig. 6.2 Selection of pressure stations on solid walls

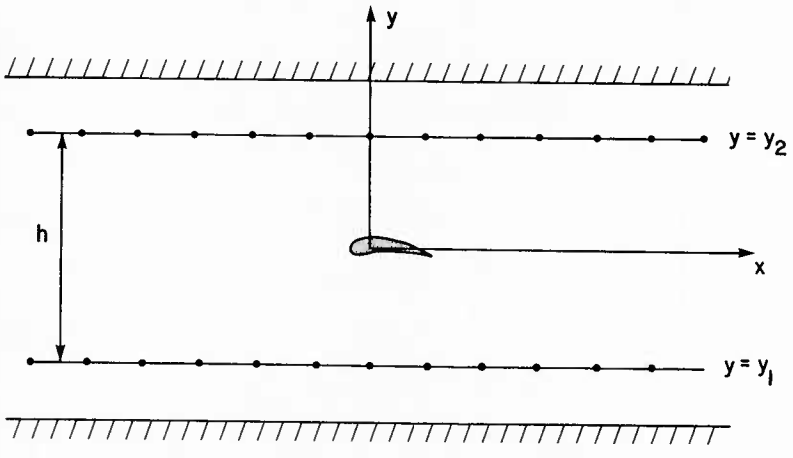

Fig. 6.3 Co-ordinate system for the infinite-length test section

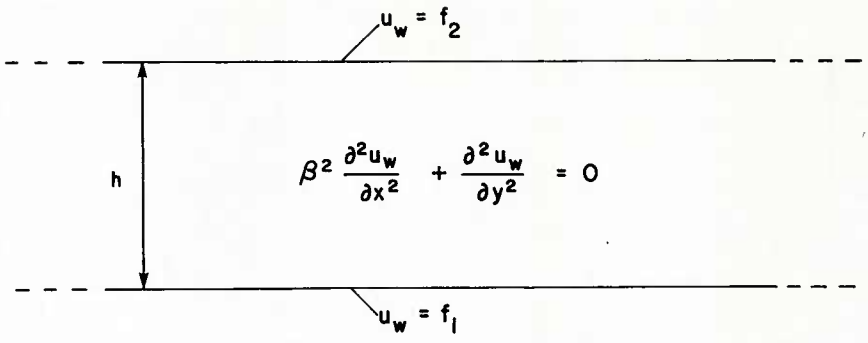

Fig. 6.4 Dirichlet problem in the infinite strip

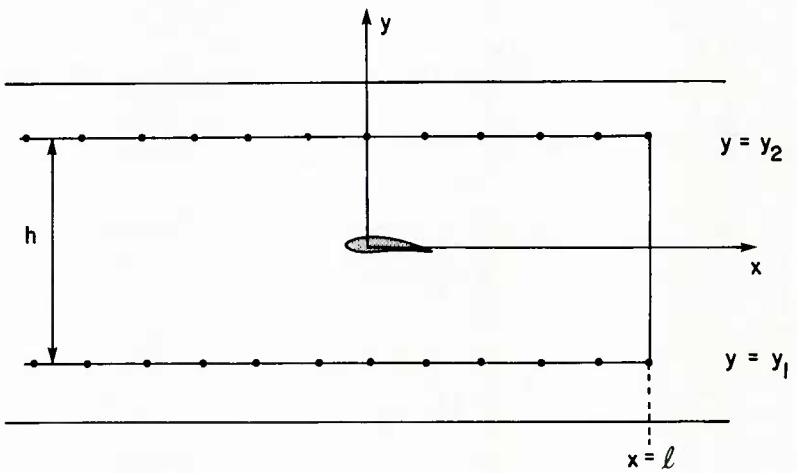

Fig. 6.5 Co-ordinate system for the semi-infinite-length test section

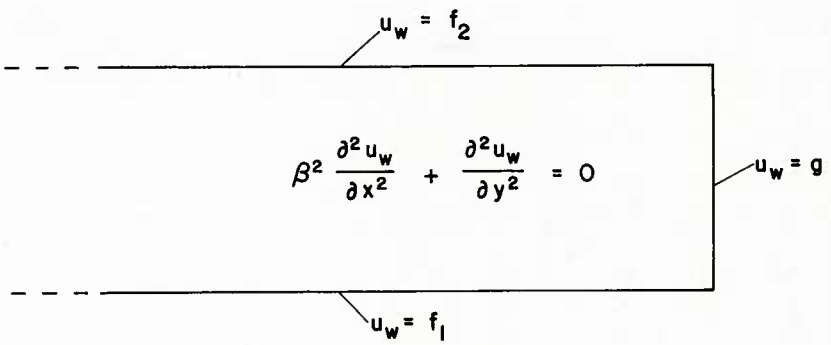

Fig. 6.6 Dirichlet problem in the semi-infinite strip

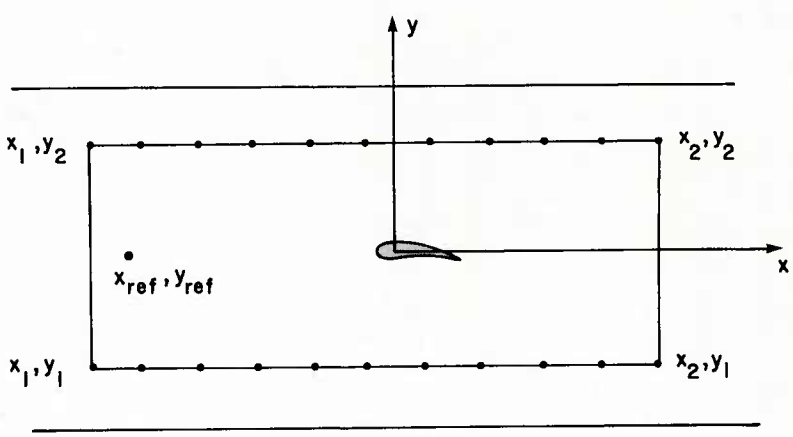

Fig. 6.7 Co-ordinate system for the finite-length test section

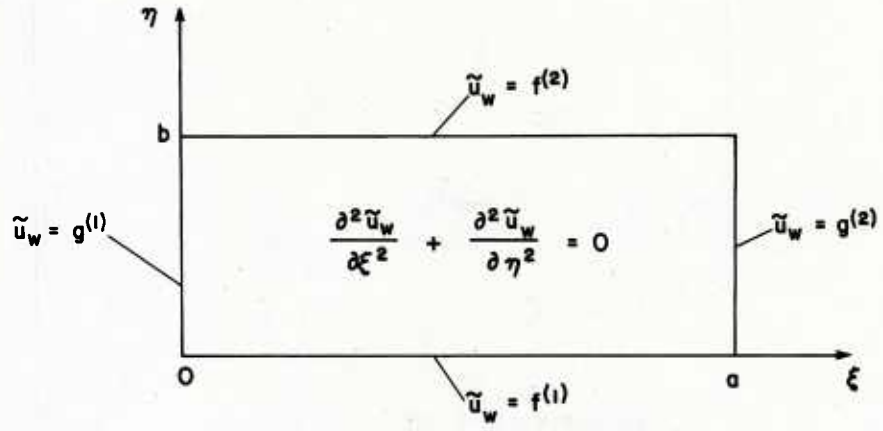

Fig. 6.8 Dirichlet problem in the rectangle

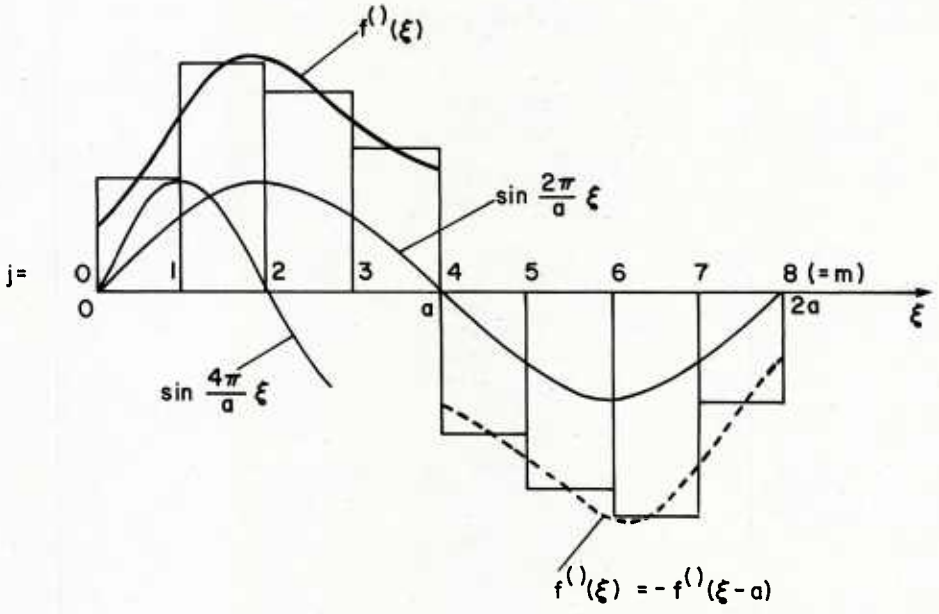

Fig. 6.9 Calculation of coefficients $A_k^{(j)}$

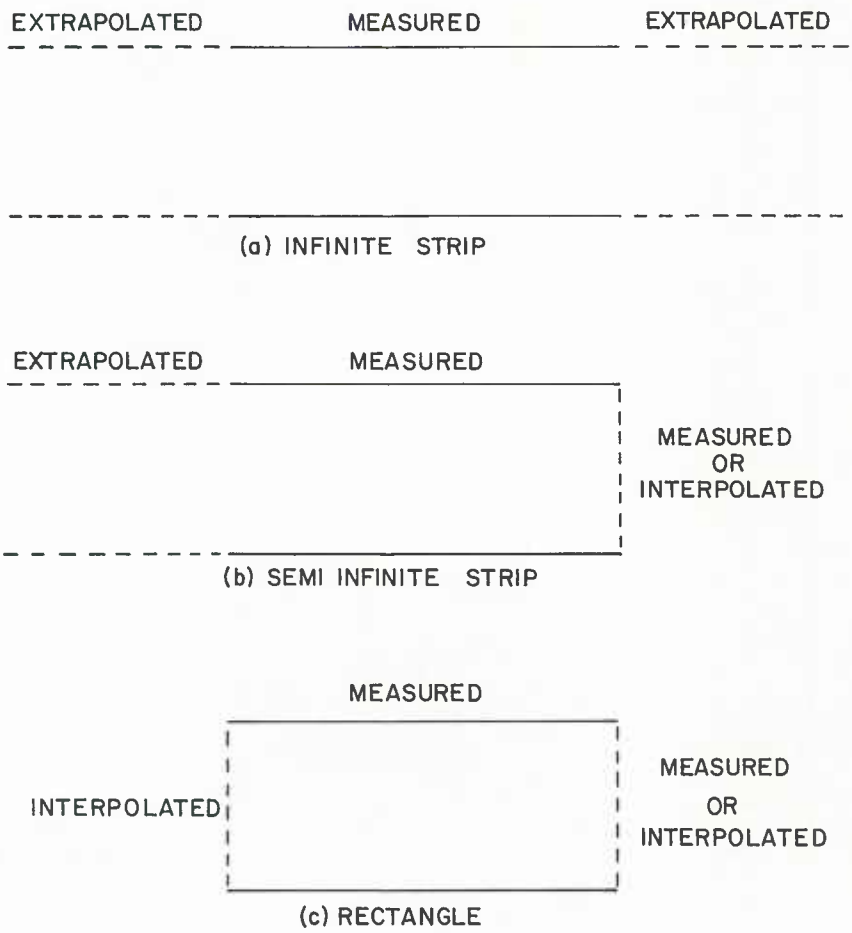

Fig. 6.10 Acquisition of boundary static pressures

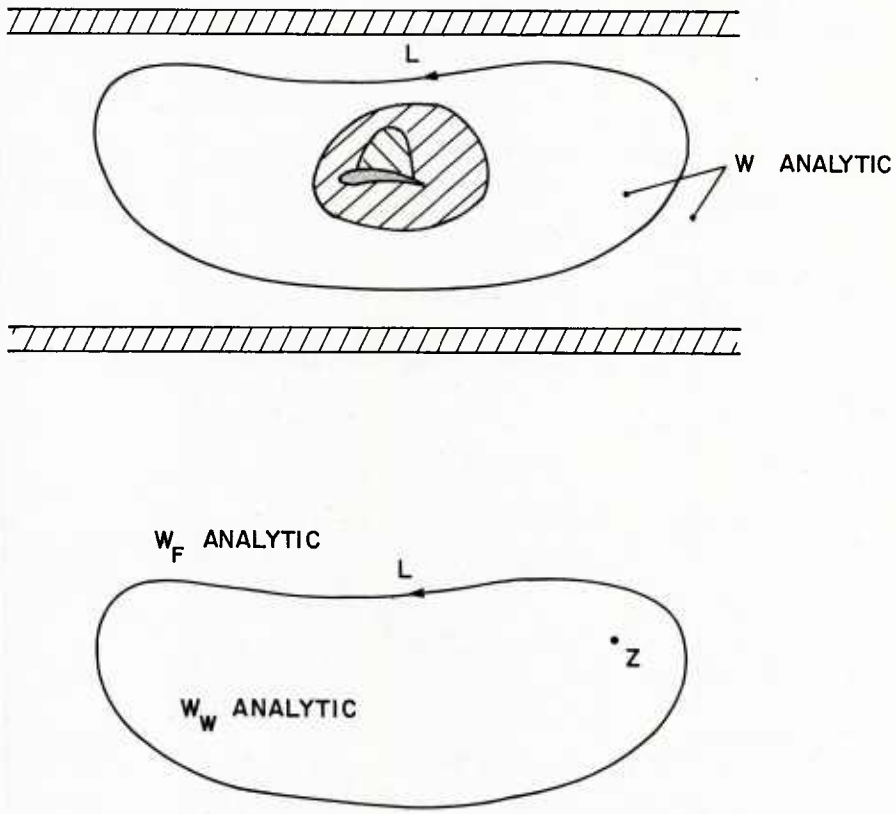

Fig. 6.11 Linearized flow regions

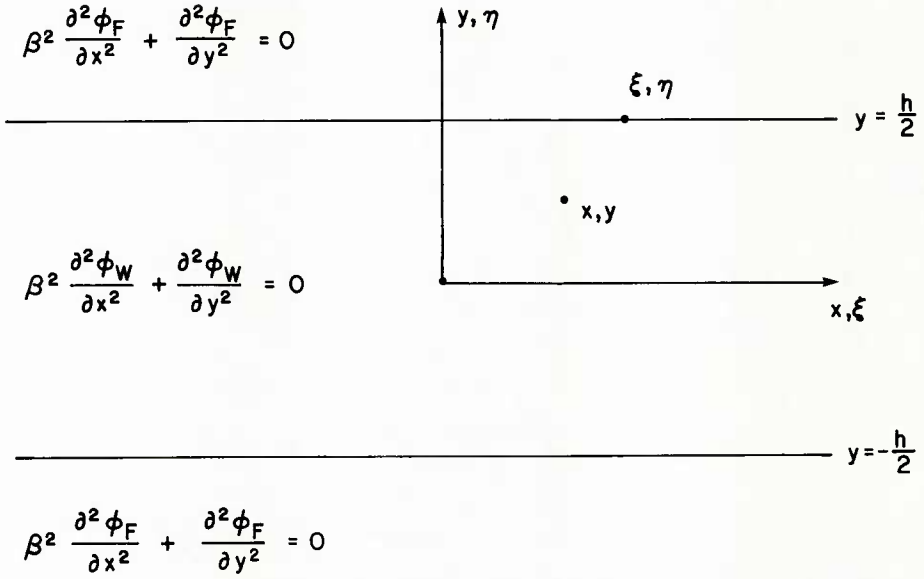

Fig. 6.12 Green's regions for the empty test section

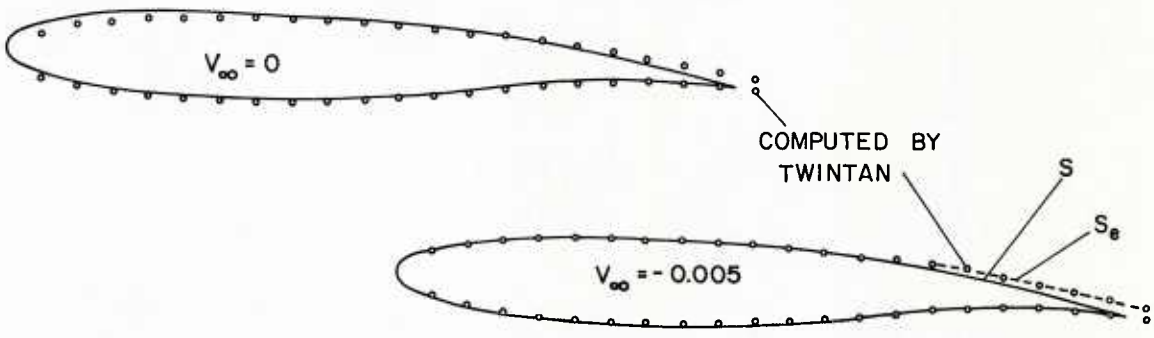

Fig. 6.13 Actual and effective airfoil contours, BGK 1 airfoil, $M_\infty = 0.784$, $\alpha = 2.56°$, c/h = 1/6, 20% wall porosity

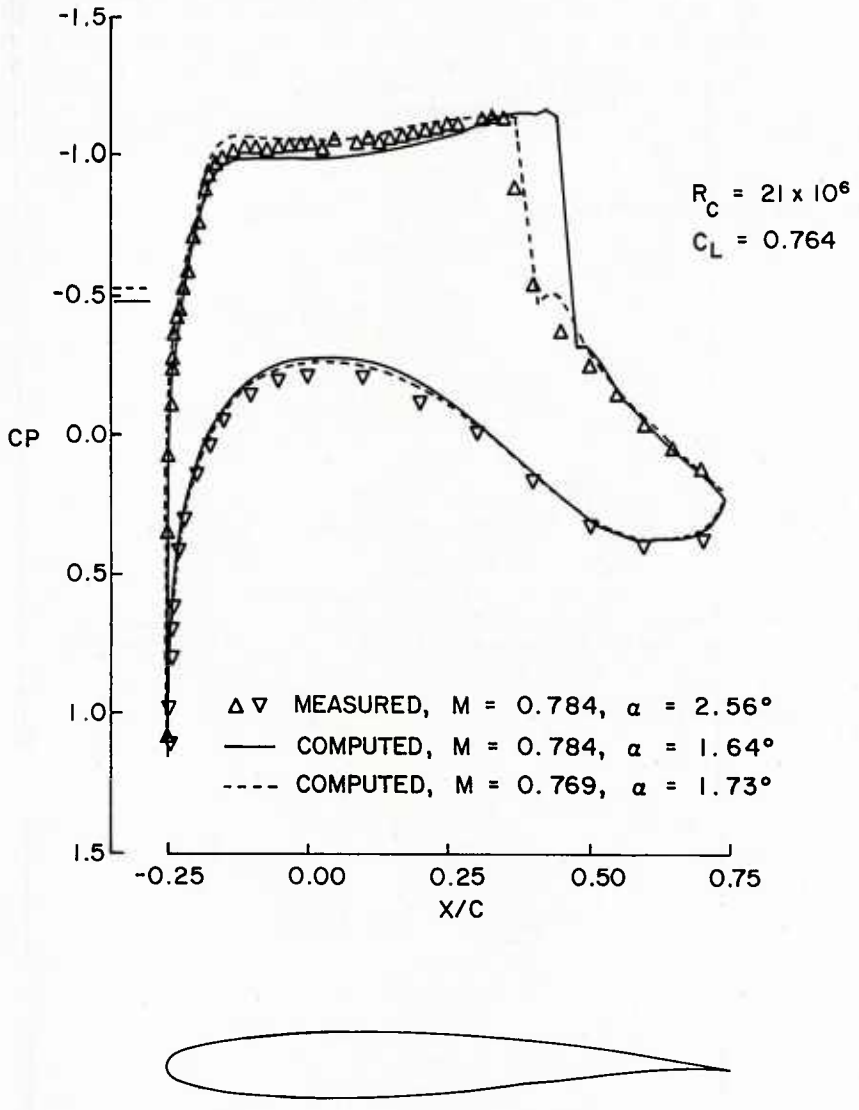

Fig. 6.14 Comparison of the pressure distribution on the BGK 1 airfoil measured in the wind tunnel with the computed ones in free air: effect of $\Delta M = -0.015$

7.0 INTEGRAL EQUATION FORMULATION OF SUBCRITICAL WALL INTERFERENCE

7.1 Green's Theorem for the Tunnel Flow Region

The present Chapter deals with the application of Green's theorem to the tunnel wall interference problem at subcritical flow conditions at the walls. It provides a partial justification for the heuristic approach to subsonic wall interference, discussed in Chapters 4 and 5. The formulation is also applicable to transonic, supersonic and unsteady flows, but the strategy of evaluating the corrections has not been fully worked out yet.

In general, the application of an appropriate Green's function leads to a singular integral equation of the Glauert or Oswatitsch type [7.1], with a kernel storing the information about the constraining effect of the particular wall. The wall interference corrections are obtained indirectly, by comparing the computed pressure distributions in the wind tunnel and free air. The advantage of the integral equation method is that it requires an order of magnitude less computing than equivalent two-dimensional numerical methods (finite difference, finite volume, etc.). However, for steady linearized flows, where wall corrections can be obtained by direct methods, the integral equation method is not the most attractive practical alternative, particularly since it works with theoretical inviscid, not the actual loadings. This probably explains why the Green's function approach has not been as widely used in wall interference, as its prominence in methods of mathematical physics would suggest. Recently, this has been improving, particularly since it has been realized that "short cuts" are possible and that wall interference corrections can be obtained explicitly from airfoil geometry and measured loadings, as in the classical approach. Of course, then the result is not drastically different from that established in the preceding chapters.

The small disturbance potential equation appropriate to transonic flow is [7.2]

$$\beta^2 \frac{\partial^2 \phi}{\partial x^2} + \frac{\partial^2 \phi}{\partial y^2} = M_\infty^2 \frac{\kappa+1}{U_\infty} \frac{\partial \phi}{\partial x} \frac{\partial^2 \phi}{\partial x^2} \tag{7.1}$$

where

$$\beta = \sqrt{1 - M_\infty^2}$$

is the Prandtl-Glauert scaling factor and κ is the ratio of specific heats (1.4 for air).

For a thin airfoil, $x_L \leqslant x \leqslant x_T$, $y = 0$, between two parallel walls, $y = -h/2$ and $y = h/2$, see Figure 7.1, the potential equation is applicable to the region $-\infty < x < \infty$, $-h/2 < y < h/2$, from which the line segment $x > x_L$, $y = 0$ is cut out. The potential ϕ is discontinuous across $x > x_L$, $y = 0$, but its derivatives are continuous across $x \geqslant x_T$, $y = 0$. Other discontinuities to be considered are the shock waves, represented here for simplicity by a single, normal shock wave along the line segment $x = x_S$, $0 \leqslant y \leqslant y_S < h/2$.

The thin airfoil boundary conditions are

$$\frac{\partial \phi}{\partial y}(x, 0+) = \frac{df^+(x)}{dx}, \qquad x_L \leqslant x \leqslant x_T$$

$$\frac{\partial \phi}{\partial y}(x, 0-) = \frac{df^-(x)}{dx}, \qquad x_L \leqslant x \leqslant x_T \tag{7.2}$$

where

$$y = f^+(x)$$

$$y = f^-(x)$$

describe the upper and lower sides of the airfoil contour.

From Equation (7.1), written in the divergence (conservative) form

$$\frac{\partial}{\partial x}\left[\beta^2 \frac{\partial \phi}{\partial x} - M_\infty^2 \frac{\kappa+1}{U_\infty} \frac{1}{2}\left(\frac{\partial \phi}{\partial x}\right)^2\right] + \frac{\partial}{\partial y}\left[\frac{\partial \phi}{\partial y}\right] = 0$$

it becomes evident that potential flow theory permits the following jump condition along our shock wave:

$$\left[\beta^2 \frac{\partial \phi}{\partial x} - M_\infty^2 \frac{\kappa+1}{U_\infty} \frac{1}{2}\left(\frac{\partial \phi}{\partial x}\right)^2\right]_{x = x_S^-}^{x = x_S^+} = 0, \qquad 0 \leqslant y \leqslant y_S \tag{7.3}$$

The tangential derivative, $\partial\phi/\partial y$, is continuous across the shock.

The Green's function

$$G = G(x,y;\xi,\eta)$$

associated with the left-hand operator of Equation (7.1), satisfies the equation

$$\beta^2 \frac{\partial^2 G}{\partial x^2} + \frac{\partial^2 G}{\partial y^2} = \delta(x-\xi)\,\delta(y-\eta), \qquad -\infty < x < \infty, \qquad -\frac{h}{2} < y < \frac{h}{2} \tag{7.4}$$

where δ is the Dirac delta function; x,y is the "fixed" point and ξ,η is the "running" point. The boundary conditions for G are as yet unspecified.

Applying Green's theorem to the tunnel flow region shown in Figure 7.2(a), we are able to write the formal solution to Equation (7.1) as

$$\phi(x,y) = I^A(x,y) + I^W(x,y) + I^D(x,y) \tag{7.5}$$

where the contributions are:

airfoil integral

$$I^A(x,y) = -\left[\int_{x_L}^{\infty} \left\{\phi(\xi,\eta)\frac{\partial G}{\partial \eta}(x,y;\xi,\eta) - \frac{\partial \phi}{\partial \eta}(\xi,\eta)\,G(x,y;\xi,\eta)\right\} d\xi\right]_{\eta = 0-}^{\eta = 0+} \tag{7.6}$$

wall integral

$$I^W(x,y) = \left[\int_{-\infty}^{\infty} \left\{\phi(\xi,\eta)\frac{\partial G}{\partial \eta}(x,y;\xi,\eta) - \frac{\partial \phi}{\partial \eta}(\xi,\eta)\,G(x,y;\xi,\eta)\right\} d\xi\right]_{\eta = -\frac{h}{2}}^{\eta = \frac{h}{2}} \tag{7.7}$$

domain integral

$$I^D(x,y) = -\beta^2\left[\int_0^{y_S} \frac{\partial \phi}{\partial \xi}(\xi,\eta)\,G(x,y;\xi,\eta)\,d\eta\right]_{\xi = x_S^-}^{\xi = x_S^+} + M_\infty^2 \frac{\kappa+1}{U_\infty} \iint_{D'} \frac{1}{2}\frac{\partial}{\partial \xi}\left(\frac{\partial \phi}{\partial \xi}(\xi,\eta)\right)^2 G(x,y;\xi,\eta)\,d\xi\,d\eta \tag{7.8}$$

where D′ denotes the continuous-flow domain, i.e. the tunnel flow region, from which the line segments representing the airfoil and the shock are taken out, Figure 7.2(a). The inclusion of the line segment $x > x_T$, $y = 0$ is of no consequence for the double integral, because the integrand is continuous across.

Since

$$\phi(\xi, 0+) - \phi(\xi,0-) = \Gamma = \text{constant}, \qquad x_T \leqslant \xi < \infty$$

$$\frac{\partial \phi}{\partial \eta}(\xi,0+) - \frac{\partial \phi}{\partial \eta}(\xi,0-) = 0 \qquad , \qquad x_T < \xi < \infty$$

we obtain

$$I^A(x,y) = -\left[\int_{x_L}^{x_T} \left\{\phi(\xi,\eta)\frac{\partial G}{\partial \eta}(x,y;\xi,\eta) - \frac{\partial \phi}{\partial \eta}(\xi,\eta)\,G(x,y;\xi,\eta)\right\} d\xi\right]_{\eta = 0-}^{\eta = 0+} - \Gamma \int_{x_T}^{\infty} \frac{\partial G}{\partial \eta}(x,y;\xi,0)\,d\xi \tag{7.9}$$

i.e. the discontinuity of ϕ needs to be integrated only along the airfoil, $x_L \leqslant x \leqslant x_T$. This form of the airfoil integral is used for example in References [7.3] and [7.4].

Another possibility is to introduce the conjugate function [7.5]

$$G^*(x,y;\xi,\eta) = -\int_{\xi}^{\infty} \frac{\partial G}{\partial \eta}(x,y;\xi,\eta)\, d\xi \tag{7.10}$$

Integration of Equation (7.6) by parts then yields

$$I^A(x,y) = \left[\int_{x_L}^{x_T} \left\{\frac{\partial \phi}{\partial \xi}(\xi,\eta)\, G^*(x,y;\xi,\eta) + \frac{\partial \phi}{\partial \eta}(\xi,\eta)\, G(x,y;\xi,\eta)\right\} d\xi\right]_{\eta = 0-}^{\eta = 0+} \tag{7.11}$$

For the wall integral (7.7) similarly

$$I^W(x,y) = -\left[\int_{-\infty}^{\infty} \left\{\frac{\partial \phi}{\partial \xi}(\xi,\eta)\, G^*(x,y;\xi,\eta) + \frac{\partial \phi}{\partial \eta}(\xi,\eta)\, G(x,y;\xi,\eta)\right\} d\xi\right]_{\eta = -\frac{h}{2}}^{\eta = \frac{h}{2}} \tag{7.12}$$

The domain integral (7.8), consisting of the line integral along the shock wave and the double integral over the continuous-flow domain D′, can also be simplified by integrating the latter by parts with respect to ξ. The integral along the shock drops out due to the shock jump condition (7.3), leaving us with

$$I^D(x,y) = -M_\infty^2 \frac{\kappa+1}{U_\infty} \iint_D \frac{1}{2}\left(\frac{\partial \phi}{\partial \xi}(\xi,\eta)\right)^2 \frac{\partial G}{\partial \xi}(x,y;\xi,\eta)\, d\xi\, d\eta \tag{7.13}$$

where D denotes the complete flow domain, i.e. the tunnel flow domain from which only the line segment representing the airfoil is removed, Figure 7.2(b). The fact that the field integral (7.13) contains the shock jump relations and that the shock waves do not have to be treated as additional cuts in the flow plane is one of the most admirable aspects of the integral formulation of potential flow past airfoils. The result, which is also transferable to oblique and curved shock waves, is due to Oswatitsch [7.6]; the present exposition, based on the divergence properties of the transonic equation, is similar to Cole [7.7], [7.8]. It need not be emphasized that Equation [7.13] is valid only for weak (isentropic) shocks, permitted by potential flow theory. On the other hand, sometimes it may be advantageous to retain the integration domain D′, using a proper fitting of the shock waves [7.9].

To summarize the above, the potential ϕ at an arbitrary field point x,y can be expressed in terms of line integrals of $\partial\phi/\partial\xi$ and $\partial\phi/\partial\eta$ over the airfoil and walls, plus a double integral of $(\partial\phi/\partial\xi)^2$ over the entire flow field.

For the free air case, whose quantities will again be denoted by subscript F, the wall integral (7.12) can be dropped, provided that the Green's function satisfies the far field condition

$$\frac{\partial G_F}{\partial x}, \frac{\partial G_F}{\partial y} \to 0 \quad \text{as} \quad r = \sqrt{(x-\xi)^2 + \beta^2 (y-\eta)^2} \to \infty \tag{7.14}$$

The formal solution for the free air potential is

$$\phi_F(x,y) = I_F^A(x,y) + I_F^D(x,y) \tag{7.15}$$

where

$$I_F^A(x,y) = \left[\int_{x_L}^{x_T} \left\{\frac{\partial \phi_F}{\partial \xi}(\xi,\eta)\, G_F^*(x,y;\xi,\eta) + \frac{\partial \phi_F}{\partial \eta}(\xi,\eta)\, G_F(x,y;\xi,\eta)\right\} d\xi\right]_{\eta = 0-}^{\eta = 0+} \tag{7.16}$$

and

$$I_F^D(x,y) = -M_\infty^2 \frac{\kappa+1}{U_\infty} \iint_{D_F} \frac{1}{2}\left(\frac{\partial \phi_F}{\partial \xi}(\xi,\eta)\right)^2 \frac{\partial G_F}{\partial \xi}(x,y;\xi,\eta)\, d\xi\, d\eta \tag{7.17}$$

where D_F is the infinite flow domain.

The Green's function G_F, satisfying Equations (7.4) and (7.14), is obtained by a scale transformation from the fundamental solution of Laplace's equation:

$$G_F = \frac{1}{2\pi\beta} \log \sqrt{(x-\xi)^2 + \beta^2 (y-\eta)^2} \tag{7.18}$$

In mathematics G_F is called the free space Green's function or the Green's function for the entire plane; in physics it is known as the potential at x,y due to a unit source located at ξ,η. The derivatives $\partial G_F/\partial\xi$ and $\partial G_F/\partial\eta$ are the potentials due to unit doublets (dipoles), oriented in the directions parallel and normal to the flow respectively.

The corresponding conjugate function

$$G_F^* = -\frac{1}{2\pi} \operatorname{atan} \frac{\beta(y-\eta)}{x-\xi} \tag{7.19}$$

is recognized as the potential at x,y due to a unit vortex at ξ,η. In accordance with Equation (7.10), G_F^* is required to vanish as $\xi \to \infty$.

Physically, the integral (7.16) represents a line distribution of vortices and sources and the integral (7.17) the area distribution of doublets. Similar interpretation of integrals (7.11) to (7.13) is also possible, if we are willing to accept G and G* as the "generalized source" and "generalized vortex" respectively. Actually, there is ample justification for this. One of the possible representation of the Green's function for the wind tunnel case is namely [7.10]:

$$G = G_F + G_W \tag{7.20}$$

where

$$G_W = G_W(x,y;\xi,\eta)$$

is a nonsingular function satisfying

$$\beta^2 \frac{\partial^2 G_W}{\partial x^2} + \frac{\partial^2 G_W}{\partial y^2} = 0, \qquad -\infty < x < \infty, \quad -\frac{h}{2} < y < \frac{h}{2} \tag{7.21}$$

By the properties of harmonic functions G_W has derivatives of all orders inside the wind tunnel, while outside G_W has singular points (images).

Briefly, the Green's function is the sum of a singular and a nonsingular function, with the sum satisfying the required boundary conditions on the tunnel boundary. Physically, G can be interpreted as the source singularity plus the induced effect of tunnel boundaries. Similar interpretation can also be lent to G*.

In conclusion, it is instructive to point out the connection between Equations (7.20) and (4.3). The decomposition, which is rigorous in the microcosm of Green's functions, is in engineering practice assumed to be valid in the macrocosm of potential functions.

7.2 Examples of Green's Functions

Although G_F and G_F^* can also be used in Equations (7.6) to (7.13), it is often advantageous to eliminate, by selection of a suitable Green's function, the unknown values of ϕ and $\partial\phi/\partial\eta$ from the wall integral (7.7) or, alternatively, the unknown values of $\partial\phi/\partial\xi$ and $\partial\phi/\partial\eta$ from Equation (7.12). The resulting form of Green's theorem for the wind tunnel case, Equation (7.5), is then similar to that for free air, Equation (7.15). Depending on the type of tunnel wall (solid, porous, slotted) or boundary measurement (static pressure, flow angle), the Green's function may be required to satisfy different boundary conditions.

Solid wall boundary conditions (Neumann problem)

Since

$$\frac{\partial\phi}{\partial y}\left(x, \pm\frac{h}{2}\right) = 0, \qquad -\infty < x < \infty$$

the wall integral (7.7) drops out if

$$\frac{\partial G}{\partial\eta}\left(x,y;\xi,\pm\frac{h}{2}\right) = 0, \qquad -\infty < \xi < \infty$$

By the symmetry property of the Green's function for the Neumann problem [7.11], the above boundary condition is equivalent to

$$\frac{\partial G}{\partial y}\left(x,\pm\frac{h}{2};\xi,\eta\right) = 0, \qquad -\infty < x < \infty \tag{7.22}$$

Using separation of variables the solution of the boundary value problem described by Equations (7.4) and (7.22) is [7.4]

$$G(x,y;\xi,\eta) = \frac{1}{2\beta h}\frac{|x-\xi|}{\beta} - \frac{1}{\beta h}\sum_{n=1}^{\infty}\frac{e^{-\lambda_n\frac{|x-\xi|}{\beta}}}{\lambda_n}\cos\lambda_n\left(y+\frac{h}{2}\right)\cos\lambda_n\left(\eta+\frac{h}{2}\right) \tag{7.23}$$

where

$$\lambda_n = \frac{n\pi}{h} \tag{7.24}$$

The isolated term in front of the sum is the zero-order cosine coefficient, corresponding to the eigenvalue $\lambda_0 = 0$.

Open jet boundary conditions (Dirichlet problem)

Since

$$\phi\left(x,\pm\frac{h}{2}\right) = 0, \quad -\infty < x < \infty$$

the wall integral (7.7) vanishes if

$$G\left(x,y;\xi,\pm\frac{h}{2}\right) = 0, \quad -\infty < \xi < \infty$$

or, by the symmetry argument

$$G\left(x,\pm\frac{h}{2};\xi,\eta\right) = 0, \quad -\infty < x < \infty \tag{7.25}$$

The Green's function for the Dirichlet problem, satisfying by Equations (7.4) and (7.25), is [7.12]

$$G(x,y;\xi,\eta) = -\frac{1}{\beta h}\sum_{n=1}^{\infty}\frac{e^{-\lambda_n\frac{|x-\xi|}{\beta}}}{\lambda_n}\sin\lambda_n\left(y+\frac{h}{2}\right)\sin\lambda_n\left(\eta+\frac{h}{2}\right) \tag{7.26}$$

The appropriate eigenvalues λ_n are again given by Equation (7.24). There is no zero-order term in the Fourier sine series.

Slotted wall boundary conditions (Mixed Dirichlet-Neumann problem)

For longitudinally slotted walls represented by the boundary condition

$$\phi\left(x,\pm\frac{h}{2}\right) \pm K\frac{\partial\phi}{\partial y}\left(x,\pm\frac{h}{2}\right) = 0, \quad -\infty < x < \infty$$

the wall integral (7.7) is made to vanish if

$$G\left(x,y;\xi,\pm\frac{h}{2}\right) \pm K\frac{\partial G}{\partial\eta}\left(x,y;\xi,\pm\frac{h}{2}\right) = 0, \quad -\infty < \xi < \infty$$

For the mixed Dirichlet-Neumann (or Robin) problem the symmetry principle is again applicable [7.11], so that G also satisfies

$$G\left(x,\pm\frac{h}{2};\xi,\eta\right) \pm K\frac{\partial G}{\partial y}\left(x,\pm\frac{h}{2};\xi,\eta\right) = 0, \quad -\infty < x < \infty \tag{7.27}$$

Using eigenfunction expansion similar to that described in Reference [7.13], the solution of the boundary value problem specified by Equations (7.4) and (7.27) can be constructed as [7.4]

$$G(x,y;\xi,\eta) = -\frac{1}{\beta h}\sum_{n=1}^{\infty}\frac{e^{-\lambda_n\frac{|x-\xi|}{\beta}}}{\lambda_n\left(1+\lambda_n^2K^2+\frac{2K}{h}\right)}\left[\lambda_n K\cos\lambda_n\left(y+\frac{h}{2}\right)+\sin\lambda_n\left(y+\frac{h}{2}\right)\right]\left[\lambda_n K\cos\lambda_n\left(\eta+\frac{h}{2}\right)+\sin\lambda_n\left(\eta+\frac{h}{2}\right)\right] \tag{7.28}$$

where the eigenvalues λ_n are the positive roots of the transcendental equation

$$\tan(\lambda_n h) = \frac{2}{K\lambda_n - \frac{1}{K\lambda_n}} \tag{7.29}$$

We can easily verify that Equation (7.28) yields the open jet solution if $K \to 0$. The closed wall solution is not obtained in the limit $K \to \infty$, but this deficiency can be corrected by formally adding the missing zero-order coefficient when $1/K = 0$. The physical aspects of the discontinuous behaviour of the blockage correction at closed wall condition are discussed in Section 4.3.

Porous wall boundary conditions (Riemann-Hilbert problem)

The ideal porous (or perforated walls) satisfy the boundary conditions

$$\frac{\partial\phi}{\partial x}\left(x,\frac{h}{2}\right) + \frac{1}{P_U}\frac{\partial\phi}{\partial y}\left(x,\frac{h}{2}\right) = 0$$

$$-\infty < x < \infty$$

$$\frac{\partial\phi}{\partial x}\left(x,-\frac{h}{2}\right) - \frac{1}{P_L}\frac{\partial\phi}{\partial y}\left(x,-\frac{h}{2}\right) = 0$$

where P_U and P_L are the upper and lower wall porosity parameters. The substitution in Equation (7.7) shows that the wall integral will be zero if G satisfies

$$\frac{\partial G}{\partial\xi}\left(x,y;\xi,\frac{h}{2}\right) - \frac{1}{P_U}\frac{\partial G}{\partial\eta}\left(x,y;\xi,\frac{h}{2}\right) = 0$$

$$-\infty < \xi < \infty$$

$$\frac{\partial G}{\partial\xi}\left(x,y;\xi,-\frac{h}{2}\right) + \frac{1}{P_L}\frac{\partial G}{\partial\eta}\left(x,y;\xi,-\frac{h}{2}\right) = 0$$

However, with respect to co-ordinates x,y the Green's function still obeys the original boundary conditions:

$$\frac{\partial G}{\partial x}\left(x,\frac{h}{2};\xi,\eta\right) + \frac{1}{P_U}\frac{\partial G}{\partial y}\left(x,\frac{h}{2};\xi,\eta\right) = 0$$

$$-\infty < x < \infty \tag{7.30}$$

$$\frac{\partial G}{\partial x}\left(x,-\frac{h}{2};\xi,\eta\right) - \frac{1}{P_L}\frac{\partial G}{\partial y}\left(x,-\frac{h}{2};\xi,\eta\right) = 0$$

The eigenfunction expansion of the Green's function for the porous wall case can be obtained by the method of Kacprzynski [7.14]. However, if we are interested only in the derivatives of G and G*, the analytic results obtained by the method of images in Chapter 5 can be utilized. Recalling that G and G* describe the potentials due to the unit source and unit vortex between the walls, we obtain from Equations (5.5) and (5.19) to (5.27) the derivatives of the wall interference parts G_W and G_W^*

$$\frac{\partial G_W}{\partial x}(x,y;\xi,\eta) = \frac{1}{\beta^2 h}\,\mathrm{Re}\left[B(x,y;\xi,\eta) + E(x,y;\xi,\eta) + \chi(P_U)\,\chi(P_L)\right] \tag{7.31}$$

$$\frac{\partial G_W}{\partial y}(x,y;\xi,\eta) = -\frac{1}{\beta h}\,\mathrm{Im}\left[B(x,y;\xi,\eta) + E(x,y;\xi,\eta)\right] \tag{7.32}$$

$$\frac{\partial G_W^*}{\partial x}(x,y;\xi,\eta) = -\frac{1}{\beta h}\,\mathrm{Im}\left[B(x,y;\xi,\eta) - E(x,y;\xi,\eta)\right] \tag{7.33}$$

$$\frac{\partial G_W^*}{\partial y}(x,y;\xi,\eta) = -\frac{1}{h}\,\mathrm{Re}\left[B(x,y;\xi,\eta) - E(x,y;\xi,\eta)\right] \tag{7.34}$$

where

$$B(x,y;\xi,\eta) = \frac{1}{2}\frac{\exp\left[\pi\frac{\tau_U+\tau_L}{2}\left(\frac{x-\xi}{\beta h}+i\frac{y-\eta}{h}\right)\right]}{\exp\left[\pi\left(\frac{x-\xi}{\beta h}+i\frac{y-\eta}{h}\right)\right]-1} - \frac{1}{2\pi\left(\frac{x-\xi}{\beta h}+i\frac{y-\eta}{h}\right)}$$

$$= \frac{1}{2}\sum_{n=1}^{\infty} B_n\left(\frac{\tau_U+\tau_L}{2}\right)\frac{\left[\pi\left(\frac{x-\xi}{\beta h}+i\frac{y-\eta}{h}\right)\right]^{n-1}}{n!}, \qquad \left|\frac{x-\xi}{\beta h}+i\frac{y-\eta}{h}\right| < 2 \tag{7.35}$$

$$E(x,y;\xi,\eta) = -\frac{1}{2}\frac{\exp\left[\pi\frac{\tau_U+\tau_L}{2}\left(\frac{x-\xi}{\beta h}+i\frac{y+\eta}{h}\right)\right]}{\exp\left[\pi\left(\frac{x-\xi}{\beta h}+i\frac{y+\eta}{h}\right)\right]+1}\exp\left(i\pi\frac{\tau_U-\tau_L}{2}\right)$$

$$= -\frac{1}{4}\exp\left(i\pi\frac{\tau_U-\tau_L}{2}\right)\sum_{n=0}^{\infty} E_n\left(\frac{\tau_U+\tau_L}{2}\right)\frac{\left[\pi\left(\frac{x-\xi}{\beta h}+i\frac{y+\eta}{h}\right)\right]^n}{n!}, \qquad \left|\frac{x-\xi}{\beta h}+i\frac{y+\eta}{h}\right| < 1 \tag{7.36}$$

and

$$\tau_U = \frac{2}{\pi}\operatorname{atan}\frac{P_U}{\beta}, \qquad 0 \leqslant \tau_U \leqslant 1$$

$$\tau_L = \frac{2}{\pi}\operatorname{atan}\frac{P_L}{\beta}, \qquad 0 \leqslant \tau_L \leqslant 1 \tag{7.37}$$

$$\chi(P) = \begin{cases} 1 & , \quad P = 0 \\ 0 & , \quad P > 0 \end{cases} \tag{7.38}$$

The symbols B_n and E_n denote the Bernoulli and Euler polynomials respectively, Equations (5.22) and (5.24).

Pressure boundary conditions (Dirichlet problem)

Assuming that the wall pressure coefficients, $C_p(x,\pm h/2)$, are known from static pressure measurement, the small disturbance boundary conditions can be specified as

$$\frac{\partial\phi}{\partial x}\left(x,\pm\frac{h}{2}\right) = -\frac{1}{2}C_p\left(x,\pm\frac{h}{2}\right)$$

To eliminate from Equation (7.12) the normal derivatives of ϕ (flow angles) we use the Green's function (7.26) for the homogeneous Dirichlet boundary condition (7.25). However, since ϕ is in fact subject to the inhomogeneous Dirichlet condition

$$\phi\left(x,\pm\frac{h}{2}\right) = -\frac{1}{2}\int_{-\infty}^{x} C_p\left(x,\pm\frac{h}{2}\right)dx$$

the wall integral will contain the (known) boundary values of ϕ and be in general non-zero. Evidently, the integral will be vanishing in the open jet case, where

$$C_p\left(x,\pm\frac{h}{2}\right) = 0, \qquad -\infty < x < \infty$$

Flow angle boundary conditions (Neumann problem)

If, on the other hand, the flow angles $\theta(x,\pm h/2)$ along the walls are known, ϕ is subject to inhomogeneous Neumann boundary conditions

$$\frac{\partial \phi}{\partial y}\left(x,\pm\frac{h}{2}\right) = \theta\left(x,\pm\frac{h}{2}\right)$$

The unknown values of ϕ are eliminated from Equation (7.7) by utilizing the Green's function (7.23) for the homogeneous Neumann condition (7.22). Solid, parallel walls are the special case

$$\theta\left(x,\pm\frac{h}{2}\right) = 0\,, \qquad -\infty < x < \infty$$

for which the wall integral (7.7) vanishes.

Combined pressure and flow angle boundary conditions

If both the pressures and flow angles along the tunnel walls are given, the potential flow problem for the region shown in Figure 7.1 is not well posed. This means that the problem may not have a solution if the boundary values are prescribed arbitrarily or are measured, subject to usual experimental errors. However, such boundary conditions are still useful for solving the tunnel exterior flow problem, allowing to obtain the wall corrections without considering the local flow conditions near the airfoil, see the method of Ashill and Weeks, Section 6.5.

7.3 Method of Sawada

Using Green's theorem, Sawada [7.5], [7.15], [7.16] developed an alternative solution to the wall interference problem by Capelier, Chevallier and Bouniol [7.17], see also Section 6.2.

The velocity correction on the tunnel axis is defined as

$$u_W(x,0) = \frac{\partial \phi}{\partial x}(x,0\pm) - \frac{\partial \phi_F}{\partial x}(x,0\pm) \tag{7.39}$$

assuming that it is continuous across $y = 0$. This is equivalent to the condition

$$\frac{\partial \phi}{\partial x}(x,0+) - \frac{\partial \phi}{\partial x}(x,0-) = \frac{\partial \phi_F}{\partial x}(x,0+) - \frac{\partial \phi_F}{\partial x}(x,0-) \tag{7.40}$$

In other words, it is from the beginning assumed that the wind tunnel test is correctable, i.e. the load distribution measured in the wind tunnel is equal to that at certain free stream conditions.

The velocity correction (7.39) can be evaluated by substituting from Equations (7.5) and (7.15). Since we wish to eliminate the (unknown) flow angles along the walls, we use the Green's function (7.26) satisfying the Dirichlet boundary condition (7.25). Utilizing Equations (7.5), (7.15), the airfoil boundary condition (7.2), and neglecting the difference between the domain integrals (7.13) and (7.17), we obtain

$$u_W(x,0) = -\left[\int_{-\infty}^{\infty} \frac{\partial \phi}{\partial \xi}(\xi,\eta)\,\frac{\partial G^*}{\partial x}(x,0;\xi,\eta)\,d\xi\right]_{\eta = -\frac{h}{2}}^{\eta = \frac{h}{2}}$$

$$+ \int_{x_L}^{x_T} \left[\frac{df^+(\xi)}{d\xi} - \frac{df^-(\xi)}{d\xi}\right] \frac{\partial G_W}{\partial x}(x,0;\xi,0)\,d\xi + \int_{x_L}^{x_T} \left[\frac{\partial \phi}{\partial \xi}(\xi,0+) - \frac{\partial \phi}{\partial \xi}(\xi,0-)\right] \frac{\partial G_W^*}{\partial x}(x,0;\xi,0)\,d\xi \tag{7.41}$$

From Equations (7.10), (7.18) and (7.26) we derive, after some manipulations,

$$\frac{\partial G^*}{\partial x}\left(x,0;\xi,\pm\frac{h}{2}\right) = \mp\frac{1}{2\beta h}\,\frac{1}{\cosh\left(\pi\,\frac{x-\xi}{\beta h}\right)}$$

$$\frac{\partial G_W}{\partial x}(x,0;\xi,0) = \frac{\partial G}{\partial x}(x,0;\xi,0) - \frac{\partial G_F}{\partial x}(x,0;\xi,0)$$

$$= \frac{1}{2\beta^2 h}\,\frac{1}{\sinh\left(\pi\dfrac{x-\xi}{\beta h}\right)} - \frac{1}{2\pi\beta(x-\xi)}$$

$$= \frac{1}{\beta^2 h}\sum_{n=1}^{\infty} B_n\left(\frac{1}{2}\right)\frac{\left(2\pi\dfrac{x-\xi}{\beta h}\right)^{n-1}}{n!}, \qquad \frac{|x-\xi|}{\beta h} < 1$$

$$= -\frac{\pi}{12\beta^2 h}\,\frac{x-\xi}{\beta h} + 0\left(\frac{x-\xi}{\beta h}\right)^3$$

$$\frac{\partial G_W^*}{\partial x}(x,0;\xi,0) = \frac{\partial G^*}{\partial x}(x,0;\xi,0) - \frac{\partial G_F^*}{\partial x}(x,0;\xi,0) = 0$$

The identical results can also be obtained from Equations (7.31) to (7.38) by putting $\tau_U = \tau_L = 1$.

Substituting the above expressions in Equation (7.41), we arrive at the solid blockage correction of Sawada [7.15]

$$u_W(x,0) = -\frac{1}{12}\,\frac{\mu\pi}{\beta^3 h^2} - \frac{1}{2\beta h}\int_{-\infty}^{\infty}\frac{C_p\left(\xi,\dfrac{h}{2}\right) + C_p\left(\xi,-\dfrac{h}{2}\right)}{2}\,\frac{d\xi}{\cosh\left(\pi\dfrac{x-\xi}{\beta h}\right)} \tag{7.42}$$

where

$$\mu = \int_{x_L}^{x_T}\left[f^+(\xi) - f^-(\xi)\right]d\xi \tag{7.43}$$

is the cross-sectional area of the airfoil.

If

$$C_p\left(\xi,\pm\frac{h}{2}\right) = 0\,, \qquad -\infty < \xi < \infty$$

Equation (7.42) reduces to the standard open jet blockage correction (4.102). The same is much less obvious for the correction formula (6.23) by Capelier, Chevallier and Bouniol. However, the connection between the two formulas is not difficult to establish [7.18]. Substituting in Equations (6.16) the doublet singularity

$$\phi_F(x,y) = \frac{\mu}{2\pi\beta}\,\frac{x}{x^2 + (\beta y)^2}$$

we obtain from Equation (6.17)

$$u_W(x,0) = -\frac{\mu}{2\beta h}\,J(x) - \frac{1}{2\beta h}\int_{-\infty}^{\infty}\frac{C_p\left(\xi,\dfrac{h}{2}\right) + C_p\left(\xi,-\dfrac{h}{2}\right)}{2}\,\frac{d\xi}{\cosh\left(\pi\dfrac{x-\xi}{\beta h}\right)}$$

where

$$J(x) = \int_{-\infty}^{\infty} \frac{\partial}{\partial \xi} \left[\frac{\xi}{\xi^2 + \left(\beta \frac{h}{2}\right)^2} \right] \frac{d\xi}{\cosh\left(\pi \frac{x-\xi}{\beta h}\right)}$$

$$= \frac{1}{6} \frac{\pi}{\beta^2 h} \left[1 - \frac{7}{20} \left(\frac{\pi x}{\beta h}\right)^2 + \ldots \right]$$

To the first order of approximation both formulas thus agree.

Similarly to Equation (7.39), Sawada defines the incidence correction as

$$v_W(x,0) = \frac{\partial \phi}{\partial y}(x,0+) - \frac{\partial \phi_F}{\partial y}(x,0\pm) \tag{7.44}$$

The continuity across $y = 0$ requires that the airfoil in free air be suitably rotated, i.e.

$$\frac{\partial \phi_F}{\partial y}(x,0+) = \frac{df^+(x)}{dx} - \Delta\alpha$$

$$\frac{\partial \phi_F}{\partial y}(x,0-) = \frac{df^-(x)}{dx} - \Delta\alpha \tag{7.45}$$

From Equations (7.5) and (7.15) it follows for the incidence correction [7.16]:

$$v_W(x,0) = -\frac{c\,C_L}{4h} + \frac{1}{2h} \int_{-\infty}^{\infty} \frac{C_p\left(\xi,-\frac{h}{2}\right) - C_p\left(\xi,\frac{h}{2}\right)}{1 + \exp\left(2\pi \frac{x-\xi}{\beta h}\right)}\, d\xi \tag{7.46}$$

Again, if

$$C_p\left(\xi,\pm\frac{h}{2}\right) = 0\,, \qquad -\infty < \xi < \infty$$

the lift-dependent part of the incidence correction (4.103) for open jet is obtained. Equivalence with the incidence correction (6.24) is verified by substituting the vortex singularity

$$\phi_F(x,y) = -\frac{c\,C_L}{\pi} \operatorname{atan} \frac{\beta y}{x}$$

in Equations (6.16).

Compared to the method of Capelier, Chevallier and Bouniol, Sawada's approach is more elaborate, but in principle adaptable to transonic flows, provided that the neglected nonlinear field contributions (double integrals) could be worked out.

7.4 Bland's Method for Steady Subsonic Interference

The method [7.19], originally developed to calculate oscillatory airfoil loadings in wind tunnels, has a very simple algorithm for the linearized, steady flow case. As is common for all integral equation methods, the wall interference corrections are obtained indirectly, by comparing the computations in the wind tunnel and free air. This guarantees a proper aerodynamic coupling between the model and the walls, which obviously is not the case in the classical interference theory, where the model boundary condition is not directly taken into account. The collocation technique, used to solve numerically the singular integral equation, is ideally suited for computing unsteady wall interference, where the coupled nature of interference between the walls and the model is of primary concern [7.20]. We shall turn to the unsteady wall interference problem in Section 8.3.

As in Reference [7.19], it will be convenient to normalize all lengths by the airfoil semi-chord, c/2. The domain integral (7.13) is neglected, assuming the flow to be subsonic linearized. The wall boundary condition is supposed to be known and the Green's function constructed in such a way that the integrals along the walls vanish. From Equations (7.5) and (7.11) in that case

$$\phi(x,y) = \left[\int_{-1}^{1} \left\{ \frac{\partial \phi}{\partial \xi}(\xi,\eta)\, G^*(x,y;\xi,\eta) + \frac{\partial \phi}{\partial \eta}(\xi,\eta)\, G(x,y;\xi,\eta) \right\} d\xi \right]_{\eta = 0-}^{\eta = 0+} \tag{7.47}$$

Furthermore, Bland's method deals only with the lift effect. The airfoil is considered infinitely thin, represented by the boundary condition

$$\frac{\partial \phi}{\partial y}(x,0) = \frac{\partial \phi}{\partial y}(x,0\pm) = \frac{df(x)}{dx} = v(x) \tag{7.48}$$

Here f describes the distribution of camber and v is the normal velocity on the airfoil, also called the upwash*. In this simplified case the second integrand in Equation (7.47) drops out. By differentiating Equation (7.47) with respect to y and introducing the vorticity distribution

$$\gamma(x) = \frac{\partial \phi}{\partial x}(x,0+) - \frac{\partial \phi}{\partial x}(x,0-) = \frac{1}{2}\left[C_p(x,0-) - C_p(x,0+) \right] \tag{7.49}$$

we obtain

$$v(x) = -\frac{\beta}{2\pi} \int_{-1}^{1} K(x-\xi)\, \gamma(\xi)\, d\xi \tag{7.50}$$

where the kernel is given by

$$K(x-\xi) = -\frac{2\pi}{\beta} \frac{\partial G^*}{\partial y}(x,0;\xi,0) \tag{7.51}$$

Since the upwash is known from the airfoil boundary condition (7.48), Equation (7.50) represents an integral equation for the vorticity γ. It can be classified as a Fredholm integral equation of the first kind; its kernel identifies it further as a Cauchy singular equation.

The factor $-2\pi/\beta$, introduced in Equation (7.51), allows to obtain from Equation (7.19) the "net" Cauchy kernel

$$K_c(x-\xi) = \frac{1}{x-\xi} \tag{7.52}$$

in the free air case. The solution of the corresponding Glauert equation

$$v(x) = -\frac{1}{2\pi} \int_{-1}^{1} \frac{\beta\gamma(\xi)}{x-\xi}\, d\xi \tag{7.53}$$

subject to the Kutta-Joukowski condition $\gamma(1) = 0$, is given by the Söhngen inversion formula

$$\beta\gamma(x) = -\frac{2}{\pi} \sqrt{\frac{1-x}{1+x}} \int_{-1}^{1} \sqrt{\frac{1+\xi}{1-\xi}}\, \frac{v(\xi)}{\xi - x}\, d\xi \tag{7.54}$$

As noted by Bland [7.19], formulas (7.53) and (7.54) can be symmetrized by introducing the pressure factor

$$\psi(x) = -\frac{\beta\gamma(x)}{2} \sqrt{\frac{1+x}{1-x}} \tag{7.55}$$

For the free air case we then obtain the transformation pair

---

*Bland, since his y axis is oriented downwards, prefers the term "downwash".

$$v(x) = \frac{1}{\pi} \int_{-1}^{1} \sqrt{\frac{1-\xi}{1+\xi}} \frac{\psi(\xi)}{x-\xi} d\xi , \qquad \psi(x) = \frac{1}{\pi} \int_{-1}^{1} \sqrt{\frac{1+\xi}{1-\xi}} \frac{v(\xi)}{\xi-x} d\xi \tag{7.56}$$

It can be shown that the pressure factor ψ is a continuous function on the interval $-1 < x < 1$ provided v is also continuous.

For the wind tunnel case, the substitution of the pressure factor (7.55) in Equation (7.50) leads to Bland's integral equation

$$v(x) = \frac{1}{\pi} \int_{-1}^{1} \sqrt{\frac{1-\xi}{1+\xi}} K(x-\xi) \psi(\xi) d\xi \tag{7.57}$$

The theoretical advantage of Equation (7.57) over (7.50) is that (7.57) has a unique solution with the correct leading and trailing edge singularities. Without the auxiliary Kutta-Joukowski condition, Equation (7.50) does not have a unique solution.

In solving the singular integral equation (7.57) it is convenient to expand the unknown pressure factor into a series of orthogonal polynomials [7.19]

$$v_n(x) = \frac{\cos\left[\left(n-\frac{1}{2}\right)\arccos x\right]}{\cos\left(\frac{1}{2}\arccos x\right)}, \qquad \psi_n(x) = \frac{\sin\left[\left(n-\frac{1}{2}\right)\arccos x\right]}{\sin\left(\frac{1}{2}\arccos x\right)} \tag{7.58}$$

It is easy to verify that these are polynomials of degree $n-1$:

$$v_1(x) = 1 \qquad \psi_1(x) = 1$$

$$v_2(x) = -1 + 2x \qquad \psi_2(x) = 1 + 2x$$

$$v_3(x) = -1 - 2x + 4x^2 \qquad \psi_3(x) = -1 + 2x + 4x^2$$

$$v_4(x) = 1 - 4x - 4x^2 + 8x^3 \qquad \psi_4(x) = -1 - 4x + 4x^2 + 8x^3$$

$$v_5(x) = 1 + 4x - 12x^2 - 8x^3 + 16x^4 \qquad \psi_5(x) = 1 - 4x - 12x^2 + 8x^3 + 16x^4$$

$$\vdots \qquad\qquad \vdots$$

see Figures 7.3 and 7.4. They can be generated by the recursion formulas

$$v_{n+2}(x) = 2x\, v_{n+1}(x) - v_n(x) \qquad \psi_{n+2}(x) = 2x\, \psi_{n+1}(x) - \psi_n(x)$$

Because of the interrelations

$$v_n(x) = \frac{1}{\pi} \int_{-1}^{1} \sqrt{\frac{1-\xi}{1+\xi}} \frac{\psi_n(\xi)}{x-\xi} d\xi , \qquad \psi_n(x) = \frac{1}{\pi} \int_{-1}^{1} \sqrt{\frac{1+\xi}{1-\xi}} \frac{v_n(\xi)}{\xi-x} d\xi \tag{7.59}$$

cf. Equations (7.56), v_n and ψ_n are called the upwash and pressure polynomials or, collectively, the airfoil polynomials.

The polynomials have the following orthogonality properties [7.19]

$$\frac{1}{\pi} \int_{-1}^{1} \sqrt{\frac{1+x}{1-x}}\, v_m(x)\, v_n(x)\, dx = \delta_{mn} , \qquad \frac{1}{\pi} \int_{-1}^{1} \sqrt{\frac{1-x}{1+x}}\, \psi_m(x)\, \psi_n(x)\, dx = \delta_{mn} \tag{7.60}$$

where δ_{mn} is the Kronecker delta. From the interval of integration $-1 < x < 1$ and the weight functions

$$\sqrt{\frac{1+x}{1-x}} \qquad \text{and} \qquad \sqrt{\frac{1-x}{1+x}}$$

it transpires that v_n and ψ_n are the Jacobi polynomials

$$P_{n-1}^{\left(-\frac{1}{2},\frac{1}{2}\right)} \qquad \text{and} \qquad P_{n-1}^{\left(\frac{1}{2},-\frac{1}{2}\right)}$$

except that they are not standardized in the usual way [7.22].

Since the airfoil polynomials form complete orthogonal bases [7.21], we can expand v and ψ in infinite series

$$v(x) = \sum_{n=1}^{\infty} b_n v_n(x), \qquad \psi(x) = \sum_{n=1}^{\infty} a_n \psi_n(x) \tag{7.61}$$

where, by the orthogonality properties (7.60)

$$b_n = \frac{1}{\pi} \int_{-1}^{1} \sqrt{\frac{1+x}{1-x}}\, v(x)\, v_n(x)\, dx, \qquad a_n = \frac{1}{\pi} \int_{-1}^{1} \sqrt{\frac{1-x}{1+x}}\, \psi(x)\, \psi_n(x)\, dx \tag{7.62}$$

For the free air case, where Equations (7.56) hold

$$a_n = \frac{1}{\pi} \int_{-1}^{1} \sqrt{\frac{1-x}{1+x}}\, \psi_n(x) \left[\frac{1}{\pi} \int_{-1}^{1} \sqrt{\frac{1+\xi}{1-\xi}}\, \frac{v(\xi)}{\xi - x}\, d\xi \right] dx$$

$$= \frac{1}{\pi} \int_{-1}^{1} \sqrt{\frac{1+\xi}{1-\xi}}\, v(\xi) \left[\frac{1}{\pi} \int_{-1}^{1} \sqrt{\frac{1-x}{1+x}}\, \frac{\psi_n(x)}{\xi - x}\, dx \right] d\xi = b_n \tag{7.63}$$

Hence, by representing the upwash by the first of Equations (7.61), we obtain the pressure factor directly as

$$\psi(x) = \sum_{n=1}^{\infty} b_n \psi_n(x) \tag{7.64}$$

For the wind tunnel case the situation is not as simple because the Fourier coefficients for the pressure factor and upwash are no longer equal. To solve the integral equation (7.57), Bland proposes the following approach. The pressure factor is approximated by the finite series

$$\psi^N(\xi) = \sum_{n=1}^{N} a_n^N \psi_n(\xi) \tag{7.65}$$

The substitution in Equation (7.57) results in

$$v(x) = \sum_{n=1}^{N} a_n^N \frac{1}{\pi} \int_{-1}^{1} \sqrt{\frac{1-\xi}{1+\xi}}\, K(x-\xi)\, \psi_n(\xi)\, d\xi \tag{7.66}$$

which, in order to determine the constants a_n^N, $n = 1, \ldots, N$, is required to be satisfied at N collocation points. These are selected to be the N zeros of the upwash polynomial v_{N+1}, that is

$$x_m^{N+1} = -\cos \frac{2m\pi}{2N+1}, \qquad m = 1, \ldots, N \tag{7.67}$$

The integral equation (7.57) is then reduced to a system of N linear algebraic equations

$$\sum_{n=1}^{N} A_{mn}^{N} \, a_n^N = c_m^N \qquad , \qquad m = 1, \ldots, N \tag{7.68}$$

where

$$c_m^N = v\left(x_m^{N+1}\right) \tag{7.69}$$

and

$$A_{mn}^{N} = \frac{1}{\pi} \int_{-1}^{1} \sqrt{\frac{1-\xi}{1+\xi}} \, K\left(x_m^{N+1} - \xi\right) \psi_n(\xi) \, d\xi \tag{7.70}$$

The determination of the kernel function, which is of a singular nature, is the crucial part of the method. The case of (idealized) porous walls is one of the few exceptions for which the cloased form of the kernel function is known in a closed form. From Equations (7.51), (7.20), (7.19) and (7.34) we have for unequal porosities

$$K(x-\xi) = \frac{\pi}{\beta h} \exp\left(\pi \frac{\tau_U + \tau_L}{2} \frac{x-\xi}{\beta h}\right) \left[\frac{1}{\exp\left(\pi \frac{x-\xi}{\beta h}\right) - 1} + \frac{\cos\left(\pi \frac{\tau_U - \tau_L}{2}\right)}{\exp\left(\pi \frac{x-\xi}{\beta h}\right) + 1} \right] \tag{7.71}$$

where τ_U and τ_L are given by Equations (7.37). For equal upper and lower wall porosities, $\tau_U = \tau_L = \tau$

$$K(x-\xi) = \frac{\pi}{\beta h} \frac{\exp\left(\pi\tau \frac{x-\xi}{\beta h}\right)}{\sinh\left(\pi \frac{x-\xi}{\beta h}\right)} \tag{7.72}$$

Finally, for solid walls, $\tau = 0$,

$$K(x-\xi) = \frac{\pi}{\beta h} \frac{1}{\sinh\left(\pi \frac{x-\xi}{\beta h}\right)} \tag{7.73}$$

and for open jet boundaries, $\tau = 1$,

$$K(x-\xi) = \frac{\pi}{\beta h} \frac{\exp\left(\pi \frac{x-\xi}{\beta h}\right)}{\sinh\left(\pi \frac{x-\xi}{\beta h}\right)} \tag{7.74}$$

Apparently, the kernel functions (7.73) and (7.74) were first given by Hantzsche and Wendt [7.23]; for more recent applications of the solid wall kernel see References [7.24] and [7.25]. The porous wall kernel (7.72) is due to Fromme and Golberg [7.26]; the unequal porosity kernel, Equation (7.71), is a new result. The kernel function for longitudinally slotted walls is not as compact as the above cases, since the corresponding Green's function (7.28) contains eigenvalues that are roots of the transcendental equation (7.29). It is given by Equation (8.64), obtained from Bland's unsteady flow kernel.

To evaluate the collocation matrix (7.70), the kernel is split into the Cauchy and analytic (wall interference parts):

$$K(x-\xi) = K_C(x-\xi) + K_W(x-\xi) \tag{7.75}$$

Using the power series expansions (7.35) and (7.36), we obtain the analytic part of the porous wall kernel (7.71)

$$K_W(x-\xi) = \frac{\pi}{\beta h} \left[\sum_{n=1}^{\infty} B_n\left(\frac{\tau_U + \tau_L}{2}\right) \frac{\left(\pi \frac{x-\xi}{\beta h}\right)^{n-1}}{n!} + \frac{1}{2} \cos\left(\pi \frac{\tau_U - \tau_L}{2}\right) \sum_{n=0}^{\infty} E_n\left(\frac{\tau_U + \tau_L}{2}\right) \frac{\left(\pi \frac{x-\xi}{\beta h}\right)^{n}}{n!} \right] \tag{7.76}$$

where B_n and E_n denote the Bernoulli and Euler polynomials, Equations (5.22) and (5.24).

For equal upper and lower wall porosities, $\tau_U = \tau_L = \tau$,

$$K_W(x-\xi) = \frac{\pi}{\beta h}\left[\sum_{n=1}^{\infty} B_n(\tau)\frac{\left(\pi\frac{x-\xi}{\beta h}\right)^{n-1}}{n!} + \frac{1}{2}\sum_{n=0}^{\infty} E_n(\tau)\frac{\left(\pi\frac{x-\xi}{\beta h}\right)^{n}}{n!}\right]$$

$$= \frac{2\pi}{\beta h}\sum_{n=1}^{\infty} B_n\left(\frac{1+\tau}{2}\right)\frac{\left(2\pi\frac{x-\xi}{\beta h}\right)^{n-1}}{n!} \tag{7.77}$$

The solid wall and open jet cases are easily obtained by substituting $\tau = 0$ and $\tau = 1$ respectively.

In accordance with Equation (7.75), the matrix is decomposed as

$$A^N_{mn} = C^N_{mn} + W^N_{mn} \tag{7.78}$$

For the Cauchy singularity we have in closed form

$$\frac{1}{\pi}\int_{-1}^{1}\sqrt{\frac{1-\xi}{1+\xi}}\,K_C(x-\xi)\,\psi_n(\xi)\,d\xi = v_n(x)$$

and hence

$$C^N_{mn} = v_n\left(x^{N+1}_m\right) \tag{7.79}$$

The analytic part is obtained numerically, using the N-point Jacobi-Gauss quadrature:

$$\frac{1}{\pi}\int_{-1}^{1}\sqrt{\frac{1-\xi}{1+\xi}}\,K_W(x-\xi)\,\psi_n(\xi)\,d\xi \simeq \frac{2}{2N+1}\sum_{j=1}^{N}\left(1-\xi^{N+1}_j\right)K_W\left(x-\xi^{N+1}_j\right)\psi_n\left(\xi^{N+1}_j\right) \tag{7.80}$$

so that

$$W^N_{mn} = \frac{2}{2N+1}\sum_{j=1}^{N}\left(1-\xi^{N+1}_j\right)K_W\left(x^{N+1}_m-\xi^{N+1}_j\right)\psi_n\left(\xi^{N+1}_j\right) \tag{7.81}$$

As quadrature points selected are the zeros of the pressure polynomial ψ_{N+1}:

$$\xi^{N+1}_j = \cos\frac{2j\pi}{2N+1}, \qquad j = 1,\ldots,N \tag{7.82}$$

We may note that the collocation and quadrature points are interleaved as

$$-1 < x_1 < \xi_N < x_2 < \ldots. < \xi_2 < x_N < \xi_1 < 1$$

Using a three-way equivalence between collocation, least squares and Galerkin's method, Fromme and Golberg [7.26], [7.27] established that

$$\lim_{N\to\infty} a^N_n = \frac{1}{\pi}\int_{-1}^{1}\sqrt{\frac{1-x}{1+x}}\,\psi(x)\,\psi_n(x)\,dx = a_n$$

which is a proof of convergence for Bland's method

Once the Fourier coefficients a_n are known, the vorticity distribution is evaluated from Equations (7.55) and (7.65) as

$$\gamma(x) = -\frac{2}{\beta}\sqrt{\frac{1-x}{1+x}}\sum_n a_n\,\psi_n(x) \tag{7.83}$$

With the help of the second Equation (7.60) the lift coefficient is obtained as [7.26]

$$C_L = \int_{-1}^{1} \gamma(x)\,\psi_1(x)\,dx \qquad \ldots \qquad \psi_1(x) = 1$$

$$= -\frac{2\pi}{\beta}\sum_n a_n \frac{1}{\pi}\int_{-1}^{1}\sqrt{\frac{1-x}{1+x}}\,\psi_n(x)\,\psi_1(x)\,dx$$

$$= -\frac{2\pi}{\beta}\,a_1 \tag{7.84}$$

and the quarter-chord pitching moment coefficient

$$C_{M_{c/4}} = -\frac{1}{4}\int_{-1}^{1}\gamma(x)\,\psi_2(x)\,dx \qquad \ldots \qquad \psi_2(x) = 1 + 2x$$

$$= \frac{\pi}{2\beta}\sum_n a_n \frac{1}{\pi}\int_{-1}^{1}\sqrt{\frac{1-x}{1+x}}\,\psi_n(x)\,\psi_2(x)\,dx$$

$$= \frac{\pi}{2\beta}\,a_2 \tag{7.85}$$

These particularly simple formulas, involving only the first two pressure Fourier coefficients, are a direct consequence of the orthogonality properties of the airfoil polynomials.

As mentioned before, in Bland's method the wall interference corrections are obtained indirectly, by comparing the free air and wind tunnel computation results. However, the connection with the standard incidence correction (4.95) of the classical wall interference theory is not difficult to show. From Equations (7.50) and (7.77) we have for a small airfoil, $c = 2 \ll h$,

$$v_W(0,0) = -\frac{\beta}{2\pi}\int_{-1}^{1} K_W(-\xi)\,\gamma(\xi)\,d\xi$$

$$\simeq -\frac{\gamma}{h}\,B_1\left(\frac{1+\tau}{2}\right) - \frac{\omega\pi}{\beta h^2}\,B_2\left(\frac{1+\tau}{2}\right)$$

where

$$\gamma = \int_{-1}^{1}\gamma(\xi)\,d\xi$$

$$\omega = -\int_{-1}^{1}\gamma(\xi)\,\xi\,d\xi$$

7.5 Method of Kraft

The integral equation formulation for transonic wall interference is due to Kraft [7.28], [7.29]. Although the equation was obtained for both lifting and nonlifting airfoils, only calculations for symmetrical flow cases were given, so that we restrict ourselves to these. The wall boundary condition is assumed to be of the porous type, and the wall integral (7.7) is eliminated employing the Green's function satisfying Equations (7.30). For symmetry reasons, the upper and lower wall porosities are assumed to be equal, $P_U = P_L = P$.

Utilizing the symmetrical airfoil boundary condition

$$\frac{\partial \phi}{\partial y}(x,0+) = -\frac{\partial \phi}{\partial y}(x,0-) = \frac{1}{2}\frac{dt(x)}{dx} \tag{7.86}$$

where t denotes the thickness distribution, we obtain from Equations (7.5), (7.6) and (7.13)

$$\phi(x,y) = \int_{-1}^{1} \frac{dt(\xi)}{d\xi} G(x,y;\xi,0)\, d\xi - M_\infty^2 \frac{\kappa+1}{U_\infty} \int_{-\frac{h}{2}}^{\frac{h}{2}} \int_{-\infty}^{\infty} \frac{1}{2}\left(\frac{\partial \phi}{\partial \xi}(\xi,\eta)\right)^2 \frac{\partial G}{\partial \xi}(x,y;\xi,\eta)\, d\xi\, d\eta \tag{7.87}$$

To be consistent with the method of Section 7.4, all lengths are again normalized by the airfoil semi-chord.* The principal value definitions of the above integrals are

$$\int_{-1}^{1} \ldots d\xi = \lim_{\epsilon \to 0} \left\{ \int_{-1}^{x-\epsilon} \ldots d\xi + \int_{x+\epsilon}^{\infty} \ldots d\xi \right\} \tag{7.88}$$

$$\int_{-\frac{h}{2}}^{\frac{h}{2}} \int_{-\infty}^{\infty} \ldots d\xi\, d\eta = \lim_{\epsilon \to 0} \int_{-\frac{h}{2}}^{\frac{h}{2}} \left\{ \int_{-\infty}^{x-\epsilon} \ldots d\xi + \int_{x+\epsilon}^{\infty} \ldots d\xi \right\} d\eta \tag{7.89}$$

although in the latter case other interpretations are also possible, see References [7.31] to [7.33].

To replace the potential function by the x component of disturbance velocity

$$u(x,y) = \frac{\partial \phi}{\partial x}(x,y) \tag{7.90}$$

we need to differentiate Equation (7.87) with respect to x. Since in the principal value definitions (7.88) and (7.89) the integration limits are x-dependent, the formula for differentiation under the integral sign has to be employed. For the thickness integral thus

$$\frac{\partial}{\partial x} \int_{-1}^{1} \frac{dt(\xi)}{d\xi} G(x,y;\xi,0)\, d\xi = \int_{-1}^{1} \frac{dt(\xi)}{d\xi} \frac{\partial G}{\partial x}(x,y;\xi,0)\, d\xi + \frac{dt(x)}{dx} \lim_{\epsilon \to 0} \left[G(x,y;x-\epsilon,0) - G(x,y;x+\epsilon,0) \right]$$

The analytic part G_W of the Green's function obviously does not contribute to the above limit, so that only the singular part G_F needs to be considered. However, even that is continuous as may be verified from Equation (7.18), so that the limit in the above expression is zero.

The situation is different with the double integral of Equation (7.87). We have

---

*Kraft uses the unit chord length.

$$\frac{\partial}{\partial x}\int_{-\frac{h}{2}}^{\frac{h}{2}}\int_{-\infty}^{\infty}\frac{1}{2}u^2(\xi,\eta)\,\frac{\partial G}{\partial \xi}(x,y;\xi,\eta)\,d\xi\,d\eta =$$

$$\int_{-\frac{h}{2}}^{\frac{h}{2}}\int_{-\infty}^{\infty}\frac{1}{2}u^2(\xi,\eta)\,\frac{\partial^2 G}{\partial x\partial \xi}(x,y;\xi,\eta)\,d\xi\,d\eta + \lim_{\epsilon\to 0}\int_{-\frac{h}{2}}^{\frac{h}{2}}\frac{1}{2}u^2(x,\eta)\left[\frac{\partial G}{\partial x}(x,y;x-\epsilon,\eta) - \frac{\partial G}{\partial x}(x,y;x+\epsilon,\eta)\right]d\eta$$

Substituting from Equation (7.18) we find that the limit is

$$\lim_{\epsilon\to 0}\left\{-\frac{1}{\pi\beta}\int_{-\frac{h}{2}}^{\frac{h}{2}}\frac{1}{2}u^2(x,\eta)\,\frac{\epsilon}{\epsilon^2+\beta^2(y-\eta)^2}\,d\eta\right\} = -\frac{1}{2\beta}u^2(x,y)$$

Accordingly, from Equation (7.87) we obtain the following integral equation for the component of the disturbance velocity

$$u(x,0) = \int_{-1}^{1}\frac{dt(\xi)}{d\xi}\,\frac{\partial G}{\partial x}(x,0;\xi,0)\,d\xi + M_\infty^2\,\frac{\kappa+1}{U_\infty}\left[\frac{1}{2\beta}u^2(x,0) - \int_{-\frac{h}{2}}^{\frac{h}{2}}\int_{-\infty}^{\infty}\frac{1}{2}u^2(\xi,\eta)\,\frac{\partial^2 G}{\partial x\partial\xi}(x,0;\xi,\eta)\,d\xi\,d\eta\right] \tag{7.91}$$

where the integrals are interpreted as principal values (7.88) and (7.89).

As pointed out in Reference [7.1], in contrast to Bland's linear integral equation (7.57) no rigorous theory seems to exist describing either the existence or uniqueness of solutions to (7.91). To facilitate its analysis, the Green's function is split according to Equation (7.20). The derivatives of its free air part are obtained from Equation (7.18) as

$$\frac{\partial G_F}{\partial x}(x,0;\xi,0) = \frac{1}{2\pi\beta}\,\frac{1}{x-\xi} \tag{7.92}$$

$$\frac{\partial^2 G_F}{\partial x\partial\xi}(x,0;\xi,\eta) = \frac{1}{2\pi\beta}\,\frac{(x-\xi)^2-\beta^2\eta^2}{\left[(x-\xi)^2+\beta^2\eta^2\right]^2} \tag{7.93}$$

The derivatives of the analytic (wall interference) part follow from Equations (7.31), (7.35) and (7.36). We have

$$\frac{\partial G_W}{\partial x}(x,0;\xi,0) = \frac{1}{\beta^2 h}\,\mathrm{Re}\left\{B(x,0;\xi,0) + E(x,0;\xi,0) + \chi(\tau)\right\}$$

$$= \frac{1}{\beta^2 h}\left\{\frac{1}{2}\sum_{n=1}^{\infty}B_n(\tau)\,\frac{\left(\pi\frac{x-\xi}{\beta h}\right)^{n-1}}{n!} - \frac{1}{4}\sum_{n=0}^{\infty}E_n(\tau)\,\frac{\left(\pi\frac{x-\xi}{\beta h}\right)^{n}}{n!} + \chi(\tau)\right\}, \quad \frac{|x-\xi|}{\beta h} < 1 \tag{7.94}$$

or, in a more compact form,

$$\frac{\partial G_W}{\partial x}(x,0;\xi,0) = \frac{1}{\beta^2 h}\left[\frac{\exp\left(2\pi\frac{x-\xi}{\beta h}\frac{\tau}{2}\right)}{\exp\left(2\pi\frac{x-\xi}{\beta h}\right)-1} - \frac{1}{2\pi\frac{x-\xi}{\beta h}} + \chi(\tau)\right]$$

$$= \frac{1}{\beta^2 h}\left[\sum_{n=1}^{\infty} B_n\left(\frac{\tau}{2}\right)\frac{\left(2\pi\frac{x-\xi}{\beta h}\right)^{n-1}}{n!} + \chi(\tau)\right] \quad , \quad \frac{|x-\xi|}{\beta h} < 1 \tag{7.95}$$

Similarly

$$\frac{\partial^2 G_W}{\partial x \partial \xi}(x,0;\xi,\eta) = \frac{1}{\beta^2 h}\,\mathrm{Re}\,\frac{\partial}{\partial \xi}\left\{B(x,0;\xi,\eta) + E(x,0;\xi,\eta)\right\}$$

$$= -\frac{\pi}{2\beta^3 h^2}\,\mathrm{Re}\left\{\sum_{n=2}^{\infty} B_n(\tau)\,\frac{\left[\pi\left(\frac{x-\xi}{\beta h} - i\frac{\eta}{h}\right)\right]^{n-2}}{n(n-2)!} - \frac{1}{2}\sum_{n=1}^{\infty} E_n(\tau)\,\frac{\left[\pi\left(\frac{x-\xi}{\beta h} + i\frac{\eta}{h}\right)\right]^{n-1}}{(n-1)!}\right\} \quad \left|\frac{x-\xi}{\beta h} + i\frac{\eta}{h}\right| < 1 \tag{7.96}$$

In the above formulas again B_n and E_n denote the Bernoulli and Euler polynomials, Equations (5.22) and (5.24).

In the free air limit, $h \to \infty$, Equation (7.91) reduces to Oswatitsch's integral equation [7.6]

$$u(x,0) = \frac{1}{2\pi\beta}\int_{-1}^{1}\frac{dt(\xi)}{d\xi}\frac{d\xi}{x-\xi} + M_\infty^2\,\frac{\kappa+1}{\beta U_\infty}\left[\frac{1}{2}u^2(x,0) - \frac{1}{2\pi}\int_{-\infty}^{\infty}\int_{-\infty}^{\infty}\frac{1}{2}u^2(\xi,\eta)\,\frac{(x-\xi)^2-\beta^2\eta^2}{\left[(x-\xi)^2+\beta^2\eta^2\right]^2}\,d\xi\,d\eta\right] \tag{7.97}$$

The numerical methods used by Kraft are straightforward generalizations of those of References [7.30] and [7.34] to [7.40], used to solve Equation (7.97). Kraft, similarly to Nørstrud [7.37], reduces Equation (7.91) to a one-dimensional integral equation assuming an exponential decay of the axial velocity in the transverse direction:

$$u(x,y) = u(x,0)\,e^{-\frac{|y|}{r(x)}} \tag{7.98}$$

The decay parameter, consistent with the irrotationality condition at the airfoil, is

$$r(x) = -\frac{u(x,0)}{\left|\frac{\partial u}{\partial y}(x,0)\right|} \tag{7.99}$$

However, its actual form does not seem to matter greatly [7.38] and it is often sufficient to consider it constant over the airfoil.

In addition, it is assumed that in transonic flow the nonlinear field contributions upstream and downstream of the airfoil can be neglected [7.39]. Accordingly, the double integral of Equation (7.91) can be reduced to

$$\int_0^{\frac{h}{2}}\int_{-1}^{1} u^2(\xi,0)\,e^{-\frac{2\eta}{r(\xi)}}\,\frac{\partial^2 G}{\partial x \partial \xi}(x,0;\xi,\eta)\,d\xi\,d\eta$$

In the numerical procedure the flow field above the airfoil, $-1 < x < 1$, $0 < y < h/2$, is divided into N vertical strips of width 2/N, see Figure 7.5. Denoting

$$x_k = -1 + \left(k - \frac{1}{2}\right)\frac{2}{N}$$

the centreline of the k th strip and putting

$$\left.\begin{aligned} u(x,0) &= u_k \\ r(x) &= r_k \end{aligned}\right\} \qquad -1 + 2(k-1)/N < x < -1 + 2k/N$$

the integral equation (7.91) reduces to a system of N nonlinear algebraic equations

$$u_k = \hat{u}_k + \frac{M_\infty^2}{\beta}\frac{\kappa+1}{U_\infty}\left[\frac{u_k^2}{2} - \sum_{j=1}^{N} A_{kj}\frac{u_j^2}{2}\right] \tag{7.100}$$

Here

$$\hat{u}_k = \int_{-1}^{1} \frac{dt(\xi)}{d\xi}\frac{\partial G}{\partial x}(x_k,0;\xi,0)\,d\xi \tag{7.101}$$

and

$$A_{kj} = 2\beta \int_0^{\frac{h}{2}} \int_{-1+2(j-1)/N}^{-1+2j/N} e^{-\frac{2\eta}{r_k}} \frac{\partial^2 G}{\partial x \partial \xi}(x_k,0;\xi,\eta)\,d\xi\,d\eta \tag{7.102}$$

The contribution of Equation (7.92) to the thickness integral (7.101) is obtained by standard techniques, e.g. using cosine substitutions for x and ξ, expanding the thickness t into Fourier series and integrating termwise, Reference [7.41]. The contribution of Equation (7.95) is an ordinary integral, whose quadrature does not pose any particular difficulties, except perhaps meeting the convergence criteria for the series representation at higher Mach numbers.

The contribution of Equation (7.93) to the influence matrix (7.102) can be obtained in closed form in terms of cosine and sine integrals, as described in References [7.28] and [7.38]. The contribution of Equation (7.96) to the influence matrix is again an ordinary integral.

Equation (7.100) must then be solved numerically via some sort of iteration procedure. For the case of subcritical flow rapid convergence can be achieved with the simple Picard iteration. However, if the flow becomes supercritical over a portion of the airfoil, this iteration method fails to converge and more sophisticated methods have to be sought, such as the fixed-shock iterative scheme by Spreiter and Alksne [7.30]. Further details are given in Reference [7.28].

A typical result for supercritical flow over a biconvex airfoil in a solid wall wind tunnel is compared in Figure 7.6 with the relaxation solution of Murman [7.42] and the time dependent solution of Laval [7.43]. Using N = 20, the integral equation solution provided in 10 or 15 iterations an excellent agreement with finite difference solutions, at a fraction of the computation cost. A similar result for flow in a porous wall wind tunnel, comparing the integral equation result of Kraft and Lo [7.29] with Murman's relaxation is shown in Figure 7.7. The comparison with experimental data of Collins and Krupp [7.44] on a 6% biconvex airfoil in a solid wall test section is shown in Figure 7.8.

For linearized subsonic flows, where the quadratic velocity terms of Equation (7.91) are negligibly small, we no longer deal with an integral equation. The axial disturbance velocity is obtained by a simple integration, as a sum of the free air and wall interference contributions

$$u(x,0) = u_F(x,0) + u_W(x,0) \tag{7.103}$$

where

$$u_F(x,0) = \frac{1}{2\pi\beta}\int_{-1}^{1} \frac{dt(\xi)}{d\xi}\frac{d\xi}{x-\xi} \tag{7.104}$$

and

$$u_W(x,0) = \int_{-1}^{1} \frac{dt(\xi)}{d\xi}\frac{\partial G_W}{\partial x}(x,0;\xi,0)\,d\xi \tag{7.105}$$

A method for correcting the measured surface pressure distribution for streamwise variations of u_W was proposed by Binion and Lo [7.45]. In spite of claiming success in some supercritical flow cases, the superposition (7.103) is justifiable only if the entire flow is governed by the linearized potential equation.

For small airfoils, $c = 2 \ll h$, it is convenient to interpret u_W instead as a correction to mainstream. Integrating Equation (7.105) by parts and using Equation (7.95), we obtain in accordance with the velocity correction (4.94)

$$u_W(0,0) = t(1)\frac{\partial G_W}{\partial x}(0,0;0,0) - \frac{\partial^2 G_W}{\partial x \partial \xi}(0,0;0,0)\int_{-1}^{1} t(\xi)\,d\xi$$

$$= \frac{\sigma}{\beta^2 h}\left[B_1\left(\frac{\tau}{2}\right) + \chi(\tau)\right] + \frac{\mu\pi}{\beta^3 h^2} B_2\left(\frac{\tau}{2}\right)$$

where

$$\sigma = t(1)$$

$$\mu = \int_{-1}^{1} t(\xi)\,d\xi$$

If the trailing edge is closed, $t(1) = 0$, the wake blockage term drops out.

REFERENCES

[7.1] Fromme, J.A. Golberg, M.A. *Integral Equations for Flows in Wind Tunnels.* Journal of Integral Equations, Vol. 1, 1979, pp. 249-273.

[7.2] Liepmann, H.W. Roshko, A. *Elements of Gasdynamics.* J. Wiley, 1957, pp. 203-206.

[7.3] Kacprzynski, J.J. *Transonic Flowfield Past Two-Dimensional Airfoils between Porous Wind-Tunnel Walls.* AIAA Journal, Vol. 14, 1976, pp. 533-535.

[7.4] Shankar, V. Malmuth, N.D. Cole, J.D. *Transonic Flow Calculations over Two-Dimensional Canard-Wing Systems.* Journal of Aircraft, Vol. 18, 1979, pp. 108-114.

[7.5] Sawada, H. *A General Correction Method of the Interference in 2-Dimensional Wind Tunnels with Ventilated Walls.* Transactions of the Japan Society for Aeronautical and Space Sciences, Vol. 21, 1978, pp. 57-68.

[7.6] Oswatitsch, K. *Gas Dynamics.* Academic Press, 1956.

[7.7] Cole, J.D. *Twenty Years of Transonic Flow.* D1-82-0878, Flight Sciences Laboratory, Boeing Scientific Research Laboratories, July 1969.

[7.8] Murman, E.M. Cole, J.D. *Calculation of Plane Steady Transonic Flows.* AIAA Journal, Vol. 9, 1971, pp. 114-121.

[7.9] Voss, R. *Berechnung ebener transsonischer Strömungen nach der Integralgleichungsmethode mit Stossanpassung.* Zeitschrift für Flugwissenschaften, Vol. 4, 1980, pp. 289-295.

[7.10] Courant, R. Hilbert, D. *Methods of Mathematical Physics.* Interscience Publishers, 1953, Vol. I, pp. 363-371.

[7.11] Duff, G.F.D. *Partial Differential Equations.* University of Toronto Press, 1956, pp. 161-162.

[7.12] Stakgold, I. *Boundary Value Problems of Mathematical Physics.* Macmillan Co., 1968, Vol. II, pp. 161-163.

[7.13] Carslaw, H.S. Jaeger, J.C. *Conduction of Heat in Solids.* 2nd Ed., Oxford at the Clarendon Press, 1959, pp. 114-120.

[7.14] Kacprzynski, J.J. *The Dynamic Problem of Thermoelasticity of a Circular Cone.* Proceedings of Vibr. Problems, Vol. 3, No. 2 (11), Warsaw, 1962.

[7.15] Sawada, H. *A New Method of Calculating Corrections for Blockage Effects in Two-Dimensional Wind Tunnel with Ventilated Walls, Using Wall Pressure Measurements.* Transactions of the Japan Society for Aeronautical and Space Sciences, Vol. 23, 1980, pp. 155-168.

[7.16] Sawada, H. — *An Experiment of Lift Interference on 2-Dimensional Wings in a Wind Tunnel with Perforated Walls.* Transactions of the Japan Society for Aeronautical and Space Sciences, Vol. 22, 1980, pp. 191-202.

[7.17] Capelier, C. Chevallier, J.-P. Bouniol, F. — *Nouvelle méthode de correction des effets de parois en courant plan.* La Recherche Aérospatiale, Jan.-Feb. 1978, pp. 1-11.

[7.18] Sawada, H. — Private communication, March 1982.

[7.19] Bland, S.R. — *The Two-Dimensional Oscillating Airfoil in a Wind Tunnel in Subsonic Compressible Flow.* Doctoral Thesis, North Carolina State University, Raleigh, 1968; also SIAM J. Appl. Math., Vol. 18, 1970, pp. 830-848.

[7.20] Fromme, J.A. Golberg, M.A. — *Aerodynamic Interference Effects on Oscillating Airfoils with Controls in Ventilated Wind Tunnels.* AIAA Journal, Vol. 18, 1980, pp. 417-426.

[7.21] Fromme, J.A. Golberg, M.A. — *Unsteady Two Dimensional Airloads Acting on Oscillating Thin Airfoils in Subsonic Ventilated Wind Tunnels.* NASA CR 2967, 1978.

[7.22] Abramowitz, M. Stegun, I.A. — *Handbook of Mathematical Functions.* National Bureau of Standards, 1964, pp. 773-802.

[7.23] Hantzsche, W. Wendt, H. — *Windkanalkorrekturen bei kompressiblen Strömungen.* Jahrbuch der deutschen Luftfahrtforschung, 1941, pp. 678-683.

[7.24] de Jager, E.M. van de Vooren, A.I. — *Tunnel Wall Corrections for a Wing-Flap System Between Two Parallel Walls.* NRL-TR W.7, National Aerospace Laboratory NLR, June 1965.

[7.25] Plotkin, A. — *Wind Tunnel Corrections for Lifting Thin Airfoils.* Transactions of the ASME, Vol. 49, 1982, pp. 448-450.

[7.26] Fromme, J.A. Golberg, M.A. — *Two Dimensional Aerodynamic Interference Effects on Oscillating Airfoils With Flaps in Ventilated Subsonic Wind Tunnels.* NASA CR 3210, 1979.

[7.27] Golberg, M.A. Fromme, J.A. — *On the L2 Convergence of Collocation for the Generalized Airfoil Equation.* Journal of Math. Analysis and Applications, Vol. 71, 1979, pp. 271-286.

[7.28] Kraft, E.M. — *An Integral Equation Method for Boundary Interference in Perforated-Wall Wind Tunnels at Transonic Speeds.* Doctoral Thesis, University of Tennessee, Dec. 1975.

[7.29] Kraft, E.M. Lo, C.F. — *Analytical Determination of Blockage Effects in a Perforated-Wall Transonic Wind Tunnel.* AIAA Journal, Vol. 15, 1977, pp. 511-517.

[7.30] Spreiter, J.R. Alksne, A. — *Theoretical Prediction of Pressure Distributions on Nonlifting Airfoils at High Subsonic Speeds.* NACA Rept. 1217, 1955.

[7.31] Schubert, H. Schleiff, M. — *Über zwei Randwertprobleme des inhomogenen Systems der Cauchy-Riemannschen Differentialgleichungen mit einer Anwendung auf ein Problem der stationären schallnahen Strömung.* Zeitschschrift für angewandte Mathematik und Mechanik, Vol. 49, 1969, pp. 621-630.

[7.32] Nixon, D. Hancock, G.J. — *Integral Equation Methods — a Reappraisal.* Symposium Transsonicum II, Springer Verlag, 1976, pp. 174-182.

[7.33] Ogana, W. Spreiter, J.R. — *Derivation of an Integral Equation for Transonic Flows.* AIAA Journal, Vol. 15, 1977, pp. 281-283.

[7.34] Oswatitsch, K. — *Die Geschwindigkeitsverteilung an symmetrischen Profilen beim Auftreten lokaler Überschallgebiete.* Acta Physica Austriaca, Vol. 4, 1950, pp. 228-271.

[7.35] Gullstrand, T.R. — *The Flow over Symmetrical Aerofoils without Incidence in the Lower Transonic Range.* KTH-AERO TN 20, Royal Inst. Techn. Stockholm, 1951.

[7.36] Zierep, J. — *Die Integralgleichungsmethode zur Berechnung schallnaher Strömungen.* Symposium Transsonicum, Springer-Verlag, 1964, pp. 92-109.

[7.37] Nørstrud, H. — *High-Speed Flow Past Wings.* NASA CR-2246, April 1973.

[7.38] Nørstrud, H. — *Numerische Lösungen für schallnahe Strömungen um ebene Profile.* Zeitschrift für Flugwissenschaften, Vol. 18, 1970, pp. 149-157.

[7.39] Nørstrud, H. — *The Transonic Aerofoil Problem with Embedded Shocks.* Aeronautical Quarterly, Vol. 14, 1972, pp. 129-138.

[7.40] Nixon, D. Hancock, G.J. — *High Subsonic Flow Past a Steady Two-Dimensional Aerofoil.* ARC Current Paper 1280, 1974.

[7.41] Bera, R.K. — *Remarks on Thin Airfoil Theory.* Journal of Aircraft, Vol. 14, 1977, pp. 508-509 and Vol. 15, 1978, p. 320.

[7.42] Murman, E.M. — *Computation of Wall Effects in Ventilated Transonic Wind Tunnels.* AIAA Paper 72-1007, 1972.

[7.43] Laval, P. *Méthodes instationnaires de calcul des effets d'interaction de paroi en écoulement bidimensionnel supercritique.* La Recherche Aérospatiale, 1973, pp. 275-288.

[7.44] Collins, D.J. Krupp, J.A. *Experimental and Theoretical Investigations in Two-Dimensional Transonic Flow.* AIAA Journal, Vol. 12, 1974, pp. 771-778.

[7.45] Binion, T.W. Lo, C.F. *Application of Wall Corrections to Transonic Wind Tunnel Data.* AIAA Paper 72-1009, Sept. 1972.

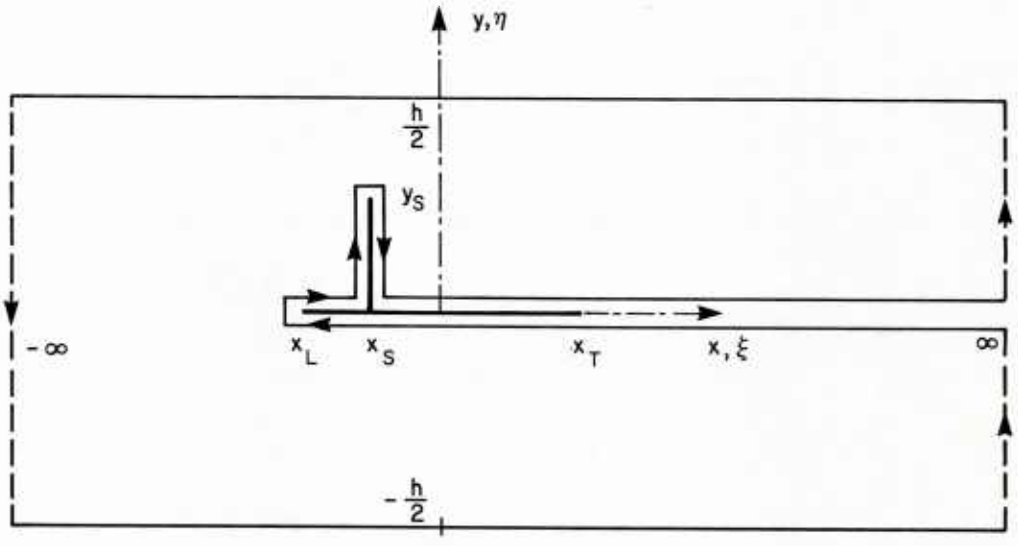

Fig. 7.1 Domain for application of Green's theorem

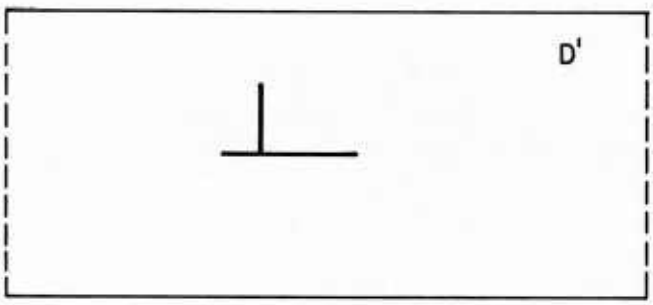

(a) CONTINUOUS-FLOW DOMAIN

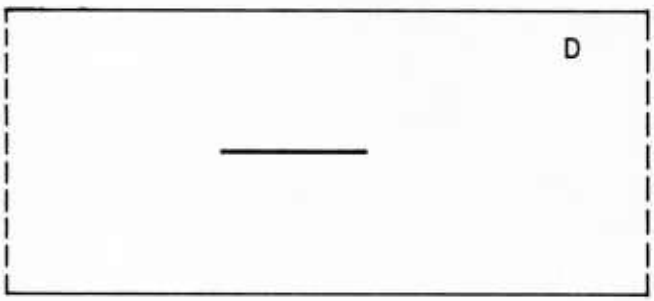

(b) COMPLETE FLOW DOMAIN

Fig. 7.2 Flow domains

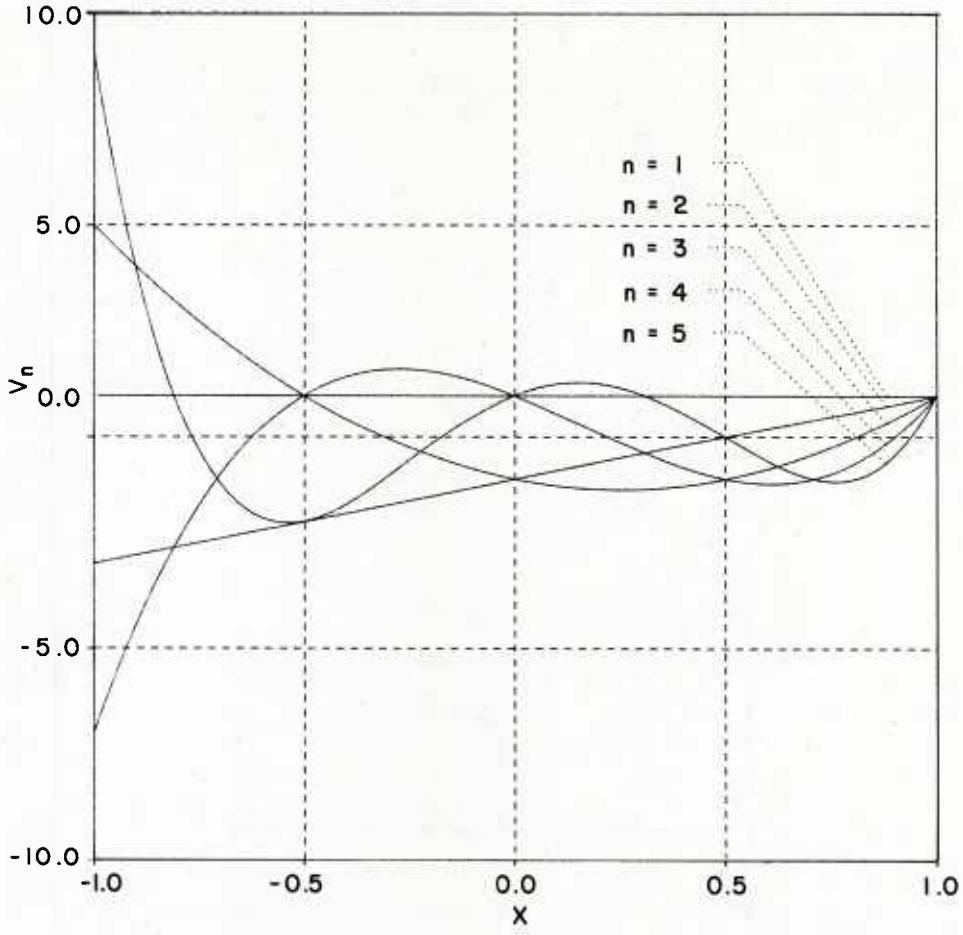

Fig. 7.3 Upwash polynomials

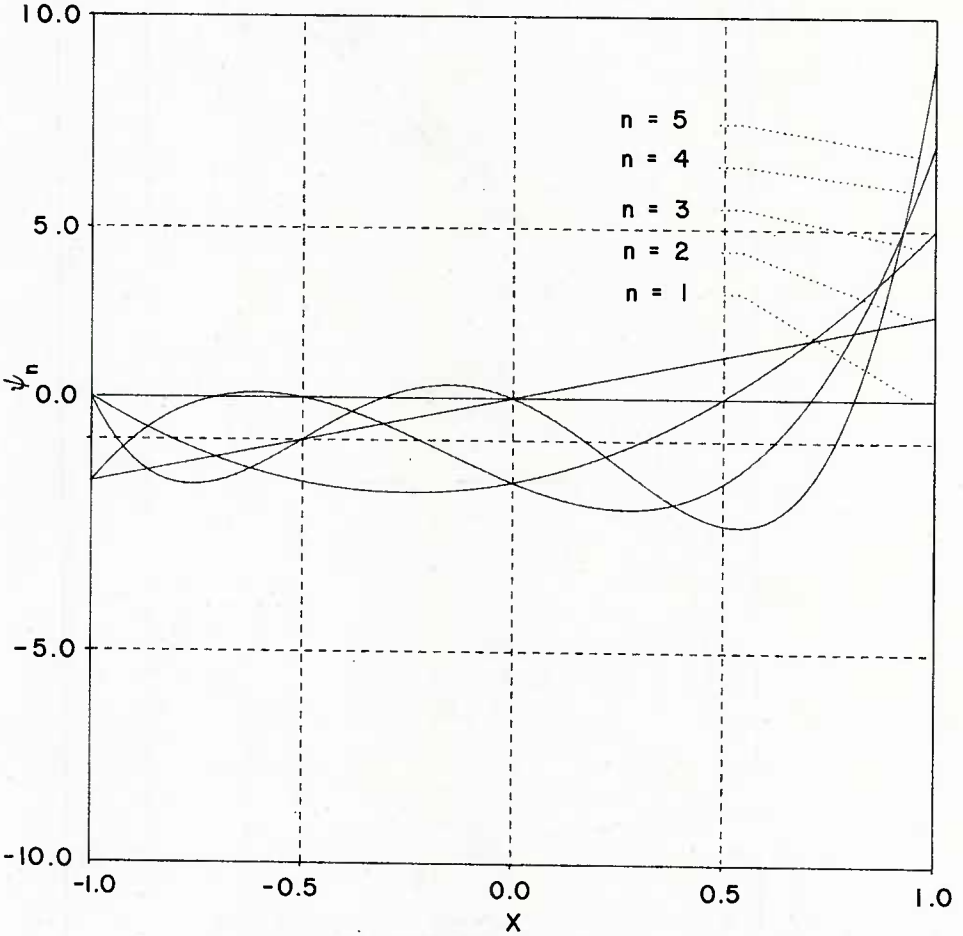

Fig. 7.4 Pressure polynomials

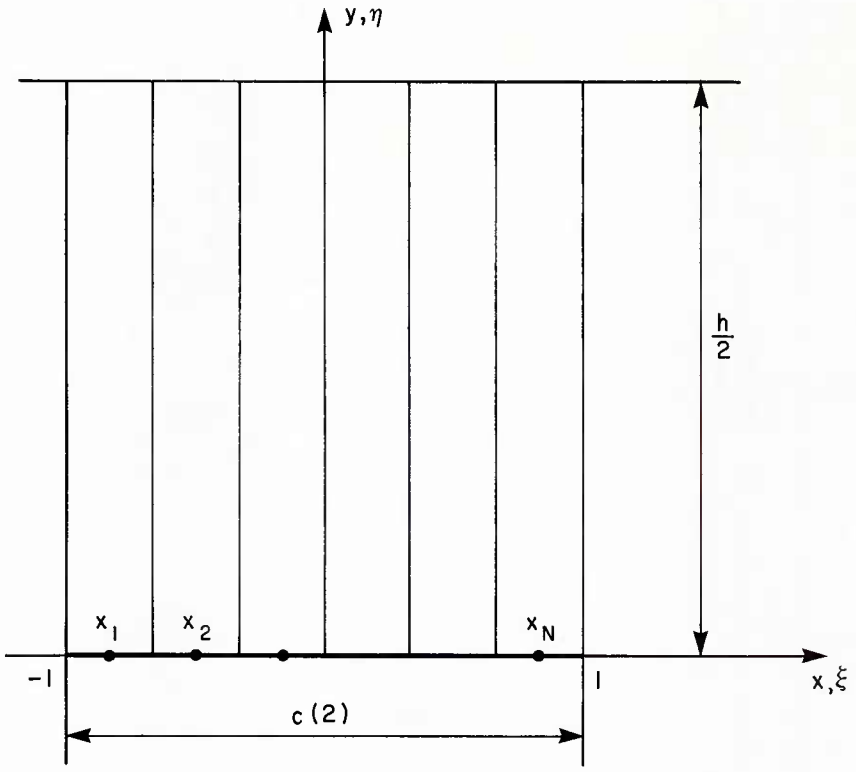

Fig. 7.5 Subdivision of flow region above the airfoil

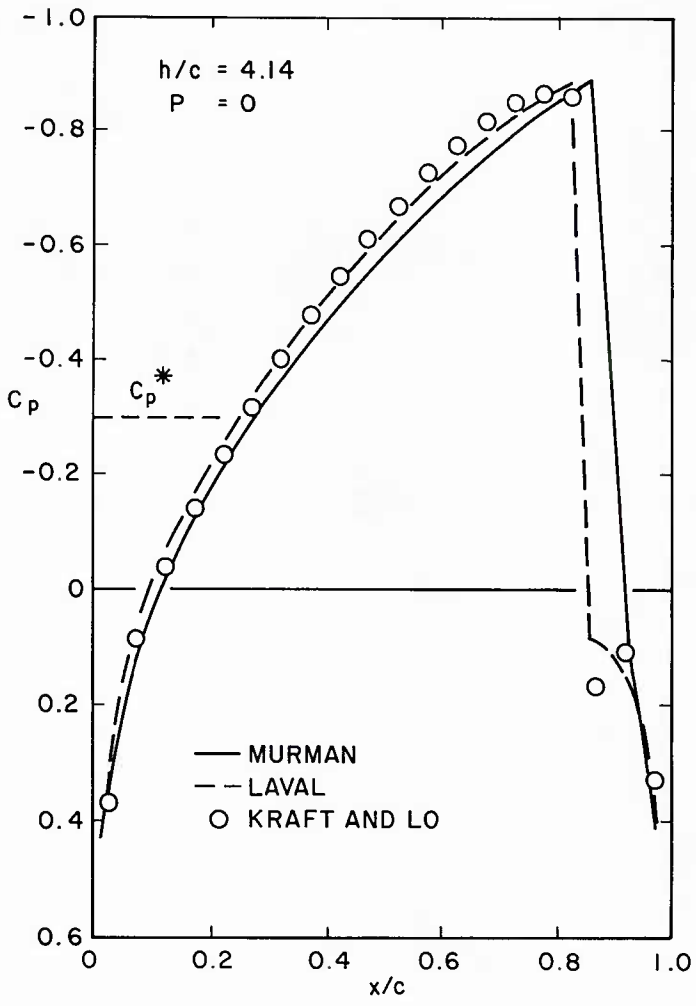

Fig. 7.6 Theoretical pressure on an 8.4% biconvex airfoil between closed walls, $M_\infty = 0.850$ (adapted from Ref. [7.29])

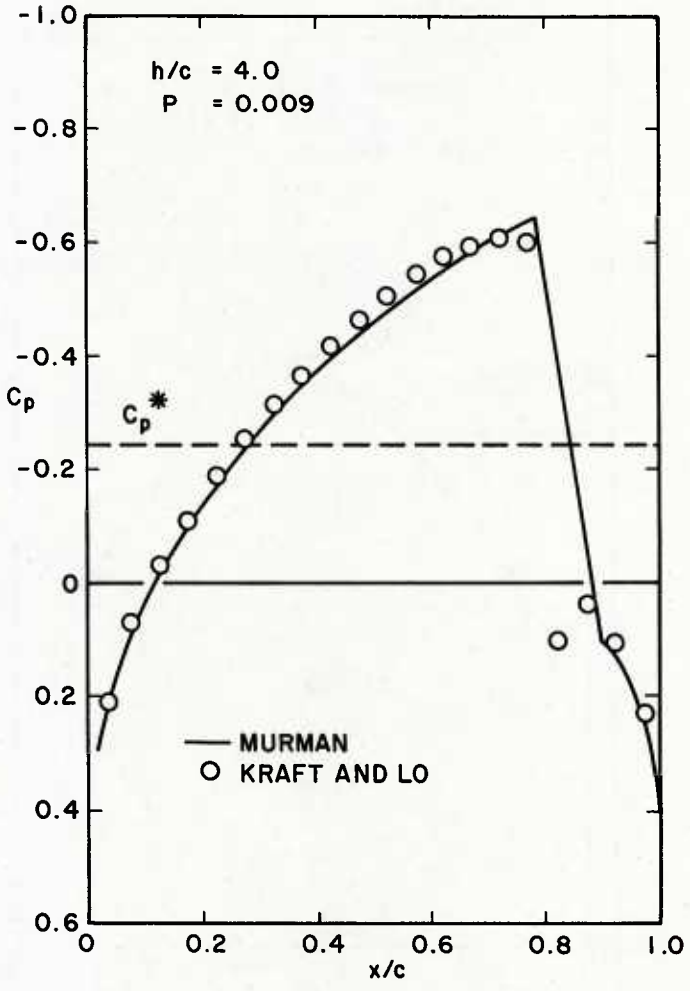

Fig. 7.7 Theoretical pressure on a 6% biconvex airfoil between porous walls, $M_\infty = 0.875$ (adapted from Ref. [7.29])

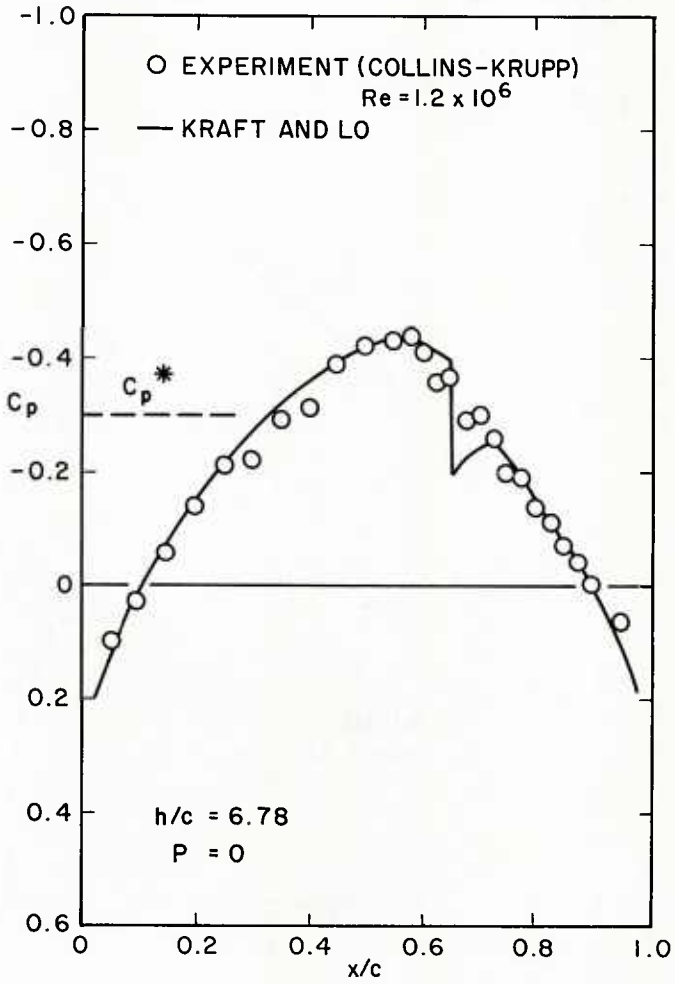

Fig. 7.8 Experimental and theoretical pressure on a 6% biconvex airfoil in a closed wall wind tunnel, $M_\infty = 0.857$ (adapted from Ref. [7.29])

8.0 UNSTEADY WALL INTERFERENCE

8.1 Governing Equations

The small disturbance equation appropriate to unsteady subsonic and supersonic flows is

$$\left(1 - M_\infty^2\right) \frac{\partial^2 \phi^t}{\partial x^2} + \frac{\partial^2 \phi^t}{\partial y^2} - 2\frac{M_\infty^2}{U_\infty} \frac{\partial^2 \phi^t}{\partial x \partial t} - \frac{M_\infty^2}{U_\infty^2} \frac{\partial^2 \phi^t}{\partial t^2} = 0 \tag{8.1}$$

It describes propagation of waves in a wind tunnel with a free stream velocity U_∞ in the x direction. By the superscript t we indicate that $\phi^t = \phi^t(x,y,t)$ is the time-dependent disturbance velocity potential. When the stream Mach number M_∞ is close to unity, we have to use [8.1]

$$\left[1 - M_\infty^2 - \frac{M_\infty^2}{U_\infty}(\kappa + 1) \frac{\partial \phi^t}{\partial x}\right] \frac{\partial^2 \phi^t}{\partial x^2} + \frac{\partial^2 \phi^t}{\partial y^2} - 2\frac{M_\infty^2}{U_\infty} \frac{\partial^2 \phi^t}{\partial x \partial t} - \frac{M_\infty^2}{U_\infty^2} \frac{\partial^2 \phi^t}{\partial t^2} = 0 \tag{8.2}$$

where we recognize the nonlinear term, present in the steady transonic equation. For flow over a harmonically oscillating airfoil, we set

$$\phi^t = \phi(x,y)\, e^{i\omega t} \,. \tag{8.3}$$

where ϕ is the (complex) amplitude of ϕ^t and ω is the angular frequency. Accordingly, from Equation (8.1) we obtain

$$\left(1 - M_\infty^2\right) \frac{\partial^2 \phi}{\partial x^2} + \frac{\partial^2 \phi}{\partial y^2} - 2ik\, M_\infty^2 \frac{\partial \phi}{\partial x} + k^2 M_\infty^2\, \phi = 0 \tag{8.4}$$

which is elliptic for subsonic flows, $M_\infty < 1$, and hyperbolic for supersonic flows, $M_\infty > 1$. The parameter

$$k = \frac{\omega}{U_\infty} \tag{8.5}$$

is the reduced frequency. It is customary to make it nondimensional by normalizing all lengths by the airfoil semichord, cf. Figure 8.1.

By substituting Equation (8.3) in (8.2), we can similarly obtain the governing equation for the amplitude of the transonic potential. For highly oscillatory flows, characterized by the condition

$$k \gg |1 - M|$$

where M is the local Mach number, the nonlinear term can be neglected [8.2]. The resultant linear transonic equation

$$\frac{\partial^2 \phi}{\partial y^2} - 2ik\, M_\infty^2 \frac{\partial \phi}{\partial x} + k^2 M_\infty^2\, \phi = 0 \tag{8.6}$$

is of parabolic type.

The unsteady pressure coefficient can be expressed as

$$C_p^t(x,y,t) = -\frac{2}{U_\infty} \frac{d\phi^t}{dt}(x,y,t) \tag{8.7}$$

where

$$\frac{d}{dt} = \left(U_\infty \frac{\partial}{\partial x} + \frac{\partial}{\partial t}\right) \tag{8.8}$$

is the linearized total time derivative. Using

$$C_p^t = C_p(x,y)\, e^{i\omega t} \tag{8.9}$$

we obtain from Equation (8.7) the relation between the amplitudes of the pressure coefficient and the potential:

$$C_p(x,y) = -2\left(\frac{\partial}{\partial x} + ik\right) \phi(x,y) \tag{8.10}$$

Applying the operator $(\partial/\partial x + ik)$ to Equation (8.4), we find that C_p satisfies the same differential equation, namely

$$\left(1 - M_\infty^2\right) \frac{\partial^2 C_p}{\partial x^2} + \frac{\partial^2 C_p}{\partial y^2} - 2ik\, M_\infty^2 \frac{\partial C_p}{\partial x} + k^2 M_\infty^2\, C_p = 0 \tag{8.11}$$

Similarly, for linearized transonic flows we obtain from Equation (8.6)

$$\frac{\partial^2 C_p}{\partial y^2} - 2ik\, M_\infty^2 \frac{\partial C_p}{\partial x} + k^2 M_\infty^2\, C_p = 0 \tag{8.12}$$

In computing subsonic flows past airfoils it is more convenient to work with C_p, since pressure, unlike the potential, is not discontinuous across the (potential) wake. In supersonic flows this is not essential, since the regions downstream of the model have no influence on airfoil pressure distribution.

For flows governed by the linear homogeneous equation (8.1) it is possible, in free air, to separate the thickness and lifting problems. If the airfoil thickness distribution is independent of time, than only the lifting problem, associated with the time-dependent camber $f^t = f^t(x,t)$, is of relevance to the unsteady flow analysis [8.3]. For harmonic oscillations

$$f^t = f(x)\, e^{i\omega t} \tag{8.13}$$

where f is the deflection amplitude. The thin airfoil boundary condition

$$\frac{\partial \phi^t}{\partial y}(x,0,t) = \frac{1}{U_\infty} \frac{d}{dt} f^t(x,t) \tag{8.14}$$

becomes, using Equations (8.3), (8.8) and (8.13)

$$\frac{\partial \phi}{\partial y}(x,0) = \left(\frac{\partial}{\partial x} + ik\right) f(x) \tag{8.15}$$

In the wind tunnel case, the separation of the unsteady lifting problem and the steady thickness problem is permissible, if additional conditions are satisfied: (1) the airfoil is located midway between the walls and (2) the wind tunnel boundary condition is linear homogeneous. Throughout this Chapter it will also be assumed that the tunnel walls are rigid, i.e. their locations are independent of time.

For solid walls, the time-dependent boundary condition is

$$\frac{\partial \phi^t}{\partial y}\left(x, \pm\frac{h}{2}, t\right) = 0$$

Substituting Equation (8.3), we obtain in terms of the potential amplitude

$$\frac{\partial \phi}{\partial y}\left(x, \pm\frac{h}{2}\right) = 0 \tag{8.16}$$

or from Equation (8.10) in terms of the pressure amplitude

$$\frac{\partial C_p}{\partial y}\left(x, \pm\frac{h}{2}\right) = 0 \tag{8.17}$$

The slotted wall boundary condition

$$\frac{d}{dt}\left[\phi^t\left(x, \pm\frac{h}{2}, t\right) \pm K \frac{\partial \phi^t}{\partial y}\left(x, \pm\frac{h}{2}, t\right)\right] = 0$$

takes similarly the form

$$\phi\left(x, \pm\frac{h}{2}\right) \pm K \frac{\partial \phi}{\partial y}\left(x, \pm\frac{h}{2}\right) = 0 \tag{8.18}$$

or

$$C_p\left(x, \pm\frac{h}{2}\right) \pm K \frac{\partial C_p}{\partial y}\left(x, \pm\frac{h}{2}\right) = 0 \tag{8.19}$$

The porous wall boundary condition for harmonically oscillating flows, as we have already observed in Chapter 2, is

$$\left(\frac{\partial}{\partial x} + ik\right) \phi \left(x, \pm\frac{h}{2}\right) \pm Z \frac{\partial \phi}{\partial y}\left(x, \pm\frac{h}{2}\right) = 0 \tag{8.20}$$

or

$$\left(\frac{\partial}{\partial x} + ik\right) C_p \left(x, \pm\frac{h}{2}\right) \pm Z \frac{\partial C_p}{\partial y}\left(x, \pm\frac{h}{2}\right) = 0 \tag{8.21}$$

The complex quantity

$$Z = R + iS \tag{8.22}$$

is the wall impedance, $R = 1/P$ is the resistance and S is the reactance.

8.2 Tunnel Resonance

The phenomenon of transverse acoustic resonance between an oscillating airfoil and wind tunnel walls was discovered analytically by Runyan and Watkins [8.4], confirmed by W.P. Jones [8.5] and verified experimentally by Runyan et al [8.6].

Tunnel resonance does not exist in incompressible flow since the velocity of propagation of a disturbance is infinite. In a compressible fluid, however, a definite time is required for a signal to reach a distant field point and phase lag enters the picture. The resonance takes place if the oscillation frequency is such that the disturbances emanating from the airfoil and those reflected by the walls form a standing wave pattern. In that case, at the position of the oscillating airfoil the normal velocity has a maximum amplitude and the pressure coefficient has a node, i.e. is of zero amplitude:

$$C_p(x,0) = 0 \qquad -\infty < x < \infty \tag{8.23}$$

Accordingly, the theoretical airloads will vanish at resonance. This certainly is the most severe case of wall interference, we have encountered so far. Fortunately, pure resonance is in practice unobtainable because of the presence of damping factors such as the viscosity, wave scattering at the walls, finite length of the test section walls, etc. A typical example is shown in Figure 8.2, which contains experimental and theoretical data obtained in a solid wall test section [8.6]. The lift and pitching moment amplitudes show pronounced dips near the (first) resonant frequency, but do not vanish entirely. Similarly, the phase angle changes are less abrupt than predicted by theory. Nevertheless, these effects are still very pronounced and tunnel testing near resonant conditions should be avoided.

For the solid and open jet boundaries the resonant frequencies can be deduced from wavefront model shown in Figure 8.3. Since the standing wave pattern (formed by emitted and reflected waves) can take place only if the disturbances propagate in the direction normal to the walls, the angle of incidence θ must satisfy

$$\sin\theta = M_\infty \tag{8.24}$$

Denoting by a the velocity of sound, the velocity of propagation of the pressure disturbance in the direction normal to the wall is $\sqrt{a^2 - U_\infty^2}$ and the time needed for it to travel from the tunnel centre line to the wall and back is

$$t = \frac{h}{\sqrt{a^2 - U_\infty^2}} = \frac{h}{\beta a} \qquad \text{where} \qquad \beta = \sqrt{1 - M_\infty^2} \tag{8.25}$$

The resonant frequencies are then obtained from the condition that the emitted and the reflected waves meet on the tunnel axis in opposite phases.

For solid walls, that do not change the phase of the wave on reflection, we obtain

$$\omega_n t = (2n-1)\pi, \qquad n = 1, 2, \ldots$$

that is

$$k_n = \frac{\omega_n}{U_\infty} = (2n-1)\pi \frac{\beta}{M_\infty}\frac{1}{h}, \qquad n = 1, 2, \ldots \tag{8.26}$$

Equation (8.26) is the well known result obtained by Runyan and Watkins [8.4] and Jones [8.5].

For open jet boundaries the phase change on reflection is π, so that

$$k_n = \frac{\omega_n}{U_\infty} = 2n\pi \frac{\beta}{M_\infty}\frac{1}{h}, \qquad n = 1, 2, \ldots \tag{8.27}$$

For ventilated walls, the phase change is more difficult to assess. As pointed out by Acum [8.7], the resonant frequencies can be determined in a simple way from the free vibration model; the theoretical background of this method can be found, for example, in Landau and Lifshitz [8.8].

Separating in Equation (8.11) the variables as

$$C_p(x,y) = Y(y)\, e^{isx} \tag{8.28}$$

we obtain for the function Y the ordinary differential equation

$$Y'' + \lambda^2 Y = 0 \tag{8.29}$$

where

$$\lambda^2 = -\beta^2 s^2 + 2M_\infty^2 sk + M_\infty^2 k^2 \tag{8.30}$$

For the homogeneous boundary conditions at $-h/2$ and $h/2$, Equation (8.29) has only a trivial solution $Y = 0$, unless

$$\lambda = \lambda_n, \qquad n = 1, 2, \ldots$$

is one of the eigenvalues of the problem.

Condition (8.23) of zero pressure amplitude on the tunnel axis yields

$$Y = 0, \qquad y = 0 \tag{8.31}$$

and we find that the eigenfunction satisfying Equations (8.29) and (8.31) is

$$Y = \sin \lambda y \tag{8.32}$$

Clearly, the formal separation of variables, Equation (8.28), represents the decomposition of the unsteady pressure field into plane waves, the quantities s and λ playing the role of the wave numbers in the x and y directions. From Figure 8.3

$$\frac{s}{\lambda} = \tan \theta$$

so that for the resonant slope, Equation (8.24)

$$s_n = \frac{M_\infty}{\beta} \lambda_n \tag{8.33}$$

Finally, substituting in Equation (8.30) and taking the positive root

$$k_n = \frac{\beta \lambda_n}{M_\infty} \tag{8.34}$$

which is Acum's relationship [8.7] between resonant frequencies and tunnel eigenvalues.

In the limit $M_\infty \to 0$ we have $k_n \to \infty$, which confirms that resonance cannot occur in incompressible flow. As M_∞ increases, resonance gradually afflicts lower and lower frequencies. Thus, acoustic resonance between the airfoil and the tunnel becomes an important phenomenon at high subsonic speeds because it occurs at relatively low values of the reduced frequency. However, no conclusion should be drawn from the very limit $k_n \to 0$ as $M_\infty \to 1$ since, clearly, Equation (8.1) is not applicable to near-sonic velocities.

The problem of determining the resonant frequency is thus reduced to finding the eigenvalues λ_n for the tunnel section. For slotted walls, substituting Equation (8.28) in (8.19), we obtain

$$Y + KY' = 0, \qquad y = \frac{h}{2} \tag{8.35}$$

Inserting Equation (8.32), we find that the eigenvalues λ_n are the roots of the transcendental equation

$$\left(\lambda_n \frac{h}{2}\right) F + \tan\left(\lambda_n \frac{h}{2}\right) = 0 \tag{8.36}$$

where

$$F = \frac{2K}{h} \tag{8.37}$$

is the nondimensional slot parameter. The points $x_n = \lambda_n h/2$ are depicted in Figure 8.4 as the projections onto the axis of the intersections of a straight line $y = -Fx$ with branches of the $y = \tan x$ function.

In the limiting cases of solid and open jet walls respectively,

$$F \to \infty \quad , \quad \lambda_n \frac{h}{2} \to \left(n - \frac{1}{2}\right)\pi$$

$$F \to 0 \quad , \quad \lambda_n \frac{h}{2} \to n\pi$$

Substituting in Equation (8.34), we arrive at the resonance frequencies (8.26) and (8.27).

For positive values of F the eigenvalues satisfy the inequalities

$$\left(n - \frac{1}{2}\right)\pi \leqslant \lambda_n \frac{h}{2} < n\pi \tag{8.38}$$

and hence are well separated. They can be calculated by the following iterative procedure: if λ_n^j, satisfying the above inequality, represents an approximation to λ_n, then

$$\lambda_n^{j+1} = \frac{2}{h}\left[n\pi - \operatorname{atan}\left(K\lambda_n^j\right)\right] \tag{8.39}$$

is a better approximation. The graphical interpretation for $n = 1$ and $j = 0$ is shown in Figure 8.5; a proof of the (geometric) convergence was given by Fromme and Golberg [8.9]. Although Newton's method can be shown to converge slightly faster for large λ_n, it requires the evaluation of two functions at each iteration, so that the formula (8.39) will generally be more convenient [8.10].

An example of calculated resonant frequencies for $M_\infty = \sqrt{3}/2$, $h = 20$, and three values of the slot parameter, $K = \infty$, 1, and 0 (K in same length units as h) is given in the following Table.

	K = ∞ (closed)	K = 1 (slotted)	K = 0 (open)
k_1	0.090690	0.165282	0.181380
k_2	0.272070	0.332586	0.362760
k_3	0.453450	0.502774	0.544133
k_4	0.634829	0.675654	0.725519
k_5	0.816209	0.850637	0.906899

As expected from inequality (8.38), the resonant frequencies for typical slotted walls ($K = 1$) lie between those for solid ($K = \infty$) and open jet ($K = 0$). The disappearance of aerodynamic loads at the resonant frequencies can be demonstrated on the absolute value of the lift coefficient amplitude, $|C_L|$, computed by Fromme and Golberg [8.9] for a flat plate undergoing a harmonic pitching motion between tunnel walls, see Figure 8.6. To show that resonance cannot occur in incompressible flow, the case $M_\infty = 0$ is also presented. Whereas the behaviour of $|C_L|$ vs. reduced frequency is smooth for $M_\infty = 0$ with the three curves for $K = \infty$, 1, and 0 merging as the frequency increases, the behaviour of $|C_L|$ for $M_\infty = \sqrt{3}/2$ is strikingly different. The closed wall solution begins with a relatively large value of $|C_L|$ at $k = 0$ and drops to zero at the first resonant frequency, $k_1 = 0.090690$. Then it increases to a maximum value of about 60% of its zero frequency value, drops again to zero at the second resonant frequency, $k_2 = 0.272070$, and so on. In accordance with the predictions in the above Table, a similar behaviour is evidenced for the ventilated wall conditions. The corresponding phase angles are shown in Figure 8.7. We observe 90° phase spikes at the resonant frequencies. The inconspicuous phase variations for the incompressible flow case indicate again the absence of resonance.

Acum's method fails to produce resonant frequencies for porous walls, if the boundary condition (8.21) is adopted in its resistance form, that is with

$$Z = R = \frac{1}{P}$$

In spite of some contradicting experimental evidence, it was for some time believed that porous walls are not subject to resonance. The dilemma was resolved by Mabey [8.11], who showed that resonance can be obtained if the porous wall is represented by the reactance boundary condition, i.e. taking

$$Z = iS \tag{8.40}$$

Inserting Equations (8.28) and (8.40) in (8.21), we obtain

$$(s+k)\,Y + SY' = 0 \quad , \quad y = \frac{h}{2} \tag{8.41}$$

The substitution from Equations (8.32), (8.33) and (8.34) yields

$$\tan\left(\lambda_n \frac{h}{2}\right) + S\beta M_\infty = 0 \tag{8.42}$$

Accordingly, for porous walls the eigenvalues are obtained explicitly as

$$\lambda_n = \frac{2}{h}\,[\operatorname{atan}(-S\beta M_\infty) + n\pi] \tag{8.43}$$

In the limiting cases of solid and open jet walls

$$S \to \infty\,, \qquad \lambda_n \frac{h}{2} \to \left(n - \frac{1}{2}\right)\pi$$

$$S \to 0\,, \qquad \lambda_n \frac{h}{2} \to n\pi$$

from which, as before, Equations (8.26) and (8.27) are obtained. For porous wall, the eigenvalues are again expected to lie on the interval, given by inequality (8.38).

Experiments with actual tunnel test sections indicate that the transmission of waves through ventilated walls is another factor affecting transverse resonance. Methods for prediction of resonant frequencies based on the acoustic interaction of the moving tunnel air and stagnant plenum air have recently been proposed by Mabey [8.11], [8.12] and Barger [8.13]. Without going into details, we mention that there are two distinct subsonic regimes of the resonant wavefront propagation. Since along the interface of the tunnel stream and plenum air the waves must have the same phase velocities, Figure 8.8, the following relationship holds for the angle of incidence θ and the angle of refraction $\bar{\theta}$:

$$\frac{a}{\sin\theta} - U_\infty = \frac{a_{plenum}}{\sin\bar{\theta}}$$

If the speed of sound in the plenum is equal to that in the test section, $a_{plenum} = a$, we obtain

$$\sin\bar{\theta} = \frac{\sin\theta}{1 - M_\infty \sin\theta} \tag{8.44}$$

where $\bar{\theta} < \pi/2$, that is

$$\sin\theta < \frac{1}{1 + M_\infty} \tag{8.45}$$

must hold. The substitution of the resonant angle, Equation (8.24), yields Mabey's condition [8.11]

$$M_\infty < (\sqrt{5} - 1)/2 \simeq 0.618 \tag{8.46}$$

If $M_\infty > 0.618$, total reflection of the resonant waves takes place. But even then, the wall does not behave entirely like a solid one: the phase change on reflection still takes place and the waves satisfying Equation (8.45) continue to refract, however none of them has the resonance slope.

8.3 Bland's Method for Unsteady Subsonic Interference

The problem of slotted wall interference on oscillating airfoils at subsonic speeds has been solved by Bland [8.15], [8.16] and extended to the porous wall case by Fromme and Golberg [8.17], [8.18].

The pressure boundary condition for the (upper) airfoil surface can be written as

$$C_p(x) = -\gamma(x) \tag{8.47}$$

The vorticity amplitude γ is actually unknown here, but the solution for C_p will be used to provide an integral equation relating the pressure amplitude and the upwash amplitude

$$v(x) = \frac{\partial \phi}{\partial y}(x,0) = \left(\frac{\partial}{\partial x} + ik\right) f(x) \tag{8.48}$$

which is known from the prescribed deflection amplitude f. Since the pressure is continuous elsewhere and antisymmetric with respect to the x axis

$$C_p(x) = 0, \qquad -1 > x \geqslant 1 \tag{8.49}$$

The condition $C_p(1) = 0$ is the Kutta-Joukowski condition for unsteady flow.

Correspondingly, the boundary value problem to be solved for the slotted wall case is

$$\frac{\partial^2 C_p}{\partial x^2}(x,y) + \frac{\partial^2 C_p}{\partial y^2}(x,y) - M_\infty^2 \left(\frac{\partial}{\partial x} + ik\right)^2 C_p(x,y) = 0, \qquad -\infty < x < \infty, \qquad 0 < y < \frac{h}{2} \tag{8.50}$$

$$C_p\left(x, \frac{h}{2}\right) + K \frac{\partial C_p}{\partial y}\left(x, \frac{h}{2}\right) = 0, \qquad -\infty < x < \infty \tag{8.51}$$

$$C_p(x,0) = \begin{cases} -\gamma(x), & -1 < x < 1 \\ 0, & -1 > x \geqslant 1 \end{cases} \tag{8.52}$$

Employing the streamwise Fourier transform

$$\hat{C}_p(s,y) = \frac{1}{\sqrt{2\pi}} \int_{-\infty}^{\infty} e^{-isx} C_p(x,y)\, dx$$

the above problem is reduced to the two-point boundary value problem

$$\frac{\partial^2 \hat{C}_p}{\partial y^2}(s,y) - \nu^2 \hat{C}_p(s,y) = 0, \qquad 0 < y < \frac{h}{2}$$

$$\hat{C}_p\left(s, \frac{h}{2}\right) + K \frac{\partial^2 \hat{C}_p}{\partial y}\left(s, \frac{h}{2}\right) = 0$$

$$\hat{C}_p(s,0) = -\frac{1}{\sqrt{2\pi}} \int_{-1}^{1} e^{-isx} \gamma(x)\, dx$$

where

$$\nu^2 = \beta^2 s^2 - 2M_\infty^2 sk - M_\infty^2 k^2 = -\lambda^2 \tag{8.53}$$

cf. Equation (8.30). The solution is

$$\hat{C}_p(s,y) = -\frac{1}{\sqrt{2\pi}} \frac{K\nu \cosh\left[\nu\left(\frac{h}{2} - y\right)\right] + \sinh\left[\nu\left(\frac{h}{2} - y\right)\right]}{K\nu \cosh\left(\nu \frac{h}{2}\right) + \sinh\left(\nu \frac{h}{2}\right)} \int_{-1}^{1} e^{-is\xi} \gamma(\xi)\, d\xi$$

Subjecting Equation (8.10) to the Fourier transform, we obtain

$$\hat{C}_p(s,y) = -2i(s+k)\, \hat{\phi}(s,y)$$

so that, with the help of the inverse transform,

$$v(x) = \frac{\partial \phi}{\partial y}(x,0) = \frac{\partial}{\partial y}\left[\frac{1}{\sqrt{2\pi}} \int_{-\infty}^{\infty} e^{isx}\, \hat{\phi}(s,0)\, ds\right]$$

$$= \frac{1}{\sqrt{2\pi}} \int_{-\infty}^{\infty} e^{isx}\, \frac{i}{2(s+k)}\, \frac{\partial \hat{C}_p}{\partial y}(s,0)\, ds$$

Accordingly, the equation for the upwash can be restated as

$$v(x) = -\frac{\beta}{2\pi} \int_{-1}^{1} K(x-\xi)\, \gamma(\xi)\, d\xi \tag{8.54}$$

where the kernel function (not to be confused with the slot parameter K) is given by

$$K(x-\xi) = -\frac{1}{\beta} \int_{-\infty}^{\infty} e^{is(x-\xi)}\, \frac{i\nu}{2(s+k)}\, \frac{K\nu \sinh\left(\nu\frac{h}{2}\right) + \cosh\left(\nu\frac{h}{2}\right)}{K\nu \cosh\left(\nu\frac{h}{2}\right) + \sinh\left(\nu\frac{h}{2}\right)}\, ds \tag{8.55}$$

The integrand is indeterminate for $\nu = i\lambda_n$, where λ_n are the eigenvalues satisfying Equation (8.36). From Equation (8.54) we readily verify that this is compatible with the resonance condition: considering the upwash to be definite, the vorticity (and hence loading) must vanish as $K(x-\xi) \to \infty$.

For the porous walls at low frequencies, the boundary condition (8.51) is replaced by

$$\left(\frac{\partial}{\partial x} + ik\right) C_p\left(x, \frac{h}{2}\right) + \frac{1}{P}\, \frac{\partial C_p}{\partial y}\left(x, \frac{h}{2}\right) = 0, \qquad -\infty < x < \infty \tag{8.56}$$

Going through the same procedure as before, the transform of the pressure amplitude is found to be [8.19]

$$\hat{C}_p(s,y) = -\frac{1}{\sqrt{2\pi}}\, \frac{\nu \cosh\left[\nu\left(\frac{h}{2} - y\right)\right] + iP(s+k) \sinh\left[\nu\left(\frac{h}{2} - y\right)\right]}{\nu \cosh\left(\nu\frac{h}{2}\right) + iP(s+k) \sinh\left(\nu\frac{h}{2}\right)} \int_{-1}^{1} e^{-is\xi}\, \gamma(\xi)\, d\xi$$

and the kernel function, to be substituted in Equation (8.54)

$$K(x-\xi) = -\frac{1}{\beta} \int_{-\infty}^{\infty} e^{is(x-\xi)}\, \frac{i\nu}{2(s+k)}\, \frac{\nu \sinh\left(\nu\frac{h}{2}\right) + iP(s+k) \cosh\left(\nu\frac{h}{2}\right)}{\nu \cosh\left(\nu\frac{h}{2}\right) + iP(s+k) \sinh\left(\nu\frac{h}{2}\right)}\, ds \tag{8.57}$$

see Reference [8.17]. Examination of the denominator shows that it is nonzero if the porosity parameter P is real, which is indicative of the fact that resonance cannot occur. However, the situation changes if Equation (8.56) is replaced by the high frequency condition, i.e. if i/S is substituted for P.

For a numerical solution of the integral equation (8.54) the singularities contained in the kernel functions need to be explicitly displayed. Unfortunately, the evaluation of the inverse Fourier transforms (8.55) and (8.57) is not an easy task. Using the method of residues and a rather arbitrary extraction of singularities, Bland [8.15] evaluated the slotted wall kernel (8.55) as

$$K(x-\xi) = \frac{1}{x-\xi} - \frac{ik}{\beta^2}\log|x-\xi|$$

$$+ \frac{\pi}{2\beta}k\left[1+\text{sign}(x-\xi)\right]e^{-ik(x-\xi)}\frac{1+Kk\tanh\left(k\frac{h}{2}\right)}{Kk+\tanh\left(k\frac{h}{2}\right)}$$

$$- \frac{\pi}{\beta}\left[\frac{2}{h}\text{sign}(x-\xi)\,S'\left(\frac{|x-\xi|}{\beta h}\right) - \frac{2ik}{\beta}S\left(\frac{|x-\xi|}{\beta h}\right)\right]e^{iM_\infty^2 k\frac{x-\xi}{\beta^2}}$$

$$+ \frac{\pi}{\beta h}\left\{\left[\frac{1}{\sinh\left(\pi\frac{x-\xi}{\beta h}\right)} - \frac{1}{\pi\frac{x-\xi}{\beta h}}\right] + \frac{e^{iM_\infty^2 k\frac{x-\xi}{\beta^2}}-1}{\sinh\left(\pi\frac{x-\xi}{\beta h}\right)}\right\}$$

$$- \frac{ik}{\beta^2}\left\{\log\left[\frac{1}{x-\xi}\tanh\left(\pi\frac{x-\xi}{2\beta h}\right)\right] + \left(e^{iM_\infty^2 k\frac{x-\xi}{\beta^2}}-1\right)\log\left[\tanh\left(\frac{\pi|x-\xi|}{2\beta h}\right)\right]\right\} \tag{8.58}$$

where S is given by the infinite series

$$S\left(\frac{|x-\xi|}{\beta h}\right) = \sum_{n=1}^{\infty}\left\{\frac{1}{\left[1+\frac{\frac{2}{h}K}{1+(K\lambda_n)^2}\right]\left[1+\left(\frac{k}{\lambda_n}\right)^2\right]}\,\frac{\exp\left[-h\lambda_n\sqrt{1-\left(\frac{M_\infty k}{\beta\lambda_n}\right)^2}\,\frac{|x-\xi|}{\beta h}\right]}{h\lambda_n\sqrt{1-\left(\frac{M_\infty k}{\beta\lambda_n}\right)^2}} - \frac{\exp\left[-(2n-1)\,\pi\frac{|x-\xi|}{\beta h}\right]}{(2n-1)\,\pi}\right\} \tag{8.59}$$

and

$$S'\left(\frac{|x-\xi|}{\beta h}\right) = \frac{dS\left(\frac{|x-\xi|}{\beta h}\right)}{d\,\frac{|x-\xi|}{\beta h}} \tag{8.60}$$

As mentioned earlier, λ_n are the roots of the transcendental equation (8.36) on the interval (8.38). The series (8.59) and (8.60) converge at $x = \xi$; however they fail to converge if

$$1-\left(\frac{M_\infty k}{\beta\lambda_n}\right)^2 = 0$$

This corresponds to Acum's resonance condition (8.34). In all that follows we assume that we are not at a resonance point.

Evidently, Equation (8.58) represents the decomposition of the kernel

$$K(x-\xi) = K_C(x-\xi) + K_L(x-\xi) + K_B(x-\xi) \tag{8.61}$$

where

$$K_C(x-\xi) = \frac{1}{x-\xi} \tag{8.62}$$

is the Cauchy kernel,

$$K_L(x-\xi) = -\frac{ik}{\beta^2}\log|x-\xi| \tag{8.63}$$

is the logarithmic kernel, and $K_B(x-\xi)$ is the remaining, bounded part of (8.58). It is clear that the wind tunnel effect must be absorbed by K_B. In contrast to Equation (8.58), the evaluation of the unsteady porous wall kernel from Equation (8.57) remains an open problem, awaiting future research [8.18].

Special cases of the kernel are:

1. Steady Flow, Slotted Walls

Substituting $k = 0$ in Equation (8.58), we readily obtain

$$K(x-\xi) = \frac{1}{x-\xi} - \frac{2\pi}{\beta h}\,\mathrm{sign}(x-\xi)\,S'\left(\frac{|x-\xi|}{\beta h}\right) + \frac{\pi}{\beta h}\left[\frac{1}{\sinh\left(\pi\frac{x-\xi}{\beta h}\right)} - \frac{1}{\pi\frac{x-\xi}{\beta h}}\right] \tag{8.64}$$

For solid walls, $1/K = 0$, the eigenvalues satisfy

$$\lambda_n \frac{h}{2} = \left(n-\frac{1}{2}\right)\pi$$

and as a result

$$S'\left(\frac{|x-\xi|}{\beta h}\right) = 0$$

Consequently

$$K(x-\xi) = \frac{\pi}{\beta h}\,\frac{1}{\sinh\left(\pi\frac{x-\xi}{\beta h}\right)}$$

in accordance with Equation (7.73).

2. Steady Flow, Porous Walls

Substituting $k = 0$ in Equation (8.53), it follows

$$\nu = \beta s$$

Inserting it together with the factor

$$\tau = \frac{2}{\pi}\,\mathrm{atan}\frac{P}{\beta}, \qquad 0 \leqslant \tau \leqslant 1$$

in Equation (8.57), we obtain

$$K(x-\xi) = -\frac{i}{2}\int_{-\infty}^{\infty} e^{is(x-\xi)}\tanh\left(\beta\frac{h}{2}s + i\frac{\pi}{2}\tau\right)ds$$

which does not exist as an ordinary (Lebesgue or Riemann) integral; instead it must be regarded as a distribution [8.17]. Only under this condition does it reduce in the limit $h \to \infty$ to the Cauchy kernel

$$K_C(x-\xi) = -\frac{i}{2}\int_{-\infty}^{\infty} e^{is(x-\xi)}\,\mathrm{sign}(s)\,ds = \frac{1}{x-\xi}$$

In contrast, the wall interference part

$$K_W(x-\xi) = K(x-\xi) - K_C(x-\xi)$$

exists as the Cauchy principal value of an ordinary integral. It can be shown [8.17] that the complete kernel is

$$K(x-\xi) = \frac{\pi}{\beta h} \frac{e^{\pi\tau \frac{x-\xi}{\beta h}}}{\sinh\left(\pi \frac{x-\xi}{\beta h}\right)} \tag{8.65}$$

in accordance with Equation (7.72). This example is indicative of difficulties which may be encountered in utilizing the general, porous wall kernel in its integral form (8.57).

3. Unsteady Flow, Free Air

The kernel covering this situation is that by Possio [8.20], [8.3], [8.21]:

$$K_F(x-\xi) = -\frac{\pi k}{2\beta^2} e^{-ik(x-\xi)} \left\{ e^{i\frac{k(x-\xi)}{\beta^2}} \left[iM_\infty \operatorname{sign}(x-\xi) H_1^{(2)}\left(\frac{M_\infty k|x-\xi|}{\beta^2}\right) - H_0^{(2)}\left(\frac{M_\infty k|x-\xi|}{\beta^2}\right)\right] \right.$$

$$\left. + \frac{2i\beta}{\pi} \log\left(\frac{1+\beta}{M_\infty}\right) + ik \int_0^{x-\xi} e^{\frac{ik\chi}{\beta^2}} H_0^{(2)}\left(\frac{M_\infty k|\chi|}{\beta^2}\right) d\chi \right\} \tag{8.66}$$

where

$$H_\ell^{(2)} = J_\ell - iY_\ell$$

denote the Hankel functions of the second kind of order ℓ. By the subscript F we indicate that Possio's kernel is a free air kernel. However, the limiting process $h \to \infty$ in which Equations (8.55) and (8.57) reduce to Equation (8.66) has yet to be demonstrated. In any case, Possio's kernel in the present form is not suitable for numerical computation. Its singularities are not explicitly displayed, it is indeterminate for $M_\infty = 0$ and it contains an integral with variable upper limit. Following an extensive analysis, Fromme and Golberg were able to reformulate it as

$$K_F(x-\xi) = \frac{1}{x-\xi} + K_1(x-\xi) \log|x-\xi| + K_2(x-\xi) \tag{8.67}$$

where

$$K_1(x-\xi) = -\frac{ik}{\beta^2} e^{-ik(x-\xi)} F_1(x-\xi) \tag{8.68}$$

$$K_2(x-\xi) = -e^{-ik(x-\xi)} F_2(x-\xi) \tag{8.69}$$

are analytic (differentiable) functions of the argument $x-\xi$. The detailed expressions for the functions F_1 and F_2 are rather lengthy and can be found in References [8.17] and [8.21].

From Equation (8.67) it can be inferred that for the wind tunnel case the kernel is of the form

$$K(x-\xi) = K_F(x-\xi) + K_W(x-\xi)$$

$$= \frac{1}{x-\xi} + K_1(x-\xi) \log|x-\xi| + K_2(x-\xi) + K_W(x-\xi) \tag{8.70}$$

where $K_W(x-\xi)$, representing the induced effect of the walls, is an analytic function.

For incompressible flow, $M_\infty \to 0$, the Possio kernel reduces to the Küssner-Schwarz kernel

$$K_F(x-\xi) = \frac{1}{x-\xi} - ik\, e^{-ik(x-\xi)} \left\{ \mathrm{Ci}\left[k|x-\xi|\right] + i\,\mathrm{Si}\left[k(x-\xi)\right] + \frac{i\pi}{2} \right\} \tag{8.71}$$

Bland [8.16] proved that also the slotted wall kernel (8.58) reduces to this expression, substituting $1/K = 0$ and $M_\infty = 0$, and taking the limit $h \to \infty$.

Representing the cosine and sine integrals by the expansions

$$\mathrm{Ci}(z) = \gamma + \log z + \sum_{n=1}^{\infty} \frac{(-1)^n z^{2n}}{(2n)(2n)!}$$

$$\mathrm{Si}(z) = \sum_{n=0}^{\infty} \frac{(-1)^n z^{2n+1}}{(2n+1)(2n+1)!}$$

where

$$\gamma = 0.577215\ldots$$

is Euler's constant, we obtain [8.17]

$$K(x-\xi) = \frac{1}{x-\xi} - ik\, e^{-ik(x-\xi)} \log|x-\xi| - ik\, e^{-ik(x-\xi)} \left[\log k + \gamma + \frac{i\pi}{2} + \sum_{n=1}^{\infty} \frac{[ik(x-\xi)]^n}{(n)(n)!} \right] \tag{8.72}$$

Clearly, this result fits much better the kernel decomposition according to Equation (8.70) than (8.61).

To enforce the Kutta-Joukowski condition (8.49), Bland introduces the pressure factor

$$\psi(x) = -\frac{\beta\gamma(x)}{2} \sqrt{\frac{1+x}{1-x}} \tag{8.73}$$

which transforms the integral equation (8.54) to

$$v(x) = \frac{1}{\pi} \int_{-1}^{1} \sqrt{\frac{1-\xi}{1+\xi}}\, K(x-\xi)\, \psi(\xi)\, d\xi \tag{8.74}$$

In his collocation method the pressure factor is expanded in pressure polynomials, Equation (7.61), and the integral equation (8.74) is reduced to a system of linear algebraic equations

$$\sum_{n=1}^{N} A_{mn}^{N} a_n^{N} = c_m^{N} \quad , \qquad m = 1, \ldots, N \tag{8.75}$$

where

$$c_m^{N} = v\left(x_m^{N+1}\right) \tag{8.76}$$

and

$$A_{mn}^{N} = \frac{1}{\pi} \int_{-1}^{1} \sqrt{\frac{1-\xi}{1+\xi}}\, K\left(x_m^{N+1} - \xi\right)\, \psi_n(\xi)\, d\xi \tag{8.77}$$

As collocation points x_m^{N+1} selected are the N zeros of the upwash polynomial v_{N+1}, Equation (7.67). Following Equation (8.61), the collocation matrix (8.77) is split as

$$A_{mn}^{N} = C_{mn}^{N} + L_{mn}^{N} + B_{mn}^{N} \tag{8.78}$$

where, according to Equations (7.79) and (7.81)

$$C_{mn}^{N} = v_n\left(x_m^{N+1}\right) \tag{8.79}$$

$$B_{mn}^{N} = \frac{2}{2N+1} \sum_{j=1}^{N} \left(1-\xi_j^{N+1}\right) K_B\left(x_m^{N+1}-\xi_j^{N+1}\right) \psi_n\left(\xi_j^{N+1}\right) \tag{8.80}$$

The quadrature points ξ_j^{N+1} are obtained from Equation (7.82). The contribution of the logarithmic kernel, which does not occur in steady flow, is evaluated in closed form using the auxiliary integral [8.15]

$$\frac{1}{\pi} \int_{-1}^{1} \sqrt{\frac{1-\xi}{1+\xi}} \log|x-\xi| \, \psi_n(\xi) \, d\xi = \begin{cases} \frac{1}{2} v_{n+1}(x) + \left(\frac{1}{2} - \log 2\right) v_n(x) , & n = 1 \\ \frac{v_{n+1}(x)}{2n} - \frac{v_n(x)}{2n(n-1)} - \frac{v_{n-1}(x)}{2(n-1)} , & n \geqslant 2 \end{cases}$$

Accordingly

$$L_{mn}^{N} = \begin{cases} -\frac{ik}{\beta^2}\left[\frac{1}{2} v_{n+1}\left(x_m^{N+1}\right) + \left(\frac{1}{2} - \log 2\right) v_n\left(x_m^{N+1}\right)\right] , & n = 1 \\ -\frac{ik}{\beta^2}\left[\frac{v_{n+1}\left(x_m^{N+1}\right)}{2n} - \frac{v_n\left(x_m^{N+1}\right)}{2n(n-1)} - \frac{v_{n-1}\left(x_m^{N+1}\right)}{2(n-1)}\right] , & n \geqslant 2 \end{cases} \tag{8.81}$$

The weakest part of the collocation method is the approximation introduced by the Jacobi-Gauss quadrature formula (8.80). Comparing Equations (8.61) with (8.70), we see that the function

$$K_B(x-\xi) = \frac{ik}{\beta^2}\left[1-e^{-ik(x-\xi)} F_1(x-\xi)\right] \log|x-\xi| + K_2(x-\xi) + K_W(x-\xi)$$

while continuous, contains singular terms of order $(x-\xi)\log|x-\xi|$. Such terms will not be integrated accurately and will result in convergence ($N \to \infty$) delay due to quadrature error in the collocation matrix. On the other hand, by splitting the kernel according to Equation (8.67), all singularities can be treated properly. For further details the reader is referred to References [8.17] and [8.21].

Once the Fourier coefficients a_n are known, the airfoil loading and force coefficients are evaluated, as for steady flow, from Equations (7.83) to (7.85). The aerodynamic work matrix, representing the work done on the airfoil as it deforms in mode (m) against the pressure due to mode (n) is

$$W_{mn} = -\frac{1}{2} \int_{-1}^{1} f^{(m)}(x) \, \overline{C_p^{(n)}(x)} \, dx \tag{8.82}$$

where the overbar denotes complex conjugation*.

Replacing the pressure amplitude by the pressure factor (8.73), we obtain

$$W_{mn} = -\frac{1}{\beta} \int_{-1}^{1} \sqrt{\frac{1-x}{1+x}} \, f^{(m)}(x) \, \overline{\psi^{(n)}(x)} \, dx$$

Expressing the deflection and the pressure factor in terms of the pressure polynomials, i.e.

$$f^{(m)}(x) = \sum_{r=1}^{\infty} h_r^{(m)} \psi_r(x) , \quad h_r^{(m)} = \frac{1}{\pi} \int_{-1}^{1} \sqrt{\frac{1-\xi}{1+\xi}} \, f^{(m)}(\xi) \, \psi_r(\xi) \, d\xi \tag{8.83}$$

and

$$\overline{\psi^{(n)}(x)} = \sum_{s=1}^{\infty} \overline{a_s^{(n)}} \, \psi_s(x) , \quad \overline{a_s^{(n)}} = \frac{1}{\pi} \int_{-1}^{1} \sqrt{\frac{1-\xi}{1+\xi}} \, \overline{\psi^{(n)}(\xi)} \, \psi_s(\xi) \, d\xi \tag{8.84}$$

*The use of the complex conjugate of the pressure amplitude is necessitated by the definition of the work matrix as an inner (scalar) product.

we obtain

$$W_{mn} = -\frac{1}{\beta}\int_{-1}^{1}\sqrt{\frac{1-x}{1+x}}\left[\sum_{r=1}^{\infty} h_r^{(m)}\,\psi_r(x)\right]\left[\sum_{s=1}^{\infty}\overline{a_s^{(n)}}\,\psi_s(x)\right]dx$$

$$= -\frac{\pi}{\beta}\sum_{r=1}^{\infty} h_r^{(m)}\,\overline{a_r^{(n)}} \tag{8.85}$$

In the special case that the deflection modes are represented by the pressure polynomials

$$f^{(m)}(x) = \psi_m(x) \tag{8.86}$$

it follows from the ortogonality properties (7.60)

$$h_r^{(m)} = \delta_{mr}$$

and

$$W_{mn} = -\frac{\pi}{\beta}\,\overline{a_m^{(n)}} \tag{8.87}$$

This simple result is due to Fromme and Golberg [8.17].

8.4 Miles' Method for Unsteady Supersonic Interference

It is assumed that the supersonic flow is governed by the linearized equation (8.4) and that the thin airfoil is mounted midway between two parallel walls, a distance h apart. The leading edge is at the origin of the co-ordinate system, Figure 8.1 b). It is remarked at the outset that the supersonic tunnel test is interference free if the leading edge Mach waves reflected from the walls intersect downstream of the airfoil. Since the Mach angle is given by

$$\sin\mu = \frac{1}{M_\infty} \tag{8.88}$$

the interference free condition is

$$c \leqslant h\,\cot\mu = Bh$$

where

$$B = \sqrt{M_\infty^2 - 1} \tag{8.89}$$

In the unit semichord co-ordinate system we have $c = 2$, so that the interference free condition reads

$$h \geqslant \frac{2}{B} \tag{8.90}$$

Unless this condition is satisfied (large h or large M_∞) or unless the porosity of the walls is such that the incident waves cancel [8.22], [8.23], the reflected waves will impinge upon the aft portion of the airfoil and induce disturbances which invalidate the simulation of free flight conditions. In wind tunnel practice, the presence of supersonic interference is often regarded as unacceptable, but it is still of some value to study it, particularly since it may not always be possible to satisfy the interference free condition.

Because of the supersonic zones of influence and dependence, given by the character of Equation (8.4) at $M_\infty > 1$, the problem of wall interference at supersonic speeds is less difficult to solve than that at subsonic speeds. To be more specific, we can directly employ the airfoil boundary condition (8.15), knowing that the flow is undisturbed upstream of the leading edge Mach wave

$$x < B|y|$$

and that the upwash downstream of the trailing edge does not influence the airfoil pressure distribution. As a result, the surface pressure can be obtained explicitly via an integral involving the deflection. This is in contrast to the subsonic case, where the dependence of pressure on deflection is implicit, leading to the solution of an integral equation.

Miles' method [8.24], originally presented for solid walls, was applied by Drake [8.19] to the low frequency porous wall case. The boundary value problem to be solved is

$$B^2 \frac{\partial^2 \phi}{\partial x^2} + 2ikM_\infty^2 \frac{\partial \phi}{\partial x} - k^2 M_\infty^2 \phi - \frac{\partial^2 \phi}{\partial y^2} = 0, \qquad -\infty < x < \infty, \qquad 0 < y < \frac{h}{2} \tag{8.91}$$

$$\left(\frac{\partial}{\partial x} + ik\right) \phi\left(x, \frac{h}{2}\right) + \frac{1}{P} \frac{\partial \phi}{\partial y}\left(x, \frac{h}{2}\right) = 0, \qquad B\frac{h}{2} < x < \infty \tag{8.92}$$

$$\frac{\partial \phi}{\partial y}(x,0) = v(x) = \left(\frac{\partial}{\partial x} + ik\right) f(x), \qquad 0 < x \tag{8.93}$$

$$\phi(x,y) = 0, \qquad x \leqslant By \tag{8.94}$$

$$\frac{\partial \phi}{\partial x}(x,y) = \frac{\partial \phi}{\partial y}(x,y) = 0, \qquad x < By \tag{8.95}$$

The form of initial conditions (8.94) and (8.95) naturally invites the Laplace transformation

$$\hat{\phi}(s,y) = \mathcal{L}\left\{\phi(x,y)\right\} = \int_0^\infty e^{-sx} \phi(x,y)\, dx \tag{8.96}$$

For a pitching motion of small amplitude α about $x = x_0$

$$f(x) = -\alpha(x - x_0) \tag{8.97}$$

from which

$$v(x) = \left(\frac{\partial}{\partial x} + ik\right) f(x) = -\alpha\left[1 + ik(x - x_0)\right] \tag{8.98}$$

and

$$\hat{v}(s) = \mathcal{L}\left\{v(x)\right\} = -\alpha\left[\frac{1}{s} + ik\left(\frac{1}{s^2} - \frac{x_0}{s}\right)\right] \tag{8.99}$$

Accordingly, the subsidiary two-point boundary value problem is

$$\frac{\partial^2 \hat{\phi}}{\partial y^2}(s,y) - \Lambda^2 \hat{\phi}(s,y) = 0, \qquad 0 < y < \frac{h}{2}$$

$$(s + ik)\, \hat{\phi}\left(s, \frac{h}{2}\right) + \frac{1}{P} \frac{\partial \hat{\phi}}{\partial y}\left(s, \frac{h}{2}\right) = 0$$

$$\frac{\partial \hat{\phi}}{\partial y}(s,0) = \hat{v}(s)$$

where

$$\Lambda^2 = B^2 s^2 + 2iM_\infty^2 sk - M_\infty^2 k^2 \tag{8.100}$$

The solution is

$$\hat{\phi}(s,y) = -\hat{g}(s,y)\, \hat{v}(s) \tag{8.101}$$

where

$$\hat{g}(s,y) = \frac{1}{\Lambda} \frac{\Lambda \cosh\left[\Lambda\left(\frac{h}{2}-y\right)\right] + P(s+ik)\sinh\left[\Lambda\left(\frac{h}{2}-y\right)\right]}{\Lambda \sinh\left(\Lambda\frac{h}{2}\right) + P(s+ik)\cosh\left(\Lambda\frac{h}{2}\right)} \tag{8.102}$$

For ideal slotted walls the wall boundary condition (8.92) is replaced by

$$\phi\left(x,\frac{h}{2}\right) + K\frac{\partial\phi}{\partial y}\left(x,\frac{h}{2}\right) = 0\,, \qquad B\frac{h}{2} < x < \infty \tag{8.103}$$

The solution of this problem is again of the form (8.101), where

$$\hat{g}(s,y) = \frac{1}{\Lambda} \frac{\sinh\left[\Lambda\left(\frac{h}{2}-y\right)\right] + K\Lambda\cosh\left[\Lambda\left(\frac{h}{2}-y\right)\right]}{\cosh\left(\Lambda\frac{h}{2}\right) + K\Lambda\sinh\left(\Lambda\frac{h}{2}\right)} \tag{8.104}$$

Taking the limit $P \to 0$ in Equation (8.102) or $K \to \infty$ in Equation (8.104), we obtain Miles' solid wall expression

$$\hat{g}(s,y) = \frac{1}{\Lambda} \frac{\cosh\left[\Lambda\left(\frac{h}{2}-y\right)\right]}{\sinh\left(\Lambda\frac{h}{2}\right)} \tag{8.105}$$

Similarly, taking the limit $P \to \infty$ or $K \to 0$ we recover Drake's open jet result [8.25]

$$\hat{g}(s,y) = \frac{1}{\Lambda} \frac{\sinh\left[\Lambda\left(\frac{h}{2}-y\right)\right]}{\cosh\left(\Lambda\frac{h}{2}\right)} \tag{8.106}$$

If $h \to \infty$, the above formulas reduce to

$$\hat{g}(s,y) = \frac{e^{-\Lambda y}}{\Lambda} \tag{8.107}$$

which is the expected free air limit [8.26].

Applying now the convolution theorem to Equation (8.101), we obtain in the physical plane

$$\phi(x,y) = -\int_0^x g(x-\xi,y)\, v(\xi)\, d\xi \tag{8.108}$$

where the influence function

$$g(x,y) = \mathcal{L}^{-1}\left\{\hat{g}(s,y)\right\} \tag{8.109}$$

is the inverse Laplace transform of $\hat{g}$.

In the free air case, the inverse transform of Equation (8.107) yields [8.26]

$$g(x,y) = \frac{1}{B} e^{-i\frac{kM_\infty^2}{B^2}x} J_0\left[k\frac{M_\infty}{B^2}\sqrt{x^2-B^2y^2}\right] H(x-By) \tag{8.110}$$

where J_0 is the Bessel function of the first kind of zero order. The Heaviside function

$$H(z) = \begin{cases} 0\,, & z < 0 \\ 1\,, & z > 0 \end{cases}$$

nullifies the influence function in the region in front of the Mach wave passing through the point x,y in accordance with the physical concept of the zone of dependence. If $y > 0$, the upper limit of the integral (8.108) is effectively reduced to

$$\xi = x - By = x - y \cot \mu$$

Of course, if $x < By$, the point is outside the domain of airfoil influence.

Expressing the hyperbolic functions of Equation (8.105) in exponentials, expanding the denominator in a geometrical series, and inverting it termwise, Miles [8.24] and Drake [8.25] obtained for the solid wall and open jet cases respectively

$$g(x,y) = \frac{1}{B} e^{-ik \frac{M_\infty^2}{B^2} x} \left\{ J_0 \left[k \frac{M_\infty}{B^2} \sqrt{x^2 - B^2 y^2} \right] H(x - By) \right.$$

$$+ \sum_{n=1}^{\infty} \epsilon^n J_0 \left[k \frac{M_\infty}{B^2} \sqrt{x^2 - B^2 (nh - y)^2} \right] H\left[x - B(nh - y)\right]$$

$$\left. + \sum_{n=1}^{\infty} \epsilon^n J_0 \left[k \frac{M_\infty}{B^2} \sqrt{x^2 - B^2 (nh + y)^2} \right] H\left[x - B(nh + y)\right] \right\} \qquad (8.111)$$

where

$$\epsilon = \begin{cases} 1 & \ldots \quad \text{closed walls} \\ -1 & \ldots \quad \text{open jet} \end{cases}$$

The single term is the free air influence function (8.110) and the sums are recognized as its images at

$$y = \pm nh \quad , \quad n = 1, 2, \ldots$$

We see that the open jet images differ from solid wall images by the alternation of signs.

The Heaviside functions cut off the contributions downstream of the supersonic zone of dependence, as illustrated in Figure 8.9. Accordingly, only a finite number of images affect the flow at any given point x,y. In particular, if

$$x < B(h - y)$$

the point is free of wall interference.

Inverse transforms of Equations (8.102) and (8.104) are not known and the method of images itself does not seem to offer any simple hints. However, in order not to disappoint the reader entirely, we mention that low frequency approximations (discarding the terms of higher powers of k) can be worked out as demonstrated by Drake [8.19]. In fact, Equation (8.92) is suitable as a low frequency boundary condition anyway. For slotted walls, whose application in supersonic test conditions is less typical, the influence function has not yet been evaluated.

From Equations (8.10) and (8.101) we obtain the transformed pressure coefficient amplitude

$$\hat{C}_p(s,0) = 2(s + ik)\, \hat{g}(s,0)\, \hat{v}(s) \qquad (8.112)$$

The actual pressure coefficient amplitude is obtained as the inverse Laplace transform

$$C_p(x,0) = \mathcal{L}^{-1} \left\{ \hat{C}_p(s,0) \right\} \qquad (8.113)$$

or, using Equations (8.10) and (8.108), as

$$C_p(x,0) = 2 \left(\frac{\partial}{\partial x} + ik \right) \int_0^x g(x - \xi, 0)\, v(\xi)\, d\xi$$

$$= 2 \lim_{x \to \xi} \left[g(x - \xi, 0)\, v(\xi) \right] + 2 \int_0^x \left[\frac{\partial}{\partial x} g(x - \xi, 0) + ik\, g(x - \xi, 0) \right] v(\xi)\, d\xi$$

Using the limit

$$\lim_{x \to \xi+} g(x-\xi,0) = \lim_{s \to \infty} s\hat{g}(s,0) = \lim_{s \to \infty} \left(\frac{s}{\Lambda}\right) = \frac{1}{B}$$

finally

$$C_p(x,0) = \frac{2}{B} v(x) + 2 \int_0^x \left[\frac{\partial}{\partial x} g(x-\xi,0) + ikg(x-\xi,0)\right] v(\xi)\, d\xi \tag{8.114}$$

The first right hand term of Equation (8.114) is the Ackeret quasi-steady result, i.e. the result obtained from the instantaneous upwash on the basis of steady flow theory (thereby neglecting all time lag effects). The unsteady and wall interference effects are obviously absorbed by the integral term.

The lift and pitching moment amplitudes can be obtained as inverse Laplace transforms, using the transformed pressure coefficient amplitude (8.109). Recalling that the airfoil chord length is $c = 2$ and that $C_p(x,0)$ represents only a half of the pressure jump across the airfoil, we have for the lift coefficient amplitude

$$C_L = -\int_0^2 C_p(x,0)\, dx = -\mathcal{L}^{-1}\left\{\frac{1}{s}\hat{C}_p(s,0)\right\}\Big|_{x=2} \tag{8.115}$$

Similarly, the amplitude of the pitching moment (about the point $x = x_0$) is

$$C_M = -\frac{1}{2}\int_0^2 (x_0 - x)\, C_p(x,0)\, dx = -\frac{1}{2}\mathcal{L}^{-1}\left\{\frac{1}{s}\left(x_0 - \frac{d}{ds}\right)\hat{C}_p(s,0)\right\}\Big|_{x=2} \tag{8.116}$$

As noted by Savkar [8.27], the Laplace transform (8.96) is also a suitable means for solving the unsteady transonic interference problem, governed by the linearized equation (8.6). In this (parabolic) case we have a single family of characteristics $x = \text{const.}$, and the problem can be considered undisturbed ahead of the leading edge characteristic $x = 0$. Thus the porous wall boundary value problem is obtained from that described by Equations (8.91) to (8.95) by taking the limit $B \to 0$, but allowing M_∞ to depart slightly from unity. Accordingly, from Equation (8.100)

$$\Lambda^2 = 2iM_\infty^2 sk - M_\infty^2 k^2 \tag{8.117}$$

The transformed potential amplitude is again given by Equations (8.101) and (8.102). The same type of interpretation applies also to solid, open and slotted wall results.

The transonic counterparts of Equations (8.110) or (8.111) can be obtained using the asymptotic formula

$$J_0(z) \sim \sqrt{\frac{2}{\pi z}} \cos\left(z - \frac{\pi}{4}\right) = \frac{e^{-i\frac{\pi}{4}}}{\sqrt{2\pi z}}\left(e^{iz} + ie^{-iz}\right)$$

where the (large) argument z stands for

$$z = k\frac{M_\infty}{B^2}\sqrt{x^2 - B^2(nh \pm y)^2} \simeq \frac{kM_\infty}{B^2} x\left[1 - \frac{1}{2}B^2\left(\frac{nh \pm y}{x}\right)^2\right]$$

Special care must be taken in the evaluation of the pressure distributions, since the supersonic pressure coefficient (8.114) does not possess a limit for $M_\infty = 1$; for more discussion see Reference [8.2]. Other interesting features of linear transonic interference are described by Savkar [8.27].

8.5 Platzer's Method for Low Frequency Supersonic Interference

As indicated in Section 8.4, the Laplace transform formulation of supersonic interference is very elegant, but for ventilated walls the evaluation of the influence function by inverse transform appears to be complicated even in low frequency approximations. The method of characteristics is an obvious alternative, whose practicality has been demonstrated on ventilated walls by Platzer and Pierce [8.28], utilizing the technique developed earlier by Teipel [8.29]. The procedure is entirely numerical, but Platzer [8.30] subsequently showed, that a closed-form estimation of supersonic wall interference is possible for low frequencies, by adapting Sauer's elementary solution [8.31]. Platzer's method is well suited for investigating the wall interference effect on stability derivatives in supersonic flow, but is feasible only for the porous and not the slotted wall boundary condition.

Considered is again the airfoil boundary value problem of Equations (8.91) to (8.95). For sufficiently small reduced frequencies it is permissible to represent the potential amplitude by its first order approximation

$$\phi(x,y) = \phi^{(0)}(x,y) + k\,\phi^{(1)}(x,y) \tag{8.118}$$

where $\phi^{(0)}$ and $\phi^{(1)}$ are understood not to be functions of k. Substituting in Equation (8.91) and separating the zero and first order terms in k, we obtain

$$B^2 \frac{\partial^2\phi^{(0)}}{\partial x^2} - \frac{\partial^2\phi^{(0)}}{\partial y^2} = 0 \tag{8.119}$$

$$B^2 \frac{\partial^2\phi^{(1)}}{\partial x^2} - \frac{\partial^2\phi^{(1)}}{\partial y^2} + 2i(B^2+1)\frac{\partial\phi^{(0)}}{\partial x} = 0 \tag{8.120}$$

Similarly, the porous wall boundary condition (8.92) splits into

$$\frac{\partial\phi^{(0)}}{\partial x}\left(x,\frac{h}{2}\right) + \frac{1}{P}\frac{\partial\phi^{(0)}}{\partial y}\left(x,\frac{h}{2}\right) = 0 \quad , \quad B\frac{h}{2} < x < \infty \tag{8.121}$$

$$\frac{\partial\phi^{(1)}}{\partial x}\left(x,\frac{h}{2}\right) + \frac{1}{P}\frac{\partial\phi^{(1)}}{\partial y}\left(x,\frac{h}{2}\right) + i\phi^{(0)}\left(x,\frac{h}{2}\right) = 0 \quad , \quad B\frac{h}{2} < x < \infty \tag{8.122}$$

Assuming that the airfoil is a flat plate undergoing pitching motion of amplitude α around the point $x_0,0$, the deflection amplitude is

$$f(x) = -\alpha(x-x_0)$$

and the airfoil boundary condition (8.93) becomes

$$\frac{\partial\phi}{\partial y}(x,0) = -\alpha - ik\alpha(x-x_0)$$

Accordingly

$$\frac{\partial\phi^{(0)}}{\partial y}(x,0) = -\alpha \tag{8.123}$$

$$\frac{\partial\phi^{(1)}}{\partial y}(x,0) = -i\alpha(x-x_0) \tag{8.124}$$

Sauer [8.31] has shown that the general solution of the system of hyperbolic equations (8.119) and (8.120), which takes the initial conditions (8.94) and (8.95) into account, is

$$\phi^{(0)}(x,y) = p(z) \tag{8.125}$$

$$\phi^{(1)}(x,y) = i\left[q(z) \mp \left(B+\frac{1}{B}\right) y\,p(z)\right] \tag{8.126}$$

where p and q are arbitrary, twice differentiable functions of the argument

$$z = x \pm By + C \tag{8.127}$$

and vanishing for all $z < 0$. The plus or minus sign depends on the family of Mach lines (characteristics) along which the disturbances propagate; the constant C serves to fix the upstream boundary of the supersonic zone of dependence.

As illustrated in Figure 8.10, the flow region above the airfoil is divided into zones $n = 1, 2, 3, \ldots$, bounded by the airfoil, the wall, and the repeated reflections of the leading edge Mach line. By the linear superposition principle Sauer's solutions (8.125) and (8.126) in the nth zone can be written as

$$\phi^{(0)}(x,y) = \sum_{j=1}^{n} p_j(z_j) \tag{8.128}$$

$$\phi^{(1)}(x,y) = i\left[\sum_{j=1}^{n} q_j(z_j) + \left(B+\frac{1}{B}\right) y \sum_{j=1}^{n} (-1)^j p_j(z_j)\right] \tag{8.129}$$

where

$$z_j = x + (-1)^j By - \frac{1}{2}\left[j - \frac{1-(-1)^j}{2}\right] Bh \tag{8.130}$$

As may be verified in Figure 8.10, the straight line corresponding to the value $z_j = 0$ defines the upstream Mach-line boundary of the jth zone.

The functions p_j and q_j can be determined consecutively by satisfying the airfoil boundary conditions in the odd-numbered zones and the wall boundary conditions in the even-numbered zones. It can be shown that

$$p_j'(z_j) = \frac{\alpha}{B} a_j \tag{8.131}$$

$$q_j'(z_j) = -\frac{\alpha}{B}(b_j z_j + c_j) \tag{8.132}$$

where a_j, b_j, and c_j are constants. Hence, p_j and q_j are obtained by simple integration*.

Starting with the airfoil boundary conditions (8.123) and (8.124) in the interference-free zone 1, we obtain [8.31]

$$p_1(z_1) = \frac{\alpha}{B} z_1 \tag{8.133}$$

$$q_1(z_1) = -\frac{\alpha}{B}\left(\frac{z_1^2}{2B^2} + x_0 z_1\right) \tag{8.134}$$

where

$$z_1 = x - By \tag{8.135}$$

Satisfying the porous wall boundary conditions (8.121) and (8.122) in zone 2, we similarly derive

$$p_2(z_2) = \frac{\alpha}{B}\frac{B-P}{B+P} z_2 \tag{8.136}$$

$$q_2(z_2) = -\frac{\alpha}{B}\left\{\left[\frac{1}{(B+P)^2} - \frac{1}{2B^2}\right] z_2^2 + \frac{B-P}{B+P} x_0 z_2 + \frac{B-P}{B+P}\left(B+\frac{1}{B}\right) h z_2\right\} \tag{8.137}$$

where

$$z_2 = x + By - Bh \tag{8.138}$$

Again, satisfying the airfoil boundary conditions (8.123) and (8.124) in zone 3, we derive

$$p_3(z_3) = \frac{\alpha}{B}\frac{B-P}{B+P} z_3 \tag{8.139}$$

*For the slotted wall boundary condition this does not apply, making Platzer's method inapplicable.

$$q_3(z_3) = -\frac{\alpha}{B}\left\{\left[\frac{1}{(B+P)^2} - \frac{1}{2B^2}\right] z_3^2 + \frac{B-P}{B+P} x_0 z_3 + \frac{B-P}{B+P}\left(B+\frac{1}{B}\right) h z_3\right\} \tag{8.140}$$

where

$$z_3 = x - By - Bh \tag{8.141}$$

This result, which takes into account just one reflection from the wall, applies to the airfoil segment $0 \leqslant x \leqslant 2Bh$, but from Equations (8.131) and (8.132) it follows that the process can be continued ad infinitum.

Using Equations (8.10), (8.118), (8.128) and (8.129), we obtain for the amplitude of the pressure coefficient at $y = 0$

$$C_p(x,0) = -2\sum_{j=1}^{n} p_j' - 2ik \sum_{j=1}^{n}\left[p_j\left(x - \frac{j-1}{2}Bh\right) + q_j'\left(x - \frac{j-1}{2}Bh\right)\right] \tag{8.142}$$

where n is an odd integer denoting the number of the zone in which the point lies:

$$\frac{n-1}{2}Bh < x < \frac{n+1}{2}Bh \tag{8.143}$$

The value of p_j', since it is always a constant, is written without an argument.

The lift coefficient amplitude is

$$C_L = -\int_0^2 C_p(x,0)\,dx = \alpha\left[c_{\ell\alpha} + ik\left(c_{\ell q} + c_{\ell\dot{\alpha}}\right)\right] \tag{8.144}$$

where

$$c_{\ell\alpha} = \frac{2}{\alpha}\int_0^2 \sum_{j=1}^{n} p_j'\,dx \tag{8.145}$$

$$c_{\ell q} + c_{\ell\dot{\alpha}} = \frac{2}{\alpha}\int_0^2 \sum_{j=1}^{n}\left[p_j\left(x - \frac{j-1}{2}Bh\right) + q_j'\left(x - \frac{j-1}{2}Bh\right)\right] dx \tag{8.146}$$

are the stability derivatives for the lift force [8.32].

Similarly, the amplitude of the pitching moment coefficient is

$$C_M = \frac{1}{2}\int_0^2 C_p(x,0)(x - x_0)\,dx = \alpha\left[c_{m\alpha} + ik\left(c_{mq} + c_{m\dot{\alpha}}\right)\right] \tag{8.147}$$

where

$$c_{m\alpha} = -\frac{1}{\alpha}\int_0^2 (x - x_0)\sum_{j=1}^{n} p_j'\,dx \tag{8.148}$$

$$c_{mq} + c_{m\dot{\alpha}} = -\frac{1}{\alpha}\int_0^2 (x - x_0)\sum_{j=1}^{n}\left[p_j\left(x - \frac{j-1}{2}Bh\right) + q_j'\left(x - \frac{j-1}{2}Bh\right)\right] dx \tag{8.149}$$

are the stability derivatives for the pitching moment.

Similar low frequency expressions for the stability derivatives are also obtainable from the Laplace-transform results of Miles [8.24] and Drake [8.19], [8.25], however with considerably bigger analytical effort. Comparisons of various theories and sample calculations can be found in Reference [8.30].

REFERENCES

[8.1] Ashley, H. *Unsteady Subsonic and Supersonic Inviscid Flow.* Unsteady Aerodynamics, AGARD-CP-227, 1977, pp. 1.1-1.32.

[8.2] Landahl, M. *Unsteady Transonic Flow.* Pergamon Press, 1961.

[8.3] Garrick, I.E. *Nonsteady Wing Characteristics, Aerodynamic Components of Aircraft at High Speeds.* (Ed. Donovan, A.F. and Lawrence, H.R.), Section F, Princeton University Press, 1957.

[8.4] Runyan, H.L. Watkins, C.E. *Considerations on the Effect of Wind-Tunnel Walls on Oscillating Air Forces for Two-Dimensional Subsonic Compressible Flow.* NACA TN 2252, Dec. 1951.

[8.5] Jones, W.P. *Wind-Tunnel Wall Interference Effects on Oscillating Airfoils in Subsonic Flow.* R. & M. 2943, Aeronautical Research Council, Dec. 1953.

[8.6] Runyan, H.L. Woolston, D.S. Rainey, A.G. *Theoretical and Experimental Investigation of the Effect of Tunnel Walls on the Forces on an Oscillating Airfoil in Two-Dimensional Subsonic Compressible Flow.* NACA Rep. 1262, 1956.

[8.7] Acum, W.E.A. *A Simplified Approach to the Phenomenon of Wind-Tunnel Resonance.* R. & M. 3371, Aeronautical Research Council, April 1962.

[8.8] Landau, L.D. Lifshitz, E.M. *Fluid Mechanics.* Pergamon Press, 1959.

[8.9] Fromme, J. Golberg, M. *Unsteady Two Dimensional Airloads Acting on Oscillating Thin Airfoils in Subsonic Ventilated Wind Tunnels.* NASA CR 2967, 1978.

[8.10] Fromme, J. Golberg, M. *Numerical Solution of a Class of Integral Equations Arising in Two-Dimensional Aerodynamics.* Journal of Optimization and Applications, Vol. 24, 1978, pp. 169-206.

[8.11] Mabey, D.G. *The Resonance Frequencies of Ventilated Wind Tunnels.* TR 78038, Royal Aircraft Establishment, April 1978.

[8.12] Mabey, D.G. *Resonance Frequencies of Ventilated Wind Tunnels.* AIAA Journal, Vol. 18, 1980, pp. 7-8.

[8.13] Barger, R.L. *A Theory for Predicting Boundary Impedance and Resonance Frequencies of Slotted-Wall Wind Tunnels Including Plenum Effects.* NASA TP 1880, 1981.

[8.14] Barger, R.L. *Reflection and Transmission of Sound by a Slotted Wall Separating Two Moving Fluid Streams.* NACA TN-4295, June 1958.

[8.15] Bland, S.R. *The Two-Dimensional Oscillating Airfoil in a Wind Tunnel in Subsonic Compressible Flow.* Doctoral Thesis, North Carolina State University, Raleigh, 1968.

[8.16] Bland, S.R. *The Two-Dimensional Oscillating Airfoil in a Wind Tunnel in Subsonic Flow.* SIAM J. Appl. Math., Vol. 18, 1970, pp. 830-848.

[8.17] Fromme, J.A. Golberg, M.A. *Two Dimensional Aerodynamic Interference Effects on Oscillating Airfoils With Flaps in Ventilated Subsonic Wind Tunnels.* NASA CR 3210, 1979.

[8.18] Fromme, J.A. Golberg, M.A. *Aerodynamic Interference Effects on Oscillating Airfoils with Controls in Ventilated Wind Tunnels.* AIAA Journal, Vol. 18, 1980, pp. 417-426.

[8.19] Drake, D.G. *The Oscillating Two-Dimensional Aerofoil Between Porous Walls.* The Aeronautical Quarterly, Vol. 8, 1957, pp. 226-239.

[8.20] Possio, C. *L'azione aerodinamica sul profilo oscillante in un fluido compressibile a velocita iposonora.* L'Aerotechnica, Vol. 18, 1938, pp. 441-458.

[8.21] Fromme, J.A. Golberg, M.A. *Reformulation of Possio's Kernel with Application to Unsteady Wind Tunnel Interference.* AIAA Journal, Vol. 18, 1980, pp. 951-957.

[8.22] Goethert, B.H. *Transonic Wind Tunnel Testing.* Pergamon Press, 1961.

[8.23] Davis, J.W. *Optimization of Wave Cancellation in Variable Porosity Transonic Wind Tunnel Flows.* NASA TN D-7432, Nov. 1973.

[8.24] Miles, J.W. *The Compressible Flow Past an Oscillating Airfoil in a Wind Tunnel.* Journal of the Aeronautical Sciences, Vol. 23, 1956, pp. 671-678.

[8.25] Drake, D.G. *The Motion of an Oscillating Aerofoil in a Compressible Free Jet.* Journal of the Royal Aeronautical Society, Vol. 60, 1956, pp. 621-623.

[8.26] Ashley, H. Landahl, M. *Aerodynamics of Wings and Bodies.* Addison-Wesley, 1965, pp. 255-257.

[8.27] Savkar, S.D. *A Note on Transonic Flow Past a Thin Airfoil Oscillating in a Wind Tunnel.* Journal of Sound and Vibration, Vol. 6, 1976, pp. 195-207.

[8.28] Platzer, M.F. Pierce, C.V. *Theoretical Investigation of Wind Tunnel Interference Effects upon Fluttering Panels and Airfoils in Low Supersonic Flow.* Proceedings of AIAA-ASME Structures, Structural Dynamics and Materials Conference, April 1970, pp. 17-24.

[8.29] Teipel, I. *Ein Charakteristikenverfahren zur Berechnung der verallgemeinerten ebenen Flatterluftkräfte.* Zeitschrift für Flugwissenschaften, Vol. 10, 1962, pp. 374-379.

[8.30] Platzer, M.F. *Wind Tunnel Interference on Oscillating Airfoils in Low Supersonic Flow.* Acta Mechanica, Vol. 16, 1973, pp. 115-126.

[8.31] Sauer, R. *Elementare Theorie des langsam schwingenden Überschallflügels.* ZAMP, Vol. 1, 1950, pp. 248-253.

[8.32] Orlik-Rückemann, K.J. *Wind Tunnel Measurements of Dynamic Derivatives.* Lecture Notes, Second Ed., National Research Council of Canada, Aug. 1963.

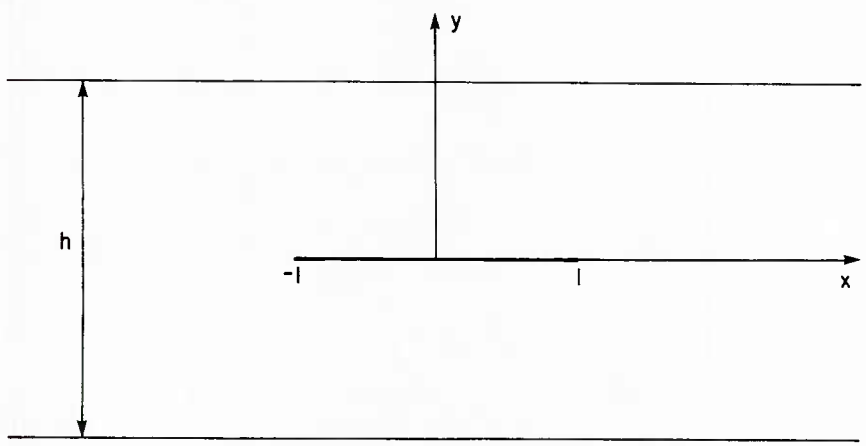

a) subsonic

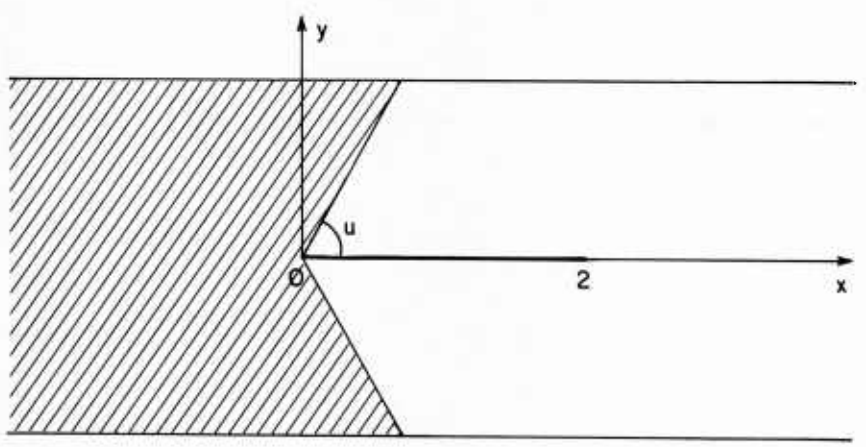

b) supersonic

Fig. 8.1 Co-ordinate system for a thin airfoil between tunnel walls

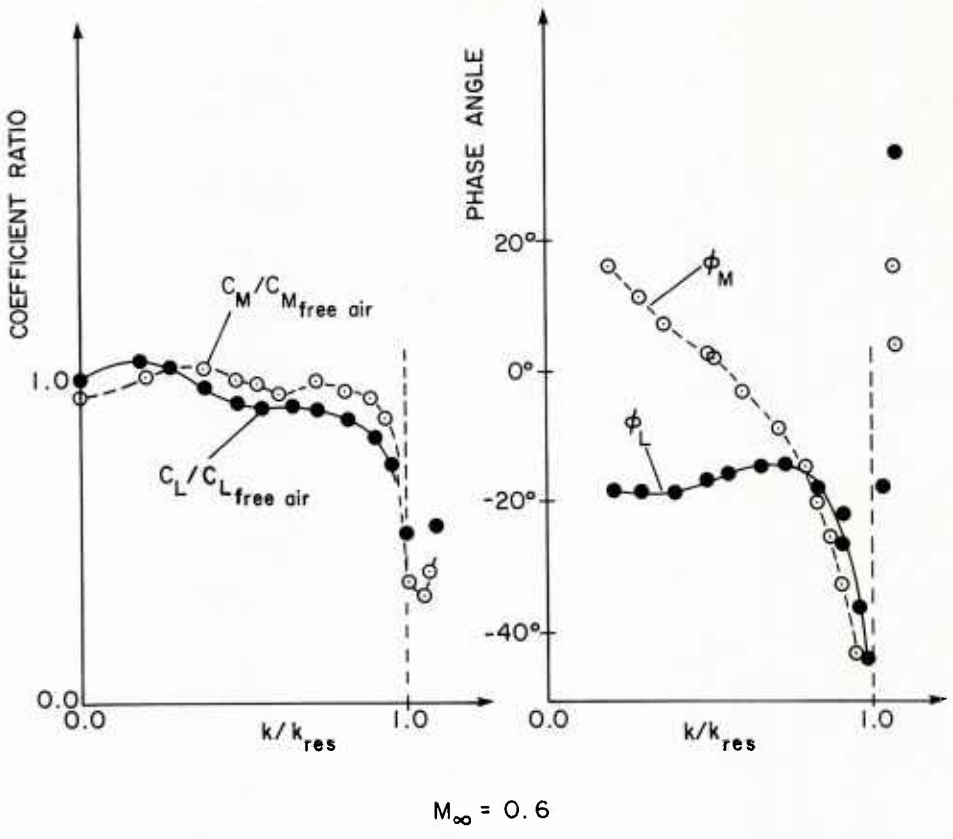

Fig. 8.2 Resonance in a solid wall test section (adapted from Ref. [8.6])

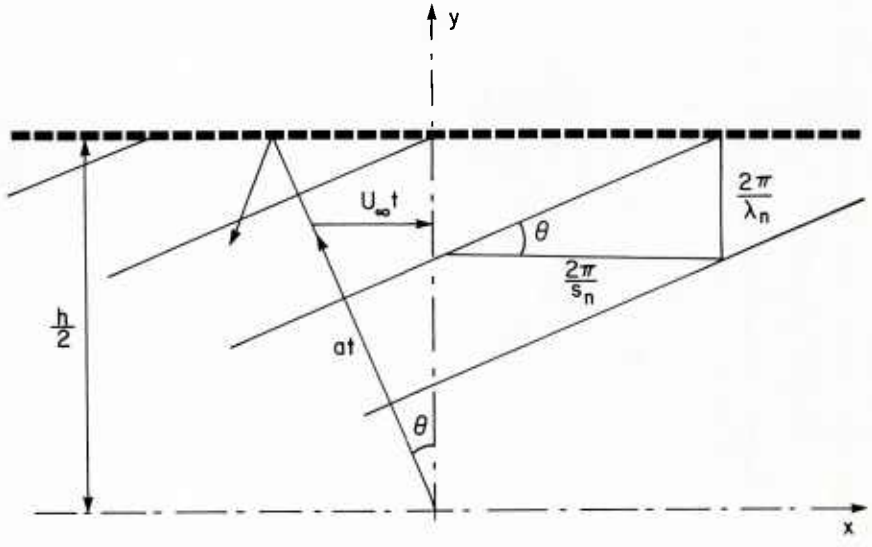

Fig. 8.3 Propagation of plane waves at resonance

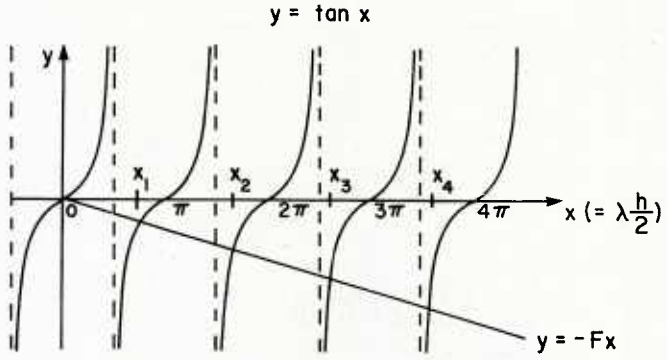

Fig. 8.4 Roots of Fx + tan x = 0
(adapted from Ref. [8.9])

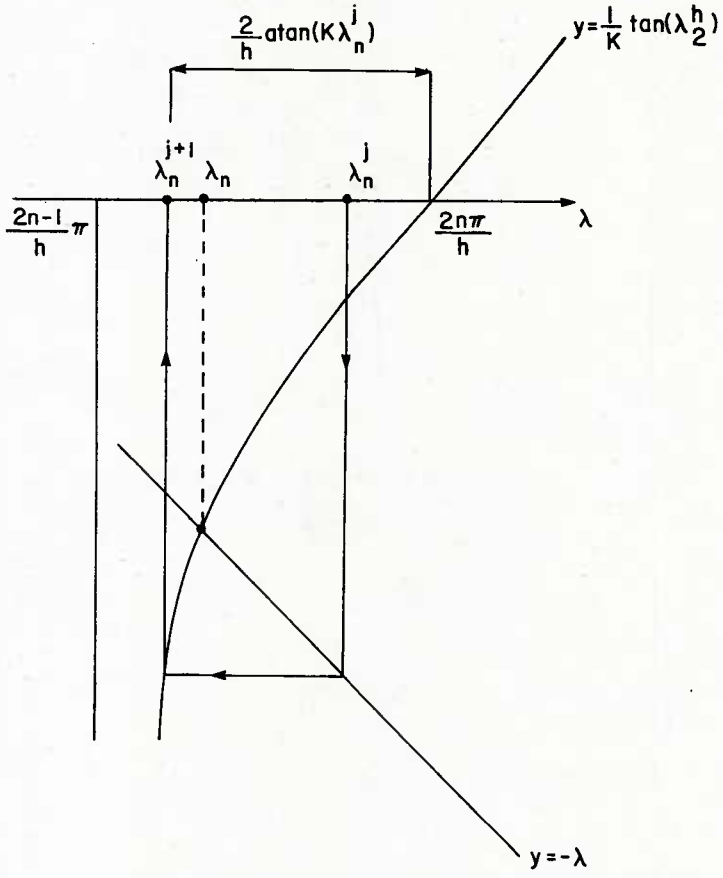

Fig. 8.5 Iteration by $\lambda_n^{j+1} = \frac{2}{h}\left[n\pi\text{-atan}\left(K\lambda_n^j\right)\right]$

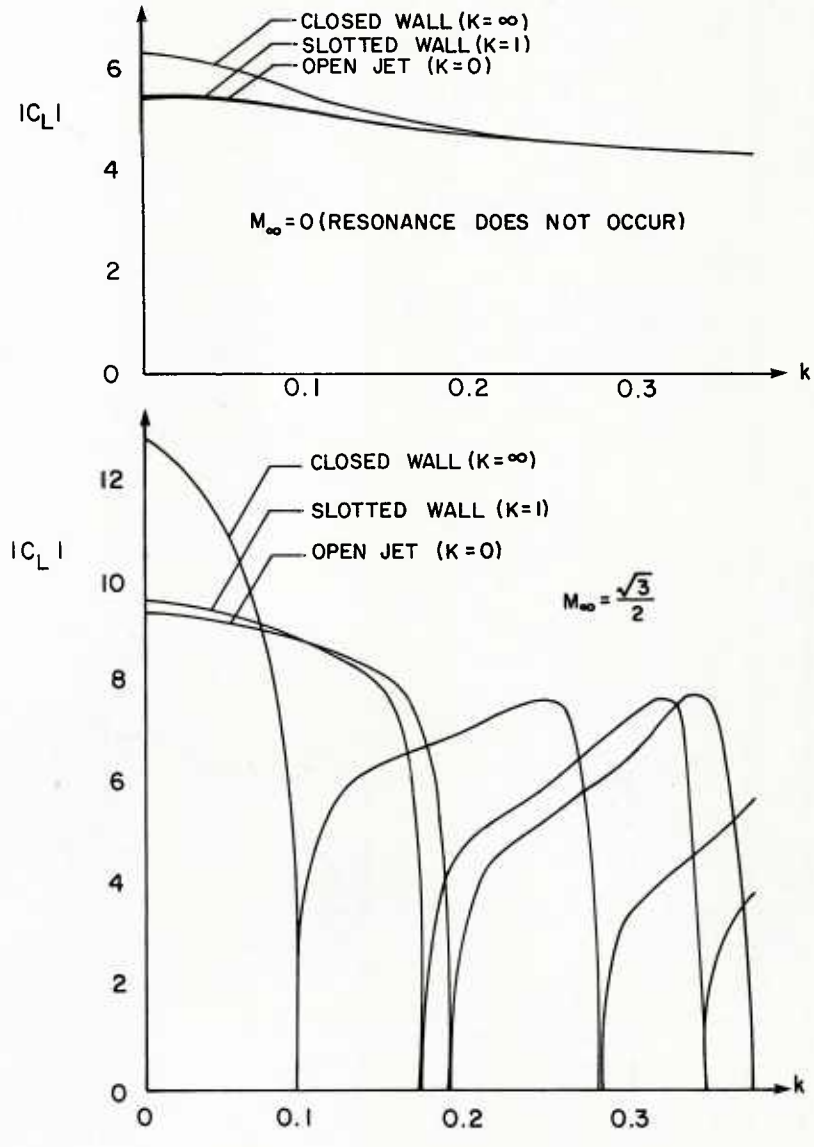

Fig. 8.6 Effect of ventilation on $|C_L|$ vs. k for a flat plate in pitching motion; c = 2, h = 20 (adapted from Ref. [8.9])

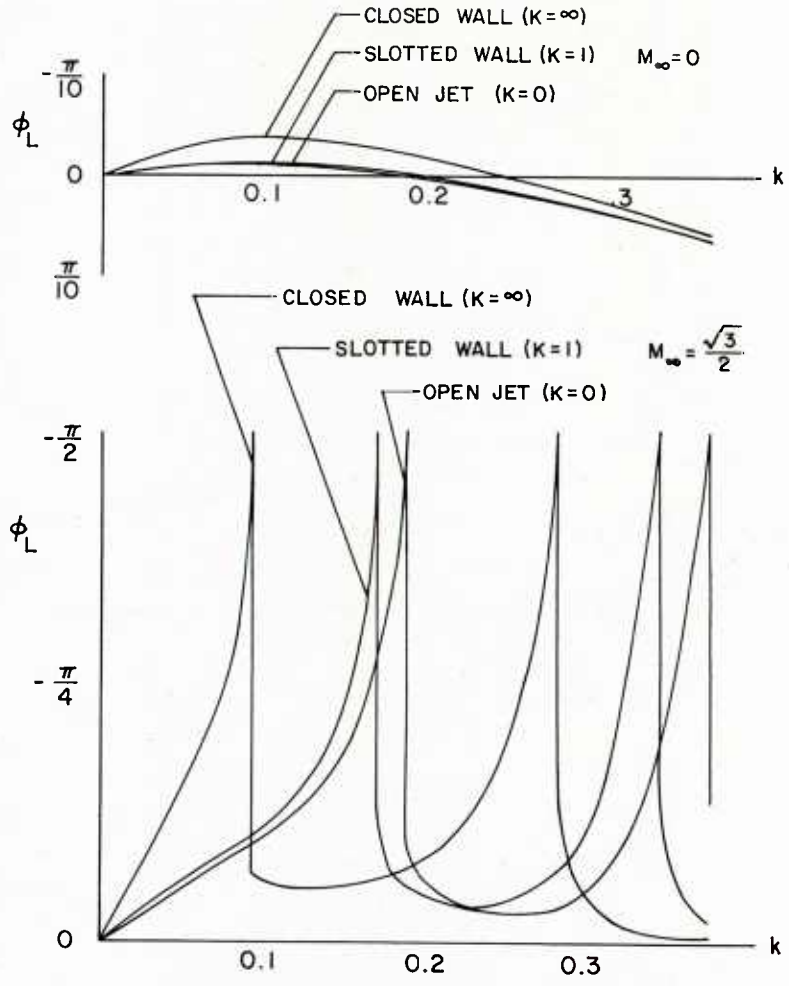

Fig. 8.7 Effect of ventilation on ϕ_L vs. k for a flat plate in pitching motion; c = 2, h = 20 (adapted from Ref. [8.9])

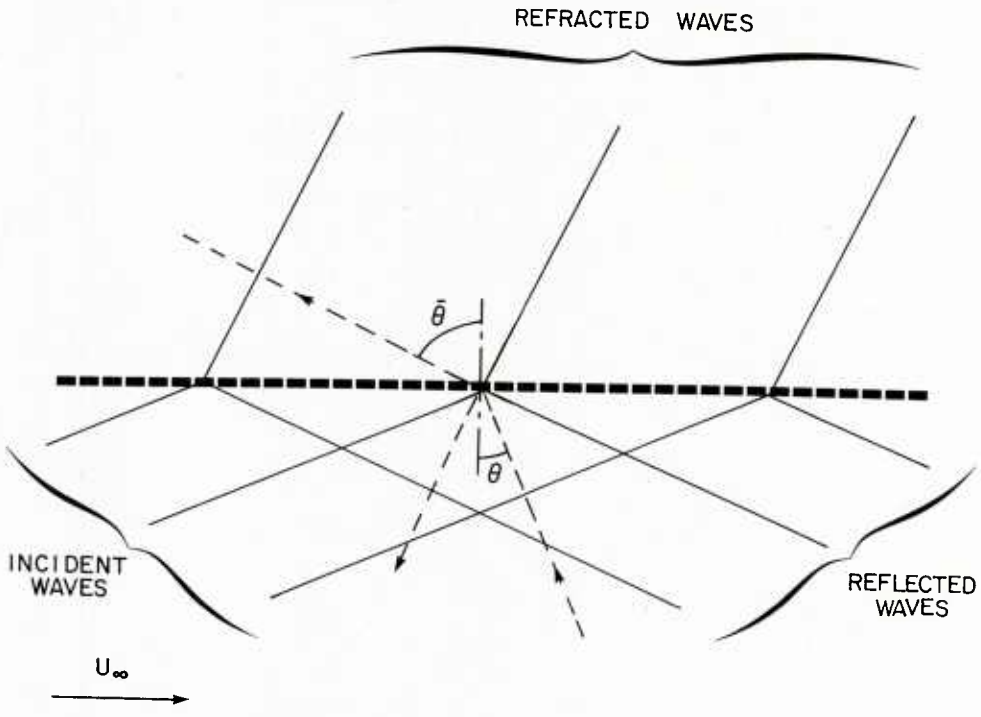

Fig. 8.8 Reflection and refraction of plane waves at a ventilated wall

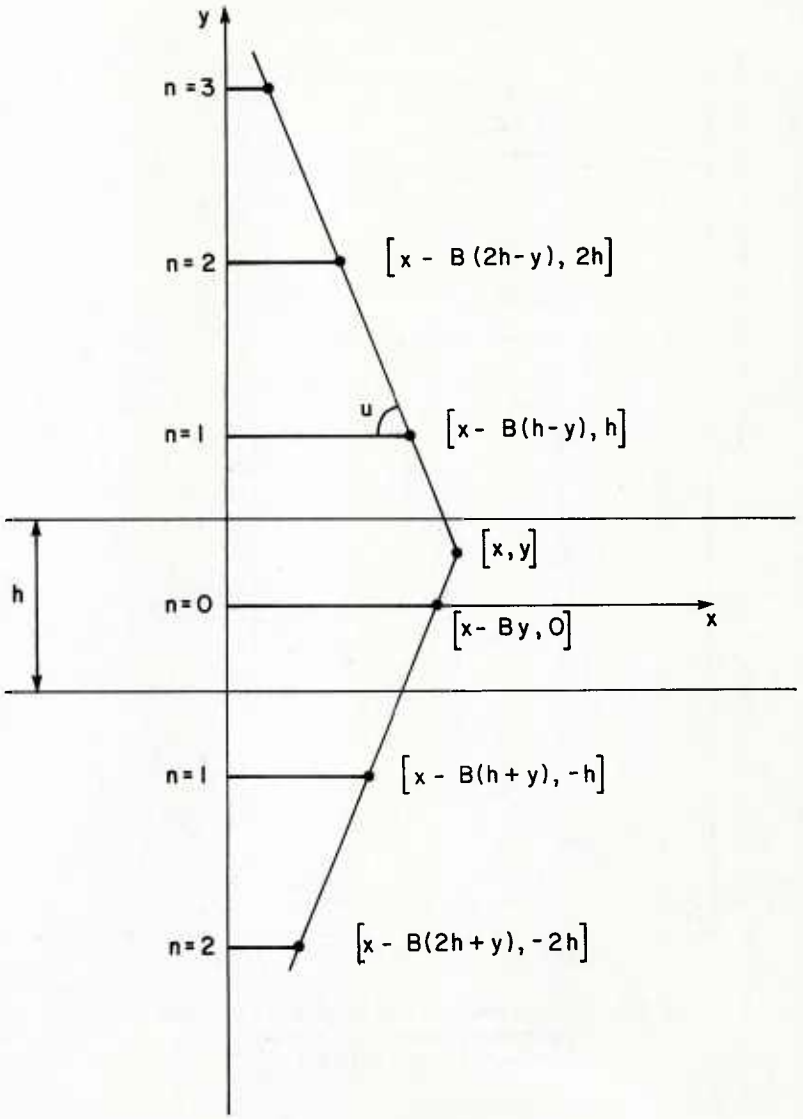

Fig. 8.9 Images for supersonic wall interference

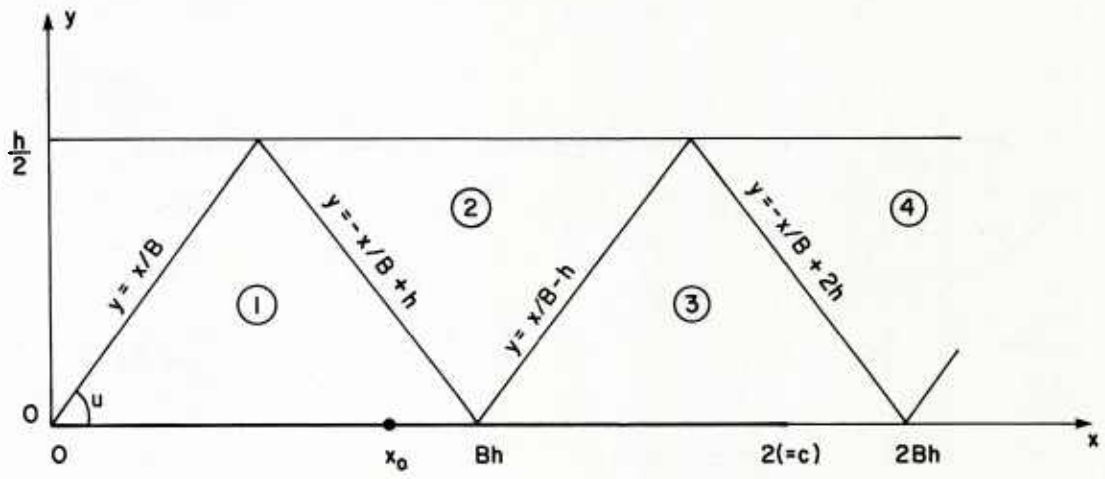

Fig. 8.10 Platzer zones

9.0 EFFECTS OF SIDE WALL BOUNDARY LAYER ON TWO-DIMENSIONAL TESTS

9.1 Introduction

In two-dimensional wind tunnel tests the airfoil model is usually mounted between two opposing solid walls, here for convenience called side walls. Ideally, then, we have a two-dimensional channel that provides flow uniformity across the span of the model. This ideal condition, however, cannot be realized in practice because of the presence of boundary layers on the side walls. The local flow at the junction of the model and the side wall becomes fully three dimensional due to the interaction of the boundary layer with the model. This local interaction, unfortunately, has far reaching effects. It does not only change the local spanwise load distributions, but also causes early separation over the rear portion of the airfoil. The rapid variation of the side wall boundary layer displacement thickness induced by the pressure field of the airfoil generates additional perturbation on the flow field about the airfoil. These effects cause the flow to deviate from the ideal two-dimensional conditions and cause errors in the measured data. Therefore it is necessary to control the boundary layer development so that these interaction effects can be minimized. For weak interaction without boundary layer control, post-test corrections must be applied to reduce the data to that of an equivalent two-dimensional condition.

9.2 Three-dimensional Flow at the Wing-Wall Junction

The side wall boundary layer has in most cases a long development length before entering the model test region and is therefore fully turbulent, with an appreciable thickness. For an empty tunnel the side wall boundary layer behaves like that of a flat plate and the growth of the boundary layer along the wall can be well predicted. The test section walls may be adjusted, if required, to compensate for the displacement effect. When a model is mounted in the test section, a pressure field is generated by the flow over the airfoil. Near the model the lateral pressure gradient is of the same order as the longitudinal one and a fully three dimensional flow develops.

At the leading edge region of the model the boundary layer at the wall sees the nose of the airfoil as a blunt protuberance [9.1]. The inviscid streamline past the round nose is highly curved and thus induces strong cross-flow normal to its direction. Away from the nose region the lateral pressure gradient is reduced and the limiting streamline (surface streamline) turns back gradually into the external inviscid stream direction. The process causes the limiting streamlines to converge forming a vortical free shear layer which separates from the wall [9.2]. This type of three-dimensional separation has been well studied for both laminar and turbulent flow [9.1]. For the case of flow past an airfoil-wall junction, excellent flow visualization of the limiting streamlines pattern can be found in the works of East [9.3], Shabaka [9.4] and Barbar [9.5]. The separated vortex sheets from the nose region roll up into a vortex pair wrapping around the airfoil-wall junction at both sides of the model. The extent of the vortex, however, is within the thickness of the boundary layer [9.3], [9.4], [9.5] and does not affect appreciably the boundary layer thickness at the region of separation. However the vortex pair energizes the boundary layer along the airfoil-wall junction downstream and at high lift condition, this favourable effect delays the separation at the side wall induced by the pressure recovery of the airfoil [9.5].

Since the side wall boundary layer is much thicker than that on the model, it is more prone to separate when facing the same adverse pressure gradient generated at the rear portion of the airfoil. Separation cells formed at the airfoil-wall junction can be observed while the pressure gradient is not yet severe enough to cause separation of the boundary layer over the model [9.5]. Barbar found that the vortex formed from the three-dimensional separation at the nose energizes the sidewall boundary layer downstream and delays the early separation. He showed that a thick boundary layer generating a large vortex had a small separation cell, while a thin boundary layer with a weak vortex had a much larger separation region. Thus the intersection drag loss is greater for a thin boundary layer than a thicker one. These observations were adopted by Jacobs in the derivation of a semi-empirical relation for the correction of drag measurements for an airfoil at incidence [9.6]. It should be noted, however, that Jacobs' correction applies to measurements at relatively low Reynolds numbers. The effect may not be so severe for high Reynolds number flows commonly used in tests with modern wind tunnels. An example of the drag correction is shown in Figure 9.1. The Reynolds number was 0.33 million for both NACA data and the DRL/PSU tests. The Jacobs' correction formula is also shown in the figure.

The three-dimensional boundary layer flow at the airfoil-wall junction also distorts the flow over the airfoil locally and thus changes the lift distribution for the portion of the model submerged in the boundary layer. This has been noted in the early experiment of Cowley and McMillan [9.7] and investigated in detail by Mendelsohn and Polhamus [9.8]. Both reports show reduction of spanwise loading as the wall is approached. The latter indicates that while the loss of the average load is small, the local spanwise load could be reduced by ten percent at the wall. At high angles of attack, separation at the airfoil-wall junction destroys the spanwise uniformity of the flow and is clearly indicated in the variation of the pitching moment along the span of the model.

For low speed flows, if there is no separation at the side wall, the airfoil-wall junction induces mainly losses in the form of additional drag and has only small effect on the average load measurements. However, with separation cells forming at the junction, the flow over the model could be so distorted that no "correction" can be reliably derived. This is particularly true for models with low aspect ratios as usually employed in facilities specially built for two-dimensional tests. For this type of flow, the only mean to establish a proper testing condition is to control the boundary layer development. A more detailed discussion on flow controls will be given in Section 9.4.

9.3 Boundary Layer Displacement Effect

As discussed in the last section, three-dimensional boundary layer flow is induced near the airfoil-wall junction by the pressure field generated by the model. Because of the slenderness of the airfoil shape, the curvature of the external streamlines decreases rapidly as the lateral distance increases. The cross-flow in the boundary layer is therefore already greatly reduced a small distance away from the airfoil. The pressure gradient along the streamline, however, varies rapidly within the extent of the chord and causes drastic changes of boundary layer thickness, which effectively alters the local width of the two-dimensional channel, causing local expansion or compression of the flow. This is particularly severe at transonic speeds, since the flow is extremely sensitive to small changes of the solid surface shape about which it passes. A detailed study of the side wall boundary layer effects at transonic speeds was conducted by Bernard-Guelle [9.9], [9.10]. It is shown, in contrast to the low speed observations discussed in the previous section, that the changes of average load and surface pressure distributions on the model depend strongly on the thickness of the incident boundary layer on the side wall. The reduction of normal force is found to be linearly proportional to the boundary layer thickness. The proportional constant assumes a near constant value for subcritical flow, but the value increases rapidly as the flow becomes supercritical. The latter is due to the movement of the shock at the upper surface of the model, where the flow is locally supersonic. As the boundary layer thickens, the shock moves forward and the section lift is further reduced.

The variation of the displacement thickness of the side wall boundary layer around an airfoil in transonic speed has been calculated by Chan [9.11] and is shown in Figure 9.2. The depression near the leading edge is due to the expansion of the flow around the nose. The adverse pressure gradient at the rear portion of the airfoil causes the rapid thickening of the boundary layer and may lead to early separation as discussed in the proceeding section. The displacement effect can be considered as a distribution of sources at the

surface [9.12]. The perturbation to the flow field due to these sources can, in principle, be evaluated. For a narrow working section this displacement thickness variation effectively changes the local width of the test channel and may locally speed up or slow down the flow about the model. The thinning of the expansion side and the thickening of the pressure side of the boundary layer, for example, would amount to a decrement of lift, as analysed by Winter and Smith [9.13].

A global analysis of the effect is given by Barnwell [9.14] and applies to subsonic or supersonic flows. The concept was later extended to the transonic range by Sewall [9.15].

In Barnwell's analysis [9.14], the changes in effective width of the test section is included in the continuity equation of the channel flow

$$(1 - M^2)\,\frac{\partial u}{\partial x} + \frac{\partial v}{\partial y} = \frac{2u}{b}\,\frac{\partial \delta^*}{\partial x} \tag{9.1}$$

where b is the width of the test section and δ^* the boundary layer displacement thickness. By observing that for a thick boundary layer with a long upstream development, the variation of the displacement thickness is dominated by the local pressure gradient [9.16], the momentum integral equation provides a direct relation for the growth of the boundary layer and the local velocity gradient as

$$\frac{\partial \delta^*}{\partial x} = -\left(2 + \frac{1}{H} - M^2\right)\frac{\delta^*}{u}\,\frac{\partial u}{\partial x} \tag{9.2}$$

The continuity equation, including the boundary layer effect, becomes

$$\left[1 - M^2 + \frac{2\delta^*}{b}\left(2 + \frac{1}{H} - M^2\right)\right]\frac{\partial u}{\partial x} + \frac{\partial v}{\partial y} = 0 \tag{9.3}$$

For subsonic linearized flow, the expression in the square bracket of Equation (9.3) amounts to an effective change of free-stream Mach number,

$$\bar{M} = \left[M^2 - \left(2 + \frac{1}{H} - M^2\right)\frac{2\delta^*}{b}\right]^{1/2} \tag{9.4}$$

The change of normal force can then be related to the change of Mach number by the Prandtl-Glauert rule,

$$\bar{\beta}\,\bar{C}_n = \beta\,C_n \tag{9.5}$$

where

$$\bar{\beta} = (1 - \bar{M}^2)^{1/2} \quad \text{and} \quad \beta = (1 - M^2)^{1/2}$$

$\bar{C}_n$ is the nearly two-dimensional normal force coefficient with side wall boundary layer and C_n the coefficient without boundary layer. Reasonable correlation of the ONERA data [9.9], [9.10] is obtained with the similarity rule as shown in Figure 9.3.

For transonic flows Sewall [9.15] applies von Karman's transonic similarity rule to correlate the free stream Mach number with and without side wall boundary layer,

$$\frac{\bar{\bar{M}}}{\bar{\bar{\beta}}^{3/4}} = \frac{\bar{M}}{\bar{\beta}^{3/4}} \tag{9.6}$$

where $\bar{\bar{\beta}} = (1 - \bar{\bar{M}}^2)^{1/2}$. The double bar denotes the condition without boundary layer. The normal force and the drag coefficients can then be correlated as

$$\frac{\bar{\bar{C}}_n}{\bar{C}_n} = \frac{\bar{\bar{C}}_d}{\bar{C}_d} = \frac{\bar{\beta}}{\bar{\bar{\beta}}} \tag{9.7}$$

Figure 9.4 shows the improvement in correlations for the normal and drag force coefficients and shock locations with Mach number when the above transonic similarity rule is applied. These results clearly indicate that the dominating effect of the sidewall boundary layer can be attributed to the displacement thickness. Taking averaged values for the boundary layer properties in the region around the airfoil, the change of the free stream Mach number due to the effective variation of the test channel width can be evaluated if thickness of the incident boundary layer is known. The scheme can readily be incorporated into programs for post-test estimations of sidewall interferences [9.17].

9.4 Boundary Layer Control by Suction

With no severe separation occurring at the side wall, the local three-dimensional flow at the airfoil-wall junction and the displacement effect from the area influenced by the model pressure field have been discussed and their global effects can be readily evaluated. However, at moderate and high lift conditions, the pressure recovery at the rear portion of the model will inevitably cause early separation at the side wall. Once the separation cell is formed, the flow over the model will be so distorted that it is doubtful that the above post-test corrections can be applied meaningfully. To reduce these adverse effects, it is necessary to control the development of the boundary layer around the model and prevent early separations at the wall. The most effective way is to apply suction locally at the regions where separations may occur [9.18] or over the area strongly influenced by the model pressure field [9.19], [9.20].

The application of boundary layer control locally to establish two dimensional test condition is adopted in the ONERA F1 tunnel [9.18]. The suction areas are strategically located at regions where flow separations both in two and three-dimensions would most likely occur. Suction can also be applied to an area surrounding the model as in the FFA 3.6m low speed tunnel [9.19] and the NAE two-dimensional test facility [9.20]. It should be noted that the suction required for these devices is moderate and does not remove the boundary layer completely. The control is achieved from the fact that the crossflow is greatly reduced by suction, thus the spread of the three-dimensional separation can be confined to a small region around the nose. With the boundary layer energized by suction, early separation at the side wall in the region of adverse pressure gradient can also be delayed. In addition, suction reduces the large variation of the displacement thickness and eliminates the need for post-test correction. An example of the displacement thickness distribution with moderate suction is shown in Figure 9.5, (compare with Fig. 9.2). That suction around the model area is of paramount importance for obtaining good two-dimensional flow at transonic conditions is amply demonstrated by the data and flow visualization pictures given in Figure 9.6 [9.23].

In some test facilities, it is not possible to accommodate suction around the model and the alternative is then to reduce the boundary layer thickness ahead of the model by suction. This scheme is employed in some two-dimensional test facilities [9.10], [9.21], [9.22]. Reducing the boundary layer thickness, however, does not imply full control of the boundary layer development as discussed above. It should be noted that the boundary layer recovers to that of a flat plate rapidly, once it leaves the suction area [9.21], [9.24] and thus reacts to the model pressure field in a similar manner as that without suction. Therefore the post-test corrections, as discussed in Sections 9.2 and 9.3, will be required to treat the measured data. The displacement effect, however, does decrease as the displacement thickness is reduced [9.14]. The validity of the post-test correction is still questionable when separations occur at the airfoil-wall junction, as a large separation cell forms because of the thin incident boundary layer [9.5].

REFERENCES

[9.1] Peake, D.J., Tobak, M., Korkegi, R.H. — *Three-Dimensional Interactions and Vortical Flows with Emphasis on High Speeds.* AGARD-AG-252, July 1980, Section 4.4.

[9.2] Lighthill, M.J. — *Introduction, Real and Ideal Fluids, in Laminar Boundary Layers.* Ed. L. Rosenhead, Oxford University Press, 1963.

[9.3] East, L.F., Hoxey, R.P. — *Boundary Layer Effects in an Idealized Wing-Body Junction at Low Speed.* TR 68161, Royal Aircraft Establishment, July 1968.

[9.4] Shabaka, I.M.M.A. — *A Preliminary Experimental Investigation of Turbulent Flow in a Simplified Wing-Body Junction.* I.C. Aero Report 75-05, Imperial College of Science and Technology, July 1975.

[9.5] Barbar, T.J. — *An Investigation of Strut-Wall Intersection Losses.* J. of Aircraft, Vol. 15, No. 10, October 1978, pp. 676-681.

[9.6] Jacobs, P.P. Jr. — *A Method of Correcting for the Effects of the Side Wall Boundary Layer in Two-dimensional Airfoil Testing.* TM 80-44, The Pennsylvania State University, Applied Research Laboratory, March 1980.

[9.7] Cowley, W.L., McMillan, G.A. — *Pressure Exploration over an Airfoil that Completely Spans a Wind Tunnel.* R. & M. 1597, British Aeronautical Research Committee, 1934.

[9.8] Mendelsohn, R.A., Polhamus, J.F. — *Effects of the Tunnel-Wall Boundary Layer on Test Results of a Wing Protruding from a Tunnel Wall.* NACA TN 1244, April 1947.

[9.9] Bernard-Guelle, R. — *Influence des Conches Limités Latérales de Soufflé dans les Essais Transsoniques en Courant Plan.* 12e Colloque D'aerodynamique Appliquée ENSMA/CEAT — Poitiers, 5-7, novembre 1976.

[9.10] Bernard-Guelle, R., Chevallier, J-P. — *Lateral Boundary Layer Effects on Two-Dimensional Tests.* 48th Semi-Annual Meeting of Supersonic Tunnel Association, Toulouse, 14-15 Sept. 1977.

[9.11] Chan, Y.Y. — *Wall Boundary-Layer Effects in Transonic Wind Tunnels, Symposium on Wall Interference in Wind Tunnel.* AGARD CP-335, London, May 1982.

[9.12] Lighthill, M.J. — *On Displacement Thickness.* Journal of Fluid Mechanics, Vol. 4, 1958, pp. 383-392.

[9.13] Winter, K.G., Smith, J.H.B. — *A Comment on the Origin of Endwall Interference in Wind-Tunnel Tests of Aerofoil.* Tech. Memo. Aero 1816, Royal Aircraft Establishment, August 1979.

[9.14] Barnwell, R.W. — *Similarity Rule for Sidewall Boundary-Layer Effect in Two-Dimensional Wind Tunnels.* AIAA Journal, Vol. 18, No. 9, Sept. 1980, pp. 1149-1150.

[9.15] Sewall, W.G. — *The Effects of Sidewall Boundary Layers in Two-Dimensional Subsonic and Transonic Wind Tunnels.* AIAA Journal, Vol. 20, No. 9, September 1982, pp. 1253-1256.

[9.16] Nash, J.F., Macdonald, A.G.J. — *The Calculation of Momentum Thickness in a Turbulent Boundary Layer at Mach Numbers up to Unity.* CP. 963, British Aeronautical Research Council, 1967.

[9.17] Kemp, W.B. Adcock, J.B. *Combined Four-Wall Interference Assessment in Two-Dimensional Airfoil Tests.* AIAA 82-0586, March 1982.

[9.18] Carrara, J.-M. Masson, A. *Three Years of Operation of the ONERA Pressurized Subsonic Wind Tunnel.* ICAS-80-23.1, Proceedings of 12th Congress of the International Council of the Aeronautical Sciences, October 1980.

[9.19] Ljungström, B.L.G. *Experimental High Lift Optimization of Multiple Element Airfoil.* AGARD CP-143, 1974.

[9.20] Ohman, L.H. Brown, D. *The NAE High Reynolds Number 15 in. × 60 in. Two-Dimensional Test Facility, Part II. Results of Initial Calibration.* Lab. Tech. Rept. LTR-HA-4, National Aeronautical Establishment, Canada, September 1970.

[9.21] McDevitt, J.B. Polek, T.E. Hand, L.A. *A New Facility and Technique for Two-Dimensional Aerodynamic Testing.* AIAA 82-0608, March 1982.

[9.22] Murthy, A.V. Johnson, C.B. Ray, E.J. Lawing, P.L. *Recent Sidewall Boundary Layer Investigations with Suction in the Langley 0.3-m Transonic Cryogenic Tunnel.* AIAA 82-0234, January 1982.

[9.23] Ohman, L.H. *Investigation of the ONERA LC 100D Supercritical Airfoil at High Reynolds Number.* Lab. Tech. Rept. LTR-HA-5X5/0083, National Aeronautical Establishment, March 1976.

[9.24] Chan, Y.Y. *Boundary Layer Controls on the Sidewalls of Wind Tunnels for Two-Dimensional Tests.* J. of Aircraft, Vol. 17, No. 5, May 1980, pp. 380-382.

$$\Delta C_d = \frac{0.000015 C_{do} C_\ell \left(\frac{C_{\ell_\infty}}{C_{\ell_{\infty_0}}} \right)^{1/2}}{\frac{\delta}{c} \left(\frac{t}{c} \right)^4 AR^{1/2}}$$

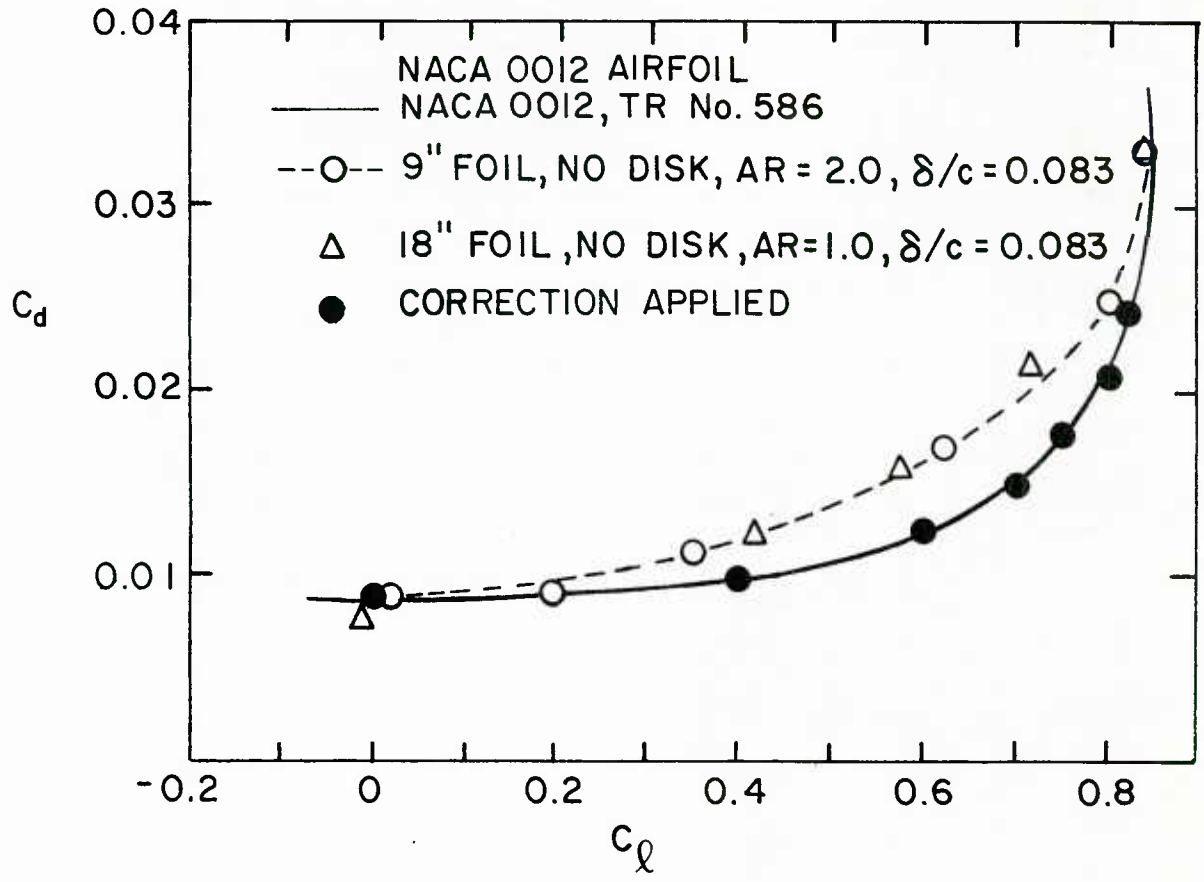

Fig. 9.1 Two-dimensional drag corrected for the airfoil-wall junction vortical flow, Reference [9.6]

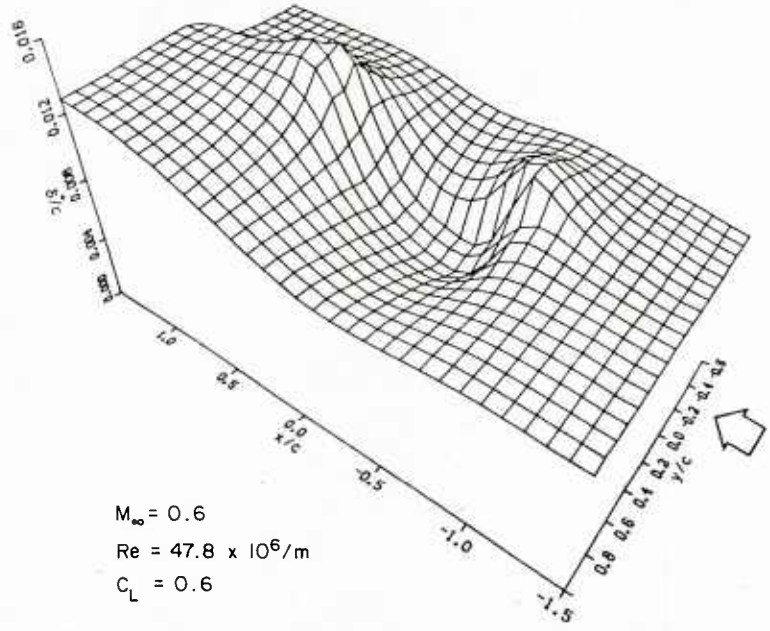

Fig. 9.2 Variation of the sidewall boundary layer displacement thickness over an area influenced by the model pressure field, Reference [9.11]

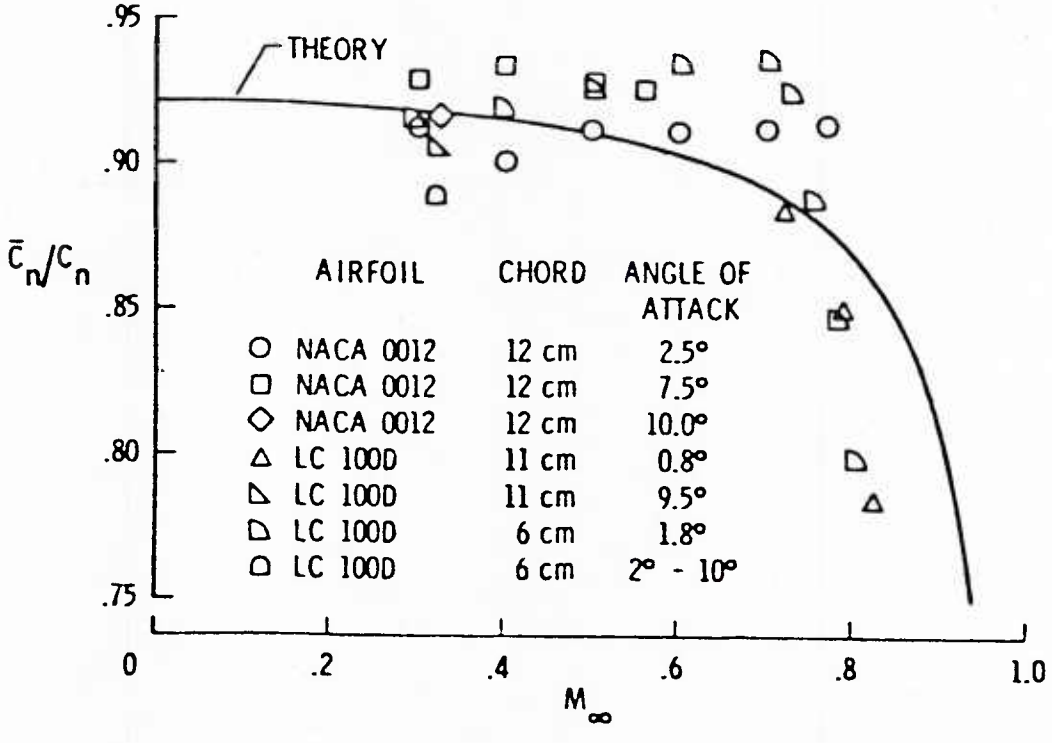

Fig. 9.3 Correlation of normal force coefficients according to the subsonic similarity rule for sidewall boundary layer displacement effects, Reference [9.14]

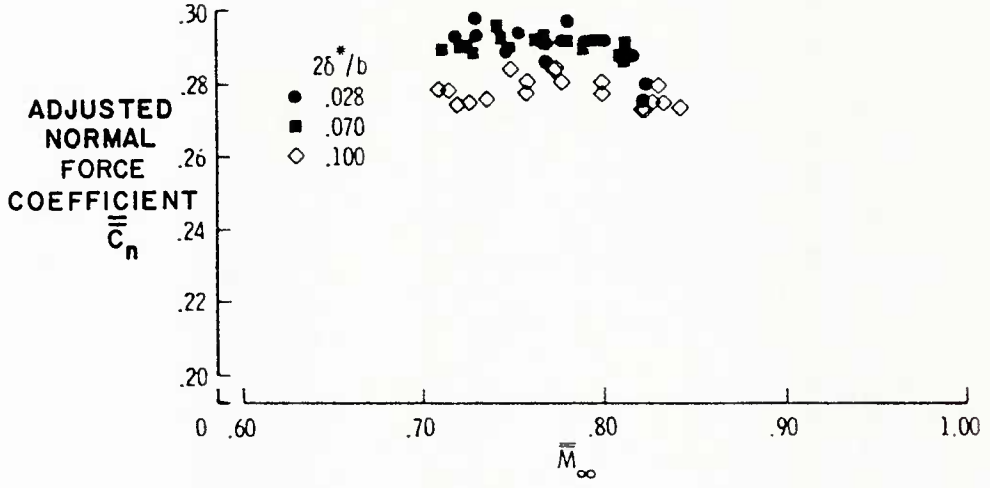

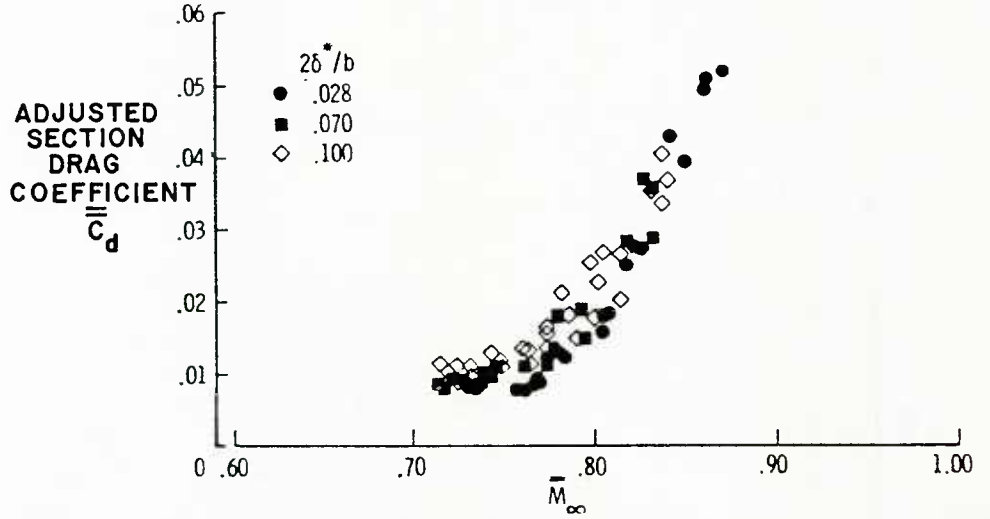

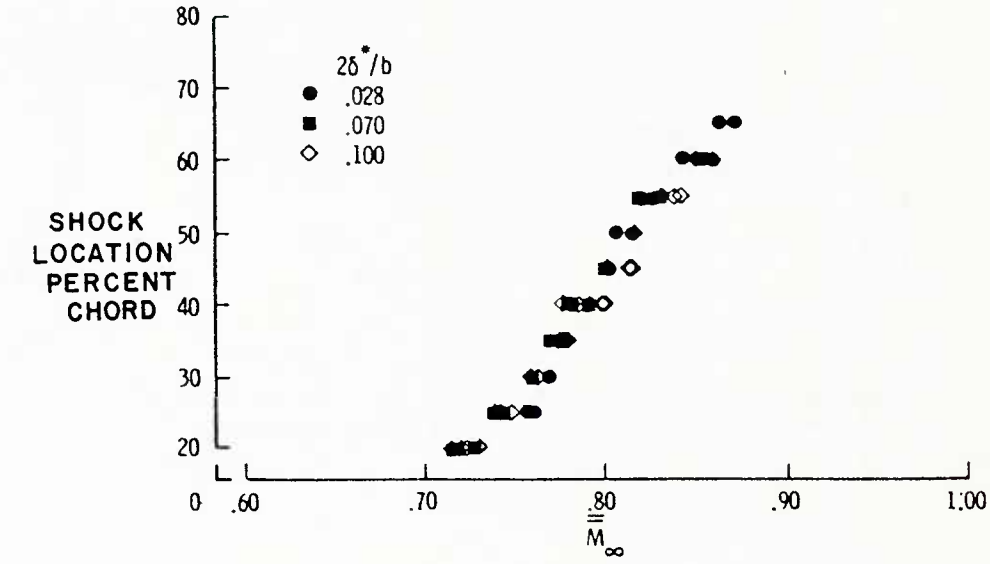

Fig. 9.4 Correlations of normal and drag force coefficients and shock locations according to the transonic similarity rule for sidewall boundary layer displacement effects, Reference [9.15]

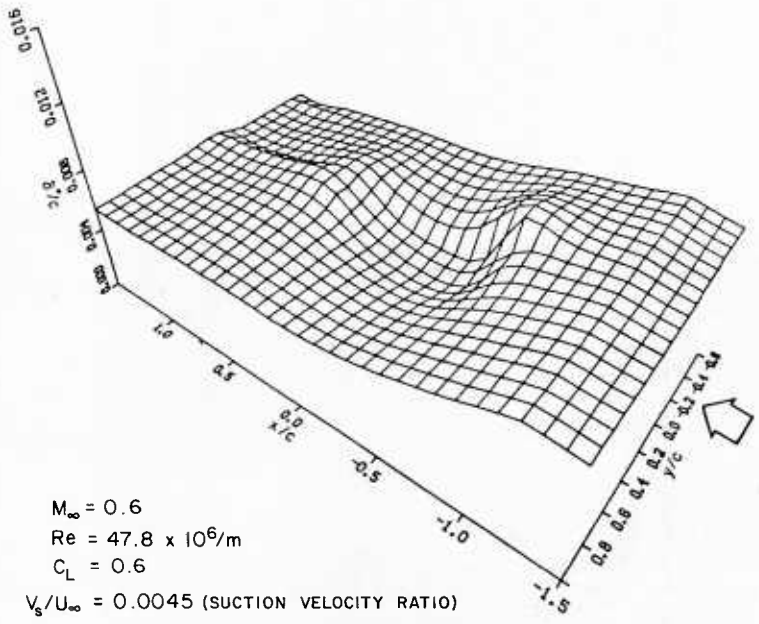

Fig. 9.5 Reduction of displacement thickness variation for sidewall boundary layer with area suction, Reference [9.11]

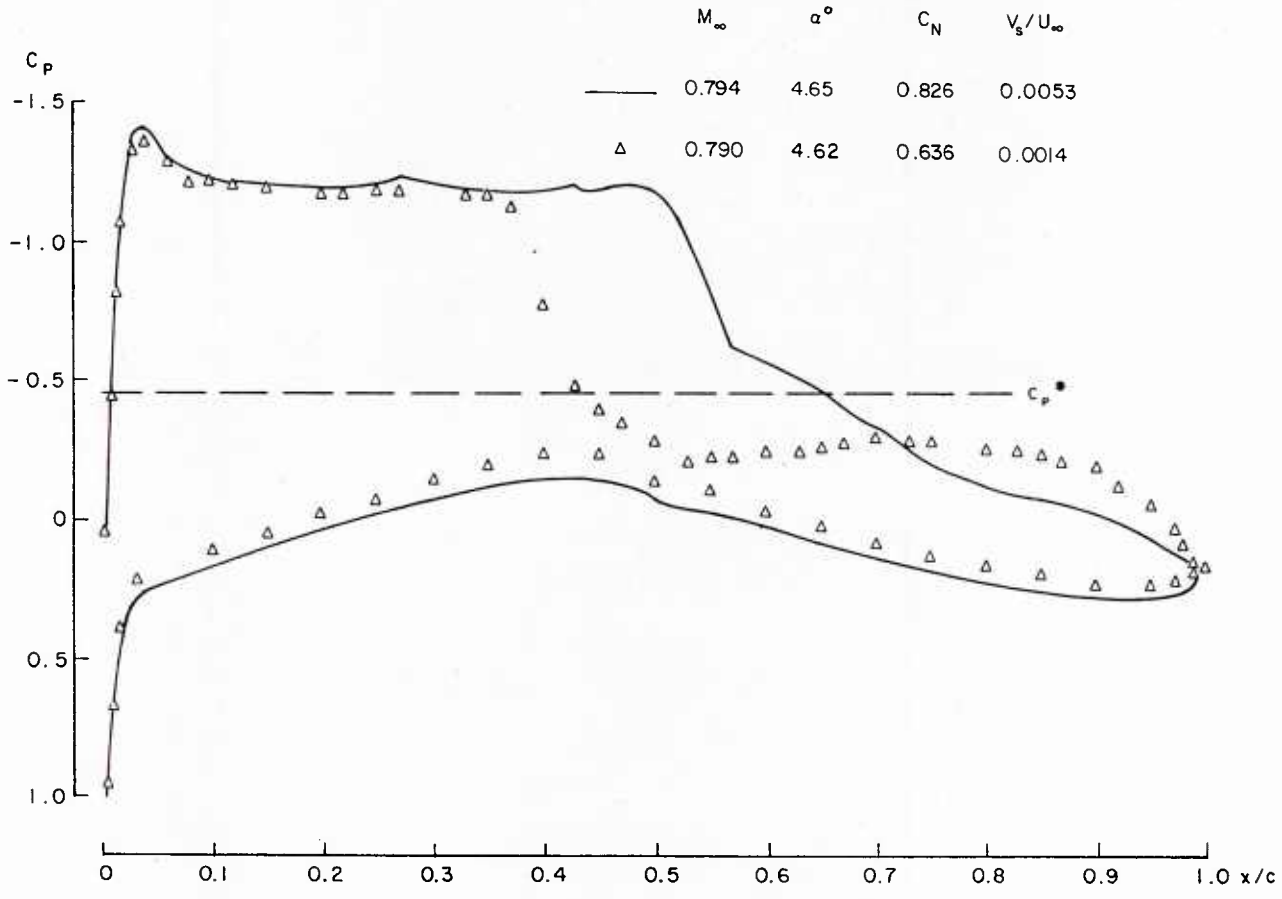

(a) Pressure distribution. Note the rearward shift of the shock and the reduction of separation aft the shock.

Fig. 9.6 Effect of suction on airfoil tests.

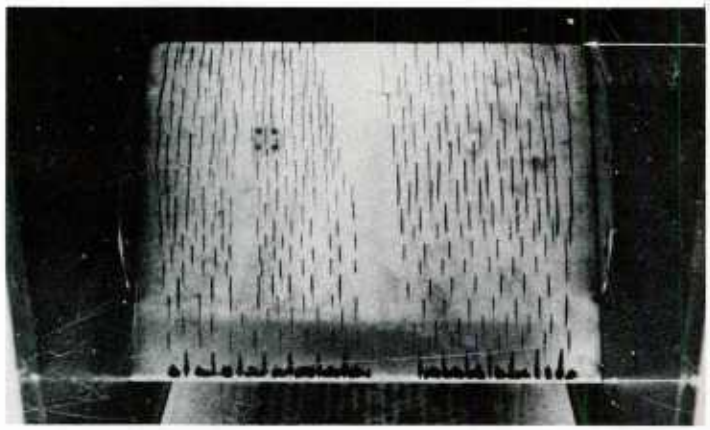

$\frac{V_s}{U_\infty}$ = 0.0053 (ADEQUATE SUCTION)

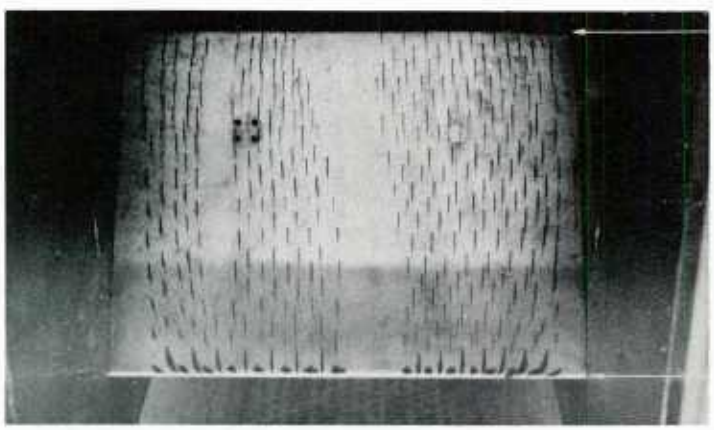

$\frac{V_s}{U_\infty}$ = 0.0014 ("ZERO" SUCTION)

(b) Surface flow visualizations for the upper surface of the airfoil for the cases shown in (a). Note, for the case of "zero" suction the convergence of the streamlines towards the centre of the model over the rear portion.

Fig. 9.6 Effect of suction on airfoil tests.

10.0 WIND TUNNELS WITH ADAPTIVE WALLS

10.1 Introduction

The undesirable effects of wall interference have been a problem as long as there have been wind tunnels. A post-test analysis of measured data and application of corrections are often unsatisfactory, particularly for large models in transonic and high incidence test regimes. In the most severe case, the tunnel flow past the model is distorted to such an extent that the measurement is uncorrectable. In principle, boundary effects can be minimized by testing smaller models in larger tunnels, but reduction of model size reduces test accuracy and Reynolds number and increasing the tunnel dimensions substantially increases the facility cost and power consumption.

A potentially attractive alternative offers the adaptive wall wind tunnel, in which wall interference is either eliminated or significantly reduced by actively controlling flow near the walls. The idea of an accommodating wall to reduce wind tunnel interference is not new. A notable example of the use of compliant tunnel walls is given in Reference [10.1], describing an NPL wind tunnel (1941). However, the early efforts lacked a methology for establishing interference free conditions. In the case of the NPL wind tunnel the setting technique was approximate, setting the contours midway between the straight and the contour giving constant static pressure. Nevertheless, the streamlining operation established an experimental procedure that is followed today, namely that the adjustment of the walls is based on measurements of wall static pressure (representing the streamwise component of disturbance velocity) and the local wall position (determining the flow angle). A revival of the adaptive wall concept is due to Ferri and Baronti [10.2] and Sears [10.3], who realized that interference free testing is feasible with the aid of on-line computers that can continually monitor tunnel flow and control the adjustment of the walls. The major contribution of Ferri and Baronti to adaptive wall technology was their pointing out the need for an iterative adjustment of adaptive walls, aimed at decreasing the differences between the measured flow variables on the tunnel boundary and the computed ones in the simulated tunnel exterior. The flow variables chosen were wall static pressure and flow deflection, in other words the x and y components of the disturbance velocity. Sears proved the correctness of this choice, drawing attention to Hilbert transforms, which for subsonic interference free flow provide the requisite functional relationship between disturbance velocity components on straight line boundaries.

Generally, adaptive (or active) walls fall into two categories: the ventilated walls with crossflow control [10.3] and solid compliant walls with contour control [10.4]. The feasibility of the first approach, using perforated adaptive walls, was established at Calspan [10.5] to [10.8] and, using slotted adaptive walls, at NASA Ames [10.9]. The applicability of the compliant wall approach was demonstrated in the University of Southamption [10.10] to [10.14], ONERA [10.15] and [10.16], and in the Technical University of Berlin [10.17] to [10.19]. Adaptive wall studies have been also pursued in other laboratories and countries, including the Soviet Union [10.20] to [10.25].

The principal objective of the ventilated walls is to allow the stream to cross the test section boundary, to generate a flow pattern resembling the one in unconstrained flow. Airflow through the ventilated wall (perforated or slotted) is regulated by adjusting the pressures in segmented plenum compartments, Figure 10.1, and by variations of the open area ratio. The measured disturbance velocity components are then analyzed to see if they are consistent with the interference free conditions in unconfined flow. If they are not, new values of wall suction and blowing are estimated, and the operation is repeated.

Compliant walls do not require any ventilation, provided that they can be contoured as streamlines in infinite field, Figure 10.2. The interference free criteria are essentially the same as for the ventilated walls, but it is also very easy to simulate the exterior flow past a given wall shape computationally and use the difference between the measured and computed wall pressures as a measure of departure from free stream conditions. The wind tunnel walls are recontoured until the pressure difference is zero all along the wall.

The appeal of solid compliant walls is that the tangent component of velocity can be measured by means of simple wall orifices and the normal component can be obtained from the local slope of the wall. However, the second of these presumed advantages is to some extent illusory, because the wall has a boundary layer and the relationship between the wall slope and the slope of streamlines at the interface (which should be outside this boundary layer) is complicated and generally unknown [10.8]. The measurement of two velocity components in the disturbed environment of ventilated walls poses a difficult technical problem, particularly for routine tunnel testing. However, the advantages of ventilated walls emerge in transonic-supersonic flow regimes, because of their natural ability to accommodate shock waves. Concerning the elimination of wall interference, neither type of the adaptive wall test section is perfect. The major factors influencing the accuracy are the finite length of the test section (truncation), and the finite number of control points (imperfect control). The compliant walls can only be constrained to coincide with streamlines at the positions of the jacks and flow through ventilated walls can only be regulated by adjusting pressures at a few plenum compartments. The error is minimized by closely spacing the jacks or plenum compartments where the velocity variations are largest, that is adjacent to the model.

10.2 Interference Free Conditions

For subcritical flow conditions at the walls, governed by the linearized potential equation

$$\beta^2 \frac{\partial^2 \phi}{\partial x^2} + \frac{\partial^2 \phi}{\partial y^2} = 0 \tag{10.1}$$

the interference free conditions can be stated explicitly, utilizing the properties of analytic functions. We shall introduce the complex co-ordinates of the observation and running points

$$z = \frac{x}{\beta} + iy \quad , \quad \zeta = \frac{\xi}{\beta} + i\eta \tag{10.2}$$

The complex disturbance velocity is

$$w(z) = \beta u(x,y) - iv(x,y) \tag{10.3}$$

where

$$u(x,y) = \frac{\partial \phi}{\partial x}(x,y) \quad , \quad v(x,y) = \frac{\partial \phi}{\partial y}(x,y) \tag{10.4}$$

are the disturbance velocity components. Consider now a simple closed, counter-clockwise oriented contour L which lies entirely in the linearized flow region governed by Equation (10.1), and which divides the plane into the interior region D_i and the exterior region D_e, see Figure 10.3. The absence of outer constraints is equivalent to the condition of analyticity of w in the exterior flow region D_e. If z is a smooth point of the contour L, we have according to the Cauchy integral formula

$$\frac{1}{2} w(z) + \frac{1}{2\pi i} \oint_L \frac{w(\zeta)}{\zeta - z} d\zeta = w(\infty) \quad , \quad z \in L \tag{10.5}$$

where the integral is the Cauchy principal value.

When the disturbance velocity at infinity vanishes, $w(\infty) = 0$, we obtain the interference free condition

$$w_F(z) = -\frac{1}{\pi i} \oint_L \frac{w_F(\zeta)}{\zeta - z} d\zeta \quad , \quad z \in L \tag{10.6}$$

The subscript F indicates the interference free case. Because of the generality of the shape of the contour, Equation (10.6) is applicable to arbitrary tunnel geometries, including the test section with compliant walls.

If the bounding contour consists of two parallel lines at $y = \pm h/2$, the exterior flow region D_e decouples into two half-planes, $y > h/2$ and $y < -h/2$, and Equation (10.6) splits into two separate conditions for top and bottom walls:

$$w_F\left(\frac{x}{\beta} \pm i\frac{h}{2}\right) = \pm\frac{1}{\pi i} \oint_{-\infty}^{\infty} \frac{w_F\left(\frac{\xi}{\beta} + i\frac{h}{2}\right)}{\xi - x} d\xi \tag{10.7}$$

Substituting from Equation (10.3) and separating the real and imaginary parts, we obtain [10.5]

$$v_F\left(x, \pm\frac{h}{2}\right) = \pm\frac{\beta}{\pi} \oint_{-\infty}^{\infty} \frac{u_F\left(\xi, \pm\frac{h}{2}\right)}{\xi - x} d\xi \tag{10.8}$$

$$u_F\left(x, \pm\frac{h}{2}\right) = \mp\frac{1}{\beta\pi} \oint_{-\infty}^{\infty} \frac{v_F\left(\xi, \pm\frac{h}{2}\right)}{\xi - x} d\xi \tag{10.9}$$

which are the compressible-flow versions of the Hilbert transforms (dispersion relations), discussed by Sears [10.3].

Replacing in Equation (10.9) x by $\hat{\xi}$, multiplying each side by

$$\pm\frac{\beta}{\pi}\frac{1}{\hat{\xi} - x}$$

and integrating with respect to $\hat{\xi}$, we obtain with the aid of the Poincaré-Bertrand transposition formula [10.25]

$$\pm\frac{\beta}{\pi} \oint_{-\infty}^{\infty} \frac{u_F\left(\hat{\xi}, \pm\frac{h}{2}\right)}{\hat{\xi} - x} d\hat{\xi} = \pm\frac{\beta}{\pi} \oint_{-\infty}^{\infty} \frac{d\hat{\xi}}{\hat{\xi} - x} \left(\mp\frac{1}{\beta\pi} \oint_{-\infty}^{\infty} \frac{v_F\left(\xi, \pm\frac{h}{2}\right)}{\xi - \hat{\xi}} d\xi \right) = \frac{1}{\pi i} \oint_{-\infty}^{\infty} \frac{d\hat{\xi}}{\hat{\xi} - x} \frac{1}{\pi i} \oint_{-\infty}^{\infty} \frac{v_F\left(\xi, \pm\frac{h}{2}\right)}{\xi - \hat{\xi}} d\xi =$$

$$= v_F\left(x, \pm\frac{h}{2}\right) + \frac{1}{\pi i} \int_{-\infty}^{\infty} v_F\left(\xi, \pm\frac{h}{2}\right) d\xi \frac{1}{\pi i} \int_{-\infty}^{\infty} \frac{d\hat{\xi}}{(\hat{\xi} - x)(\xi - \hat{\xi})}$$

Since the last integral is zero, Equation (10.8) is established. It can be likewise shown that Equation (10.9) follows from (10.8). These important results imply that any one of the Hilbert transforms (10.8) and (10.9) is sufficient for specifying the interference free case.

For the general (simple closed) contour L we obtain, upon substituting Equations (10.2) and (10.3) in (10.6) and separating the real and imaginary parts [10.26],

$$v_F(x,y) = -\frac{\beta}{\pi} \oint_L \frac{\left[(\xi - x)\, u_F(\xi,\eta) - (\eta - y)\, v_F(\xi,\eta)\right] d\xi + \left[\beta^2 (\eta - y)\, u_F(\xi,\eta) + (x - \xi)\, v_F(\xi,\eta)\right] d\eta}{(\xi - x)^2 + \beta^2 (\eta - y)^2} \tag{10.10}$$

$$u_F(x,y) = \frac{1}{\beta\pi} \oint_L \frac{\left[\beta^2 (\eta - y)\, u_F(\xi,\eta) + (\xi - x)\, v_F(\xi,\eta)\right] d\xi - \left[\beta^2 (\xi - x)\, u_F(\xi,\eta) - \beta^2 (\eta - y)\, v_F(\xi,\eta)\right] d\eta}{(\xi - x)^2 + \beta^2 (\eta - y)^2} \tag{10.11}$$

Again, only one of the Equations (10.10) and (10.11) will be needed for specifying the interference free case; the other part will be redundant.

In the operator form, the transform pairs (10.8), (10.9) and (10.10), (10.11) can be written

$$v_F = \mathcal{H}\, u_F \tag{10.12}$$

$$u_F = \mathcal{H}^{-1}\, v_F \tag{10.13}$$

where

$$\mathcal{H}^{-1} = -\frac{1}{\beta^2}\, \mathcal{H}$$

In practice the velocity components will be measured at only a finite number of points along the control contour and the above integral relationships will have to be discretized [10.15], [10.26]. The linear relationship (10.12) becomes

$$\{v_H\} = [H]\, \{u_F\} \tag{10.14}$$

where $\{u_F\}$ is the column vector of the values of u_F at m measurement points, $\{v_H\}$ is the column vector of the transformed velocity component v_H at n measurement points, and $[H]$ is the (n X m) transform matrix. Because of the approximation involved, $\{v_H\}$ is not necessarily equal to the interference free vector $\{v_F\}$. However, it is presumed that in the limit of vanishing distance between measurement points the exact interference free relationship

$$\{v_F\} = [H]\, \{u_F\} \tag{10.15}$$

is established. The inverse relationship is

$$\{u_F\} = -\frac{1}{\beta^2}\, [H]\, \{v_F\} \tag{10.16}$$

In contrast to Equation (10.13) we do not use the symbol $[H]^{-1}$ since the matrix $[H]$ is not necessarily square and its rank is less than n.

Examples of possible errors resulting from the stepwise and linear interpolations of u_F are depicted in Figure 10.4 to 10.7. The upper graphs in the figures show the interference free disturbance velocity components

$$u_F\left(x,\pm\frac{h}{2}\right) = \frac{\partial \phi_F}{\partial x}\left(x,\pm\frac{h}{2}\right) \quad , \quad v_F\left(x,\pm\frac{h}{2}\right) = \frac{\partial \phi_F}{\partial y}\left(x,\pm\frac{h}{2}\right) \tag{10.17}$$

calculated from Equations (4.14) to (4.18) for $M_\infty = 0.0$ and 0.8, and selected singularity strengths σ, γ, μ, and ω. The bottom portions show the interpolated values of u_F (solid lines), the transformed values v_H (symbols), and the theoretical interference free values v_F (broken lines). In Figure 10.4 we see that with 20 control points along each boundary the step interpolation is too crude for determining whether interference free conditions have in fact been established or not. The linear interpolation, Figures 10.5 to 10.7, is far more satisfactory.

These numerical examples are closely related to the problem of the imperfect control of adaptive walls [10.27]. Because of nonzero size and finite number of control elements (plenum compartments, jacks, etc.) and limited number of measurement points (pressure orifices, flow angle probes, etc.), the interference free relationships can be established only approximately. However, interference can be substantially reduced compared to that in conventional, nonadaptive test sections. An adaptive wall wind tunnel with imperfect control can achieve what is, for most practical purposes, interference free flow about the model [10.28].

The linear interference free relationships (10.6) to (10.11) are applicable to supercritical flows past the model, provided that the embedded supersonic regions are not excessive and do not reach the walls. The flow is then nearly parallel to the walls and can be linearized up to very high subsonic Mach numbers. However, if the flow near the walls is distinctly nonlinear, it is appropriate to replace the governing equation (10.1) by the transonic small disturbance equation

$$\beta^2 \frac{\partial^2 \phi}{\partial x^2} + \frac{\partial^2 \phi}{\partial y^2} = M_\infty^2 \frac{\kappa + 1}{U_\infty} \frac{\partial \phi}{\partial x} \frac{\partial^2 \phi}{\partial x^2} \tag{10.18}$$

In this case, the interference free relationships cannot be obtained analytically.

For subcritical flows, where Equation (10.18) is elliptic, the evaluation of interference free relationships entails calculation of the fictitious flowfield exterior to the interface L, with the contour distribution of one of the measured disturbance velocity components prescribed as boundary values [10.8]. The agreement of the remaining velocity component with its computed exterior counterpart indicates interference free flow inside the test section.

For example, for a straight line interface at $y = h/2$ we solve Equation (10.18) in the upper half plane, $y > h/2$, subject to the far field conditions

$$\frac{\partial \phi}{\partial x} \quad , \quad \frac{\partial \phi}{\partial y} \to 0 \qquad \text{as} \qquad \sqrt{x^2 + \beta^2 y^2} \to \infty$$

and the (Neumann) boundary condition

$$\frac{\partial \phi}{\partial y}\left(x, \frac{h}{2}\right) = v\left(x, \frac{h}{2}\right) \qquad , \qquad -\infty < x < \infty$$

The numerical solution can be obtained by finite difference, finite element or other suitable methods; for some interesting theoretical aspects see Reference [10.24].

The resultant disturbance velocity component

$$u_F\left(x, \frac{h}{2}\right) = \frac{\partial \phi}{\partial x}\left(x, \frac{h}{2}\right)$$

gives the interference free counterpart of

$$v_F\left(x, \frac{h}{2}\right) \equiv v\left(x, \frac{h}{2}\right)$$

If the measured value agrees with the computed one,

$$u\left(x, \frac{h}{2}\right) = u_F\left(x, \frac{h}{2}\right) \qquad , \qquad -\infty < x < \infty$$

the interference free flow, as far as the upper interface $y = h/2$ is concerned, is established.

For highly curved compliant walls it is more appropriate to calculate the external flow past the actual wall contour, corrected for the displacement thickness of the boundary layer [10.4], [10.11].

Formally, the obtained (numerical) dependence of v_F on u_F or u_F on v_F can again be written in the operational form (10.12) or (10.13), but of course the (nonlinear) operators $\mathcal{H}$ and $\mathcal{H}^{-1}$ are not known explicitly.

10.3 Iterative Schemes for Achieving Interference Free Conditions

In practice, the disturbance velocity components u and v along the control contour will not comply with the interference free relationships. A simple iterative scheme [10.5] for achieving interference free conditions is readily obtained from Equation (10.12):

$$v^{(j+1)} = (1 - r)\, v^{(j)} + r\, \mathcal{H}\, u^{(j)} \tag{10.19}$$

where r is a relaxation factor on the interval $0 < r < 1$. For linearized subsonic flow and straight line interfaces $y = \pm h/2$, $\mathcal{H}$ is the Hilbert operator [10.29] and

$$\mathcal{H}\, u^{(j)} = \pm \frac{\beta}{\pi} \oint_{-\infty}^{\infty} \frac{u^{(j)}\left(\xi, \pm \frac{h}{2}\right)}{\xi - x}\, d\xi \tag{10.20}$$

The matrix form of the above iterative scheme follows from Equation (10.15):

$$\{v\}^{(j+1)} = (1-r)\{v\}^{(j)} + r\,[H]\,\{u\}^{(j)} \tag{10.21}$$

In the iterative step (j) the walls are adjusted to produce the required $v^{(j)}$. The newly obtained $u^{(j)}$, together with $v^{(j)}$, serves to determine $v^{(j+1)}$ that has to be produced in the wall adjustment step (j+1). The process is continued until (with adequate accuracy)

$$v^{(j+1)} = v^{(j)}$$

From Equation (10.19) then

$$v^{(j)} = \mathcal{H}\, u^{(j)}$$

so that

$$u^{(j)} = u_F \qquad \text{and} \qquad v^{(j)} = v_F$$

An alternative procedure for specifying u instead of v can be similarly devised from Equation (10.13) or (10.16).

As shown by Lo and Kraft [10.30], the subsonic iterative procedure is convergent independently of the initial values $u^{(0)}$ and $v^{(0)}$ and the relaxation factor $0 < r < 1$. However, for a successful application of the method in practice, requiring a small number of wall adjustment steps, the selection of the initial values and the relaxation factor plays an important role.

Of great interest in this connection is the single-step convergence formula, proposed by Lo and Kraft [10.30] for subcritical conditions at the walls and nonlifting flows; the extension to lifting flows is due to Paquet [10.31]. The formula is based on the classical wall interference concept, utilizing the splitting of the complex disturbance velocity

$$w(z) = w_F(z) + w_W(z) \tag{10.22}$$

where w_F is a function analytic in the exterior region D_e and w_W is a function analytic in the interior region D_i, Figure 10.3.

For a smooth point z of the simple closed contour L, according to Cauchy's integral formula

$$\frac{1}{2} w_F(z) + \frac{1}{2\pi i} \oint_L \frac{w_F(\zeta)}{\zeta - z}\, d\zeta = 0 \qquad , \qquad z \in L \tag{10.23}$$

$$-\frac{1}{2} w_W(z) + \frac{1}{2\pi i} \oint_L \frac{w_W(\zeta)}{\zeta - z}\, d\zeta = 0 \qquad , \qquad z \in L \tag{10.24}$$

Adding Equations (10.23) and (10.24) and eliminating w_W from Equation (10.22), we obtain the single-step formula

$$w_F(z) = \frac{1}{2} w(z) - \frac{1}{2\pi i} \oint_L \frac{w(\zeta)}{\zeta - z}\, d\zeta \qquad , \qquad z \in L \tag{10.25}$$

which determines the value of w_F at a contour point z in terms of values of w on the contour.

For the contour consisting of two straight lines at $y = \pm h/2$, we obtain

$$w_F\left(\frac{x}{\beta} \pm i\frac{h}{2}\right) = \frac{1}{2} w\left(\frac{x}{\beta} \pm i\frac{h}{2}\right) \pm \frac{1}{2\pi i} \oint_{-\infty}^{\infty} \frac{w\left(\frac{\xi}{\beta} \pm i\frac{h}{2}\right)}{\xi - x}\, d\xi \mp \frac{1}{2\pi i} \int_{-\infty}^{\infty} \frac{w\left(\frac{\xi}{\beta} \mp i\frac{h}{2}\right)}{\xi - x \mp i\beta h}\, d\xi \tag{10.26}$$

If $w = w_F$, the ordinary integral drops out, according to the Cauchy integral formula for a function analytic in the half-plane, and Equation (10.26) reduces to the interference free relationship (10.7).

Using Equation (10.3) and separating the real and imaginary parts, we obtain

$$v_F\left(x,\pm\frac{h}{2}\right) = \frac{1}{2}\,v\left(x,\pm\frac{h}{2}\right) \pm \frac{\beta}{2\pi}\,\oint_{-\infty}^{\infty} \frac{u\left(\xi,\pm\frac{h}{2}\right)}{\xi - x}\,d\xi$$

$$-\frac{\beta h}{2\pi}\int_{-\infty}^{\infty} \frac{v\left(\xi,\mp\frac{h}{2}\right)}{(\xi - x)^2 + \beta^2 h^2}\,d\xi \mp \frac{\beta}{2\pi}\int_{-\infty}^{\infty} \frac{\xi - x}{(\xi - x)^2 + \beta^2 h^2}\,u\left(\xi,\mp\frac{h}{2}\right)d\xi \qquad (10.27)$$

$$u_F\left(x,\pm\frac{h}{2}\right) = \frac{1}{2}\,u\left(x,\pm\frac{h}{2}\right) \mp \frac{1}{2\pi\beta}\,\oint_{-\infty}^{\infty} \frac{v\left(\xi,\pm\frac{h}{2}\right)}{\xi - x}\,d\xi$$

$$-\frac{\beta h}{2\pi}\int_{-\infty}^{\infty} \frac{u\left(\xi,\mp\frac{h}{2}\right)}{(\xi - x)^2 + \beta^2 h^2}\,d\xi \pm \frac{1}{2\pi\beta}\int_{-\infty}^{\infty} \frac{\xi - x}{(\xi - x)^2 + \beta^2 h^2}\,v\left(\xi,\mp\frac{h}{2}\right)d\xi \qquad (10.28)$$

Equations (10.27) and (10.28) demonstrate that for the case of subsonic flow at the walls the boundary measurement of u and v is sufficient for the determination of the corresponding disturbance velocity components u_F and v_F in free air. It is also seen that u_F and v_F are determined from u and v uniquely, which means that the adjustable walls cannot be manipulated to produce any u_F and v_F satisfying Equations (10.8) and (10.9). For finite size airfoils, where the assumption (10.22) is not exact, each of Equations (10.27) and (10.28) can easily be converted into a new iterative scheme. The left hand side is not considered to be the interference free value, but the new estimate of v or u that has to be established in the next wall adjustment step. When finally $v_F = v$ or $u_F = u$, the interference free relationship (10.8) or (10.9) is established.

The comparison with the iterative scheme (10.19) and (10.20) shows that the first two right-hand side terms of Equation (10.27) can be produced by selecting the relaxation factor $r = 0.5$, the value first proposed by Ferri and Baronti [10.2]. The ordinary integrals of Equation (10.27), which accelerate convergence, cannot be obtained from Equations (10.19) and (10.20). On the other hand, the basic iterative scheme (10.19) is also applicable to supercritical flows near the walls [10.7]. Because the operator $\mathcal{H}$ is nonlinear, the questions of convergence is a difficult one and, besides experimentation, there are no reliable quidelines available as yet concerning the selection of an optimum relaxation factor.

10.4 Initial Setting of Adaptive Walls

So far we have considered the iterative establishing of the components u_F and v_F of the interference free disturbance velocity on the control boundary, ignoring the actual control of the flow parameters at the walls, that must accompany such a procedure. This may appear more or less as an academic exercise, particularly since there is no guarantee there that the available wall control (suction, blowing, open area distribution, wall deflection, etc.) enables the iterative steps leading to interference free flow.

The simplest approach to wall adjustment uses a far field estimation of u_F and v_F and idealized wall boundary conditions. In this case the flow inside the tunnel agrees to within certain accuracy with the unconstrained infinite flow [10.23], [10.24]. The measured boundary velocity components u and v can be analyzed for residual corrections, for example as described in Section 6.5, or used as initial values for the subsequent iterative adjustment of the walls. Chances are that the initial wall setting will bring us close to interference free conditions, so that only a small corrective action will be required to establish them fully. This is of great value for facilities with short run times, where rapid wall adjustment is very essential.

As described in Section 4.1, the subsonic far field of an airfoil in free air can be estimated from Equations (4.14) to (4.18), and a quick assessment of the required ventilated wall adaptation made by substituting in the wall boundary conditions discussed in Chapter 2.

For example, according to Equation (2.23) the required distribution of the porosity parameter along the walls at $y = \pm h/2$ is

$$P_U(x) = -\frac{\frac{\partial \phi_F}{\partial y}\left(x,\frac{h}{2}\right)}{\frac{\partial \phi_F}{\partial x}\left(x,\frac{h}{2}\right)} \quad , \quad P_L(x) = \frac{\frac{\partial \phi_F}{\partial y}\left(x,-\frac{h}{2}\right)}{\frac{\partial \phi_F}{\partial x}\left(x,-\frac{h}{2}\right)} \qquad (10.29)$$

where the subscripts U and L denote the upper and lower walls respectively. The calculated parameters

$$\tau_U(x) = \frac{2}{\pi}\,\mathrm{atan}\,\frac{P_U(x)}{\beta} \quad , \quad \tau_L(x) = \frac{2}{\pi}\,\mathrm{atan}\,\frac{P_L(x)}{\beta} \qquad (10.30)$$

for the earlier used free air case in Figure 10.7a is shown in Figure 10.8a. Admittedly, a suitable distribution of porosity can be used to attenuate certain adverse features of wall interference [10.32], but a complete elimination is impossible, since negative values of the porosity parameter have no physical correspondence.

The slot parameter distributions, required to eliminate interference of longitudinally slotted test section is obtained from Equation (2.40):

$$K_U(x) = -\frac{\frac{\partial \phi_F}{\partial x}\left(x, \frac{h}{2}\right)}{\frac{\partial^2 \phi_F}{\partial x \partial y}\left(x, \frac{h}{2}\right)} \quad , \quad K_L(x) = \frac{\frac{\partial \phi_F}{\partial x}\left(x, -\frac{h}{2}\right)}{\frac{\partial^2 \phi_F}{\partial x \partial y}\left(x, -\frac{h}{2}\right)} \tag{10.31}$$

The calculated parameters

$$\psi_U(x) = \left[1 + \frac{2}{h} K_U(x)\right]^{-1} \quad , \quad \psi_L(x) = \left[1 + \frac{2}{h} K_L(x)\right]^{-1} \tag{10.32}$$

for the same free air case are shown in Figure 10.8b. Because of the presence of the second derivative of ϕ_F in Equations (10.31), the streamwise variations of ψ_U and ψ_L are even more rapid. Again, it is beneficial to vary the slot parameter by suitably shaping the slots [10.33], but it is impossible to eliminate interference completely, since the slot parameter cannot be negative.

Until now it was assumed that the plenum pressure is constant, equal to the undisturbed static pressure of the tunnel stream. The unfavorable situation concerning the elimination of wall interference can be changed by permitting the plenum pressures to vary in the streamwise direction. This essential feature of adaptive test sections with ventilated walls is achieved by subdividing the upper and lower plenum chambers into compartments, where the pressures can be controlled individually [10.3].

For ideal porous walls, some interesting studies were performed by Byrkin and Mezhirov [10.21]; we will here present an illustrative example only. For simplicity, it is assumed that the plenum pressures $p_U(x)$ and $p_L(x)$ can be varied continuously. The upper and lower plenum pressure coefficients are defined as

$$C_{p_U}(x) = 2\frac{\frac{p_U(x)}{p_\infty} - 1}{\kappa M_\infty^2} \quad , \quad C_{p_L}(x) = 2\frac{\frac{p_L(x)}{p_\infty} - 1}{\kappa M_\infty^2} \tag{10.33}$$

where $\kappa = 1.4$ and p_∞ and M_∞ are the reference pressure and Mach number. The only limitation imposed on plenum pressure coefficients is the vacuum condition

$$C_{p_U}(x), \; C_{p_L}(x) > -\frac{2}{\kappa M_\infty^2} \tag{10.34}$$

Provided that the walls are sufficiently open, this, as we shall see, is a relatively mild restriction.

For porous walls, utilizing the boundary condition (2.20) with the constant term given by Equation (2.22), the distributions of upper and lower plenum pressure coefficients needed to eliminate interference are

$$C_{p_U}(x) = -2\left[\frac{\partial \phi_F}{\partial x}\left(x, \frac{h}{2}\right) + \frac{1}{P_U}\frac{\partial \phi_F}{\partial y}\left(x, \frac{h}{2}\right)\right] \quad , \quad C_{p_L}(x) = -2\left[\frac{\partial \phi_F}{\partial x}\left(x, -\frac{h}{2}\right) - \frac{1}{P_L}\frac{\partial \phi_F}{\partial y}\left(x, -\frac{h}{2}\right)\right] \tag{10.35}$$

The porosity parameters P_U and P_L can also be considered to be functions of x. As suggested by Sears [10.3], the variable porosity may be advantageous in regions near the airfoil, where the variations of u and v are most rapid.

Figure 10.9 shows the distributions of the plenum pressure coefficients needed to eliminate wall interference for the same stream Mach number and singularity strengths as used in the variable porosity example in Figure 10.8a. The condition $C_p > -2.23$ following from Equation (10.34) is met for both selected porosity parameters $P_U = P_L = 1.0$ and 0.5. It is seen that the less porous (more resistive) wall requires more pressure regulation. For very low values of the porosity parameters Equations (10.35) indicate that the vacuum condition would be violated and the adjustment for interference free conditions made impossible.

For longitudinally slotted walls the analysis is similar. Using the nonhomogeneous boundary condition (2.39), the plenum pressure coefficient distributions needed to establish interference free flow are

$$C_{p_U}(x) = -2\left[\frac{\partial \phi_F}{\partial x}\left(x, \frac{h}{2}\right) + K_U \frac{\partial^2 \phi_F}{\partial x \partial y}\left(x, \frac{h}{2}\right)\right] \quad , \quad C_{p_L}(x) = -2\left[\frac{\partial \phi_F}{\partial x}\left(x, -\frac{h}{2}\right) - K_L \frac{\partial^2 \phi_F}{\partial x \partial y}\left(x, -\frac{h}{2}\right)\right] \tag{10.36}$$

The slot parameters K_U and K_L can again be considered to be functions of x.

Figure 10.10 shows the plenum pressure coefficients, evaluated for the same free air case as in Figure 10.9. The utilized nondimensional slot parameters are defined as

$$F_U = \frac{2}{h} K_U \quad , \quad F_L = \frac{2}{h} K_L \tag{10.37}$$

For the selected values $F_U = F_L = 0.20$ and 0.40 the plenum pressure regulation is again possible. As in the porous wall case, very low values of open area ratio lead to $K_U, K_L \to \infty$ and the condition (10.34) would then be violated.

From the comparison of Figures 10.9 and 10.10 it appears that the slotted walls do not require pressure regulation over such a large length as the porous walls do. However, since it is not known to what extent the plenum segmentation reduces the transfer of streamwise momentum through the slotted wall, and thus affects the idealized slotted wall boundary condition, this result is only hypothetical.

The initial setting plays an equally important role for solid, compliant walls [10.16]. To construct streamlines for a given free air potential ϕ_F, we can use the simple marching scheme

$$x_{n+1} = x_n + \Delta x_n \quad , \quad y_{n+1} = y_n + \frac{\frac{\partial \phi_F}{\partial y}(x_n, y_n)}{1 + \frac{\partial \phi_F}{\partial x}(x_n, y_n)} \Delta x_n \tag{10.38}$$

where Δx_n is the n th step in the streamwise direction. The limitation of the wall adjustment are mechanical, given by elastic properties of the walls [10.12], and topological, disallowing the wall to cross the airfoil. To hold the airfoil near the centreline of a narrow test section, there should be provision for moving the airfoil vertically with change of angle of attack [10.4].

An example of top and bottom wall deflections δy_U and δy_L is shown in Figure 10.11b. The starting (anchor) points of the streamlines were set at $x/h = -5.0$ and $y/h = \pm\frac{1}{2}$. The wall divergence

$$\frac{\delta y_U - \delta y_L}{h} = \sigma$$

observed far downstream is due to the presence of the source of strength σ in the free air potential ϕ_F. It is also noted that the deflections δy_U and δy_L have nonvanishing slopes at the distances as large as $|x|/h = 5$, which indicates that test sections with solid, compliant walls have to be quite long to provide interference free conditions with a good accuracy [10.11]. The disturbance velocity components u_F and v_F in Figure 10.11a differ slightly from those in Figure 10.7a, since the walls are no longer straight. The initial wall contours can be made more accurate by making an allowance for the boundary layer thickness, estimated from the theoretical wall pressure distributions.

10.5 Linear Control Wind Tunnels

If the wind tunnel can be treated as a linear control system, the interference free condition can be established in a single adjustment step. Linearity is most likely a valid assumption if the walls are already preset (on basis of far field computation, previous test, etc.) and only a small corrective adjustment is required to achieve interference free flow.

Let f denote a general control variable (pressure in the plenum compartment, wall deflection, etc.) and δf its variation. The linear dependence of the disturbance velocity increments δu and δv at m and n measurement points respectively on δf at k control points can be expressed in matrix forms as

$$\{\delta u\} = [U]\{\delta f\} \quad , \quad \{\delta v\} = [V]\{\delta f\} \tag{10.39}$$

where $\{\delta f\}$, $\{\delta u\}$ and $\{\delta v\}$ are the column vectors of the values δf, δu and δv respectively and $[U]$ and $[V]$ are the $(m \times k)$ and $(n \times k)$ influence matrices. A summary of the matrix dimensions is given in the Table below.

column vector	rows × columns	matrix	rows × columns
$\{\delta f\}$	$k \times 1$	$[H]$	$n \times m$
$\{\delta u\}, \{u\}, \{u_F\}$	$m \times 1$	$[U]$	$m \times k$
$\{\delta v\}, \{v\}, \{v_F\}$	$n \times 1$	$[V]$	$n \times k$

Denoting by $\{u\}$ and $\{v\}$ the column vectors of measured x and y disturbance velocity components, the following adjustment is required to obtain interference free flow

$$\{u\} + \{\delta u\} = \{u_F\} \quad , \quad \{v\} + \{\delta v\} = \{v_F\} \tag{10.40}$$

With the help of Equations (10.39)

$$\{u\} + [U]\{\delta f\} = \{u_F\} \quad , \quad \{v\} + [V]\{\delta f\} = \{v_F\}$$

Substituting in the interference free relationship (10.15), we obtain

$$\left([V] - [H][U]\right)\{\delta f\} = [H]\{u\} - \{v\} \tag{10.41}$$

When n = k, Equation (10.41) represents a system of n linear equations for the n unknown values of δf. If further $[V] - [H]\,[U]$ is a nonsingular matrix, we obtain Dowell's formula [10.34]

$$\{\delta f\} = \left([V] - [H]\,[U]\right)^{-1}\left([H]\,\{u\} - \{v\}\right) \tag{10.42}$$

which determines the column vector of the control variable needed to establish interference free conditions.

When the number n of measurement points exceeds the number k of control points (expected condition in practice), Equation (10.41) represents an overdetermined system of linear equations that can be solved only in a least-square or some similar sense.

It is clear that the success of the method depends on the knowledge of the influence matrices $[U]$ and $[V]$. For ventilated walls the natural choice of the control variable is the pressure coefficient in the plenum compartment. As demonstrated by Satyanarayana, Schaier, and Davis [10.9], the influence matrices can be obtained experimentally from the disturbance velocity changes at the measurement points induced by k linearly independent combinations of compartment pressure increments. Because of aerodynamic interactions, this procedure is faster than that of changing the pressure in one plenum compartment at a time while keeping the pressures in other compartments constant. In principle, the measurements leading to influence matrices should be done in the presence of the model and at the given, preadjusted tunnel conditions. The experimental data of Reference [10.9] indicate that in the range of small plenum pressure increments, the velocity changes are indeed almost linear.

For solid compliant walls the best choice of the control variable is the y component of the disturbance velocity, given by the local slope of the wall. In this case

$$[V] = [I]$$

is the unit (identity) matrix and Equation (10.42) becomes

$$\{\delta v\} = \left([I] - [H]\,[U]\right)^{-1}\left([H]\,\{u\} - \{v\}\right) \tag{10.43}$$

The matrix $[U]$, providing now the relationship

$$\{\delta u\} = [U]\,\{\delta v\} \tag{10.44}$$

can be approximated, neglecting the aerodynamic influence of the model, from test section geometry. Using the Fourier transform method, an example for straight line walls and stepwise variations of δv was given by Erickson and Homicz [10.28].

An alternative derivation provides the Cauchy integral formula. We introduce the complex variables (10.2) and the variation of the complex velocity

$$\delta w(z) = \beta\,\delta u(x,y) - i\,\delta v(x,y) \tag{10.45}$$

which is assumed to be analytic in the interior region D_i. For a smooth point z of the contour L then

$$\delta w(z) = \frac{1}{\pi i}\oint_L \frac{\delta w(\zeta)}{\zeta - z}\,d\zeta \qquad , \qquad z \in L \tag{10.46}$$

In particular, for straight line contours at $y = \pm h/2$

$$\delta w\left(\frac{x}{\beta} \pm i\frac{h}{2}\right) = \mp\frac{1}{\pi i}\oint_{-\infty}^{\infty} \frac{\delta w\left(\frac{\xi}{\beta} \pm i\frac{h}{2}\right)}{\xi - x}\,d\xi \pm \frac{1}{\pi i}\int_{-\infty}^{\infty} \frac{\delta w\left(\frac{\xi}{\beta} \mp i\frac{h}{2}\right)}{\xi - x \mp i\beta h}\,d\xi \tag{10.47}$$

Substituting from Equation (10.45) and taking the real part, we obtain

$$\delta u\left(x, \pm\frac{h}{2}\right) - \frac{\beta h}{\pi}\int_{-\infty}^{\infty} \frac{\delta u\left(\xi, \mp\frac{h}{2}\right)}{(\xi - x)^2 + \beta^2 h^2}\,d\xi$$

$$= \pm\frac{1}{\beta\pi}\left[\oint_{-\infty}^{\infty} \frac{\delta v\left(\xi, \pm\frac{h}{2}\right)}{\xi - x}\,d\xi - \int_{-\infty}^{\infty} \frac{\xi - x}{(\xi - x)^2 + \beta^2 h^2}\,\delta v\left(\xi, \mp\frac{h}{2}\right)\,d\xi\right] \tag{10.48}$$

which can be further discretized to yield the required linear dependence (10.44).

This simple result, together with the control formula (10.43), is suitable for solid compliant walls if they are only mildly curved, or straight ventilated walls if it is known how to set up any desired normal velocity distributions along the walls by varying plenum pressures. Empirical formulae of the type described in Reference [10.28] might be helpful, but it should be also remembered that, in general, the plenum pressure affects both δu and δv in a coupled fashion.

REFERENCES

[10.1] Lock, C.N.H.; Beavan, J.A. *Tunnel Interference at Compressibility Speeds Using Flexible Walls of the Rectangular High Speed Tunnel.* British ARC R.&M. 2005, 1944.

[10.2] Ferri, A.; Baronti, P. *A Method for Transonic Wind Tunnel Corrections.* AIAA Journal, Vol. 11, 1973, pp. 63-66.

[10.3] Sears, W.R. *Self-Correcting Wind Tunnels.* (The Sixteenth Lanchester Memorial Lecture) Aeronautical Journal, Vol. 78, 1974, pp. 80-89.

[10.4] Goodyer, M.J. *The Self Streamlining Wind Tunnel.* NASA TM X-72699, Aug. 1975.

[10.5] Erickson, J.C.; Nenni, J.P. *A Numerical Demonstration of the Establishment of Unconfined-Flow Conditions in a Self-Correcting Wind Tunnel.* RK-5070-A-1, Calspan Corp., Nov. 1973.

[10.6] Vidal, R.J.; Catlin, P.A.; Chudyk, D.W. *Two-Dimensional Subsonic Experiments With an NACA 0012 Airfoil.* RK-5070-A-3, Calspan Corp., Dec. 1973.

[10.7] Vidal, R.J.; Erickson, J.C.; Catlin, P.A. *Experiments with a Self-Correcting Wind Tunnel.* Wind Tunnel Design and Testing Techniques, AGARD-CP-174, Oct. 1975, pp. 11.1-11.13.

[10.8] Sears, W.R.; Vidal, R.J.; Erickson, J.C.; Ritter, A. *Interference-Free Wind Tunnel Flows by Adaptive-Wall Technology.* ICAS Paper No. 76-02, Oct. 1976; also Journal of Aircraft, Vol. 14, 1977, pp. 1042-1050.

[10.9] Satyanarayana, B.; Schairer, E.; Davis, S. *Adaptive-Wall Wind-Tunnel Development for Transonic Testing.* Journal of Aircraft, Vol. 18, 1980, pp. 273-279.

[10.10] Goodyer, M.J. *A Low Speed Self Streamlining Wind Tunnel.* Wind Tunnel Design and Testing Techniques, AGARD-CP-174, Oct. 1975, pp. 13.1-13.8.

[10.11] Judd, M.; Wolf, S.W.D.; Goodyer, M.J. *Analytical Work in Support of the Design and Operation of Two Dimensional Self Streamlining Test Sections.* NASA CR 145019, 1976.

[10.12] Wolf, S.W.D.; Goodyer, M.J. *Self Streamlining Wind Tunnel — Low Speed Testing and Transonic Test Section Design.* NASA CR 145257, Oct. 1977.

[10.13] Wolf, S.W.D.; Goodyer, M.J. *Studies of Self Streamlining Wind Tunnel Real and Imaginary Flows.* NASA CR 158831, Aug. 1979.

[10.14] Wolf, S.W.D.; Cook, I.D.; Goodyer, M.J. *The Status of Two- and Three-Dimensional Testing in the University of Southampton Transonic Self-Streamlining Wind Tunnel.* AGARD-CP-335, Wall Interference in Wind Tunnels, May 1982, pp. 15.1-15.14.

[10.15] Chevallier, J.P. *Soufflerie transsonique à parois auto-adaptables.* Wind Tunnel Design and Testing Techniques, AGARD-CP-174, Oct. 1975, pp. 12.1-12.8.

[10.16] Archambaud, J.P.; Chevallier, J.P. *Utilisation de parois adaptables pour les essais en courant plan.* AGARD-CP-335, Wall Interference in Wind Tunnels, May 1982, pp. 14.1-14.14.

[10.17] Ganzer, U. *Windkanäle mit adaptiven Wänden zur Beseitigung von Wandinterferenzen.* Zetschrift Flugwiss. Weltraumforsch., Vol. 3, 1979, pp. 129-133.

[10.18] Ganzer, U. *Adaptable Wind Tunnel Walls for 2-D and 3-D Model Tests.* ICAS Paper No. 80-23.3, Oct. 1980.

[10.19] Ganzer, U. *On the Use of Adaptive Walls for Transonic Wind Tunnel Testing.* AGARD-CP-335, Wall Interference in Wind Tunnels, May 1982, pp. 13.1-13.8.

[10.20] Sychev, V.V.; Fonarev, A.S. *Bezinduktsionnye aerodinamicheskie truby dlia transzvukovych issledovanii.* Uchenye zapiski TsAGI, Vol. 6, 1975, pp. 1-14.

[10.21] Byrkin, A.P.; Mezhirov, I.I. *K probleme induktsii pronitsaemykh stenok rabochei chasti aerodinamicheskoi truby malykh skorostei.* Uchenye zapiski TsAGI, Vol. 9, 1978, pp. 11-20.

[10.22] Fonarev, A.S. *Induktsia stenok transzvukovych trub i puti ee umen'shenia.* Uchenye zapiski TsAGI, Vol. 10, 1979, pp. 1-15.

[10.23] Sayadian, K.G.; Fonarev, A.S. *O maloinduktsionnych rezhimach obtekania profilei i tel vrashchenia v transzvukovych trubach.* Uchenye zapiski TsAGI, Vol. 12, 1981, pp. 51-61.

[10.24] Fonarev, A.S. Sherstyuk, A.V. *Algorithms and Methods for Computer Simulation of Transonic Flow.* Transl. from Avtomatika i Telemekhanika, No. 7, July 1982, pp. 5-18.

[10.25] Gakhov, F.D. *Boundary Value Problems.* Pergamon Press, 1966.

[10.26] Everhart, J.L. *A Method for Modifying Two-Dimensional Adaptive Wind Tunnel Walls Including Analytical and Experimental Verification.* NASA TP-2081, Feb. 1983.

[10.27] Sears, W.R. *Adaptive Wind Tunnels with Imperfect Control.* Journal of Aircraft, Vol. 16, 1979, pp. 344-348.

[10.28] Erickson, J.C. Homicz, G.F. *Numerical Simulations of a Segmented-Plenum, Perforated, Adaptive-Wall Wind Tunnel.* AIAA Journal, Vol. 20, 1982, pp. 612-623.

[10.29] Sneddon, I.N. *The Use of Integral Transforms.* McGraw-Hill, 1972, pp. 233-238.

[10.30] Lo, C.F. Kraft, M. *Convergence of the Adaptive-Wall Wind Tunnel.* AIAA Journal, Vol. 16, 1978, pp. 67-72.

[10.31] Paquet, J.B. *Perturbations induites par les parois d'une soufflerie, méthodes intégrales.* Thèse Doc. Ing., Université de Lille, juin 1979.

[10.32] Lo, C.F. *Wind-Tunnel Wall Interference Reduction by Streamwise Porosity Distribution.* AIAA Journal, Vol. 10, 1972, pp. 547-550.

[10.33] Berndt, S.B. *Flow Properties of Slotted-Wall Test Sections.* AGARD-CP-335, Wall Interference in Wind Tunnels, May 1982, pp. 6.1-6.7.

[10.34] Dowell, E.H. *Control Laws for Adaptive Wind Tunnels.* AIAA Journal, Vol. 19, 1981, pp. 1486-1488.

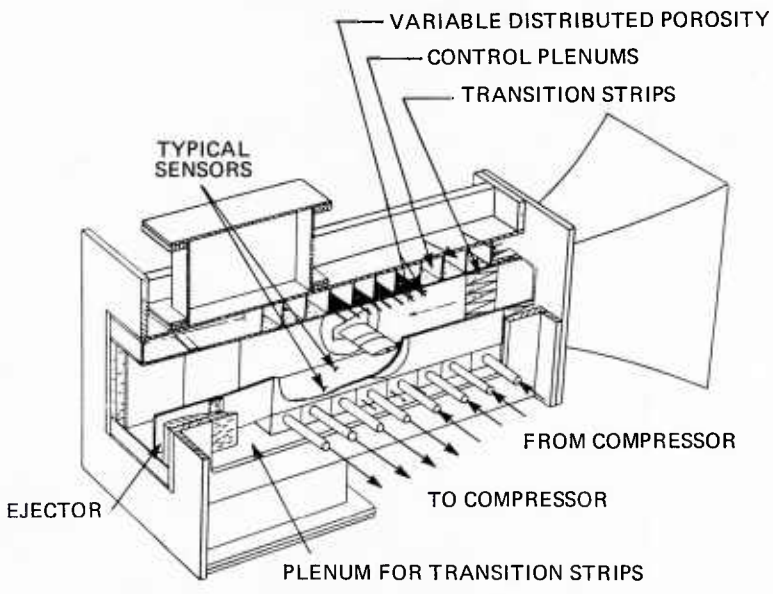

Fig. 10.1 Calspan adaptive test section with porous walls, Reference [10.3]

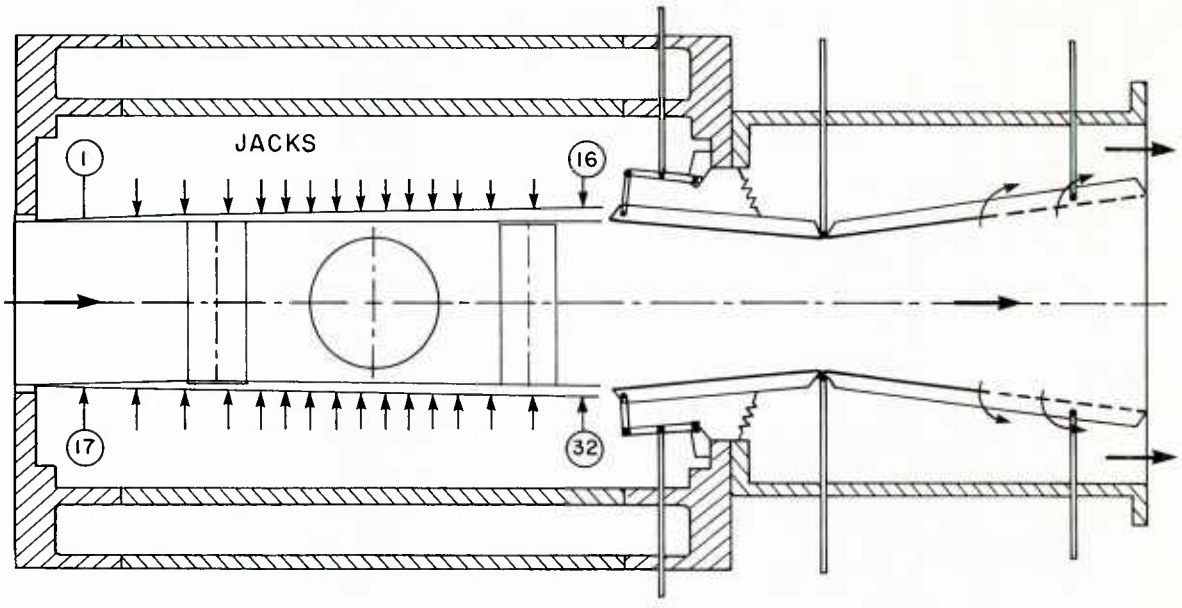

Fig. 10.2 ONERA adaptive test section with compliant walls, Reference [10.16]

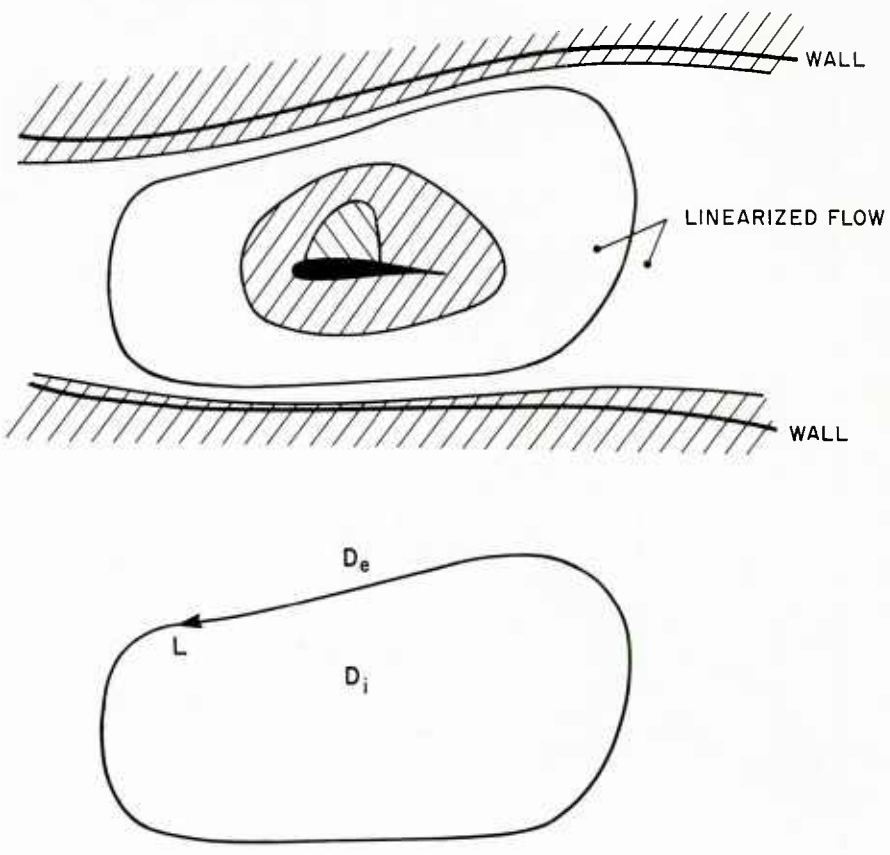

Fig. 10.3 Interior and exterior flow regions

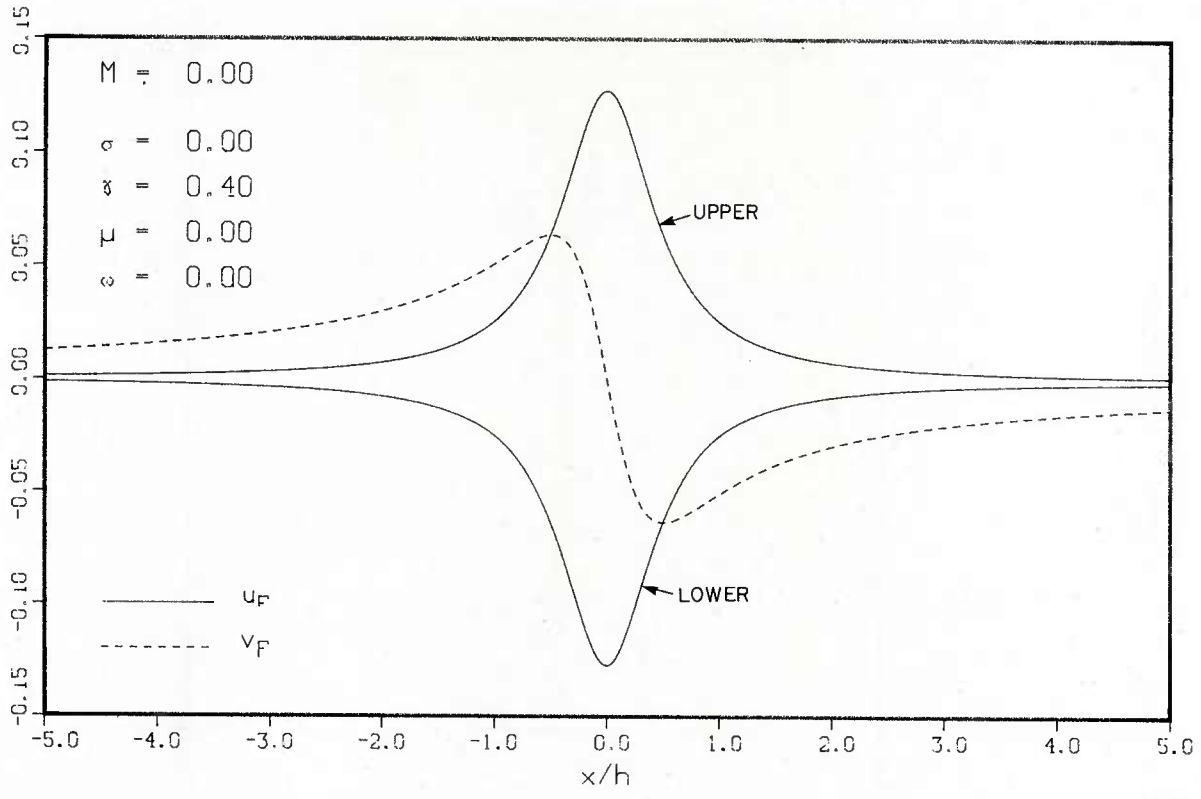

Fig. 10.4a Free air disturbance velocity components u_F and v_F at y/h = ± 0.5 for a point vortex in incompressible flow

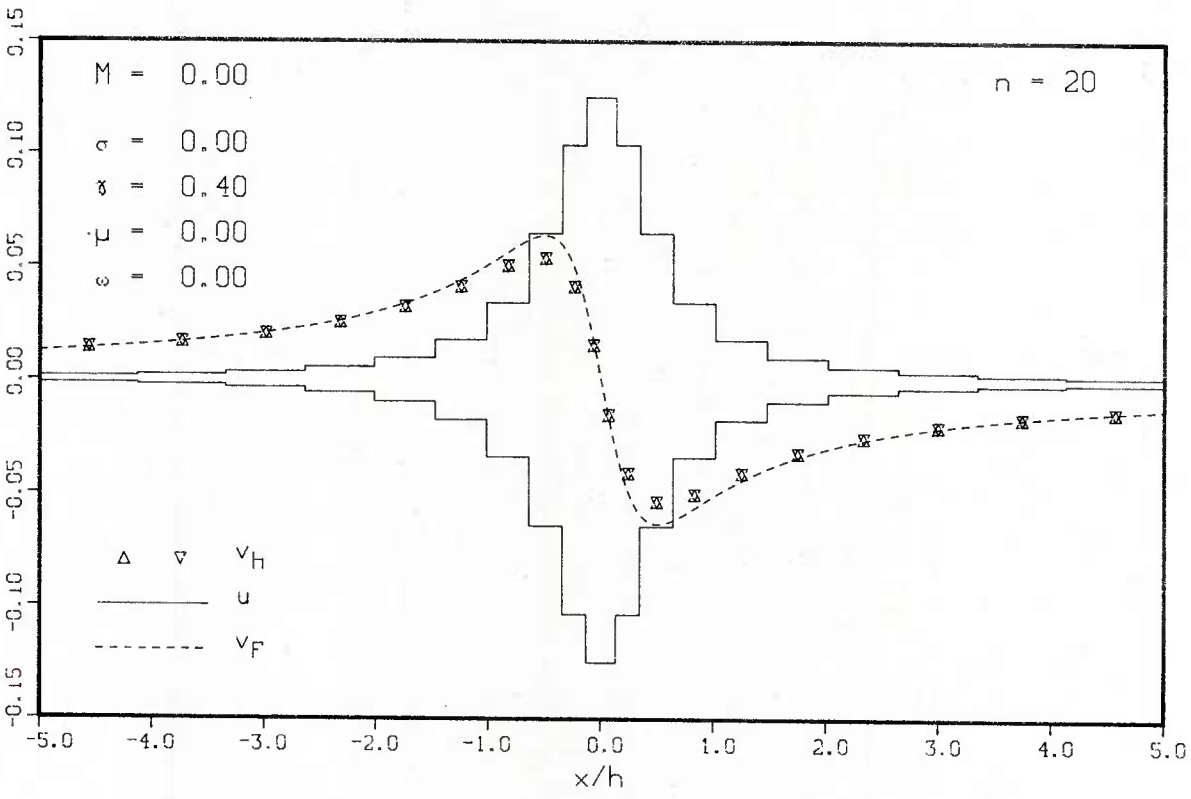

Fig. 10.4b Transformed velocity component v_H, evaluated from stepwise interpolated component u_F

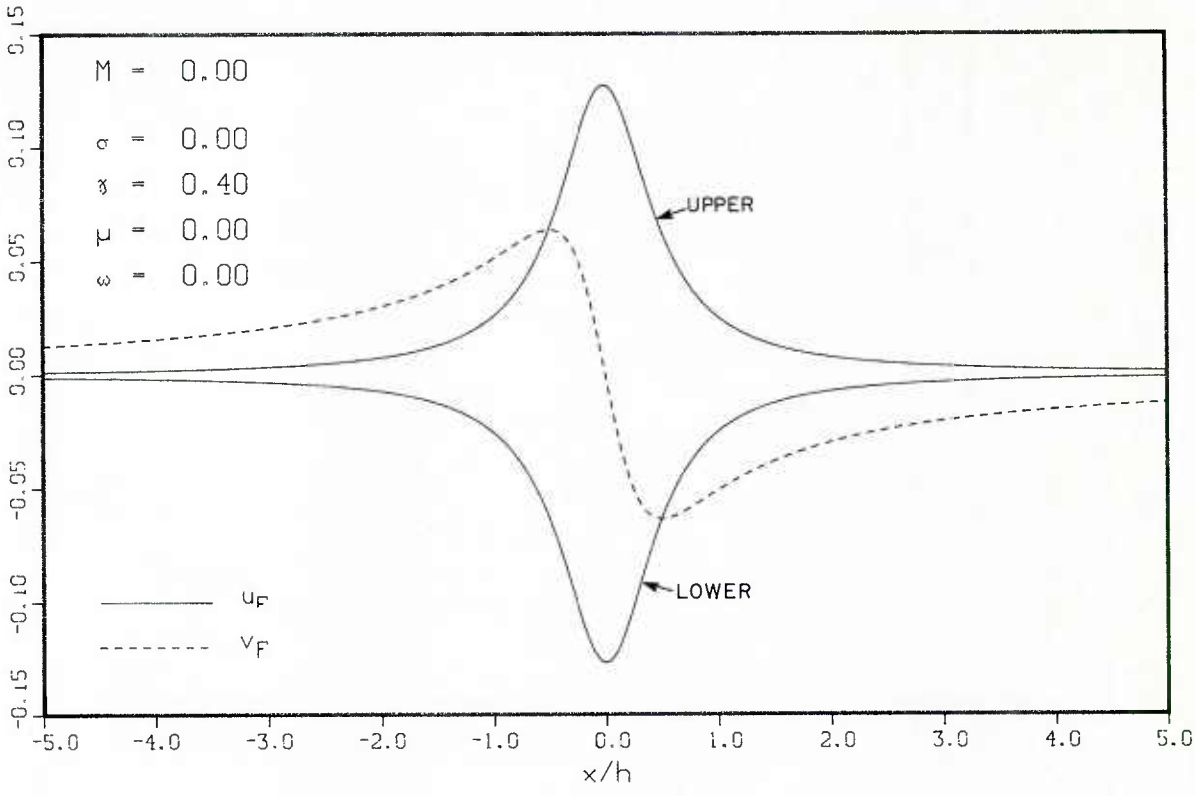

Fig. 10.5a Free air disturbance velocity components u_F and v_F at $y/h = \pm 0.5$ for a point vortex in incompressible flow

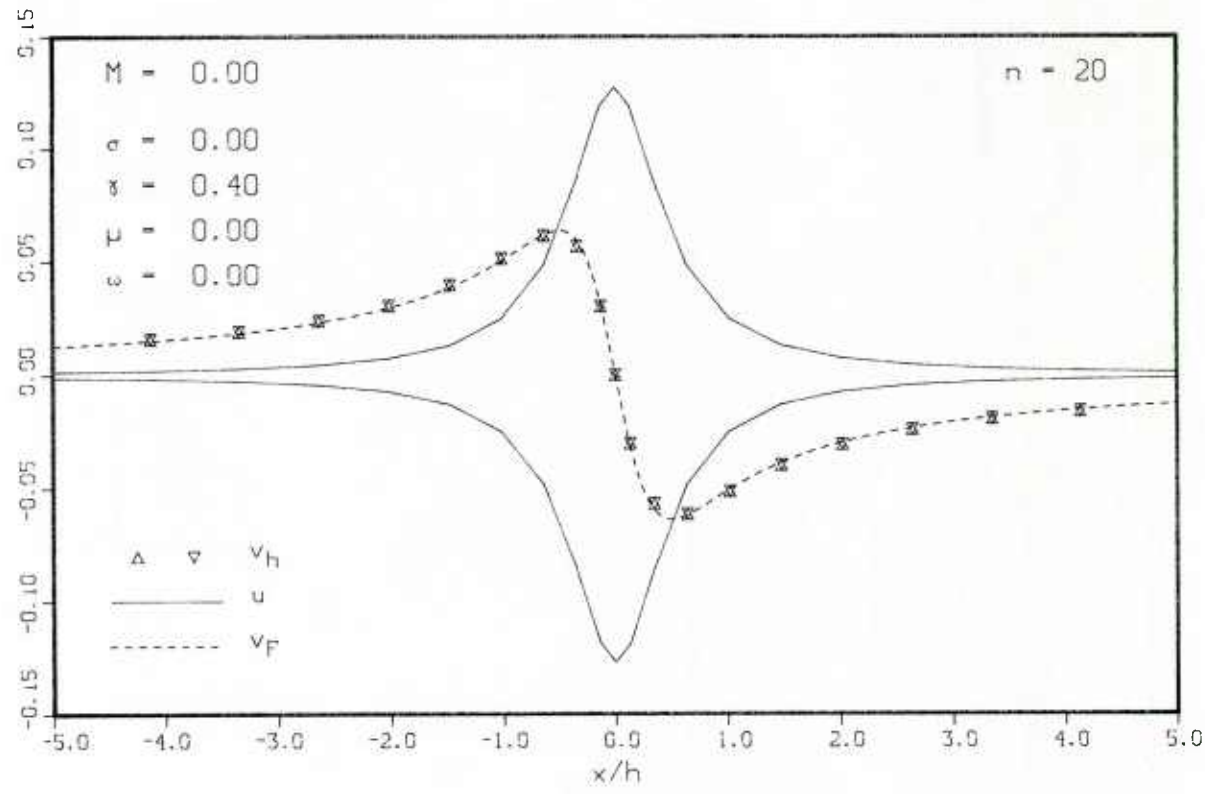

Fig. 10.5b Transformed velocity component v_H, evaluated from linearly interpolated component u_F

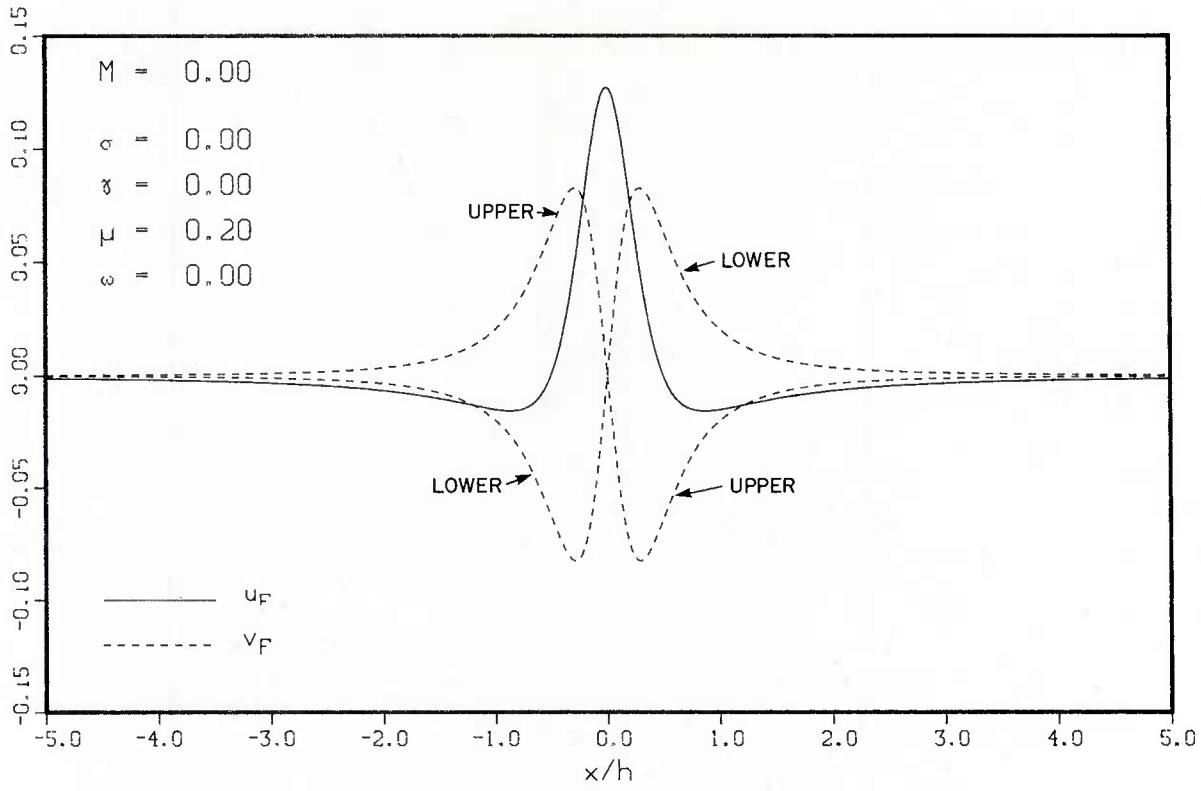

Fig. 10.6a Free air disturbance velocity components u_F and v_F at y/h = ± 0.5 for a doublet in incompressible flow

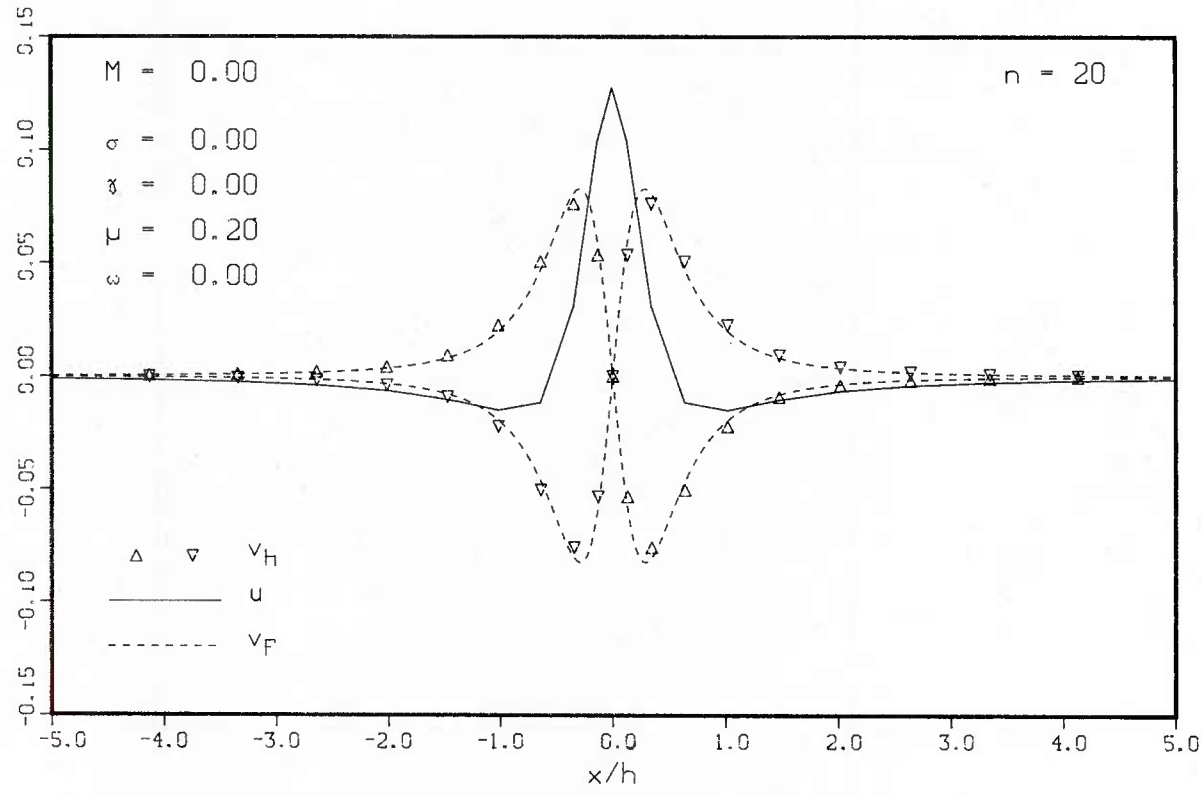

Fig. 10.6b Transformed velocity component v_H, evaluated from linearly interpolated component u_F

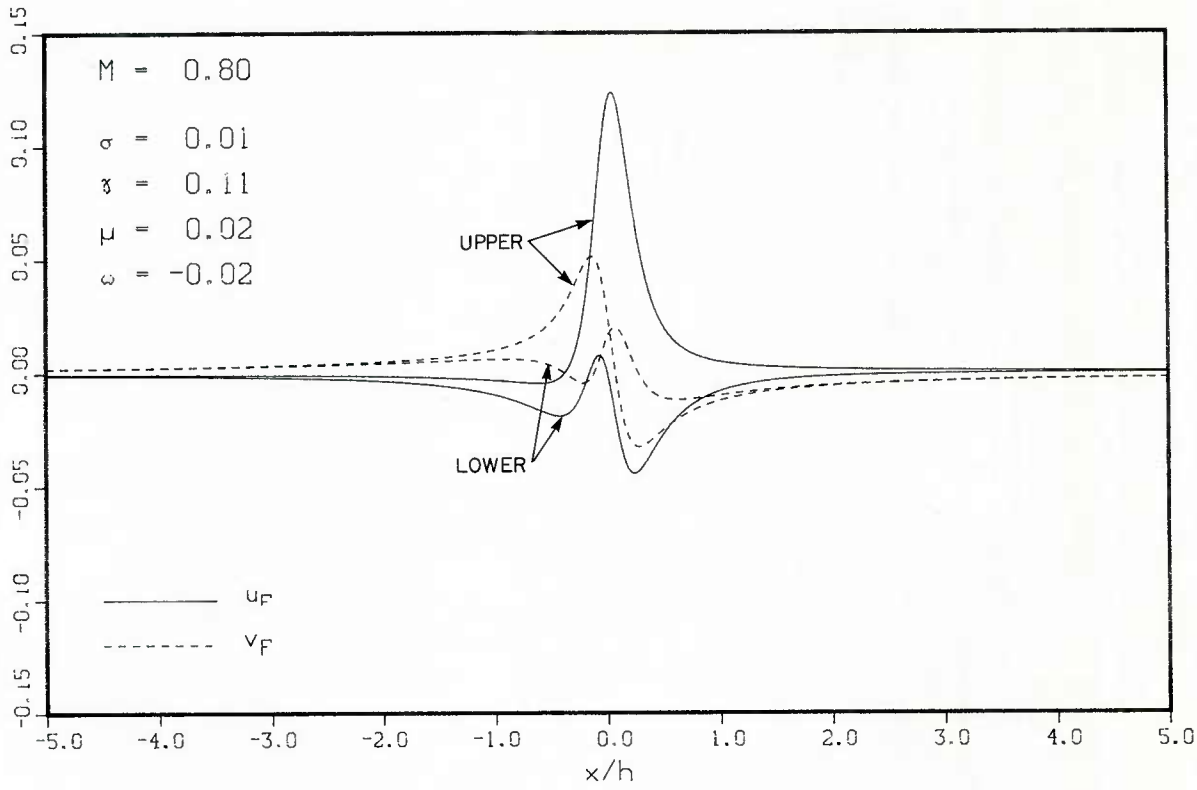

Fig. 10.7a Free air disturbance velocity components u_F and v_F at y/h = ± 0.5 for a source-vortex-doublet combination in compressible flow

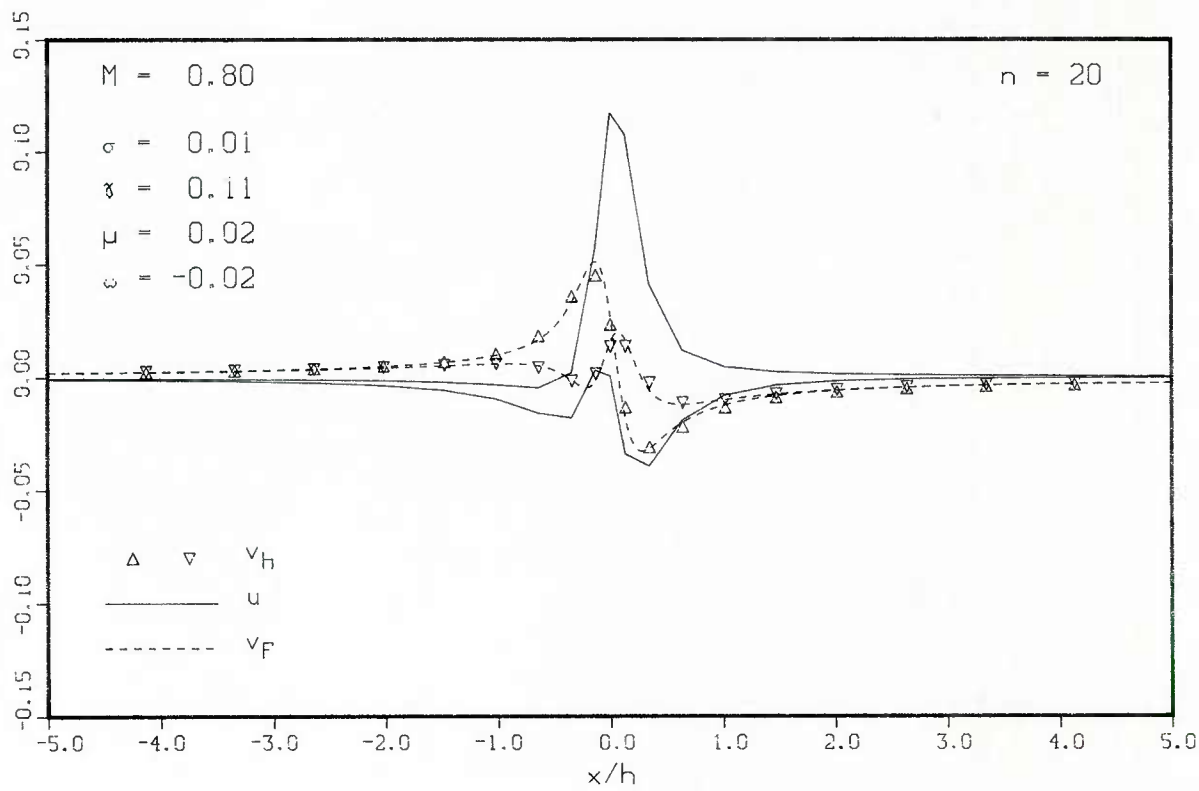

Fig. 10.7b Transformed velocity component v_H, evaluated from linearly interpolated component u_F

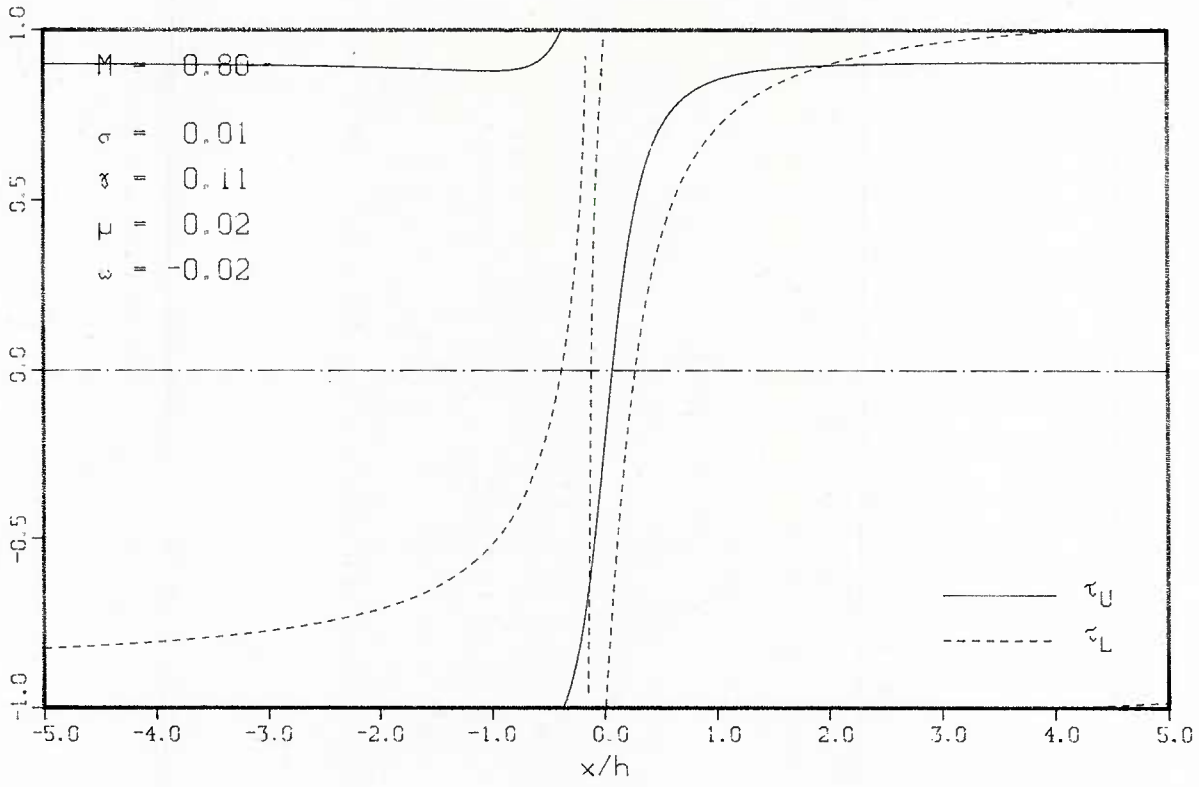

Fig. 10.8a Distribution of upper and lower wall porosity parameters for elimination of wall interference

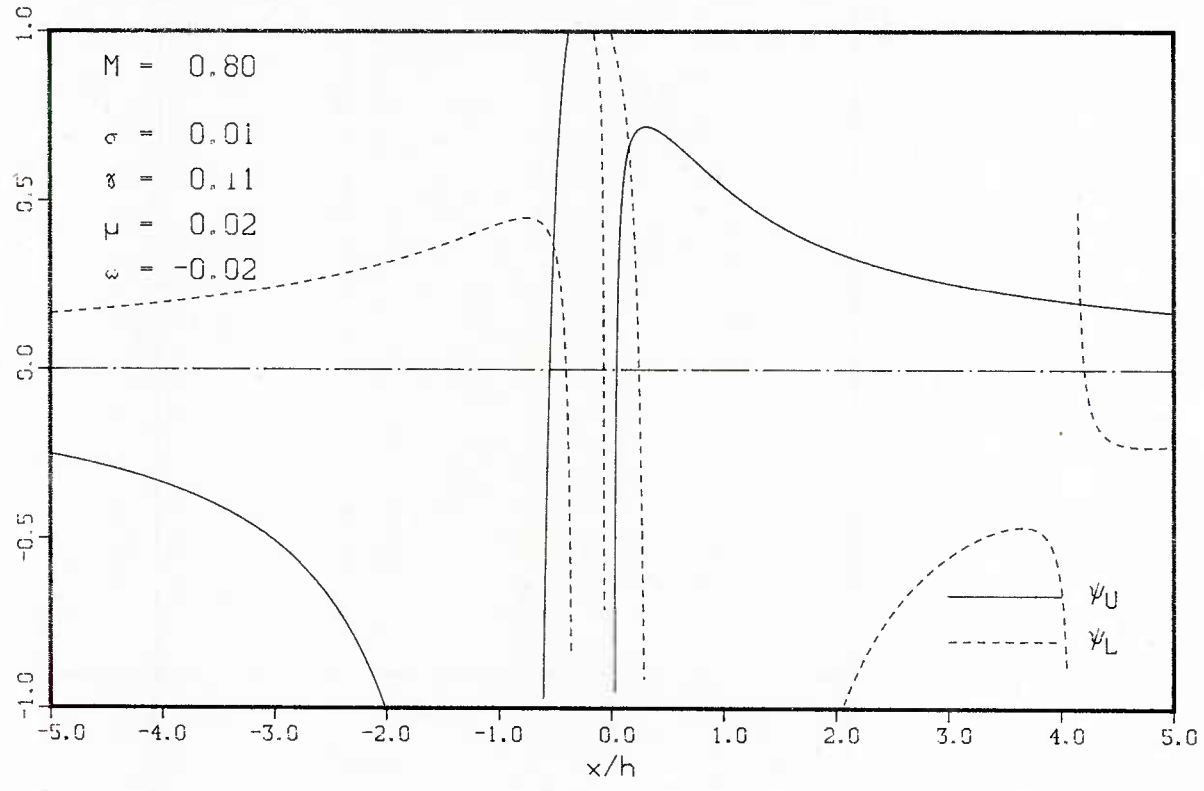

Fig. 10.8b Distribution of upper and lower wall slot parameters for elimination of wall interference

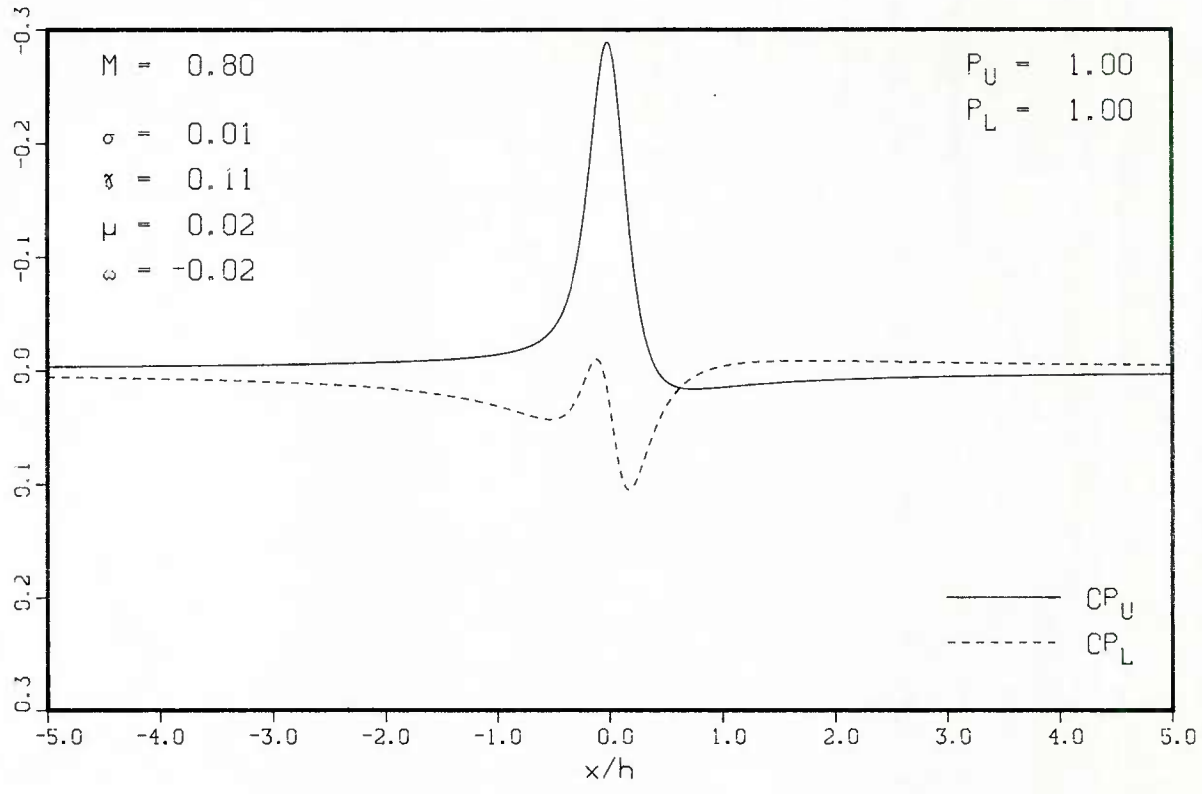

a) more open wall

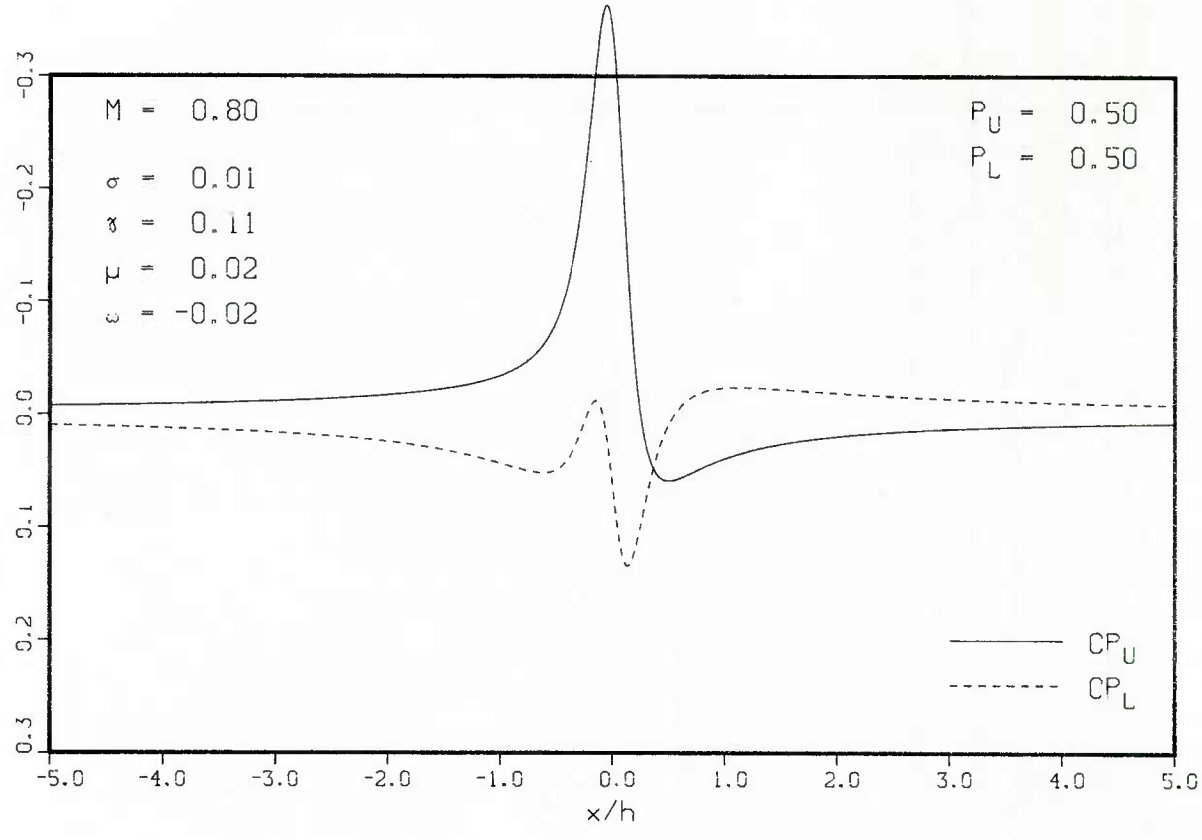

b) less open wall

Fig. 10.9 Distribution of upper and lower plenum pressure coefficients for elimination of porous wall interference

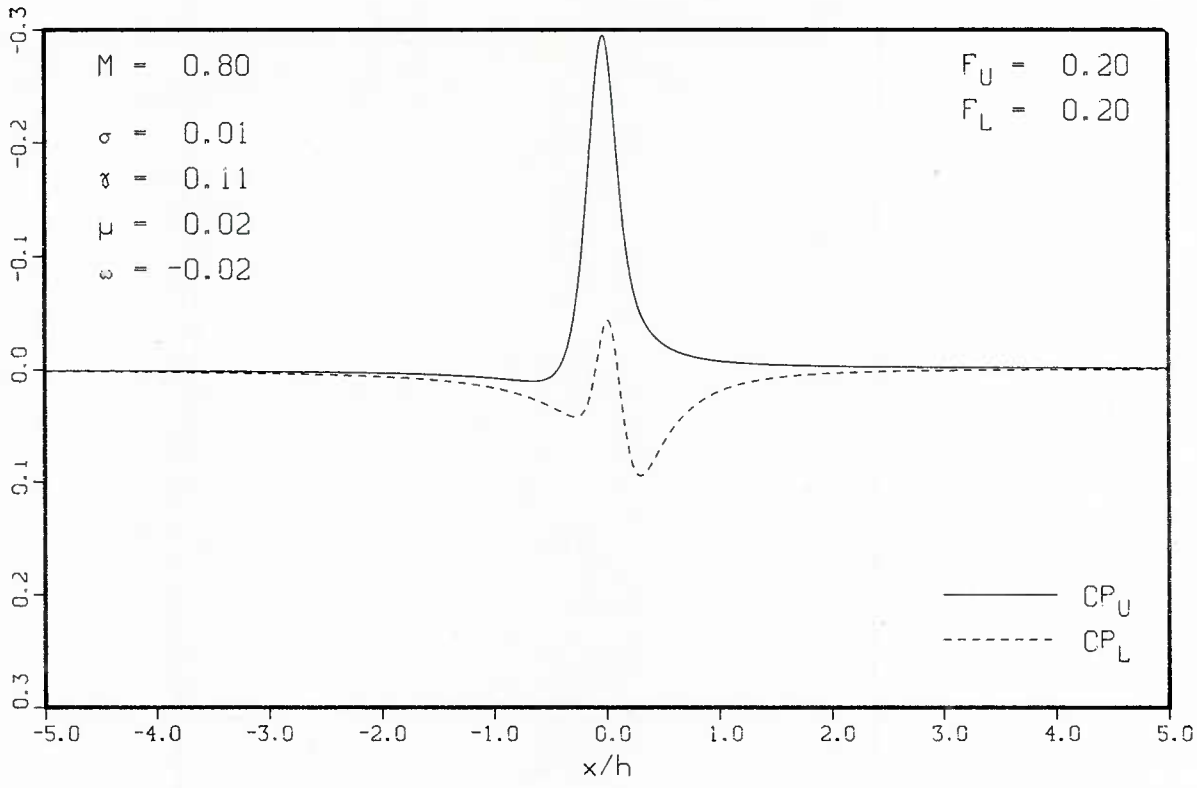

a) more open

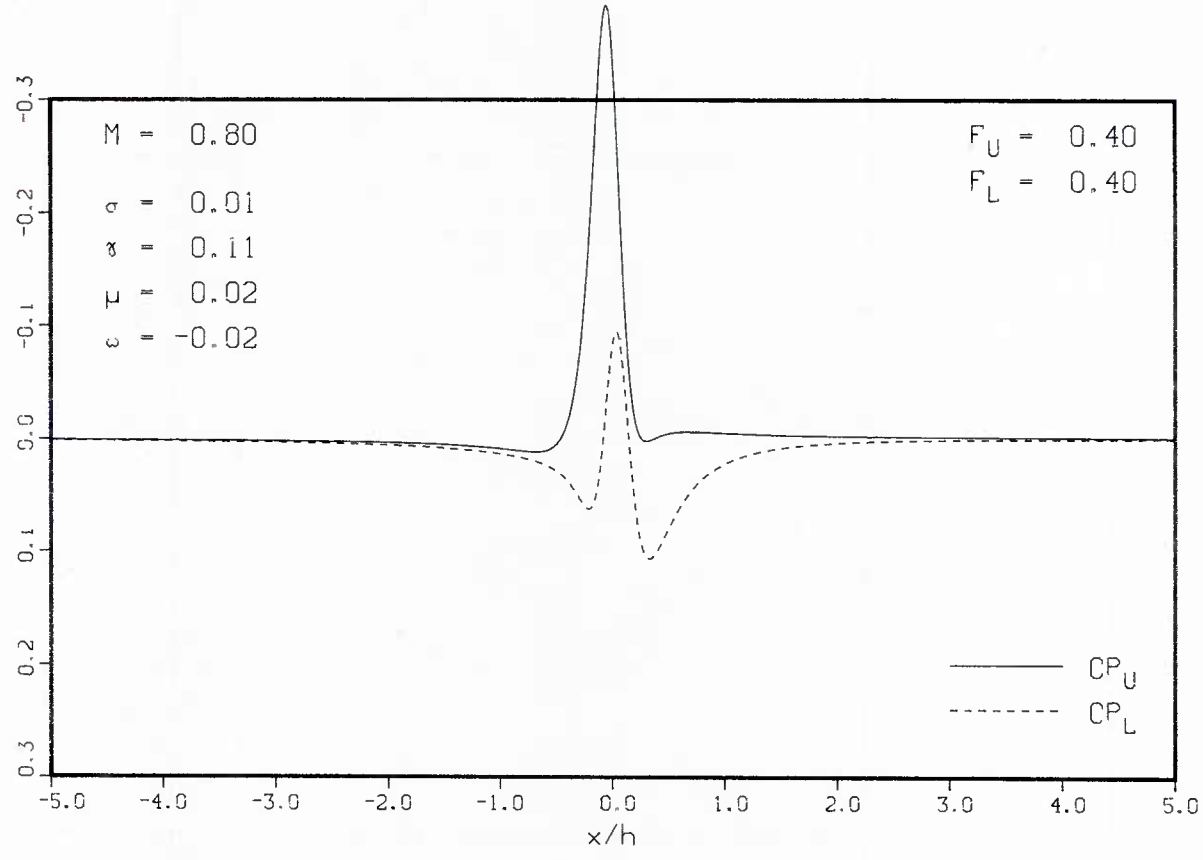

b) less open

Fig. 10.10 Distribution of upper and lower plenum pressure coefficients for elimination of slotted wall interference

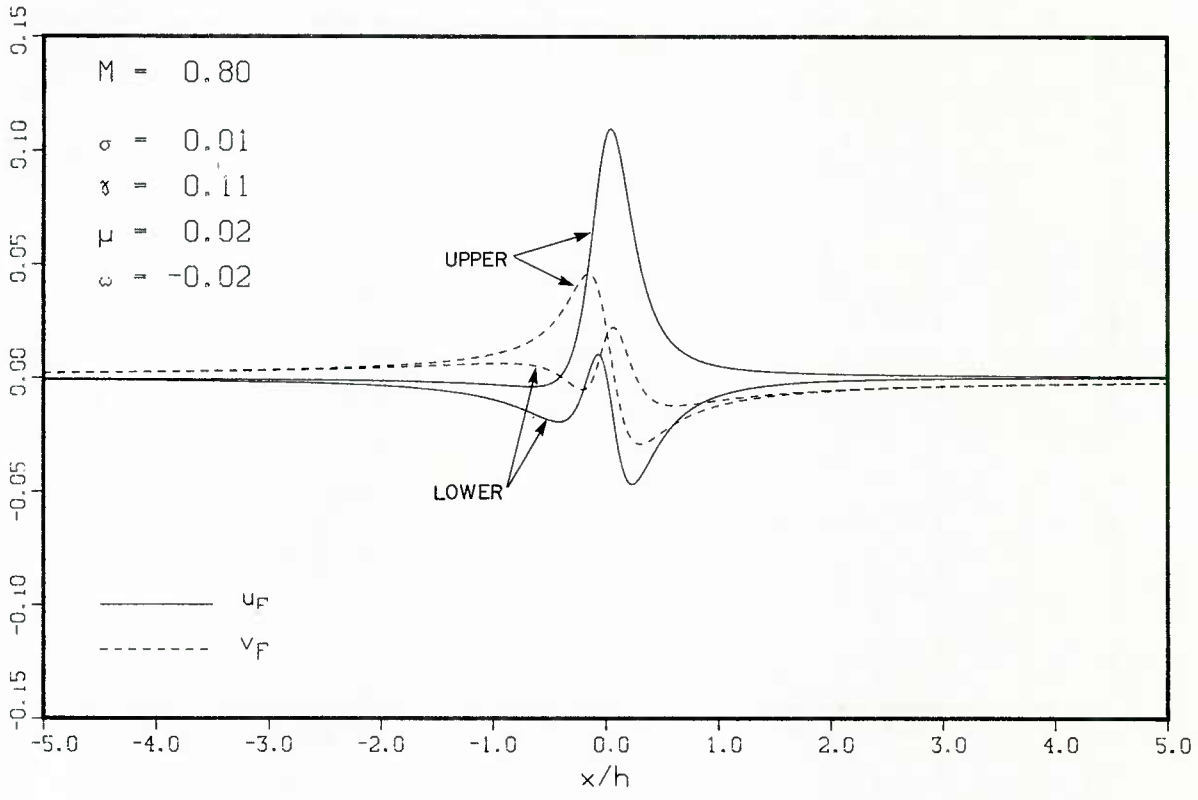

Fig. 10.11a Free air disturbance velocity components u_F and v_F along upper and lower streamlines for a source-vortex-doublet combination in compressible flow

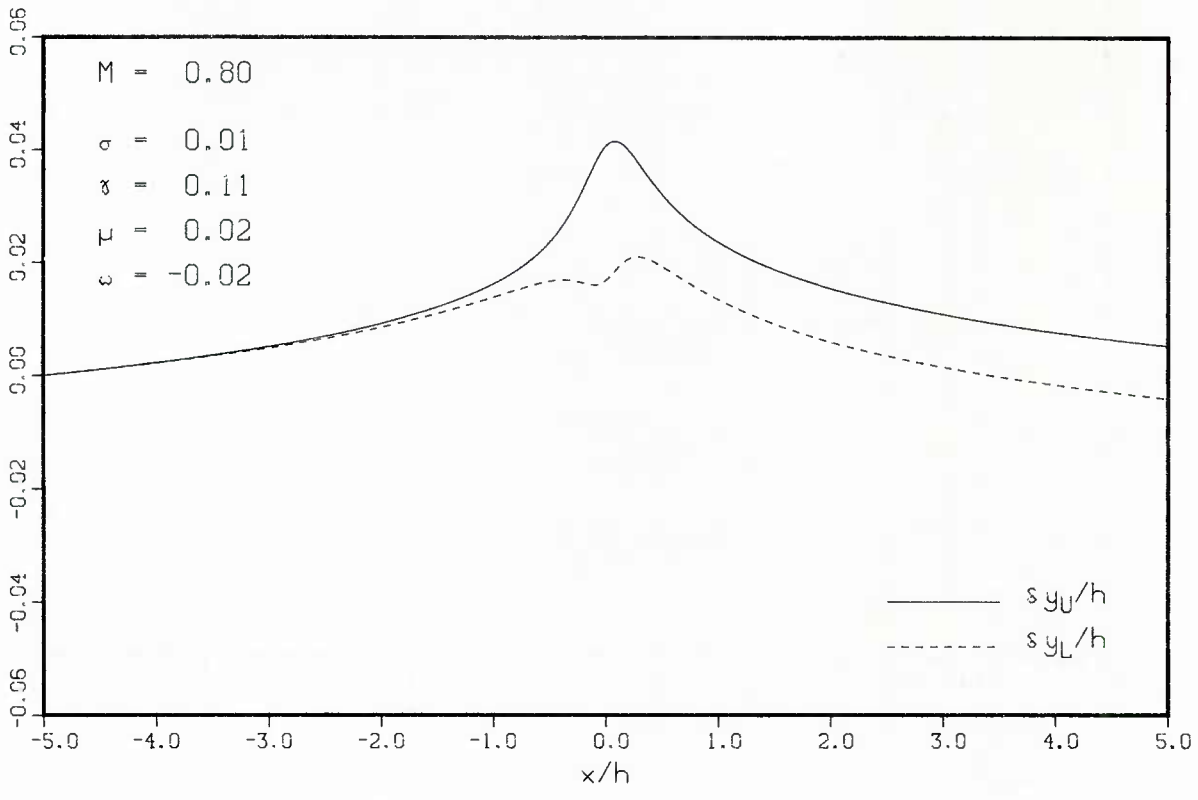

Fig. 10.11b Relative deflections of upper and lower walls for elimination of wall interference

AGARDograph No.281
Advisory Group for Aerospace Research and Development, NATO
TWO-DIMENSIONAL WIND TUNNEL WALL INTERFERENCE
by M.Mokry, Y.Y.Chan and D.J.Jones
Published November 1983
194 pages

A description and analysis is presented of the more important developments during the past decade in the understanding of the wall interference problem associated with two-dimensional wind tunnel testing at subsonic and transonic speeds. Discussed are wall boundary conditions, asymptotic analysis of wall interference, classical and extended wall interference,

P.T.O

AGARD-AG-281

Wind tunnels
Subsonic flow
Transonic flow
Walls
Aerodynamic interference
Aerodynamics

AGARDograph No.281
Advisory Group for Aerospace Research and Development, NATO
TWO-DIMENSIONAL WIND TUNNEL WALL INTERFERENCE
by M.Mokry, Y.Y.Chan and D.J.Jones
Published November 1983
194 pages

A description and analysis is presented of the more important developments during the past decade in the understanding of the wall interference problem associated with two-dimensional wind tunnel testing at subsonic and transonic speeds. Discussed are wall boundary conditions, asymptotic analysis of wall interference, classical and extended wall interference,

P.T.O

AGARD-AG-281

Wind tunnels
Subsonic flow
Transonic flow
Walls
Aerodynamic interference
Aerodynamics

AGARDograph No.281
Advisory Group for Aerospace Research and Development, NATO
TWO-DIMENSIONAL WIND TUNNEL WALL INTERFERENCE
by M.Mokry, Y.Y.Chan and D.J.Jones
Published November 1983
194 pages

A description and analysis is presented of the more important developments during the past decade in the understanding of the wall interference problem associated with two-dimensional wind tunnel testing at subsonic and transonic speeds. Discussed are wall boundary conditions, asymptotic analysis of wall interference, classical and extended wall interference,

P.T.O

AGARD-AG-281

Wind tunnels
Subsonic flow
Transonic flow
Walls
Aerodynamic interference
Aerodynamics

AGARDograph No.281
Advisory Group for Aerospace Research and Development, NATO
TWO-DIMENSIONAL WIND TUNNEL WALL INTERFERENCE
by M.Mokry, Y.Y.Chan and D.J.Jones
Published November 1983
194 pages

A description and analysis is presented of the more important developments during the past decade in the understanding of the wall interference problem associated with two-dimensional wind tunnel testing at subsonic and transonic speeds. Discussed are wall boundary conditions, asymptotic analysis of wall interference, classical and extended wall interference,

P.T.O

AGARD-AG-281

Wind tunnels
Subsonic flow
Transonic flow
Walls
Aerodynamic interference
Aerodynamics

theories, wall interference corrections from boundary measurements, integral equation formulation of subcritical wall interference, and effects of side wall boundary layer on two-dimensional tests. Unsteady wall interference at subsonic and supersonic flow conditions is reviewed. Recent advances in the adaptive wall technique, which actively reduces or eliminates wall interference, are also described.

This AGARDograph has been produced at the request of the Fluid Dynamics Panel of AGARD.

ISBN 92-835-1463-7

theories, wall interference corrections from boundary measurements, integral equation formulation of subcritical wall interference, and effects of side wall boundary layer on two-dimensional tests. Unsteady wall interference at subsonic and supersonic flow conditions is reviewed. Recent advances in the adaptive wall technique, which actively reduces or eliminates wall interference, are also described.

This AGARDograph has been produced at the request of the Fluid Dynamics Panel of AGARD.

ISBN 92-835-1463-7

theories, wall interference corrections from boundary measurements, integral equation formulation of subcritical wall interference, and effects of side wall boundary layer on two-dimensional tests. Unsteady wall interference at subsonic and supersonic flow conditions is reviewed. Recent advances in the adaptive wall technique, which actively reduces or eliminates wall interference, are also described.

This AGARDograph has been produced at the request of the Fluid Dynamics Panel of AGARD.

ISBN 92-835-1463-7

theories, wall interference corrections from boundary measurements, integral equation formulation of subcritical wall interference, and effects of side wall boundary layer on two-dimensional tests. Unsteady wall interference at subsonic and supersonic flow conditions is reviewed. Recent advances in the adaptive wall technique, which actively reduces or eliminates wall interference, are also described.

This AGARDograph has been produced at the request of the Fluid Dynamics Panel of AGARD.

ISBN 92-835-1463-7

AGARD
NATO OTAN
7 RUE ANCELLE · 92200 NEUILLY-SUR-SEINE
FRANCE
Telephone 745.08.10 · Telex 610176

DISTRIBUTION OF UNCLASSIFIED AGARD PUBLICATIONS

AGARD does NOT hold stocks of AGARD publications at the above address for general distribution. Initial distribution of AGARD publications is made to AGARD Member Nations through the following National Distribution Centres. Further copies are sometimes available from these Centres, but if not may be purchased in Microfiche or Photocopy form from the Purchase Agencies listed below.

NATIONAL DISTRIBUTION CENTRES

BELGIUM
Coordonnateur AGARD – VSL
Etat-Major de la Force Aérienne
Quartier Reine Elisabeth
Rue d'Evere, 1140 Bruxelles

CANADA
Defence Science Information Servic
Department of National Defence
Ottawa, Ontario K1A OK2

DENMARK
Danish Defence Research Board
Østerbrogades Kaserne
Copenhagen Ø

FRANCE
O.N.E.R.A. (Direction)
29 Avenue de la Division Lecl
92320 Châtillon sous Bagneu

GERMANY
Fachinformationszentrum F
Physik, Mathematik GmbH
Kernforschungszentrum
D-7514 Eggenstein-Leopo

GREECE
Hellenic Air Force General Staff
Research and Development Directorate
Holargos, Athens

ICELAND
Director of Aviation
c/o Flugrad
Reykjavik

ITALY
Aeronautica Militare
Ufficio del Delegato Nazionale all'AGARD
3, Piazzale Adenauer
ma/EUR

UNITED KIN
Defence Research
Station Square House
St. Mary Cray
Orpington, Kent BR5 3RE

UNITED STATES
National Aeronautics and Space Administration (NASA)
Langley Field, Virginia 23365
Attn: Report Distribution and Storage Unit

THE UNITED STATES NATIONAL DISTRIBUTION CENTRE (NASA) DOES NOT HOLD STOCKS OF AGARD PUBLICATIONS, AND APPLICATIONS FOR COPIES SHOULD BE MADE DIRECT TO THE NATIONAL TECHNICAL INFORMATION SERVICE (NTIS) AT THE ADDRESS BELOW.

PURCHASE AGENCIES

Microfiche or Photocopy
National Technical
Information Service (NTIS)
5285 Port Royal Road
Springfield
Virginia 22161, USA

Microfiche
ESA/Information Retrieval Service
European Space Agency
10, rue Mario Nikis
75015 Paris, France

Microfiche or Photocopy
British Library Lending
Division
Boston Spa, Wetherby
West Yorkshire LS23 7BQ
England

Requests for microfiche or photocopies of AGARD documents should include the AGARD serial number, title, author or editor, and publication date. Requests to NTIS should include the NASA accession report number. Full bibliographical references and abstracts of AGARD publications are given in the following journals:

Scientific and Technical Aerospace Reports (STAR)
published by NASA Scientific and Technical
Information Branch
NASA Headquarters (NIT-40)
Washington D.C. 20546, USA

Government Reports Announcements (GRA)
published by the National Technical
Information Services, Springfield
Virginia 22161, USA

Printed by Specialised Printing Services Limited
40 Chigwell Lane, Loughton, Essex IG10 3TZ

ISBN 92-835-1463-7